2022

Applications of Advanced Computational Modelling for Principal Underground Mining Hazards Management and Control

Ming Qiao

UNIVERSITY
OF WOLLONGONG
AUSTRALIA

Faculty of Engineering & Information Sciences

School of Civil, Mining and Environmental Engineering

Applications of Advanced Computational Modelling for Principal Underground Mining Hazards Management and Control

A thesis submitted in fulfilment of the requirement for the award of the degree of Doctor of Philosophy of University of Wollongong

By

Ming Qiao

30 November 2022

THESIS DECLARATION

I, Ming Qiao, declare that this thesis, submitted in fulfilment of the requirements for the award of Doctor of Philosophy, in the School of Civil, Mining and Environmental Engineering, University of Wollongong, is wholly my own work unless otherwise referenced or acknowledged. The thesis is completed under the supervision of Professor Ting Ren, Dr Jon Roberts, and Professor Alex Remennikov. The document has not been submitted for qualifications at any other academic institution.

Ming Qiao

November 2022

ACKNOWLEDGEMENTS

I would like to express my deepest gratitude to my supervisors, Professor Ting Ren, Dr Jon Roberts, and Professor Alex Remennikov, for their invaluable guidance and considerable support throughout the studying period in Australia. Although the outbreak of Covid19 impacted my study and life for a long period of my PhD study, considerate care from Professor Ren and Dr Roberts allows me to enjoy my stay in Australia, which are beautiful memories and precious wealth in my life.

I am thankful for the financial support from the China Scholarship Council (CSC) and the University of Wollongong (UOW) for providing me with the living allowance and tuition fees, respectively.

I would like to express my sincere appreciation to Visiting Professor Jianming (William) Wu for sharing his in-depth knowledge and making precious suggestions on spontaneous combustion throughout my study.

Special thanks go to the mine staff at the underground coal mines introduced in the thesis for providing me with onsite geological and mining information, gas monitoring data and other supports for computational modelling and result validation.

I am grateful to the Australian Coal Association Research Program (ACARP) for the support of project C28006 entitled “Impact of gas composition on outburst propensity of coal”, project C33029 entitled “Optimise longwall face ventilation to mitigate goaf gas emissions onto walkways and tailgate end” and project C33030 entitled “VR-CFD based simulation tool for dust control in gateroad development panels”.

I would like to show my gratitude to Dr Jennifer Hines for her support in the underground coal mine visit and dust monitoring at the heading development.

I owe my sincere gratitude to the technical staff in the School of Civil, Mining and Environmental Engineering (CME), especially Richard Berndt for his laboratory assistance and Ben O’Brien from IMTS for software technical assistance.

I would like to extend my gratitude to all our mining group members, including Professor Naj Aziz, Dr Jan Nemcik, Dr Patrick Booth, Dr Zhenjun Shan, Dr Anxiu Liu, Dr Jia Lin, Dr Hongchao Zhao, Dr Xiaohan Yang, Dr Hongwei Liu, Dr Lihai Tan, Dr Shuo Liu, Dr Bo Zhao, Mr Zhongbei Li for their friendly support and motivation during the course of this study.

I would like to thank my loved father, mother, sister and brother-in-law for their consistent encouragement and support. They have endured so much for these four years. I dedicate this thesis

to them. Lastly, and most importantly, to my lovely and gorgeous girlfriend, and her kind-hearted parents. This study would not have been completed without their love and encouragement.

PUBLICATIONS

1. **M Qiao**, T Ren, J Roberts, X Yang, Z Li, & J Wu. Insight into proactive inertisation strategies for spontaneous combustion management during longwall mining of coal seam with various orientations. **Energy Sources, Part A: Recovery, Utilization, and Environmental Effects**, 2023. (Accepted)

2. **M Qiao**, T Ren, J Roberts, H Liu, X Yang, L Tan, & J Wu. Improved computational fluid dynamics modelling of coal spontaneous combustion control and gas management. **Fuel**, 2022, 324, 124456.

3. **M Qiao**, T Ren, J Roberts, X Yang, Z Li, & J Wu. New insight into proactive goaf inertisation for spontaneous combustion management and control. **Process Safety and Environmental Protection**, 2022, 161, 739-757.

4. **M Qiao**, Z Li, P Booth, T Ren, & D Black. Lab studies of gas compositions on coal outburst. **2022 Resource Operators Conference**, February 2022, Wollongong, Australia.

5.Z Li, T Ren, X Li, **M Qiao**, X Yang, L Tan, & B Nie. Multi-scale pore fractal characteristics of differently ranked coal and its impact on gas adsorption. **International Journal of Mining Science and Technology**, 2023.

6. T Ren, **M Qiao**, J Roberts, & J Hines. Monitoring and computational modelling of ventilation and dust flow in development panel. **2023 Resource Operators Conference**, February 2023, Wollongong, Australia.

7. J Roberts, R Liao, **M Qiao**, D Hastie, & P Wypych. Research into the selection and efficiency of nozzles for airborne dust suppression. **2023 Resource Operators Conference**, February 2023, Wollongong, Australia.

8. H Liu, F Wang, T Ren, **M Qiao**, & J Yan. Influence of methane on the prediction index gases of coal spontaneous combustion: A case study in Xishan coalfield, China. **Fuel**, 2021, 289, 119852.

9. L Tan, T Ren, L Dou, X Yang, **M Qiao**, & H Peng. Analytical stress solution and mechanical properties for rock mass containing a hole with complex shape. **Theoretical and Applied Fracture Mechanics**, 2021, 114, 103002.

10. L Tan, T Ren, L Dou, X Yang, X Cai, & **M Qiao**. Analytical stress solution for rock mass containing two holes based on an improved Schwarz alternating method. **Theoretical and Applied Fracture Mechanics**, 2021, 116, 103092.

PARTICIPATED PROJECTS

1. Studies of goaf gas flow dynamics and inertisation strategies for goaf heating controls. (Industrial project, completed, 2020).

2. CFD modelling studies of longwall goaf gas flow ventilation dynamics and respirable dust dispersion on a longwall face. (Industrial project, completed, 2020)

3. Studies of gas reservoir properties of Wongawilli Seam at Dendrobium Mine. (Industrial project, completed, 2021)

4. Impact of Gas Composition on Outburst Propensity of Coal. (ACARP project C28006, completed, 2021)

5. Tracer gas study of goaf gas flow dynamics and evaluation of inertisation effectiveness. (Industrial project, completed, 2021)

6. CFD modelling studies of goaf flow dynamics during panel sealing process. (Industrial project, completed, 2021)

7. CFD modelling studies of booster fan exhaust shock losses. (Industrial project, completed, 2021)

8. Optimise longwall face ventilation to mitigate goaf gas emissions onto walkways and tailgate end. (ACARP project C33029, Final (draft) report to ACARP, 2022)

9. VR-CFD based simulation tool for dust control in gateroad development panels. (ACARP project C33030, Final (draft) report to ACARP, 2022)

10. CFD modelling studies of outburst induced overpressure in a development panel. (Industrial project, completed, 2022)

ABSTRACT

Underground coal mining is facing increased threats from the hazards of spontaneous combustion and heating of coal, abnormal mine gas emissions, and harmful dust concentrations in underground workings, due to increased production outputs and extraction depth of cover. To control and mitigate these engineering problems, there is a need to gain critical knowledge of spontaneous heating in the longwall (LW) goaf, gas migration patterns onto the LW face, and ventilation dynamics and dust dispersion in complex underground environments. Advanced Computational Fluid Dynamics (CFD) modelling can be used to simulate various scenarios portraying these hazards that may occur in underground LWs and provide much-needed knowledge and fundamental science that can be used to develop robust and effective control and mitigation strategies against these hazards.

A comprehensive literature review has been conducted to understand these principal mining hazards (PMH), with a particular emphasis on the applications of CFD modelling in the prevention management and control of those PMH arising during coal extraction process. The insufficiencies and gaps in research on spontaneous combustion in active LW goaf, gas migration onto the LW face, and dust dispersion and transport in the development heading were identified. In addition, several field studies were carried out in underground coal mines in Australia to gain a better understanding of these mining issues and collate essential data for the CFD modelling studies.

In recent years, goaf heating and spontaneous combustion incidents have been reported in several Australian underground coal mines during normal production cycles. The onset of these heating incidents was dictated by many operational and environmental parameters. Based on the site-specific conditions of an underground coal mine, where the coal seam gas is of approximately 80% carbon dioxide (CO_2) and 20% methane (CH_4) with a gas emission rate of 2000 l/s, CFD models were developed and validated with field gas monitoring data collected from the Tube Bundle System. The CFD models incorporated a user defined function (UDF) of gas emission and permeability variations in a three-dimensional (3D) space of computational domain representing the LW panels and goaf areas. Simulation results indicated that better goaf inertisation could be achieved when nitrogen (N_2) was injected via cut-throughs (C/T) at about 250 m behind the LW face on the maingate (MG) side and surface boreholes at 100 m and 700 m on the tailgate (TG) side, with a total injection rate greater than 1750 l/s. The oxygen concentration on the MG and TG side dropped below 5% at distances of 120 m and 75 m behind the LW face, with a confined oxidation zone area of 35375 m^2, which was approximately one-third of the oxidation zone area without inert gas injection. The impact of geological variations (i.e., coal seam orientations and goaf gas composition) on spontaneous combustion prevention and management was further

studied using CFD models. The influence of ventilation design and operational parameters (e.g., tightness of the goaf seals) on spontaneous combustion control was also investigated by additional CFD models based on field data.

During LW sealing-off, the ventilation flow dynamics change within the goaf, which considerably increases the risk of spontaneous combustion and gas explosion. To prevent these hazards, CFD models were developed and calibrated with field gas monitoring data to simulate a range of operational scenarios of different ventilation arrangements. The modelling studies indicated that at least six gas sensors should be employed and positioned appropriately to ensure effective goaf atmosphere monitoring for risk management during the LW sealing-off process.

Extensive CFD-DPM (Discrete phase model) coupling modelling studies were conducted to investigate dust-related issues in LW gateroad development panels. Based on site-specific conditions, a CFD model incorporating a Continuous Miner (CM), Shuttle Car (SC) and exhausting ventilation tube was established and validated with onsite dust monitoring data. Three scenarios of CM cutting at the middle, floor and roof positions were considered and simulated. In all cases, the simulation results indicated that high levels of dust exposure would occur to left-hand-side (LHS) operators and consequently they should be equipped with high-quality personal protective equipment and stay behind the ventilation duct inlet during coal cutting process, while miners standing at the right-hands-side (RHS) of the CM for roof and/or rib bolting and machine operation should stay immediately behind the bolting rig where dust concentration was relatively low.

The studies conducted in this thesis provided new insights into the current goaf inertisation practices to effectively manage and control spontaneous heating in LW goaf by considering geological variations and mining design. Furthermore, the CFD modelling study of gas flow dynamics during the panel sealing-off process provides new knowledge of ventilation and goaf gas dynamics, which is critical to the positioning of gas monitoring sensors to reliably measure goaf atmosphere changes, thus minimizing spontaneous heating and gas explosion risks with much-improved mine safety. The research work also shed light on the dust and ventilation behaviour in gateroad development panels, and provided several recommendations for operators' locations and dust mitigation strategies to improve the health and safety of miners. The research outcomes from this study contribute to the improvement of current practices and guidance for PMH management and control in underground mines and tunnelling projects.

TABLE OF CONTENTS

LIST OF ABBREVIATIONS

CFD	Computational Fluid Dynamics
PMH	Principal Mining Hazards
LW	Longwall
UDF	User Defined Function
3D	Three Dimensional
C/T	Cut-Through
MG	Maingate
TG	Tailgate
DPM	Discrete Phase Model
CM	Continuous Miner
SC	Shuttle Car
LHS	Left Hand Side
RHS	Right Hand Side
CO_2	Carbon Dioxide
CH_4	Methane
N_2	Nitrogen
O_2	Oxygen
CO	Carbon Monoxide
H_2	Hydrogen
C_2H_2	Acetylene
C_2H_4	Ethylene
C_2H_6	Ethane
NSW	New South Wales
CWP	Coal Workers' Pneumoconiosis
PMF	Progressive Massive Fibrosis
PPE	Personal Protective Equipment
AFC	Armoured Face Conveyor
SHT	Self-Heating Temperature
DEM	Discrete Element Method
PFC	Particle Flow Code
EGZ	Explosive Gas Zone
GVB	Gob Ventilation Borehole
BSL	Beam Stage Loader

DSMC	Direct Simulation Monte Carlo
TARP	Trigger Action Response Plan
GC	Gas Chromatograph
TB	Tube Bundle
PHMP	Principal Hazard Management Plan
MHMP	Major Hazard Management Plan
SCMP	Spontaneous Combustion Management Plan
PCI	Pulverized Coal Injection
BH	Borehole
OZA	Oxidation Zone Area
GA	Goaf Area

LIST OF FIGURES

LIST OF TABLES

CHAPTER 1 GENERAL INTRODUCTION

1.1 Backgrounds

Coal is a key resource that has played a crucial role in industrial development and technological advances. A recent report released by British Petroleum (2020) revealed that coal remained the biggest contributor to electricity generation by fuel worldwide in 2019, accounting for approximately 36.4%, which was followed by natural gas (23.3%) and hydroelectricity. Particularly in Australia, the share of electricity produced by coal reached around 56.4% in 2019. As the fifth-largest coal producer, Australia annually produces 450~500 Mt of coal in recent years, accounting for approximately 6% of global total coal production, as shown in Figure 1.1 (International Energy Agency 2020).

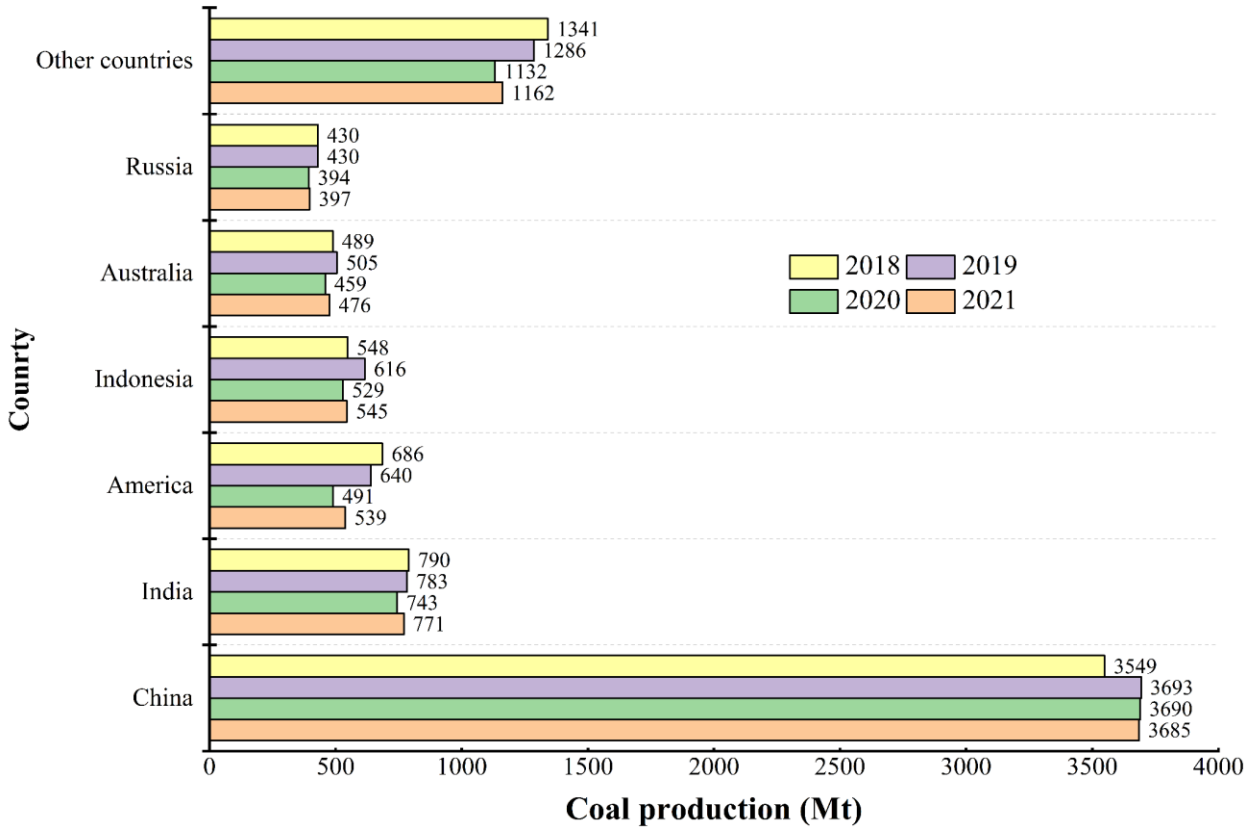

Figure 1.1 Coal production of major countries worldwide (International Energy Agency 2020)

Coal mining technology is driven worldwide by the need for high-yield and high-efficiency production, and this is achieved by increasing longwall (LW) panel width and advancing distance in Australia, which results in new challenges of effectively managing and controlling principal mining hazards (PMH) commonly taking place in the process of coal extraction. According to the guideline issued by NSW Resources Regulator (2016), nine specific hazards are identified for the mine site, including roads or other vehicle operating areas, air quality or dust or other airborne contaminants, fire or explosion, ground or strata failure, inundation or inrush of any substance, mine shafts and winding system, gas outbursts, spontaneous combustion and subsidence (NSW

South Wales 2021).

Spontaneous combustion and heating of coal have become a significant hazard faced by many underground coal mines, especially those in New South Wales (NSW) and Queensland, where most coal resources are distributed in Australia. In the last century, many gas explosions triggered by spontaneous combustion took place in underground coal mines in Australia, bringing about heavy economic losses, severe injury and even loss of lives. Particularly the violent explosions occurring in Box Flat in 1972 and Kianga No.1 coal mine in 1975 which took the lives of 17 and 13 miners, respectively, and it was revealed that these two fatal accidents were caused by explosive methane being ignited by spontaneous combustion (Loane et al. 1975; Queensland Government 1972). Ham (2005) reported that 51 mining incidents associated with spontaneous combustion happened in Queensland over 32 years (1972～2004), and several coal mines in NSW suffered from spontaneous-combustion-related hazards, resulting in mines having to close either temporarily or permanently since 1972. Despite considerable advances in techniques and technologies for spontaneous combustion management and control, it is expected that at least one spontaneous-combustion-induced incident will occur annually on average, causing miners to be withdrawn and evacuated from the mine site (Cliff 2015).

When coal resources are extracted from the underground seam, a large void area termed goaf is formed behind the LW face. With the continuous advance of the working face, the mined-out area becomes bigger, and the overlying strata above the mining seam are highly liable to bend and even collapse under the effect of self-gravity. The mining-induced fractures and cracks provide channels for seam gas emitted from gas-bearing strata overlying or underlying the mining seam. If not properly and effectively managed and controlled, the in-situ seam gas in large quantity is likely to expel onto the working face or accumulate at the upper corner of the tailgate end, leading to production stoppages, mine evacuation, and even uncontrolled mining hazards, such as coal and gas outburst and gas explosions.

On 5 January 2011, a fire and explosion took place in the proximity of the TG area of LW1 at the Blakefield South Mine, and subsequently, the mine was sealed for about 5 months before the underground environment was sufficiently safe for workers to re-enter the mine. All underground miners working at the LW panel in the course of the explosion were safely withdrawn as a result of the accurate judgment of potential risks and early evacuation decisions made by the deputy (Flowers & Stewart 2011). This incident caused some damage to the ventilation control devices and mining equipment, as shown in Figure 1.2. A technical report released by Stewart and Hsin (2012) revealed that there were some occasions where methane concentration built up and exceeded the minimum explosive limit on the tailgate side of the goaf area just behind the chock

line.

(a) Stopping blown out

(b) Joy Mimic Unit

Figure 1.2 Damage caused by fire and explosion at the Blakefield South Mine (Flowers & Stewart 2011)

More recently, an unanticipated build-up of methane and carbon dioxide in both LW and main return gateroad caused 70 coal workers to be withdrawn from Metropolitan Coal Mine on 21 March 2019, and the mine was barred from entering for 7 days until both methane and carbon dioxide concentration reduced below safe trigger values (Australasian Mine Safety Journal 2019). In the LW return gateroad, the maximum methane concentration registered by remote gas monitoring system had reached as high as 16.1%, which is slightly higher than the maximum explosive limit of 15%. An investigation conducted by NSW Resources Regulator (2019) identified that the LW supports experienced unforeseen increased loading pressure as a result of the rising depth of cover and localized specific geological conditions, which resulted in floor heave and chain pillar fracturing. Thus, many pathways were created to allow gas to migrate from gas-bearing strata under the mining seam to mined-out goaf areas.

With the increase in coal production, an enormous amount of coal or silica dust can be produced by mining-related activities, including but not limited to cutting, drilling, crushing as well as transporting, which has become a hard-to-eradicate problem plaguing the mining industry.

Prolonged exposure to the harsh environment where dust concentrations remain at a high level could lead to coal workers being highly likely to contract mining-induced respiratory diseases that are irreversible and hard to cure, such as coal workers' pneumoconiosis (CWP, also termed as "black lung disease"), silicosis, mixed dust pneumoconiosis, chronic obstructive pulmonary diseases, occupational asthma, bronchitis symptoms, and even progressive massive fibrosis (PMF) that is considered as the most severe form of CWP (Chen et al. 2012; Fishwick & Barber 2012; Graber et al. 2017; McBean et al. 2018; Smith 2017; Wang et al. 2020). Due to significant technological progress in dust control, stringent legislation for dust management, better personal protective equipment (PPE) available for miners, and comprehensive medical surveillance and screening on a regular basis, it has been about 30 years since the 1970s that no case of coal workers diagnosed with CWP was formally reported (McBean et al. 2018; Zosky et al. 2016). That was until May 2015 when the first CWP case re-emerged in Queensland (Parliament of Australia 2016; Penrose 2020; Queensland Audit Office 2019). In the following approximate 5-year period, a total of 207 workers employed in the mining-related industry in Queensland were identified as victims of mine dust lung diseases by 31 March 2021, among which 50, 46, and 27 workers were diagnosed with CWP, silicosis, and mixed dust pneumoconiosis respectively (Queensland Government 2021). It is noted from Figure 1.3 that CWP cases identified annually remained at 6~7 in the recent 5 years in Queensland except in 2017 when 14 employees working in the mining industry contracted CWP. In NSW, it was reported that 8 male workers employed in the mining industry contracted either CWP or silicosis from December 2016 to May 2020, while another two cases of interstitial lung disease and pneumoconiosis have not been confirmed (NSW Government 2021).

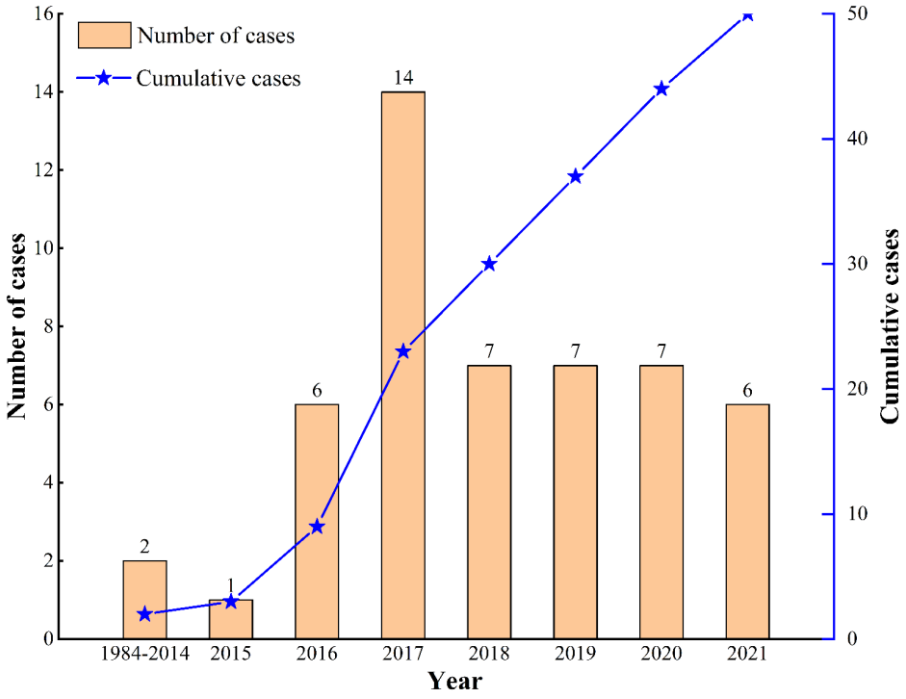

Figure 1.3 Cases of CWP in Queensland since 1984 (Queensland Government 2021)

Coal Services (2010) is commissioned to regularly monitor onsite dust levels at different coal mines in NSW in an attempt to evaluate the effectiveness of various dust control techniques and recognize the potentially risky areas where workers are highly likely to suffer from respiratory diseases. According to an annual report released by Coal Services (2020), the average exposure for respirable dust, respirable quartz, and inhalable dust was all below the statutory workplace exposure standard of 2.5 mg/m^3, 0.1 mg/m^3, and 10 mg/m^3 respectively. However, in spite of the great effort put into controlling dust concentration below the legislative standard, there were still some occasions where airborne dust sampled in the required workplace exceeded the allowable maximum exposure values (Coal Services 2020), as depicted in Figure 1.4. It is noted that the exceedances of dust exposure limits generally showed a downward trend in recent years, especially for respirable dust whose exceedance rates remained only at 0.1%. In contrast, the exceedance rates for respirable quartz were as high as 1.8%. As a result, much emphasis should be laid on the management and control of respirable crystalline silica because it is widely accepted that silica can cause more serious harm to the lung than coal dust (Coal Workers' Pneumoconiosis Select Committee 2017). The new workplace exposure standards for respirable coal dust (1.5 mg/m^3) and respirable crystalline silica (0.05 mg/m^3) took effect in NSW on 1 February 2021 and 1 July 2020, respectively (NSW Government 2020). From 1 September 2020, the statutory occupational exposure limits for respirable coal dust and respirable crystalline silica are 1.5 mg/m^3 and 0.05 mg/m^3, respectively, for Queensland (Queensland Government 2020).

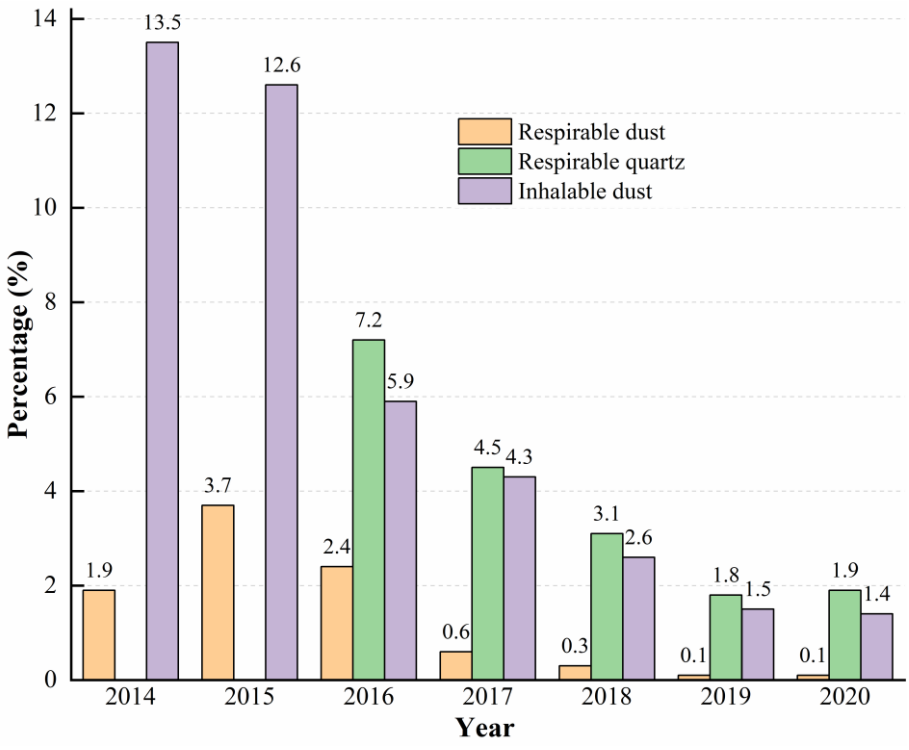

Figure 1.4 The percentage of sampling dust exceeding the statutory exposure standard (Coal Services 2020)

Due to the competitive advantages of data visualization, time-saving, and cost-saving over

traditional physical lab experiments and field testing, computational fluid dynamics (CFD) modelling has been widely used to help solve mining-related problems, such as spontaneous combustion and heating control (Balusu et al. 2019; Qiao et al. 2022a; Ren & Balusu 2005; Zhuo et al. 2021), gas explosion formation and propagation (Brune et al. 2016; Gilmore et al. 2016; Li et al. 2020b), dust management and control (Ren & Wang 2019; Ren et al. 2018b; Wang et al. 2017b), effective management and control of elevated gas emitted from the goaf areas (Mishra et al. 2016; Ren et al. 2018a; Tanguturi et al. 2020), prediction of ventilation airflow in the LW face and heading development (Guo et al. 2012; Tutak & Brodny 2018; Wang et al. 2018e), and diesel particulate matter control (Thiruvengadam et al. 2016; Xu et al. 2018; Zheng et al. 2017). It has been proven that comprehensive utilization of CFD modelling in the mining industry is of great benefit to solving fluid-dynamics-related problems and optimizing equipment design, thus not only reducing the likelihood of risk associated with mining activities but also saving a significant amount of time and cost (Ren & Balusu 2009; Xu et al. 2016).

1.2 Statement of Problems

The LW face in underground coal mines is characterized by expanded LW panel width (normally 250～400 m), longer advance distance (2～3 km) and increased advance rates. When coal is extracted from the underground space, a void area is formed behind the LW face, and the strata above the mining seam will cave as a result of gravity and re-distributed surrounding stress. The falling roof is compacted and consolidated in the centre of the goaf area under the effect of overlying strata and periodic weighting, resulting in low permeability in this area; however, the caving roof cannot be compacted tightly at the edge of the goaf due to the support of the coal pillar, resulting in many cracks and fractures providing pathways for air to ingress into the goaf area (Qian & Xu 1998). The distribution of fractures and cracks induced by mining activities on the plane view is featured as an "O-ring" in shape, which is commonly utilized for post-drainage (Qu et al. 2015). Once the air in large volume migrates into the goaf area via the leakage pathways at the periphery of the goaf area and fractured chain pillars, coal left in these areas will be subject to oxidation under ambient temperature, leading to the occurrence of spontaneous combustion and heating, and even a fire threatening the safety of mine. A famous proverb goes that "prevention is always better than cure". In order to effectively manage and control the onset of spontaneous combustion, various strategies have been proposed and successfully implemented in mine sites, such as ventilation measures by blocking off the leakage pathways and reducing ventilation pressure difference; goaf inertisation by carbon dioxide, nitrogen, boiler gas or seam gas; remote sealing by fly ash, filling material, ventilation door, etc., among which goaf inertisation is widely applied in Australian coal mines. Many scholars have conducted extensive research on the effect

of different mining parameters on spontaneous combustion control in the goaf area, including the inert gas injection location via underground cut-throughs and surface boreholes, injection flow rate, inert gas type, ventilation air flowrate through the LW face, the negative pressure within gas drainage boreholes or roadways, gas drainage rate, the barometric pressure, the permeability within the goaf area as well as coal properties. However, few studies comprehensively cover the impacts of other geological parameters (coal seam orientations and seam gas composition) and mining factors (e.g., different ventilation patterns of LW panels and the tightness of seals built in the cut-throughs) on ventilation dynamics and gas distribution patterns and the determination of fit-for-purpose proactive goaf inertisation strategies. In addition, there is limited research on the ventilation dynamics and goaf gas atmosphere change (methane and oxygen) in the LW panel at different stages of the panel sealing-off process, during which period the LW face is stopped for face recovery and spontaneous combustion is likely to occur and develop due to strong air leakage and heat built up.

As shallow coal reserves have been severely depleted in many countries worldwide and underground coal extraction progresses into deep and gassy coal seams, the management and control of the high volume of goaf gas emissions have become a more challenging problem for the mining industry. Once improperly and ineffectively controlled and managed, the excessive emission of gas, particularly methane, has given rise to problems of production delays, mine evacuation, fires and gas explosions in the worst-case scenario. In view of mining hazards associated with elevated gas levels in the LW face or goaf area, various control measures and engineering designs have been developed and utilized in underground coal mines (Qu et al. 2016; Ren et al. 2018a; Si & Belle 2019; Stewart Gillies 2013), including pre-drainage and post drainage (e.g., the surface to in-seam boreholes, underground in-seam directional drilling, surface goaf wells or holes, cross-measure boreholes), different ventilation systems (e.g., maingate belt headings with homotropal ventilation, fresh air flowing to tailgate gateroads, bleeder ventilation) and control measures (e.g., curtains, brattices, wings, back over bleed, and back return airway). Although these mining practices have been successfully implemented in most of the coal mines in Australia for the purpose of effectively reducing the high volume of goaf gas emission to the LW face, there are still several underground coal mines that have experienced goaf gas leakage into the LW face via the rear of supports and elevated gas levels in the vicinity of the TG drive (armoured face conveyor (AFC) motor and gearbox), resulting in face stoppage, production delays, additional operational cost as well as unanticipated safety issues. By in-depth analysis of real-time gas monitoring data provided by eight underground coal mines over the course of two years from 2016 to 2018, the Mines Inspectorate of Queensland indicated that there were some occasions where the general body methane levels exceeded 2.0% and even 2.5% in six mines (Inspectorate

2019), as illustrated in Figure 1.5. It is not unusual that the methane concentration may be below the practicably acceptable threshold limit in the outbye return airway, while localized unexpected high methane levels, particularly at the TG end as the LW shearer cuts in the direction towards the tailgate, are likely to be present and lie in the explosive range of 5%～15%. Effectively reducing the gas exceedance incidents caused by LW air flushing out goaf gases has become an urgent problem plaguing many underground coal mines, especially those that are extracting coal resources from gassy or multiple seams with high goaf gas emissions (>5000 l/s) and low permeability. As a result, there is an immediate need to determine the optimum ventilation and gas management practices that can be implemented on the LW face to effectively manage and control high-gas-emission-related problems, particularly at some localized areas around the TG ends. In addition, When the LW face approaches the finish-off line, the LW equipment is required to relocate to the new installation face, which usually takes at least one month. During this period, the LW face stops advancing, and both the ventilation dynamics and goaf gas atmosphere change, which significantly increases the risk of spontaneous combustion and gas explosion. To prevent these hazards from arising during the LW panel sealing-off process, a detailed understanding of ventilation dynamics and goaf gas atmosphere in the active goaf and LW face is of vital importance to improve the panel sealing-off process design and mitigate the risk of spontaneous combustion and gas explosion.

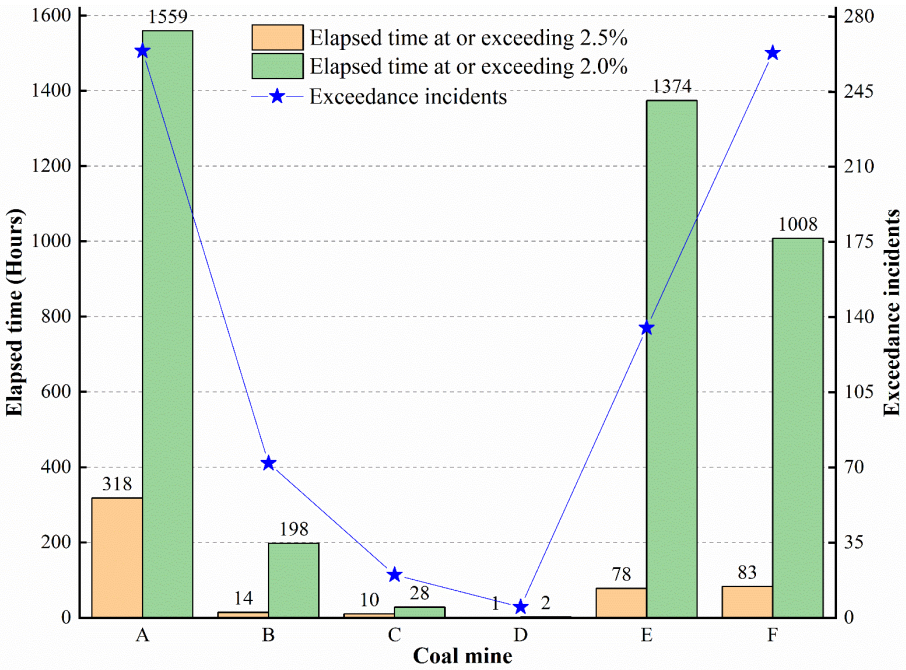

Figure 1.5 Summary of methane exceedances in six mines (Inspectorate 2019)

Exposure to respirable coal dust and silica dust in underground mines is becoming a growing concern due to the re-occurrence of dust-induced lung disease in both Queensland and NSW. Airborne dust monitoring data collected from thousands of workers employed in the mining

industry by Coal Services (2017) under Order 43 revealed that the continuous miner (CM) operators experience the second-highest dust exposures, just followed by the LW workers. A similar trend has also been reported by Queensland Government (2020). The dust sampling and monitoring are conducted on a regular basis at specific sites susceptible to high dust levels, and the determination of workers' exposure to respirable dust is traditionally done in accordance with AS2985: 2009-Workplace Atmosphere-Method for Sampling and Gravimetric Determination of Respirable Dust. This method is favourable as it enables people to directly make comparisons between sampling results and the stipulated workplace exposure standards. However, several limitations exist as it only provides an overall dust concentration at specific sites over the sampling period, and the granularity of specific tasks or processes that contribute most to exposure cannot be defined when the process changes during monitoring. As a result, real-time dust monitors are required to provide continuous dust data and assist in comprehensively understanding how the exposure levels behave when the specific task changes. For the sake of obtaining the dust profile at the whole development heading, CFD modelling has been increasingly used. According to site-specific conditions, CFD numerical model can be built and calculated. By comparing the onsite dust data collected using continuous real-time monitors and personal gravimetric monitoring devices, the simulation results from CFD modelling can be verified and validated. Although extensive CFD modelling works pertaining to dust control in the heading face have been conducted, few studies investigate the dust migration patterns in the CM-driven heading with single exhaust ventilation, which is much more common in the mining industry in Australia. In addition, the impact of various cutting operations on dust migration patterns in the development panel is hardly ever studied, such as the coal cutting and dumping process, different cutting positions of the drums and the distance of the exhausting duct from the heading face. What is more, there are limited studies with regard to the dispersion regularity of respirable coal and silica dust (particle sizes below 10 μm), which is more harmful to miners' bodies due to the fact that it is hard to exhale these kinds of dust out of mouth and dust can penetrate deeply into lung and cause irreversible harm.

1.3 Significance of This Study

Many PMHs, including but not limited to spontaneous combustion and heating in large goaf areas, abnormal gas emissions and elevated gas levels at the TG end, and high respirable coal and silica dust levels at underground workings, pose increasing threats to health and safety in underground coal mines. Although significant progress has been made to manage and control these hazards, some accidents unexpectedly occur, resulting in adverse worker health outcomes, production delays and mine evacuations. In the worst cases, mine fire and gas explosions or excessive dust inhalation present a risk to human life.

It has been reported that many accidents involving spontaneous combustion and heating occurred in Australian underground coal mines in recent years, resulting in production delays, panel seals and even mine closure. Due to the LW goaf being characterized as an inaccessible area, CFD modelling has superior advantages over traditional research methods in studying heating-related problems in the goaf area. Based on site-specific conditions, three-dimensional (3D) goaf models can be constructed and adequately calibrated using on-site data, enabling other scenarios to be simulated with a high level of confidence. Thereafter, extensive parametric studies can be conducted to investigate the effect of different geologic variations (e.g., goaf gas composition and coal seam orientations) and mining designs (e.g., ventilation patterns and the tightness of seals built in the cut-throughs) on goaf gas distribution, which will cast light on improving current goaf inertisation practices to effectively manage and control spontaneous heating problems in the goaf areas, particularly those with large panel size and advancing distance.

High goaf gas emissions (methane and carbon dioxide) and elevated gas levels at localized TG ends have recently plagued some underground coal mines, as evidenced by recent accidents in NSW and Queensland. To effectively mitigate and manage these problems, it is essential to improve the knowledge of ventilation behaviour and gas flow dynamics. With the aid of CFD modelling, 3D LW models can be built based on defined scenarios and simulated with accurate boundary conditions. The simulation results will be validated and calibrated with onsite monitoring data, and extensive parametric studies of various LW ventilation controls and practices can be evaluated with sufficient confidence. The methane dispersion characteristics at various stages of the LW sealing-off process could also be simulated, which allows for identifying appropriate gas sensor locations to monitor goaf gas atmosphere change. The modelling results can provide immediate benefits to coal mines facing serious goaf gas emission problems or those whose LW face approaches the finish-off line.

Long-term exposure to the underground workings where high respirable coal dust or respirable silica dust exists can pose a significant threat to the health of coal mine workers. The alleviation and mitigation of dust exposure depend not only on effective engineering controls but also on ongoing innovative education and training programs for the employee on the job. Based on specific development panel scenarios, numerical models can be built and calculated using the CFD-DPM (Discrete Phase Model) coupling method, with simulation results being compared with onsite datasets for model validation. Then extensive parametric studies can be carried out to better understand dust and ventilation behaviour around CM in various development operations and cutting scenarios (e.g., cutting roof and floor, cutting, conveying and loading process, the distance of ventilation duct from the heading face).

1.4 Objectives

The main objective of this research is to investigate various practices and measures to manage and control PMHs faced by most underground coal mines in Australia using CFD modelling methods, including spontaneous combustion and heating in large goaf areas, elevated goaf gas emissions at localized TG end and gas-related problems during the LW panel sealing-off process, and fugitive airborne dust in the gateroad development panels. Specifically, this research aims:

- To better understand the PMHs occurring in the underground coal mines and their countermeasures by comprehensive literature review and field study;
- To qualitatively and quantitatively investigate the impact of various inertisation strategies on spontaneous combustion management and control in the active goaf where the seam gas is primarily composed of carbon dioxide;
- To study and determine the optimal inertisation parameters (e.g., injection locations, injection rate, inert gas type) for better spontaneous heating management in the active goaf with various seam gas composition and coal seam orientations;
- To qualitatively and quantitatively study the influence of ventilation and mining design (e.g., ventilation patterns, tightness of goaf seals built in the cut-throughs, and goaf inertisation strategies) on goaf gas flow dynamics and patterns in the LW goaf where the seam gas is predominantly comprised of methane;
- To advance knowledge of ventilation dynamics, evaluate ventilation arrangements, and provide critical knowledge of appropriate positioning of monitoring points to reliably reflect goaf atmosphere change during different stages of the panel sealing-off process for the purpose of preventing spontaneous heating and gas explosion;
- To improve the understanding of ventilation patterns and dust dispersion around the CM and operators in the development heading and evaluate the effectiveness of dust mitigation practices by conducting extensive CFD-DPM coupling simulations.

1.5 Scope of Work

In order to address research problems and achieve the thesis objectives, thorough literature reviews and extensive CFD modelling will be conducted to shed new insight into the management and control of three PMHs: spontaneous combustion and heating in the goaf areas, elevated gas levels at the TG end of the LW face, and high airborne dust concentration at the development panels. Necessary field data are collected and analyzed to calibrate the computational modelling, thus increasing confidence in investigating scenarios out of the base case. Figure 1.6 illustrates the scope of work and research framework in this study.

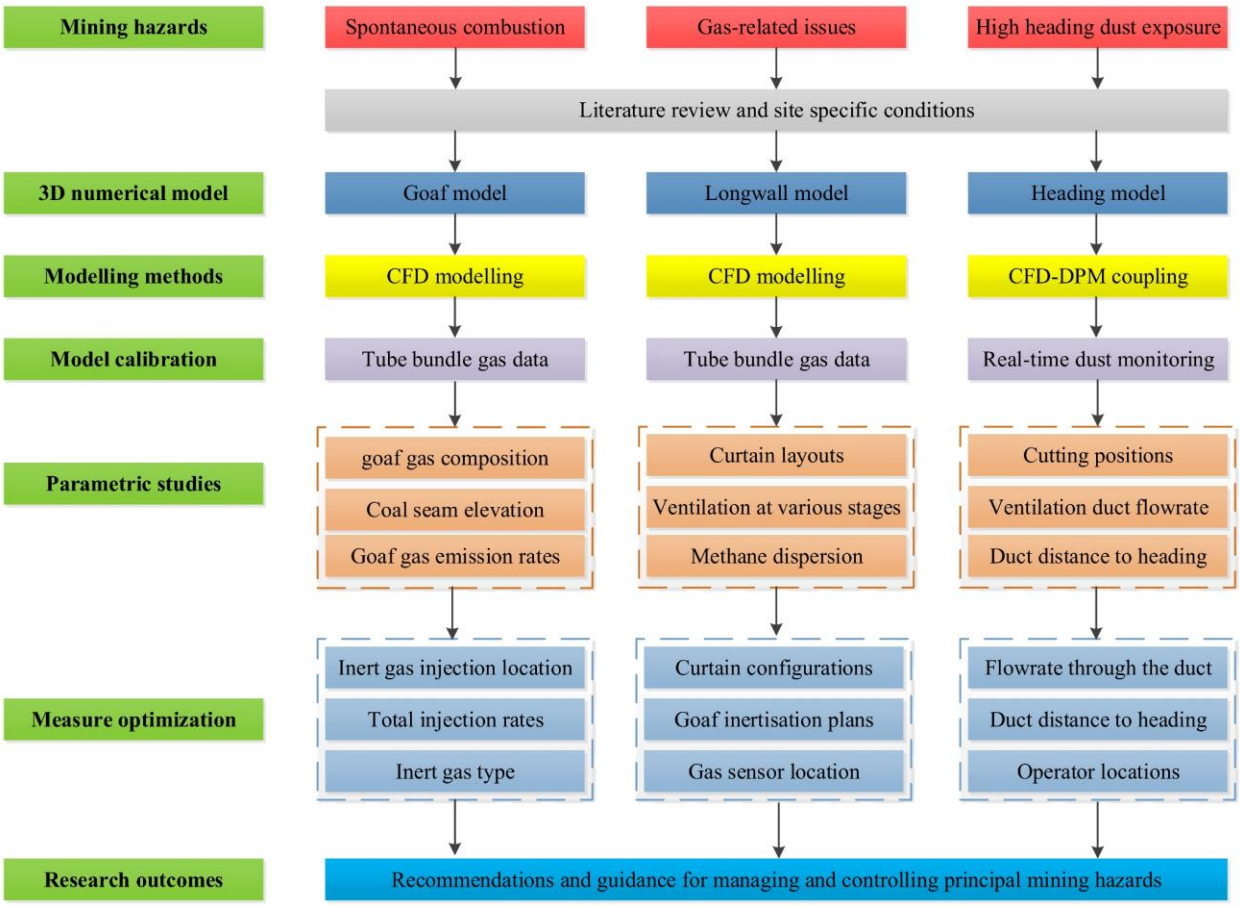

Figure 1.6 Scope of work and research framework

1.6 Thesis Outline

This thesis contains the following nine chapters:

Chapter 1 is a general introduction to the thesis topic, which includes background, statement of problems, significance, objectives, the scope of work, research framework and thesis outline.

Chapter 2 provides a thorough literature review of the PMHs occurring in underground coal mines, with an emphasis on spontaneous combustion in the active goaf, elevated gas levels at the localized TG end and over-exposure dust issues in the development heading. In particular, the application of the CFD techniques for solving problems arising from the mentioned PMHs is introduced, including managing and controlling spontaneous combustion in the active LW goaf, mitigating abnormal gas emissions in the LW goaf and on the LW face, and reducing dust levels in the development heading.

Chapter 3 is based on the paper entitled **New insight into proactive goaf inertisation for spontaneous combustion management and control** published in **Process Safety and Environmental Protection**. The spontaneous heating management system typically employed in Australian underground coal mines is first reviewed. Then based on site-specific conditions of an underground coal mine (in NSW) where coal seam gas is predominantly comprised of carbon

dioxide, CFD models are constructed and calibrated with gas monitoring data, after which extensive parametric studies are performed for proactive goaf inertisation optimization by qualitatively and quantitatively analyzing simulation results.

Chapter 4 is based on the paper entitled **Insight into proactive inertisation strategies for spontaneous combustion management during longwall mining of coal seams with various orientations** published in **Energy Sources, Part A: Recovery, Utilization, and Environmental Effects.** Based on the computational models employed in Chapter 3, extensive CFD simulations are carried out to investigate the impact of coal seam orientations, dictated by the elevation of the MG and TG, and the height of the working face and the starting-off line, on spatial gas distribution patterns and proactive goaf inertisation strategies, in which nine different scenarios are considered.

Chapter 5 is based on the paper entitled **Ventilation flow dynamics and proactive inertisation strategies for spontaneous heating management in active goaf with various seam gas composition**. The validated CFD models in Chapter 3 are applied, and parametric studies are conducted to study the effect of seam gas composition on oxygen distribution characteristics in the active goaf area and fit-for-purpose goaf inertisation plans, in which five different scenarios of seam gas composition are taken into account.

Chapter 6 is based on the paper entitled **Improved computational fluid dynamics modelling of coal spontaneous combustion control and gas management** published in **Fuel**. Based on the geological and mining conditions of an Australian underground coal mine (in Queensland) where seam gas is almost composed of methane, CFD models are built and verified by real-time gas monitoring data. The impact of ventilation design and operational measures on the management and control of spontaneous combustion and gas exceedance is investigated qualitatively and quantitatively, including goaf gas emission rates, the tightness of goaf seals at the cut-throughs, ventilation layouts, proactive goaf inertisation strategies, as well as abnormal gas emission control on the LW face with the application of curtains and brattices.

Chapter 7 is based on the paper entitled **Ventilation arrangement evaluation and proactive goaf inertisation for spontaneous heating and gas explosion management during longwall panel sealing-off process**. Based on site-specific geologic and mining conditions of an Australian underground coal mine in Queensland, two three-dimensional CFD models are built and validated with onsite gas monitoring data. Extensive computational modelling is performed to shed new insight on ventilation dynamics and goaf atmosphere in the active goaf, evaluate the proposed ventilation arrangements, and provide critical knowledge of appropriate positioning of gas monitoring sensors to timely and reliably reflect the goaf atmosphere change during the panel sealing-off process, thus managing spontaneous combustion and gas explosion and improving coal

mining safety.

Chapter 8 is based on the paper entitled **Dispersion and migration characteristics of respirable dust in development panels**. Based on site-specific conditions of a development heading, a 3D CFD model that incorporated a CM, SC and exhausting ventilation tube was built and validated with field measuring data, where a good agreement is reached. Extensive simulations are conducted to investigate the airflow migration patterns and temporal-spatial dust dispersion characteristics in the heading, and dust mitigation strategies are evaluated. This modelling study can advance the understanding of multi-source dust diffusion characteristics in the heading face and provide guidance on dust mitigation, thus improving the health and safety of miners and creating a cleaner underground working environment.

Chapter 9 summarises the major conclusions achieved from the research, and recommendations for future work are provided in this chapter.

CHAPTER 2 LITERATURE REVIEW

2.1 Introduction

Spontaneous combustion and heating, abnormal excessive gas emissions onto the working face, and fugitive airborne dust generated in mining activities are significant problems plaguing underground coal mines worldwide. If not prevented, managed, and controlled in a timely and effective manner, these PMHs could bring about production delay and stoppage, personnel death and injury, and even temporary or permanent mine closure. As a result, it is of vital importance to improve the knowledge of goaf gas flow dynamics and ventilation migration patterns in both LW panels and development headings using CFD modelling methods to figure out the optimal solutions to these PMHs. Therefore, the application of CFD modelling in solving problems associated with spontaneous heating is first discussed, and research limitations are identified. Then, methane distribution characteristics and various control measures practically employed in underground coal mines for reducing high gas emissions and methane accumulation in localized TG end areas are reviewed from the perspective of CFD simulations. Finally, the review of dust dispersion and diffusion characteristics in heading development is undertaken, through which the deficiency in CFD investigation into dust-related problems is discovered.

2.2 CFD Modelling of Spontaneous Combustion and Heating

Spontaneous combustion or heating of coal is a long-term thermal dynamic hazard that is plaguing many underground coal mines worldwide, particularly those extracting underground coal with a high propensity for spontaneous combustion. The mined-out goaf area expands correspondingly as the coal resources are continuously extracted from the underground working coal seam. Depending on the specific geologic conditions (e.g., faults, folds, dykes, seam thickness, coal seam orientations and seam gas composition) and different mining techniques utilized (e.g., mining methods, panel layouts, ventilation system), the issues associated with spontaneous combustion in the active goaf area tend to be complex, and the active goaf is commonly characterized by inaccessible area, which makes it difficult to solve these problems by traditional laboratory experiments or time-consuming frequent fieldwork at the mine site (Liu & Qin 2017a). As a result, numerical simulation, particularly the application of CFD modelling, has become an effective tool for solving spontaneous-combustion-related problems in the active LW goaf.

After verifying and calibrating the base model using on-site monitoring data, Ren et al. (2005) and Ren and Balusu (2009; 2010) conducted extensive parametric studies with a view to comprehensively investigating the influence of inert gas injection location, injection rate and inert gas type on spontaneous combustion control in the goaf area. It was recommended that a decent

goaf inertisation result could be produced by pumping inert gas at a distance of 200～400 m behind the LW face rather than in close proximity to the LW face, as the majority of inert gas would disperse along with main ventilation airflow and directly ventilate out of face if the injection site was too close to the LW face. The second significant finding from the modelling was that an injection rate of 0.5 m^3/s could meet the requirements for desirable goaf inertisation performance.

Yuan et al. (2006) studied the influence of different ventilation systems (e.g., one-entry and two-entry bleederless systems and three-entry bleeder system) on flow paths and spontaneous heating distribution in the goaf area using CFD modelling. It was to be noted that there was a marginal difference in airflow patterns for one-entry and two-entry bleederless systems, whereas the air velocity behind the shields and close to the goaf back end was much higher with the three-entry bleeder system.

Li et al. (2007) and Li (2008) conducted numerical simulations and found that although gas drainage could shorten the spontaneous combustion period and reduce gas contents within the goaf area to a certain degree, it could enlarge the self-ignition area, making spontaneous combustion more serious. Further, Zhu et al. (2011) investigated the influence of three different drainage patterns (e.g., end tunnel, high-level suction tunnel and buried pipe) on the drainage efficiency and spontaneous combustion risk. The simulation results indicated that spontaneous combustion was more likely to occur in the goaf areas where a more effective drainage pattern was employed, thus additional measures, especially nitrogen injection, should be complemented to prevent the oxidation zone from enlarging.

A grid-based modelling method complementarily made up of both CFD modelling and reservoir modelling was developed by Karacan et al. (2008) and was considered a helpful and powerful tool for researchers to systematically improve the fundamental knowledge of ventilation dynamics and gas migration patterns under different geological and mining conditions and to develop fit-for-purpose countermeasures for managing spontaneous combustion and other gas-related problems.

The permeability distribution within the goaf area, as an indispensable parameter of gas flow simulation, was obtained by Yuan and Smith (2008) using FLAC modelling, and the results were validated by onsite caving data, after which the permeability distribution was imported into Fluent to investigate the influence of coal properties on spontaneous heating in the goaf area, mainly including self-heating temperature (SHT), coal particle size, coal surface area and heat of reaction. The results showed that the SHT, coal particle size and surface area had a profound impact on spontaneous heating, while the influence of the heat of reaction was marginal.

Extensive CFD simulations were conducted by Taraba and Michalec (2011) to study the impact

of face advance rate on the development of spontaneous heating. It was confirmed that a favourable zone where spontaneous heating was more likely to occur and develop could be found in the goaf area. With the reduction in the advance rate, the maximum temperature within the favourable zone increased, and this favourable zone moved towards the face.

Ren et al. (2012) conducted CFD modelling to investigate the proactive inertisation strategy for containing spontaneous heating in the LW goaf at Fenghuangshan coal mine where typical U-type ventilation was employed along with a retraining bleeder return road serving for removing contaminated gases out of the mine, as shown in Figure 2.1. The simulation results showed that a better inertisation result could be obtained by injecting nitrogen at an approximate distance of 100 m behind the LW face on the belt roadside or via a surface borehole in a practical location.

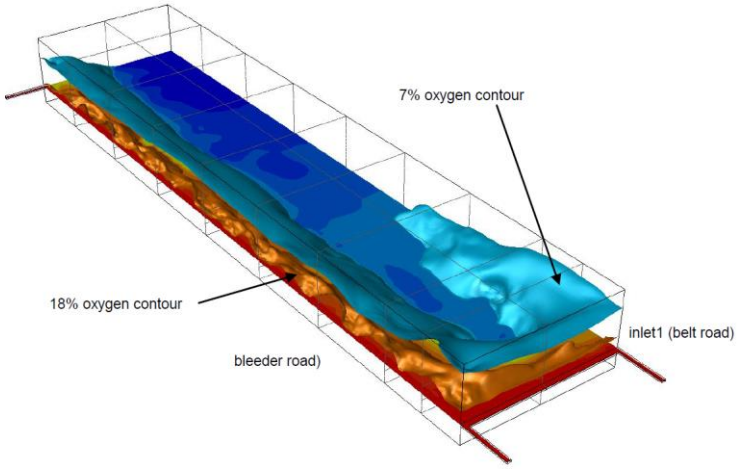

Figure 2.1 Spatial distribution of potential spontaneous combustion area (Ren et al. 2012)

Based on works by Li et al. (2007), Zhu et al. (2011) and Qin et al. (2016b) thoroughly investigated the influence of drainage pressure on controlling symbiotic hazards of spontaneous combustion and gas explosion. Although gas drainage could help prevent gas from accumulating at the upper corner of the LW face and reduce gas levels below the allowable threshold limit value, part of the fresh air could be sucked into the drainage pipes from the LW face through various air leakage pathways, thus increasing the risk of spontaneous combustion. As a result, a reasonable balance between gas drainage and spontaneous heating control should be reached to determine optimal drainage parameters, especially drainage pressure.

In the light of gas drainage and oxygen consumption due to coal oxidation, Shi et al. (2015) carried out CFD simulations to obtain oxygen dynamic ingress into the goaf area, and the results indicated that the residual coal in the upper part of the goaf was more easily subjected to spontaneous combustion than that located at the lower part.

Liu et al. (2016a) performed numerical research on the determination of different inert gases (nitrogen or carbon dioxide) in better controlling spontaneous combustion in the LW goaf. The

modelling results showed that the injection of carbon dioxide performed better than nitrogen, particularly when injection points were located on the MG side of the goaf.

Given the dynamic advance of the LW face, Liu et al. (2017a; 2017b) utilized moving coordinates of the goaf area and investigated the distribution characteristics of oxygen and temperature as well as factors influencing spontaneous combustion. It was found that an increase in the advancing rate and a reduction in both crushed coal and ventilation flux assisted in solving problems associated with spontaneous combustion.

Taking account of the oxygen consumption rate, carbon monoxide generation rate, and heat release rate, Huang et al. (2018) investigated the impact of periodic weighting on the distribution of three zones in the goaf area using Fluent. With the increase in weighting interval, the area of high temperature rose, while the area liable to spontaneous combustion shrank and moved to the deeper goaf.

Particular attention was paid by Wang et al. (2018a) to numerical solutions to hazards associated with spontaneous combustion and gas explosion that may co-exist in the goaf area under the condition of gas drainage. It was concluded that both buried pipes and cross-measure boreholes performed better in reducing methane concentration at the upper corner of the TG panel and in shrinking the area of the oxidation zone as much as possible. As the coupled hazard zone tended to move toward the deeper goaf under the condition of gas drainage, additional nitrogen injection should be performed in the deep goaf rather than the shallow counterpart to yield a better cooling performance.

Chu et al. (2018) constructed a 3D numerical model to study the influence of gas drainage via an upper tunnel on gas control performance and spontaneous combustion management. With an increase in gas drainage rate, gas capture efficiency gradually improved, while the area of coal spontaneous combustion rose. Therefore, a risk assessment method was put forward to optimize the drainage rate in an attempt to reach a balance between gas drainage performance and spontaneous combustion control.

From the perspective of safe mining and saving time and cost, Zhang et al. (2019a; 2019b) thoroughly undertook scenario-based research on injecting inert gas into the goaf area for self-heating control, proactively or reactively, as illustrated in Figure 2.2. It would be better to proactively inject inert gas in the initial phase of coal extraction as a heating event was highly likely to evolve at the starting-off area without taking any preventive measures, whereas a reactive goaf inertisation strategy was recommended when the LW face had already advanced a certain distance at a normal rate at which the incubation period of heating was longer than its window period, and the potential heating would be located in the consolidation zone where oxygen was

insufficient to sustain heating.

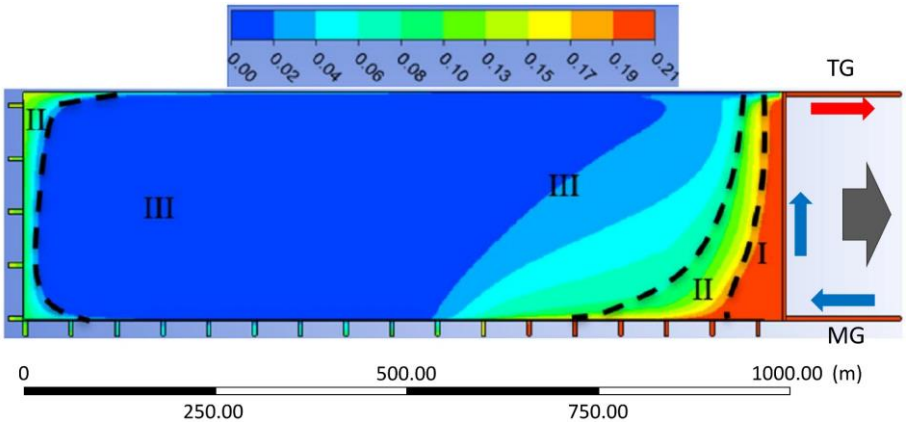

Figure 2.2 Oxygen levels in the active goaf with air leakage (Zhang et al. 2020)

A discrete fracture-pore goaf model was proposed by Zhuo et al. (2019) to numerically study the impact of air leakage pathways connecting surface ground to the mined-out seam with a shallow-buried depth on spontaneous combustion management. In comparison to the distribution of oxygen and gaseous products of spontaneous combustion within the active goaf area and overlying adjacent goaf area, it was found that the upper goaf area could be easily subjected to spontaneous combustion once the wind speed arising from air leakage exceeded the minimum speed required by spontaneous combustion, while the active goaf area faced the problem of higher carbon monoxide concentration than that in overlying goaf due to air leakage from the LW face.

A similar study to Zhuo et al. (2019) was conducted by Zhang et al. (2020), who focused on the influence of various air leakage originating from seals at the MG side of the goaf area, mining-induced cracks, and adjacent goaf area on coal self-heating within the active LW goaf. It was noted that two heating sites existed, with one in close proximity to the starting-off area and the other one immediately behind the LW face. Practical precautions were required to be taken with the heating spot at the starting-off area where coal self-heating could easily evolve and progress into an open fire 25 days later, while there was no need to take action with the other heating site as it would be suffocated by the consolidated caved roof with the continuous advance of working face at a certain rate.

Extensive CFD simulations were conducted by Balusu et al. (2019) to investigate the optimal proactive goaf inertisation strategies for the panel with a length of 1000 m and 3000 m. The seam dip angle and goaf gas emission rate were observed to have a significant influence on oxygen distribution within the goaf area. To effectively reduce the oxygen levels within the goaf with a length of 3000 m, nitrogen injection at a flow rate of 1500 l/s via multiple points could produce better inertisation performance when compared to injection through a single location.

Chen et al. (2020a) examined the effectiveness of negative pressure of cross-cut on the three-zone

distribution in the LW goaf, and the simulation results tallied well with the filed measurement. The modelling results showed that the potential spontaneous combustion zone could be shrunk to a certain degree when the cross-cut was located in the heat dissipation zone or the oxidation zone, while the negative pressure regulation should be stopped as the cross-cut progressed into the suffocating zone.

Combined with laboratory experiments, field measurements, and numerical simulations, Liu et al. (2020b) studied the air leakage patterns and nitrogen inertisation performance with three adjacent goafs, as depicted in Figure 2.3. It was concluded that air leakage from the chain pillars posed a great threat of spontaneous combustion to the adjacent working face and the optimum inertisation strategy was to inject nitrogen through the area located between the heat dissipation zone and the coal oxidation zone.

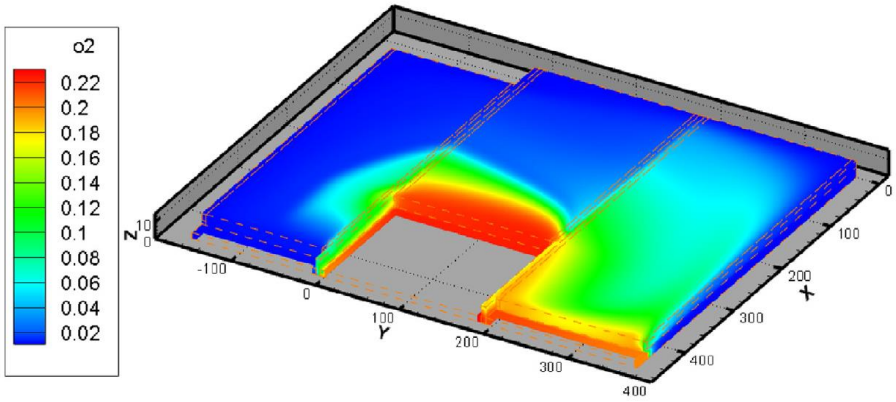

Figure 2.3 Oxygen distribution in triple adjacent goaf areas (Liu et al. 2020b)

Based on the specific geological conditions of the Daxing underground coal mine, a 3D computational model incorporating the actual inclination angle of the working face was built by Gao et al. (2020) to investigate the effect of operational parameters (e.g., air flowrate on the working face, gas drainage capacity and location as well as nitrogen injection location and rate) on the oxidation zone distribution to control spontaneous combustion and excessive gas accumulation within the goaf area. It was concluded that the problem associated with gas accumulation at the upper corner of the working face was hard to solve merely by an increase in the airflow volume, and other measures (e.g., gas drainage and nitrogen injection) should be performed under optimum operating conditions.

A CFD-DEM (Discrete element method) coupling method was employed by Zhang et al. (2021) to obtain fracture-pore evolution characteristics from Particle flow code (PFC), which was then compiled and imported into Fluent to get gas distribution in LW goaf and identify spontaneous combustion area.

Yang et al. (2021) verified the numerical model with onsite experimental data and analyzed the

influence of the supplied air volume on the hazardous zone where both spontaneous combustion and gas explosion may simultaneously occur under the condition of a Y-type ventilation system. A positive correlation was found between air volume and the area of the compound hazardous zone.

Li et al. (2021b) numerically studied the distribution patterns of oxygen and methane in the active goaf using a moving mesh method, and the potential danger zone where both spontaneous combustion and methane accumulation could occur simultaneously was identified. The impact of influencing factors on the location of the potential danger zone was further evaluated, including ventilation flow rate, face advancing rate as well as attenuation coefficient of methane emission.

An attempt was made by Shi et al. (2021) to study the evolution characteristics of temperature and methane during the fire zone sealing and reveal the mechanism of methane explosion induced by the sealing operation. The changes in ventilation flow rate, temperature, methane and oxygen distribution were evaluated during and after the sealing process, which assisted in shedding insight into preventing and controlling gas explosions.

Targeting spontaneous combustion in the mined-out goaf with a shallow buried depth, Zhuo et al. (2021) performed extensive CFD simulations to study the distribution patterns of oxygen and velocity under different conditions of surface air leakage. The hazardous zone in the overlying and underlying goaf was determined by superposing oxygen and velocity.

In combination with laboratory experiments, field monitoring and CFD simulations, Gui et al. (2022) studied the evolution characteristics of oxygen within the goaf area with a U-type ventilation system under different airflow ratios of the machine roadway to the air roadway. Linear regression was used to evaluate the status of spontaneous combustion by estimating oxygen concentration at a specific location along the active goaf.

More recently, Hou et al. (2022) built computational models of three adjacent goafs and validated the modelling results with onsite gas data. The impact of adjacent goafs and chain pillar porosities on the spontaneous combustion zone was evaluated, and countermeasures for reducing both porosities were proposed to prevent and control fire.

In summary, many scholars have investigated the influence of various mining and geological parameters on the development and control of spontaneous combustion, including but not limited to ventilation patterns, gas drainage location and rate, particle size and surface area of coal left in the goaf area, face advance rate, the volume of air supplied to face, air leakage from various potential sources, the weight interval induced by mining, the panel size (length and width), and adjacent goaf areas. However, the impacts of other geological parameters (coal seam orientations

and seam gas composition) and mining factors (e.g., different ventilation patterns of LW panels and the tightness of seals built in the cut-throughs) on ventilation dynamics and gas distribution patterns and the determination of fit-for-purpose proactive goaf inertisation strategies are rarely studied. In addition, almost all modelling results are analyzed qualitatively rather than quantitatively. What is more, there is no research on the ventilation dynamics and goaf gas atmosphere change (methane and oxygen) in the LW panel at different stages of the panel sealing-off process, during which period the LW face is stopped for face recovery and spontaneous combustion and gas explosion are likely to occur and develop due to strong air leakage and heat built up.

2.3 CFD Modelling of Gas Migration in the LW Goaf and Working Face

Abnormal gas emissions from the active goaf, adjacent goaf and methane-bearing strata underlying or overlying the mining seam have potentially posed significant threats to mining safety and regular production. Thus, many scholars have dedicated themselves to investigating the gas flow dynamics both in LW goaf and the working face and evaluating preventative measures or strategies for solving methane-related problems both physically and numerically.

2.3.1 Numerical simulations of methane flow dynamics in the goaf area

Marts et al. (2014a; 2014b; 2015) numerically analyzed the explosive gas zone (EGZ) distribution within the goaf under U-type and back return ventilation patterns, and evaluated the dynamic sealing performance of nitrogen injection at different locations in minimizing the EGZ area, thus reducing the likelihood of gas explosion in the active goaf.

Brune et al. (2016; 2015) and Gilmore et al. (2014; 2015) conducted extensive CFD modelling work on the EGZ distribution in the goaf area under bleeder and progressively sealed ventilation patterns. The analysis of simulation results indicated that EGZ area could be formed in both types of ventilation systems, and a reduction in airflow quantity, proper nitrogen injection, and the implementation of back returns could be helpful in reducing EGZ area to a certain degree. To reduce and even eliminate explosion risk in progressively sealed goaf areas, a dynamic seal strategy was put forward by Brune and Saki (2017) by injecting nitrogen inbye of the face and behind the shields both on the MG and TG side and arranging a back return system to push goaf fringe methane back into the goaf.

Taking the permeability model and gas release conditions into account, Qin et al. (2015) numerically researched how goaf gas drainage affected the gas migration patterns within the goaf area. The analysis of simulation results indicated that a better gas capture performance could be generated, and gas emission onto the working face could be mitigated when gas drainage was operated at the perimeter of the LW goaf with the borehole bottom located in the lower fractured

zone. Later, Qin et al. (2019) studied the relationship between barometric pressure and methane concentration and recommended that the ventilation system should be designed effectively to minimize the pressure differential between intake and return.

Saki et al. (2015) undertook extensive CFD research on the influence of air quantity flowing through the LW face on the reduction in methane concentration at the TG return and EGZ in the gobs progressively sealed. It was interesting that an increase in face quantity could result in an increase in EGZ and methane levels at the TG corner, which was contrary to popular belief. A recent study by Saki et al. (2020) revealed that the operating parameters of gob ventilation boreholes (GVBs) had a profound effect on methane extraction and air ingress, which should be considered thoroughly from the viewpoint of safety and benefits, and designed based on site-specific conditions of mines.

An alternative horizontal directionally gas drainage strategy was proposed by Guo et al. (2015) to control methane-related problems in the goaf area, and extensive CFD simulations and field trial work were undertaken to evaluate the effectiveness of the strategy. It was observed from simulations that an optimal gas drainage performance was achieved by locating directional boreholes at the bottom of the fracture zone where low-pressure sinks could be created amid drainage, and surrounding gas flow dynamics were changed to avoid goaf gas from emitting into the face, in particular at the return airway. The field trial successfully demonstrated that this alternative gas drainage strategy was capable of consistently capturing substantial amounts of methane and minimizing fugitive gas emissions onto the LW face (Qin et al. 2017).

To advance the knowledge of gas flow dynamics and pressure distribution within the goaf area under the condition of gas drainage, Liu et al. (2016b) developed both mathematical and CFD models. The simulation results showed that venthole gas drainage had great advantages of higher drainage efficiency and reducing fugitive gas emissions onto the working face over other traditional drainage methods, which was in good agreement with field measurements.

Tang et al. (2016) numerically analyzed the impact of gas extraction via a high drainage roadway on air leakage within a goaf area, and it was concluded that the gas extraction volume should be no more than the total volume of air leakage and gas emission; Otherwise, a significant air leakage could be observed.

Cheng et al. (2016a) studied the impact of increasing airflow quantity supplied to the LW face and gas drainage pressure on the management and control of abnormal gas levels and spontaneous combustion using CFD modelling. It was revealed that the methane levels at the TG roadway could be reduced by an increase in face airflow quantity or negative drainage pressure employed in the high-level roadway, while increasing airflow rate produced superior performance in lowering

methane levels at the TG roadway and upper corner of face intersection than rising negative drainage pressure.

Lolon et al. (2017) investigated the phenomenon of gob breathing resulting from a sudden barometric change in the active goaf with a bleeder ventilation pattern by means of CFD simulation, and it was observed that as the barometric pressure reduced, the EGZ was enlarged and had a tendency to move from the goaf area towards the active working areas, thus increasing the risk of potential explosion and fire accidents. To combat this problem, a real-time pressure monitoring system was suggested to be well-established in combination with fit-for-purpose gas drainage via GVBs (Lolon et al. 2020).

Li et al. (2018) investigated the influence of different gas drainage strategies on reducing the methane level at the upper corner of the face, including surface well, buried pipe, cross-measure pipe, and their combinations. It was obtained that gas emission rate had a significant influence on the determination of drainage method, and a combination of the three mentioned drainage measures was recommended for coal mines experiencing high gas emission (> 45 m^3/min).

Liu et al. (2019a) numerically simulated the spatial distribution of methane in the LW goaf and optimized the best methane drainage strategy. The simulation results indicated that the bottom of the surface drainage hole should be located at 16 m above the mining seam and the distance between the drainage hole and the return roadway was 45 m, under which condition the best gas extraction effect was reached.

Li et al. (2020b) numerically studied the spatial distribution of oxygen and methane in the active goaf and found that increasing airflow rate could contribute to a drop in hazardous areas where both methane and oxygen concentration lay in the explosive range under certain goaf gas emission rates. Once the gas emission rate exceeded a critical value (50 m^3/min), solely increasing air quantity had a limited impact on shrinking the hazardous zones, and other actions were required to be taken.

Li et al. (2021a) studied methane migration characteristics within the goaf area where spontaneous combustion of coal occurred. The simulation results revealed that although ventilation dilution assisted in mitigating and even eliminating methane accumulation, a rise in temperature induced by spontaneous combustion would lead to methane accumulation as a result of the enhanced chimney effect of upward airflow.

An effort was put by Zhu et al. (2022) to study the evolution characteristics of the goaf gas (e.g., methane, oxygen and carbon monoxide) and temperature in the active goaf, and a novel model was put forward to determine explosion limits of explosive gas and provide guidance on

controlling explosions. The simulation results showed that an increase in airflow rate resulted in an increase in explosion degrees.

2.3.2 Numerical simulations of gas flow patterns on the LW faces

Tanguturi et al. (2014; 2015; 2020) built CFD models consisting of the face area and goaf area to gain a better understanding of goaf gas distribution within the LW goaf under different panel orientations and to evaluate the effectiveness of various measures, such as gas drainage, back returning and curtain configurations on control high methane levels at the TG area. Simulation results indicated that part of the airflow would deviate from the main airstream and push methane back towards the goaf area at the TG fringe with the utilization of the face curtains at the TG walkway or back returning system, thus reducing localized methane levels. In addition, gas drainage at the appropriate location and rate played a part in reducing methane concentration emitted onto the face area, particularly at the goaf fringe.

Previous studies by Mishra et al. (2016; 2018) focused on the methane dispersion and distribution characteristics in the TG area under the different velocities of air flowing through the face, and it was concluded that an airflow velocity of 3 m/s was sufficient to disperse and reduce methane concentration to an allowable level and prevent methane from layering. Although the results from simulations and experiments showed a reasonable agreement, the model was too simplified without consideration of the impact of equipment.

A complicated numerical model embodying LW supports, shearer, AFC, beam stage loader (BSL), crusher and conveyor was built by Wang et al. (2017d; 2017e; 2018e) to thoroughly investigate the methane dispersion and distribution patterns on the LW face. Scenario-based CFD modelling was conducted to study the impact of cutting direction and shearer location on methane distribution on the LW face, and extensive parametric studies were carried out to evaluate the effectiveness of various measures on the mitigation of methane on the LW face, mainly including the quantity of air flowing through the face, seam gas content, adjacent gas-bearing strata, cut-through at the TG side, drum sprays as well as curtains installed on the MG side.

CFD modelling was employed by Ren et al. (2019; 2018a) to gain a better understanding of carbon dioxide behaviour at the goaf fringe and propose countermeasures to reduce high gas levels at the TG corner. A good agreement between simulation results and onsite measurement was reached, and the effectiveness of increasing airflow rate and gas drainage on fringe gas reduction was examined. It was noted that an increase in airflow rate could lower the gas level at the TG fringe to a certain extent, and both the back-return system and gas drainage via the TG borehole could be conducive to reducing the localized gas level.

Taking account of methane emitted from goaf caving and coal cutting on the face, Tutak and

Brodny (2018) mainly investigated the methane distribution at the corner where the face intersected with the return airway and the usage of auxiliary ventilation equipment for methane mitigation. It was proved that auxiliary ventilation equipment with reasonable flow quantity could reduce methane concentration at the TG corner, but the insufficiency of this study was the absence of the actual equipment configuration in the model.

Considering the actual condition where both the LW shearer and AFC moved along the face, Krawczyk (2020) conducted preliminary numerical work using moving and deforming meshes to advance the knowledge of methane propagation on the LW face. It was revealed that both local mesh variability and overset meshes were considered promising tools for solving fluid problems associated with movement, and further study was required to verify and calibrate the numerical model results with experimental data.

In view of the applicability of Darcy's law to the highly porous area, Juganda et al. (2020) set the perimeter of the goaf area as a discrete medium simulated with rock rubbles and set the centre of goaf as a porous medium, thus investigating the airflow dynamics at the headgate and TG corner. It was proved that using the discrete method on the edge of the goaf area was necessary for problems related to flame and explosion propagation.

Song et al. (2021a; 2021b) built a complicated LW model highly identical to the actual geometry and investigated the dust and gas distribution on the LW face. Two hazardous areas where dust and gas concentrations were high were identified at the mining area and TG fringe. Also, it was observed that increasing airflow quantity could reduce dust and gas concentrations to a certain degree, and an optimal airflow rate of 2500 m^3/min was determined by considering that the gas-dust reduction performance was weakened when air quantity exceeded this critical value.

To summarise, the majority of numerical simulations study the ventilation dynamics and gas distribution in the active goaf and on the LW face, while no research focuses on the impacts of various controls and practices on a range of gas events and gas migration characteristics during the LW sealing-off process, during which period spontaneous combustion and gas explosion is highly likely to occur without effective control measures. In addition, the impact of configurations of curtains and brattices on the LW face and in the TG end on methane mitigation at the goaf fringe are under-researched.

2.4 CFD Modelling of Dust and Airflow Patterns in the Heading Development

With the increase in coal demand, there is a growing need for quick heading drivage and high production capacity, which is achieved by significant scientific and technological advancement. The airborne fugitive dust generated during mining operations rises correspondingly, posing great

threats to underground miners who are exposed to a high-concentration dust environment during the long period of a working shift. If not managed and controlled effectively, airborne dust particles, especially respirable coal dust and silica dust, can penetrate deeply into the pulmonary alveoli, resulting in irreversible harm to lung function and physical health. Compared with traditional laboratory experiments which are normally characterized as time-consuming and cost-consuming, CFD has been widely used in solving dust-related problems arising in dust-rich underground spaces (e.g., LW face and heading development) due to its great advantages of dust visualization and easy design and evaluation of dust control measures. The CFD numerical models are established based on the specific conditions of underground spaces and calibrated with onsite dust monitoring data to guarantee the accuracy of models, after which extensive parametric studies can be carried out to improve the knowledge of airflow and dust migration patterns and to evaluate the performance of various dust control techniques available. As the thesis focuses on dust issues existing in the heading development, only the application of CFD modelling for solving dust problems in the heading face is reviewed.

It was not until 1993 that many scholars began applying CFD simulations to investigate the airflow and dust migration patterns in underground coal mines. In order to study the airflow and dust migration characteristics within a heading development driven by a CM, Heerden and Sullivan (1993) carried out CFD modelling, but a major drawback of their study was that the simulation results were not verified. Another study by Srinivasa et al. (1993) emphasized the prediction of airflow patterns using CFD modelling, and it was considered that CFD was a promising tool for solving dust-related problems.

Funded by National Institute for Occupational Safety and Health, Wala et al. (2003) constructed a 3D model identical to the self-designed scaled benchmark model to simulate the airflow patterns. The validation of the simulation results with experimental data boosted the confidence in the application of CFD modelling to predict, evaluate and design appropriate ventilation systems in a short period.

Based on an actual dead-end coal-mine gallery, Parra et al. (2006) established a simple model and conducted CFD simulations with results verified by experiment results, after which extensive simulations were undertaken to investigate the influence of three typical ventilation systems (forcing, exhausting, and mixed ventilation system) on the spatial distribution of velocity and localized mean age of air.

A simplified model only incorporating fan duct and heading development was built by Wang et al. (2006), and the DPM model was used to improve the understanding of dust migration regularities in a heading ventilated by an exhaust duct. It was concluded that the exhaust ventilation system

performed better in dust removal than the forcing counterpart.

Hargreaves and Lowndes (2007) conducted extensive steady-state CFD modelling to study the impact of various operational parameters on the airflow patterns within a development heading, including two different cutting stages of the CM, cutting height, the distance between the blowing duct and heading face, and the working conditions of scrubber fan. The onsite velocity was measured by a multisensor unit and anemometer to map the airflow patterns for validation purposes, and it was proved that simulation results from validated CFD modelling could be beneficial for designing auxiliary ventilation systems and mitigating the amount of dust produced amid the cutting operations of the CM.

A 2D CFD model was built by Aminossadati and Hooman (2008) to probe into the impact of brattice serving the function of deflecting airflow toward the cross-out blind heading on ventilation efficiency. It was reported that the brattice with a higher length was beneficial for removing contaminants from this area.

Taking time factors into account, Toraño et al. (2011) mapped out the dust distribution characteristics within a roadheader-tunnelled mine roadway ventilated by a forcing and exhaust duct, with CFD simulation results verified by both dust concentration and air velocity measured on-site. It was pointed out that calibrated CFD models were capable of predicting dust behaviour and optimizing auxiliary ventilation parameters, mainly including airflow supplied by ducts and the location of the duct, thus enabling improvement in working conditions and coal production.

Niu et al. (2011) employed a simplified heading model to enquire into the impact of various ventilation parameters (e.g., exhaust duct diameter, the distance between the duct and heading face, and the height of the duct) on dust migration characteristics and the optimum ventilation parameters were determined in accordance with the simulation results.

Utilising the CFD-DSMC (Direct Simulation Monte Carlo) coupling method, Hu et al. (2016; 2015) studied the spatiotemporal distribution of dust particles ranging from 0.1 μm to 100 μm within a roadway after blasting, which provided theoretical guidance for designing a dust removal system and evaluating the ventilation efficiency. Later, Hu et al. (2021; 2019; 2020) focused on CFD-DPM simulation of dust dispersion in roadways driven by the roadheader and revealed how different airflow velocities of the forcing duct impacted the dust migration patterns, after which decent roadheader driver location and airflow velocity supplied by forcing fan were determined.

A hybrid brattice system consisting of a physical brattice and flexible curtains was proposed by Kurnia et al. (2015) to direct more airflow toward the heading face and disperse dust particles with concentration dropping below a safe level. Several key parameters influencing system

performances were evaluated, and it was observed that a better dust dispersion result was obtained with full blockage of brattice, U-shaped air curtains, and shorter setback distance.

Unlike many CFD simulation studies in which the Euler-Lagrange model was employed to track dust trajectory, Wang et al. (2015) applied the Euler-Euler model to simulate the dust migration and distribution characteristics in a laneway where ventilation was sourced from a forcing and exhausting duct. After simulation results from the simple geometry model were compared with experimental data, they studied the influence of many parameters on dust movement, such as dust releasing rate, forcing air velocity, and ventilation patterns.

Using the CFD-DEM coupling method, Cheng et al. (2016b) investigated the dust diffusion characteristics within a heading driven by a fully mechanized heading machine at a mesoscopic level and analyzed the relationships between dust particle size and diffusion distance and velocity. It was recommended that the diffusion distance of dust particles of various sizes was required to be considered when specific dust prevention measures were taken.

Li et al. (2016) carried out extensive numerical simulations aimed at studying whether normal ventilation parameters could meet the minimum requirements for providing sufficient oxygen, removing contaminants (dust and carbon monoxide), and maintaining comfortable air temperature in a super-large underground development heading. The existing ventilation system could fulfil the requirements for dust and temperature control, but particular attention should be given to the control of carbon monoxide concentration amid blasting.

In order to advance the knowledge of dust dispersion characteristics in a roadway under the condition of a hybrid ventilation pattern, Geng et al. (2018; 2017) treated the dust particle collision with the hard-sphere model and numerically simulated the distribution of dust with different particle sizes over time. The influence of different ventilation patterns and supplied air velocity from the fan duct on dust movement and sediment were in-depth analyzed, and the mechanism of intense circumfluence of dust was also discussed. Later, Geng et al. (2020) studied the dust migration patterns in a roadway driven by a roadheader under a forcing ventilation system, and the effect of dust particle sizes and the flow rate of the ventilation duct on dust dispersion characteristics were analyzed.

In an investigation into the spatial and temporal characteristics of coal dust produced during the roadway drivage with a roadheader, Liu et al. (2017) conducted a series of parametric studies pertaining to the impact of the variation of supply air velocity on energy save and dust removal efficiency using CFD-DPM method. Among the seven scenarios proposed, better performance in dust mitigation and energy saving could be yielded when intermittent flow where a high velocity of 15.6 m/s lasting for 110 s and a low velocity of 12 m/s lasting for 50 s were applied.

An attempt was made by Shi et al. (2017) to explore the optimum arrangement of the dedusting air duct in a heading face driven by a roadheader. Three significant factors influencing dust control efficiency were examined, including the presence of a dedusting fan, the specific location of the fan (in the middle of the heading or close to the return side), and the distance between the fan absorbing inlet to the heading face. It was reported that the total dedusting efficiency could be as high as 75.88% with the best arrangement of the dedusting fan.

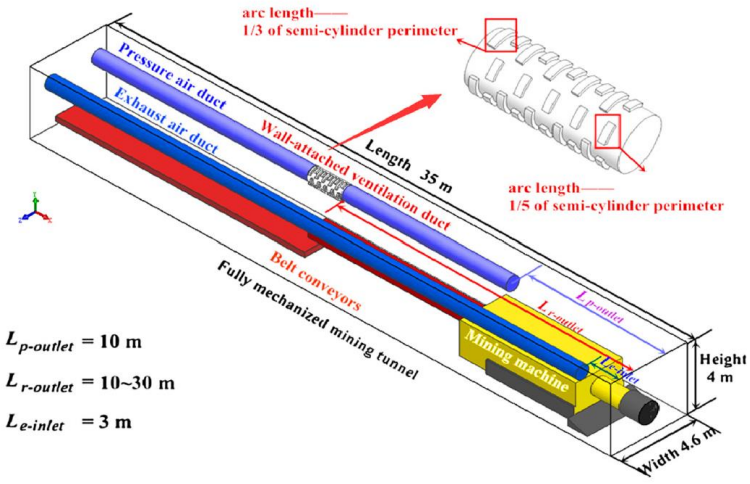

Figure 2.4 CFD model of the heading driven by a roadheader (Wang et al. 2017a)

For the purpose of confining dust within a certain area, considerable effort was made by Wang et al. (2017a; 2018b) to optimize the operating parameters of the air-curtain generator in a roadheader-driven heading face under the hybrid ventilation system, including the radial airflow rate from the generator, the distance between the heading face and air-curtain generator, the axial-to-radial flow ratio of the wall-attached air cylinder, the forced-to-exhaust airflow ratio of the hybrid ventilation system as well as the duct distance from the heading face, as illustrated in Figure 2.4. Later, Wang et al. (2018c; 2021b) modified their CFD models by connecting the exhausting fan duct with a dust-removal fan, and analyzed the effect of ventilation arrangements on dust mitigation performances, such as axial-to-radial flow ratios of air duct, the forced-to-exhaust ratio of the ventilation system, forced-air quantity, as well as the location of the suction duct.

To evaluate the performance of water spray for dust control, Wang et al. (2017b) built a CFD model with a simplified roadheader geometry and thoroughly analyzed the influence of spray pressure on dust suppression results. The airflow was simulated as a continuous phase, while the water spray was simulated as a discrete phase. The simulation results indicated that the optimal spray pressure was 2.4 MPa.

With the aid of the CFD-DEM coupling method, Yu et al. (2017a; 2017b) numerically studied the impact of the air-curtain generator and its operating parameters on dust dispersion characteristics

in a heading driven by a roadheader under a forced-exhaust ventilation system. Then, using the same coupling method, Yu et al. (2018b) investigated the dust diffusion characteristic in a heading excavated by blasting under a single forcing or exhausting ventilation condition. It was obvious that single-exhausting ventilation was superior to the single-forcing counterpart in terms of dust suppression. Later, Yu et al. (2018a; 2020) focused on research on dust suppression in the heading face by means of water spray and optimized the water spray parameters for the best dust mitigation performance under a single forcing or hybrid ventilation system.

In a study investigating the spatiotemporal evolution characteristics of dust particles in the tunnels driven by a heading machine, a full-scale physical model highly identical to the actual dimension was built by Hua et al. (2018a; 2020a). The airflow-dust coupled fields under blowing and hybrid ventilation (far-pressing-near-adsorption) were analyzed, and a conclusion was drawn that hybrid ventilation performed better in dust suppression than blower ventilation. In addition, a multi-radial swirling flow generator was fitted on the compressed air duct at a certain distance from the duct outlet for the purpose of containing the harmful dust, and key parameters were examined, including the distance between the newly fitted flow generator and tunnelling face, the pressurized air volume and inflow-to-outflow ratio (Hua et al. 2020b; Hua et al. 2018b).

A complicated numerical model incorporating a boom-type roadheader was constructed by Cao et al. (2018a; 2018b) to evaluate the dust mitigation efficiency in large-cross tunnels under the combined forcing-and-exhausting ventilation pattern. The influences of many operational conditions (e.g., cutting position, the distance from the exhausting pipe outlet to the tunnelling face, the ratio of forcing to exhaust airflow rate, the location of forcing and exhausting pipe) on dust concentration distribution at different elevations were investigated, and optimal parameters for significant improvements in dust removal were determined.

Liu et al. (2019b; 2018) established a 3D numerical model incorporating major equipment (including a roadheader, pressure duct, exhaust duct, wet dust removal fan, belt conveyor, and multi-radial air-curtain generator), and simulated the airflow migration and dust diffusion characteristics under different influencing factors, such as the distance of air-curtain generator from tunnelling face, the ratio of axial to radial airflow (generator), and the ratio of exhaust to pressurized airflow (the dust removal fan). The recommended parameters were provided to protect the roadheader driver from excessive exposure to dust.

Zhou et al. (2018) built a simple arched heading model and numerically studied the impact of different ventilation parameters on dust concentration distribution under the far-pressing-near-adsorption ventilation arrangement, such as the distance between heading face and pressurized duct outlet or exhaust duct inlet, the volume ratio of pressurized duct to exhaust duct as well as the

location of ducts.

Chang et al. (2019), Gong et al. (2019), Liu et al. (2019c), and Mishra et al. (2019) all carried out CFD modelling of dust distribution and migration patterns within a heading face, but the models they built were too simplified. They either built simplified geometry of the mining machine (CM or roadheader) in the numerical model or constructed a heading panel without the mining machine.

In combination with laboratory experiments, Liu et al. (2019e) numerically investigated the influence of the spray pressure and nozzle orifice diameter on dust control efficiency within a roadheader-driven heading where a hybrid ventilation pattern was employed, and simulation results were verified by field measurements. A similar study was conducted by Guo et al. (2020a), who investigated the influence of spray pressure and nozzle offset degrees on dust mitigation performance within a 12-CM-15-10D CM-driven tunnel under single forcing ventilation.

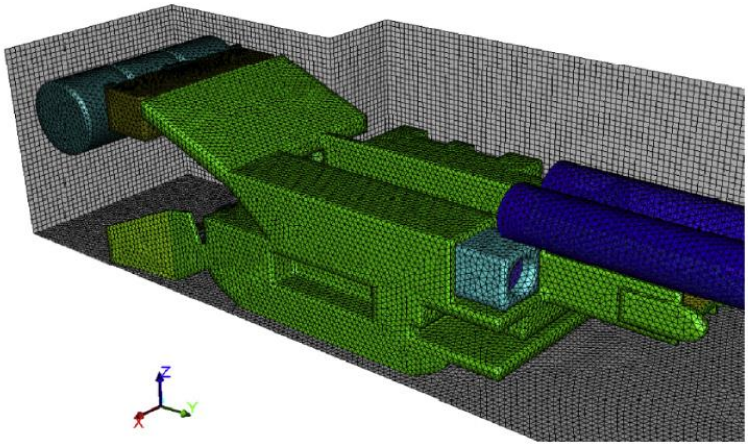

Figure 2.5 Meshed model of heading tunnelled by a continuous miner (JOY12CM27) (Wang et al. 2019)

To improve the understanding of airflow movement and respirable dust migration in a heading driven by a CM (JOY12CM27) under two different cutting scenarios, Wang et al. (2019) performed a series of CFD works and put forward a solution to alleviating high dust concentration confronting the mine site, as shown in Figure 2.5. It was reported that a high dust reduction rate of 90% could be achieved when these proposed measures were taken properly, including the installation of a dust scrubber and venturi spray system, re-arrangement of the cutting sequence and intake ventilation location.

Yin et al. (2020; 2019) numerically evaluated the usage of a multi-radial air curtain generator for dust suppression within a tunnel face excavated by a roadheader under the hybrid ventilation system and examined the impact of locations of the generator and forced air cylinder.

To improve the knowledge of temporospatial characteristics of airflow patterns and dust diffusion in a tunnel driven by a Cantilever-typed tunnelling machine and ventilated by a single compressed air duct, Guo et al. (2020b) undertook extensive CFD simulations and verified base-model results

with onsite dust monitoring data, after which the influence of airflow quantity on diffusion distance of both high and low concentration dust was further evaluated.

Based on site-specific conditions of a heading face excavated by EBZ-160 roadheader, Cai et al. (2021) built complicated models to investigate the dust migration under the far-pressure-near-absorption ventilation scheme, and the optimal airflow rate from the exhaust fan and the location of forcing duct were obtained.

Focusing on dust problems sourced from different locations of a heading face driven by a tunnelling machine, Jiang et al. (2021) performed simulations to better understand the migration patterns of dust from different sources, and the simulation results could shed insight on countermeasures for dust controls.

Lu et al. (2022a; 2022b) built a heading model that incorporated a roadheader, bridge transfer machine, belt conveyor and forcing duct, and investigated the impact of various mining parameters on dust dispersion characteristics, mainly including rotation speed of the cutter head and cutting sequences.

An attempt was made by Xu et al. (2022) to enhance the knowledge of how roadway inclination impacted dust migration within a heading face driven by roadheader and ventilated by a forcing fan, and it was concluded that a reduction in airflow rate in elevation roadway and a rise in the airflow rate in depression roadway assisted in dust control.

Nie et al. (2022a; 2022b; 2022d) studied airflow and dust migration patterns within a roadheader-driven heading under the exhaust-and-forcing ventilation system, and a series of operational parameters were optimized to achieve the best dust mitigation performance.

A novel modularized airflow diverging system was proposed by Yang et al. (2022a; 2022b), and extensive CFD simulations were conducted to study the airflow, dust and gas migration characteristics in a heading face excavated by a roadheader. The working parameters of the ventilation system were optimized to control both dust and gas issues in the heading.

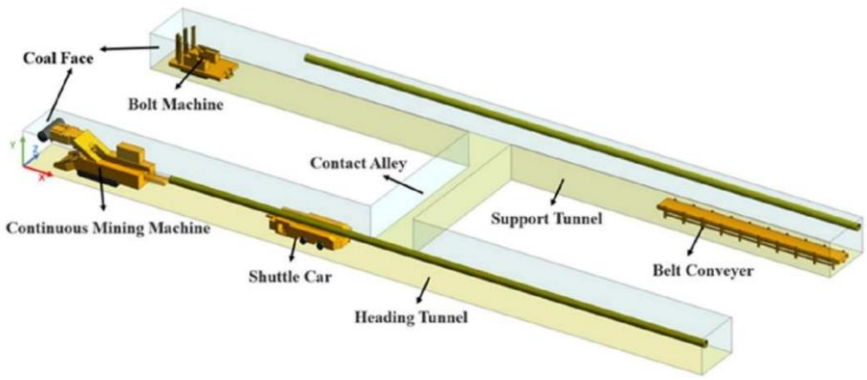

Figure 2.6 CFD model of two connected tunnels (Zhou et al. 2022)

Zhou et al. (2022) studied the spatiotemporal distribution of dust in two connected tunnels with a forcing ventilation system, and dust levels at the different driver locations (e.g., CM, SC and bolt machine) were evaluated, with the CFD model illustrated in Figure 2.6.

From the above literature review, it is noted that the machine for heading or tunnel drivage is either roadheader or tunnelling machine, and the ventilation patterns employed are either single forcing ventilation or hybrid ventilation in the vast majority of studies, while limited research investigates the dust migration patterns in the CM-driven heading with single exhaust ventilation, which is much more common in the mining industry in Australia. In addition, the impact of various cutting operations on dust migration patterns in the development panel has received limited studies, such as the coal cutting and dumping process, different cutting positions of the drums and the distance of the exhausting duct from the heading face. What is more, there are limited studies with regard to the dispersion regularity of respirable coal and silica dust (particle sizes below 10 μm), which is more harmful to miners' bodies due to the fact that it is hard to exhale these kinds of dust out of mouth and dust can penetrate deeply into lung and cause irreversible harm.

2.5 Summary

A comprehensive review of the spontaneous combustion and heating in the goaf areas, ventilation dynamics and gas distribution characteristics in the active goaf and the LW face, as well as dust dispersion and diffusion characteristics in the heading development, has been undertaken in this chapter, with a particular emphasis on the utilization of CFD modelling to prevent, manage and control those PMHs arising during the coal extraction process.

Reviews on CFD modelling of spontaneous combustion in the active goaf show that the impacts of fundamental geological parameters (coal seam orientations and seam gas composition) and mining factors (e.g., different ventilation patterns of LW panels and the tightness of seals built in the cut-throughs) on ventilation dynamics and gas distribution patterns and the determination of fit-for-purpose proactive goaf inertisation strategies have received limited attention. In addition, an improved post-processing method is required to analyze the CFD simulation results both qualitatively and quantitatively to enhance confidence in comparing different scenarios and optimizing goaf inertisation strategies. What is more, there is limited research on the ventilation dynamics and goaf gas atmosphere change (methane and oxygen) in the LW panel at different stages of the panel sealing-off process, during which period the LW face is stopped for face recovery and spontaneous combustion is likely to occur and develop due to strong air leakage and heat built up.

In addition, CFD modelling studies of ventilation dynamics and gas distribution characteristics in the active goaf and LW face have been reviewed. There is an immediate need to evaluate various

ventilation and gas management practices that can be implemented to effectively manage and control high gas emissions, particularly at the localized TG ends of the LW face. In addition, gas migration characteristics during the LW sealing-off process require further investigation to prevent gas explosions and spontaneous combustion.

Furthermore, reviews on solving the dust-related problems in the heading development by means of CFD modelling indicate that limited research studies dust migration and dispersion patterns in the heading face driven by a CM, particularly under a single exhaust ventilation system, which is much more common in the mining industry in Australia. In addition, the impact of various cutting operations and handling processes on dust dispersion characteristics in the development panel has received limited attention, such as the process of coal cutting, conveying and dumping, different drum cutting positions and the distance of the exhausting duct from the heading face. What is more, there are limited studies with regard to the dispersion regularity of respirable coal dust (particle sizes below 10 μm), which are more harmful to miners' health.

To conclude, this comprehensive literature review illustrates the insufficiencies in research on spontaneous combustion in the active LW goaf, elevated gas levels at the TG end and dust diffusion and migration in the heading development. With the aid of CFD modelling, the management and control measures of these PMHs can be identified and evaluated, which will shed new insight on improving current control practices and mining safety.

CHAPTER 3 NEW INSIGHT INTO PROACTIVE GOAF INERTISATION FOR SPONTANEOUS COMBUSTION MANAGEMENT AND CONTROL

Summary

This chapter provides new insight into proactive goaf inertisation for spontaneous combustion management and control. The spontaneous heating management system typically employed in Australian underground coal mines is introduced, including early detection and prediction of spontaneous combustion, detection and monitoring of spontaneous combustion, principal hazard management plans, as well as proactive spontaneous combustion control technology. The method to numerically determine the parameters for proactive control measures is presented. Based on the site-specific conditions of an underground coal mine in NSW, a 3D CFD model was constructed and validated with on-site gas monitoring data, which allowed for goaf gas flow dynamics and flow patterns to be determined and analyzed. Goaf inertisation strategies were qualitatively and quantitatively investigated from three aspects, including inert gas injection locations, injection rates, and inert gas type. The study provides guidance to underground coal mines for the control and prevention of spontaneous combustion and heating of coal in the goaf areas during the normal mining process and to improve the health and safety of miners.

Citation

M Qiao, T Ren, J Roberts, X Yang, Z Li, & J Wu. New insight into proactive goaf inertisation for spontaneous combustion management and control. **Process Safety and Environmental Protection**, 2022, 161, 739-757.

https://doi.org/10.1016/j.psep.2022.03.074

Abstract

Spontaneous heating in the active goaf area during normal mining processes poses increased threats to mine productivity and safety, as evidenced in events induced by the spontaneous combustion of coal. To control and mitigate this engineering problem, there is a need to gain critical knowledge of spontaneous combustion in the longwall (LW) goaf area, which can be achieved through a combination of field tests and numerical modelling. This paper introduces the spontaneous combustion management system widely used in Australia and presents Computational Fluid Dynamics (CFD) models for the simulation of gas flow dynamics in the goaf area, based on the site conditions of an underground coal mine where coal seam gas is predominantly comprised of carbon dioxide. The models were validated with gas monitoring data and used to conduct parametric studies for proactive goaf inertisation optimization. Qualitative and quantitative analysis of simulation results indicated that better goaf inertisation could be achieved when nitrogen was injected via cut-through at 250 m on the maingate (MG) side and surface boreholes at 100 m and 700 m on the tailgate (TG) side, with a total injection rate greater than 1750 l/s. The oxygen concentration on the MG and TG side dropped below 5% at distances of 120 m and 75 m behind the LW face, with an oxidation zone area of 35375 m^2, which was approximately one-third of the oxidation zone area of the scenario without inert gas injection. Simulation results help shed light on improving current goaf inertisation practices to effectively reduce the risk of heating in goaf areas and improve mining process safety based on Australian conditions and practices.

Keywords

Spontaneous heating; Principal hazard management plan; Computational modelling; Proactive goaf inertisation; Inertisation parameter optimization; Mining process safety.

3.1 Introduction

Despite the significant advances in mining technology and safety management, coal mining worldwide is still facing severe challenges of effectively preventing and controlling hazards induced in the process of normal mining, and Australia is no exception. As hard-to-eradicate longstanding thermal dynamic events, spontaneous combustion and heating have been a significant hazard plagued by many underground coal mines, especially those in Queensland and New South Wales where most coal resources are located. If not managed and controlled effectively, heating-related events could result in the loss of coal resources, environmental pollution from toxic and suffocating gas emissions (e.g., carbon monoxide, carbon dioxide, methane), and production delay and stoppage (Bai et al. 2020; Deng et al. 2016; Liu & Qin 2017b; Xia et al. 2016; Zhang et al. 2020; Zhuo et al. 2019). When a mixture of air with methane concentration lying in the explosive

range (5%~15%) presents in the vicinity of the heating location, a gas explosion is likely to be initiated by the energy generated by combustion and heating, culminating in disastrous consequences, such as coal miner injury and death, mine closure, and significant economic losses (Brune et al. 2016; Li et al. 2021b; Lolon et al. 2020; Ren & Balusu 2010; Tutak et al. 2020; Yang et al. 2021). Massive explosions occurring in Box Flat Colliery on 31 July 1972 and Kianga No.1 coal mine on 20 September 1975, claimed the lives of 17 and 13 coal miners, respectively, and the following inquiry launched by the official government revealed that both explosions were triggered by sufficient heating sourced from spontaneous combustion (Loane et al. 1975; Queensland Government 1972). A thorough review of incidents related to spontaneous combustion was conducted by Ham (2005) amid a 32-year period from 1972 to 2004, and it was reported that 51 hazardous events involving spontaneous combustion happened in Queensland, causing coal mines to close either temporarily or permanently. Cliff (2015) predicted that at least one incident associated with spontaneous combustion could occur on average each year, causing coal miners to be withdrawn and evacuated from the mine and even mine closure in some cases.

With significant advances in computer technology, Computational Fluid Dynamics (CFD) modelling has been increasingly used in solving problems arising in the process of coal mining, and spontaneous heating related problems are no exception. In combination with CFD modelling and field studies in two underground coal mines in Australia, Balusu et al. (2005b) proved that proactive inertisation could successfully reduce oxygen ingress into the goaf area and develop an inert goaf atmosphere, thus effectively containing the spontaneous combustion and heating in the goaf areas while the longwall (LW) face was retreated slowly or even stopped. It was indicated from simulation results that effective goaf inertisation could be achieved when inert gas was injected into the goaf area at 200 to 400 m behind the LW face with an injection flow rate of approximately 0.5 m^3/s (Ren & Balusu 2009). Yuan and Smith (2008) conducted CFD simulations to study the evolution of temperature and oxygen concentration in two adjacent goaf areas and revealed the impact of coal surface area and heat of reaction on spontaneous heating. Taraba and Michalec (2011) built 3D models of LW with a U-type ventilation system to investigate the impact of face advancing rate on spontaneous combustion, and a critical advancing rate was determined to reduce the likelihood of spontaneous heating. Xia et al. (2015) numerically studied the self-heating process of coal in an underground coal seam that is rich in methane, and parametric studies were conducted on the impact of coal properties on self-heating. After validating the base model with filed measured data, Liu et al. (2016a) numerically researched the efficiency of carbon dioxide or nitrogen on spontaneous combustion control, and ideal injection was determined. Targeting at problems of co-occurrence of spontaneous combustion and methane explosion in the goaf areas, many scholars carried out extensive numerical simulations and investigated the

influence of different parameters on controlling these co-existing hazards (Li et al. 2021b; Qin et al. 2016a; Wang et al. 2018a; Xia et al. 2017; Yang et al. 2021). Huang et al. (2018) focused on probing into the effect of periodic weighting on "three-zone" and temperature distribution in the goaf area, which was helpful in the management and control of spontaneous combustion. Considering the high risk of spontaneous combustion during mining stoppage, Liu et al. (2019d) optimized the mining parameters to mitigate this dynamic problem. Numerical simulations were conducted by Shi et al. (2019) and Liu et al. (2020b) to study the impact of nitrogen injection on spontaneous combustion control in the goaf area. With the aid of orthogonal tests and numerical simulations, Si et al. (2019) optimized the carbon dioxide injection parameters, and the results indicated that multisource injection of carbon dioxide could suppress spontaneous combustion in the goaf area. Numerical simulations were performed by Zhang et al. (2020) to improve the knowledge of oxygen and temperature distribution in the goaf area with obvious air leakage induced by mining activities, and goaf inertisation by means of nitrogen injection was optimized. Zhou et al. (2021) numerically investigated oxygen distribution in the goaf area and proposed integrated fire prevention measures, including injecting nitrogen and inhibitor and plugging leakage. Based on specific conditions of a fully mechanized top coal caving face, Qi et al. (2021) divided the goaf area into three different zones and numerically optimized the nitrogen injection locations for spontaneous combustion control.

In addition, various goaf inertisation techniques have been developed to prevent and control heating, including goaf inertisation with three-phase foam (Zhou et al. 2006), two-phase nitrogen foam (Ray & Singh 2007), fly-ash foam (Qin et al. 2014), inorganic solidified foam (Lu et al. 2020b), gel-stabilized foam (Shi et al. 2022), injection of methane sourced from inseam gas drainage (Claassen 2011), inertisation with water and ash mixture and carbon dioxide (Szurgacz et al. 2020), fire extinguishing gel (Li et al. 2019). Compared with these goaf inerting techniques, proactive goaf inertisation with inert gas (e.g., nitrogen, carbon dioxide, or boiler gas) injected into the goaf area during normal mining cycles has the advantages of easy transport, deployment and management, which has been widely applied in Australia to suppress the onset of spontaneous combustion and heating (Salisbury et al. 2022; Terry Martin SC & Clough 2021).

In the light of frequent spontaneous combustion and heating events in the active goaf area during the normal mining process, a robust and integrated system has been established in Australia, which includes early prediction and detection of spontaneous heating, onsite gas sampling and monitoring, principal hazard management plan, and proactive control measures. However, many Australian underground coal mines, working seams prone to spontaneous combustion, face severe challenges of obvious oxygen ingress into the goaf area as a result of fast advance rates, high

ventilation rates and increased production outputs. This results in less time for compaction of the caved roof, and more air leakage pathways can therefore exist in the goaf area, resulting in more air penetrating into the goaf area. High ventilation rates can cause a significant pressure difference between the maingate (MG) side and the goaf area, and more fresh air is likely to flow into the goaf area, thus increasing the likelihood of spontaneous combustion. In comparison to high ventilation rates and serious air leakage, the current goaf inertisation practices with low inert gas injection rates cannot fully meet the requirement of suppressing the onset of spontaneous combustion and heating. Therefore, there is a need to investigate the optimum goaf inertisation strategies for spontaneous combustion management and control, including injection location, type of inert gas and injection rate.

Based on the specific site conditions of an underground coal mine in NSW, this paper introduces the spontaneous heating management system typically employed in Australian underground coal mines and presents how to numerically determine the parameters for proactive control measures. The numerical simulations are validated based on on-site gas monitoring data allowing for goaf gas flow dynamics and flow patterns to be determined and analyzed. The verified CFD model can then be used to qualitatively and quantitatively investigate goaf inertisation strategies. The study will provide guidance to underground coal mines for the control and prevention of spontaneous combustion and heating of coal in the goaf areas during the normal mining process and improve the health and safety of miners.

3.2 Early Detection and Prediction of Spontaneous Combustion

An early indication of the onset of spontaneous combustion and heating prior to mining operation can provide valuable time for effective action to be immediately taken to prevent the heating from spreading and escalating into an open fire. This relatively small window of opportunity to detect a heating event often relies on the propensity of mined coals to spontaneous combustion and the timely detection and interpretation of gaseous products released from this heating process. In Australia, the R_{70} index is widely used to evaluate the spontaneous combustion propensity, while a combination of various single indicator gases and gas ratios is applied for the early detection of spontaneous heating.

3.2.1 R_{70} index

The adiabatic self-heating method was first used by Davis and Byrne (1924) and further developed into the adiabatic R_{70} test in Australia and NewZealand with a view to evaluating the susceptibility of coal to spontaneous combustion (Beamish et al. 2001; Beamish et al. 2000; Ren et al. 1999). The 150 g coal samples with particles size smaller than 212 μm are placed in an adiabatic oven where the temperature rises from 40 ℃ to 70 ℃ as a result of coal self-heating, and the temperature

change as the function of time is referred to as the R_{70} value, in the unit of °C/h (Beamish 2005; Beamish & Arisoy 2008; Beamish & Blazak 2005). Typically, the higher the R_{70} index value, the higher the coal propensity for spontaneous combustion and self-heating (Arısoy 2010; Wang et al. 2018d).

Depending on the different geological conditions and coal properties, the spontaneous combustion propensity is classified differently by NSW and Queensland based on the R_{70} index (NSW Department of Industry and Investment 2011b), as listed in Table 3.1.

Table 3.1 Coal spontaneous combustion propensity classification

Classification	Propensity level	Queensland	NSW
1	Low	$R_{70}<0.5$	$R_{70}<1.0$
2	Low-to-medium	$0.5\leq R_{70}<1.0$	$1.0\leq R_{70}<2.0$
3	Medium	$1.0\leq R_{70}<2.0$	$2.0\leq R_{70}<4.0$
4	High	$2.0\leq R_{70}<4.0$	$4.0\leq R_{70}<8.0$
5	Very-high	$4.0\leq R_{70}<8.0$	$8.0\leq R_{70}<16.0$
6	Ultra-high	$8.0\leq R_{70}<16.0$	$16.0\leq R_{70}<32.0$
7	Extremely-high	$R_{70}>16.0$	$R_{70}>32.0$

The R_{70} test is carried out on a dry basis and eliminates inherent moisture and the associated delay in thermal runaway due to evaporating water, which does not indicate the moderating impact of moisture within the coal on self-heating behaviour at low temperatures. To address this problem, the incubation test method was developed by Beamish and Beamish (2010), and it has been routinely employed in the coal mining industry in Australia (Beamish et al. 2018; Beamish & Theiler 2019). The significant modifications to the normal R_{70} test include testing the coal samples with their as-received moisture content, starting the test at ambient mine temperature, using coal samples with an approximate weight of 200 g, and applying a low oxygen flow rate (Beamish & Beamish 2011).

3.2.2 Interpretation of indicator gases and gas ratios

3.2.2.1 Interpretation of indicator gases

Combustion is likely to occur and sustain in the goaf area when sufficient oxygen (O_2), fuels (residual coal left in the goaf), and heat in support of the reaction are present. It has also been shown that spontaneous combustion and heating could occur even at low ambient temperature (Zhang et al. 2016; Zhang et al. 2013; Zhou et al. 2017). During the process of coal oxidation, particular gases will be progressively produced at certain temperatures, including but not limited to carbon monoxide (CO), carbon dioxide (CO_2), hydrogen (H_2), methane (CH_4), acetylene (C_2H_2),

ethylene (C_2H_4), ethane (C_2H_6), and other higher hydrocarbons, with concentrations varying significantly due to the differences in intrinsic properties of coal. Gas evolution tests have been widely used to investigate the gas production trends with increasing temperature and provide a reference for formulating Trigger Action Response Plans (TARP) specific to the coal mine. Although the gas evolution occurring with increasing temperature varies from coal to coal, the characteristics of gas appearing at the specific temperature can be utilized to predict the onset of spontaneous combustion and determine the different oxidation stages, thus guiding the early detection and prevention of spontaneous heating during its incubation period. As a result, many gases released in coal oxidation with rising temperature are selected as indicator gases of spontaneous combustion and self-heating.

Among all gases potentially produced as a result of spontaneous combustion, CO is the most common indicator of coal heating. CO could generally appear at a low temperature of 20～30 ℃ and was detectable throughout the whole period of combustion (Liu et al. 2020a). The production of CO emitted rose rapidly when the temperature exceeded 110 ℃ (Ma et al. 2020b). Although CO has been considered a reliable indicator of spontaneous heating, concerns must be given with the other likely sources of CO from underground vehicles powered by diesel and the appearance of CO at ambient temperature, and it is a kind of toxic gas (Tutak & Brodny 2017b). Therefore, different stages of spontaneous combustion should be judged by the increasing trend of CO levels continuously monitored rather than the absolute CO concentration of a single reading.

Another typical gas produced during low-temperature coal oxidation is CO_2. Currently, there is limited use of CO_2 as a good indicator of early prediction of spontaneous combustion because CO_2 can emanate from various sources besides combustion and heating. Firstly, CO_2 can originate from the virgin coal seam, and the CO_2 is likely to emit when the original adsorption-desorption equilibrium is broken as a result of mining activities and flow to the working face via fissures and fractures existing in the goaf areas and coal pillars. Secondly, it can be produced by long-term microbial oxidation or acid mine water containing calcium carbonate (Timko & Derick 2006).

H_2, as a characteristic gas liberated during coal combustion and heating, has gained tremendous popularity in Australia to forecast whether a heating event has already progressively developed into an escalated stage (Cliff et al. 2014). In the course of low-temperature coal oxidation, a minute trace of H_2 can be released, and its quantity increases when the temperature exceeds 100 ℃ (Wang et al. 2017c). Two significant concerns with H_2 as an indicator gas are that H_2 is likely to be produced when galvanized steels contained in the sampling pipes react with acid water (Liu et al. 2021), and it is not easy to discriminate between helium and H_2 in the gas analysis using gas chromatography as they have similar retention times. As a result, it is much better to use sampling

tubes of non-reactive materials rather than galvanized steel.

C_2H_4 is a significant characteristic gas used by many countries, such as China and Australia. Studies conducted by Chen et al. (2020b), Levi et al. (2015), and Liu et al. (2021) revealed that C_2H_4 first appeared when the temperature reached 110 ℃, 140 ℃, and 190 ℃, respectively. The lower the temperature required for the coals to produce C_2H_4, the more prone to spontaneous combustion (Cai et al. 2019). C_2H_4 can be regarded as a good indicator of advanced heating and is widely used as the upper trigger level for the TARPs.

In practice, there are many problems associated with the use of characteristic gases to predict the onset of spontaneous heating and assess the heating stages, as summarised by Cliff (2015):

- The absolute gas concentration may be diluted by ventilation to a lower level and even beyond the detection limit when gas intermingles with the incoming air, resulting in underestimating the severity of heating;
- Gases selected as indicator gas could originate from other sources besides spontaneous combustion and heating, such as coal seam and diesel-powered vehicles.
- It is difficult to distinguish between small-scale and large-scale heating, as they may demonstrate almost the same gas concentration.

3.2.2.2 Interpretation of gas ratios

To compensate for the drawbacks of sole use of characteristic gas concentration for spontaneous heating prediction, a variety of gas ratios have been considered, including CO make, Graham's ratio, CO/CO_2 ratio, Tricket''s Ratio, Young's Ratio, H_2/CO ratio, and air-free analysis (NSW Department of Industry and Investment 2011b). Among these gas ratios, CO make, Graham's ratio and CO/CO_2 ratio are the most useful indicators for TARPs.

(1) CO make

It is defined as the volume of CO that flows past a specific monitoring point per unit of time, in the unit of litre/minute.

$$CO\ make = 0.06 \times CO \times airflow\ volume \qquad (3-1)$$

Where: the unit of CO and airflow volume are ppm and m^3/s, respectively.

CO make is always used in panel return gateroads and back bleeder roads in Australia to indicate the CO conditions, eliminating the influence of ventilation dilution by air leakage. CO make trigger values should be set based on site-specific mine conditions.

(2) Graham's ratio

It is defined as the ratio of CO in the air to oxygen deficiency (Graham 1920), which is widely

used to evaluate the intensity of coal oxidation. The ratio is calculated using the following equations:

$$\mathrm{O_2\ deficiency} = \frac{20.93}{79.04} \times \mathrm{N_2} - \mathrm{O_2} \qquad (3-2)$$

$$\mathrm{Graham's\ ratio} = \frac{\mathrm{CO\ in\ the\ air}}{\mathrm{O_2\ deficiency}} \times 100\% = \frac{CO_{out} - CO_{in}}{O_{2_{out}} - O_{2_{in}}} \times 100\% \qquad (3-3)$$

Where: CO is the carbon monoxide concentration, %; O_2 is the oxygen concentration, %; the unit of CO in the air is %; the subscript "in" represents the intake condition, while the subscript "out" represents the return condition.

Considering the circumstances where O_2 probably alters due to dilution with other gases or the return airflow is likely to contain more than one airstream, Graham's ratio was modified based on the assumption that N_2 remained unchanged throughout the whole process. The modified Graham's ratio can be obtained by the following equation:

$$Graham's\ ratio = \frac{CO_{out} - CO_{in} \times \frac{N_{2\ out}}{N_{2\ in}}}{\frac{N_{2\ out}}{N_{2\ in}} \times O_{2\ in} - O_{2\ out}} \times 100\% \qquad (3-4)$$

Where: N_2 is the nitrogen concentration, %.

In underground areas where gas sensors or monitors are placed, a change in CO concentration could be caused by ventilation fluctuation, such as goaf breathing attributed to a change in barometric pressure. However, the revised Graham's ratio is almost independent of ventilation dilution and has become one of the significant indexes commonly used in both sealed areas and well-ventilated roadways to be indicative of early heating. A rise in Graham's ratio typically shows an accelerated coal oxidation process. It can give a warning of abnormal conditions and provide a small window of opportunity to take countermeasures several weeks before any distinct odour could be detected and a fire event occurs.

There are some non-negligible drawbacks in the use of Graham's ratio to interpret the atmospheric conditions, listed as follows (Cliff 2015):

(a) Its accuracy is not reliable in circumstances where less oxygen is consumed and oxygen deficiency is lower than 0.35, which is a shared disadvantage for other gas ratios involving oxygen deficiency;

(b) It could be potentially influenced by other sources of CO besides heating, such as underground equipment fueled by diesel and the supplied air containing a blackdamp.

(c) It will become invalid when nitrogen is used for LW goaf inertisation, as it is assumed that nitrogen should be kept constant to reflect the original oxygen condition.

(3) CO/CO_2 ratio

The oxide of carbon ratio is only correlated with CO and CO_2, so it has the advantage of being free from the impact of oxygen deficiency compared to the many other ratios that are obtained by that deficiency (Şensöğüt 2011). The CO/CO_2 ratio can be calculated by the following equation:

$$Oxide\ of\ carbon\ ratio = \frac{CO_{out} - CO_{in}}{CO_{2\ out} - CO_{2\ in}} \qquad (3-5)$$

Each mine should set trigger levels for CO/CO_2 ratio based on site-specific conditions. The advantage of the oxide ratio of carbon over Graham's ratio is that it is free from the influence caused by excess nitrogen. However, the oxide ratio of carbon could become inaccurate if CO or CO_2 emanates from other sources, such as coal seam and diesel equipment.

3.3 Detection and Monitoring of Spontaneous Combustion

An understanding of potential heating locations plays a vital role in heating prevention and control during the mining process. In general, with the continuous advance of the LW face, the area of the unsupported roof suspended above the mined-out seam increases correspondingly and then collapses in a large area. The caved roof in the centre of the goaf area will be consolidated by the overburden strata, which is characterized by low permeability and an oxygen-lean environment. Thus, heating or fire is unlikely to occur in this area on account of insufficient oxygen to sustain the self-oxidation of coal. On the contrary, many air leakage pathways exist at the periphery of the goaf area where the roof incompletely collapses and ribs spall, which could provide channels for oxygen to penetrate into the goaf area. Due to the ventilation pressure difference between the inbye and outbye of the active goaf, more oxygen can leak into the goaf area via various pathways and react with residual coal. When the heat produced by coal oxidation overtakes the heat removed by the air, a heating event is highly likely to occur. As a result, monitoring points should be arranged at the perimeter of the active goaf and sealed areas to monitor the change of airflow rate, temperature, and typical gas concentration. Gas samples should be taken periodically at adjacent sealed goaf areas and analyzed in detail using the Gas Chromatograph (GC) in an attempt to identify the likelihood of a potential heating event based on the deviation of sampled gas from the normal gas background. In addition, continuous monitoring and routine sampling are required at the intake of a district, in the panel return outbye of the starting-up line, the main return, across the LW face, inbye of development heading, and other suspected locations, as illustrated in Figure 3.1. Depending on the site-specific conditions of an underground coal mine, sampling locations and

frequency should be determined and changed as required.

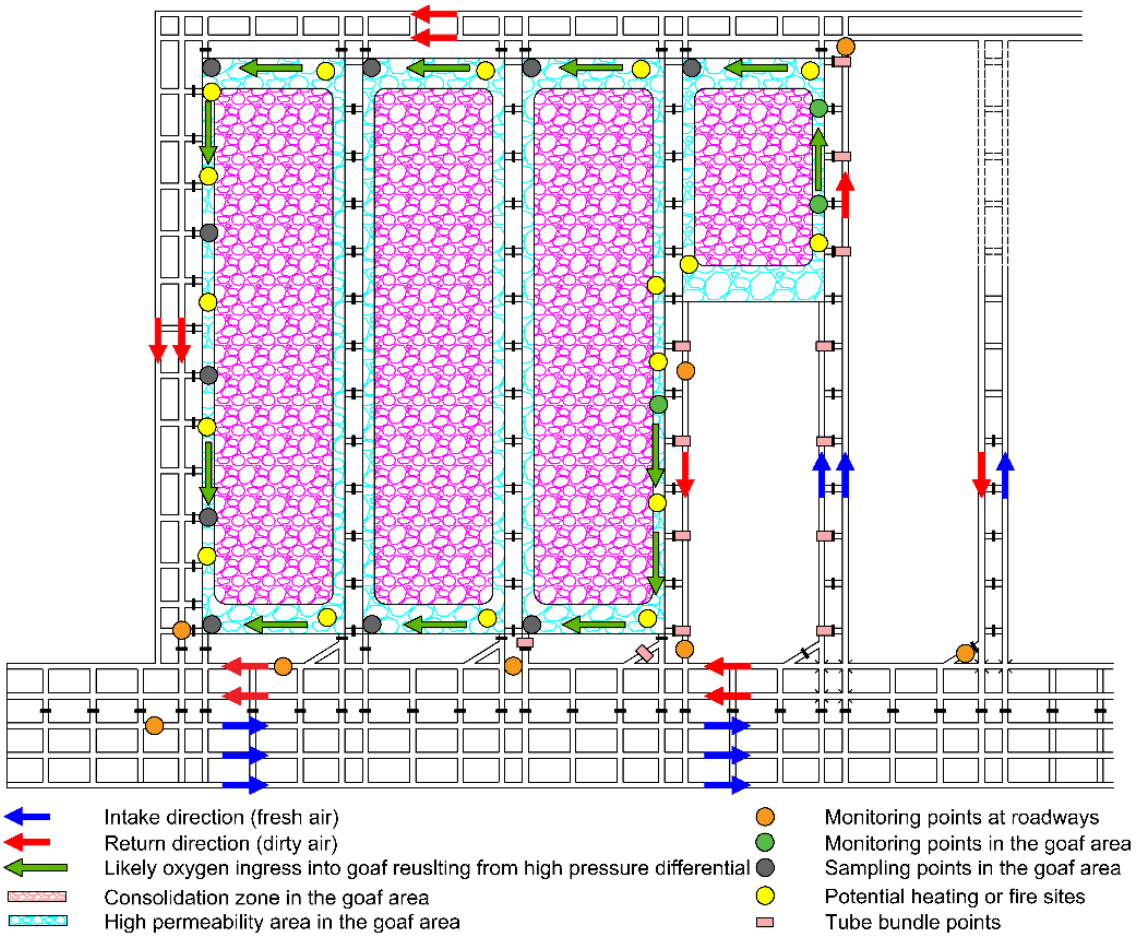

Figure 3.1. Gas sampling and monitoring locations in a typical Australian underground mine

As an integral part of gas management, gas monitoring plays an indispensable role in potential heating indications. An integrated gas monitoring system has been widely applied in Australia, including real-time sensors, the tube bundle system, personal portable sensors, and periodic bag samples, to assist in establishing the normal gas background and immediate alert of any variations from the normal value, which could be conducive to early prediction and prevention of spontaneous heating.

There are different types of real-time sensors capable of continuously monitoring different gases. Dependent on specific requirements, some real-time sensors are able to detect four typical gases: CO, CO_2, O_2 and CH_4, while other sensors serve the detection of a single particular gas, such as CO or CH_4. In several coal mines, real-time sensors can detect CO and CH_4 simultaneously. Although real-time telemetric sensors enable different typical gas at strategic locations to be monitored in a real-time and continued manner, it still suffers some disadvantages, such as limited gas detection range and service life, cumbersome sensor maintenance and adjustment, and unsuitable for oxygen-lean environment.

The tube bundle (TB) system can continuously draw samples from multiple underground locations

of interest to the surface through plastic tubes and analyze them sequentially in a dedicated surface TB hub. Typical gases that the system is capable of analyzing are CO, CO_2, O_2 and CH_4. Gas samples from the underground TB locations can be collected in the surface TB hub using special gas bags for further analysis of characteristic gases with the GC. TB system has great advantages of long-term trending of characteristic gases, wide gas detection range, easy-to-maintain with long service life, being able to work in sealed areas and may still function after an explosion. However, it still faces several drawbacks, such as the time delay mainly depending on the distance from underground TB locations to the surface TB hub, regular TB inspection and maintenance to avoid tube blockage or leakage, and cycling of result analysis between each TB location.

In Australian underground coal mines, both the real-time telemetric system and the TB system are ordinarily incorporated into a software system named "Safegas" (Terry Martin SC & Clough 2021), which can display the gas concentration and ratios at specific monitoring locations and issue warnings if the trigger gas levels are reached. The monitoring data and warnings are also synchronized in the central control room far away from the TB hub so that abnormal conditions can be timely noticed by officers and action can be taken.

Hand-held portable gas monitors are also widely used in underground coal mines. When performing underground works, coal workers are equipped with one hand-held gas monitor that enables detailed monitoring of gas levels at areas of concern. Also, this portable gas monitor helps to protect underground miners from the potential high gas levels in risky areas, such as areas close to seals or stoppings.

Gas samples are routinely taken at areas of concern to further analyze gas composition using GC. GC is capable of accurately detecting a wide variety of gases other than the four-typical gas, such as C_2H_4, C_2H_6, C_2H_2, and H_2. Thus, operators are required to have a good grip on GC control and data analysis.

In addition to the above gas sampling and monitoring techniques, air velocity monitoring sensors are installed in critical underground locations to register airflow rates at a particular place. Depending on the specific site, the airflow rate should be regulated and controlled accordingly.

3.4 Principal Hazard Management Plan

In order to effectively manage and control problems associated with spontaneous combustion and heating, different regulations and acts have been promulgated and strictly enforced in different states in Australia. Coal Mining Safety and Health Regulation 2017 enacted by the Queensland Government (2017) states that an integrated safety and health management system is required to be well established prior to mining activities commencing. The safety management system mainly

consists of three different parts: principal control plans, principal mining hazard management plan and management of other hazards. For underground coal mines, Principal Hazard Management Plan (PHMP) is compulsorily required. In terms of fire-related problems, the safety and health management system must contain essential information about fire prevention and control, an effective fire fighting capability, the safety of persons fighting fires, and a risk assessment to identify all potential fire hazards at the mine.

Coal Mine Safety and Health Act 2002, amended and enacted in 2002 by New South Wales (2002), states that coal mining operation is allowed to be carried out with the prerequisite that a health and safety management system complying with this Act and regulations is well established. The health and safety management system should be reviewed on a regular basis and amended as required to ensure the safe and effective assessment and control of potential hazards arising from mining activities. Similar to PHMP enacted by Queensland, Major Hazard Management Plan (MHMP) is required prior to the operator commencing coal extraction. It is required by MHMP that the coal operation arrangement necessary for preventing, detecting, and combating fire or spontaneous combustion and heating should be established and maintained, the training of personnel involved in the arrangement should be performed in a timely manner, as well as the apparatus aimed at preventing, detecting and combating fires or spontaneous heating should be provided in sufficient quantity and maintained in good conditions.

In recent years, it is not uncommon that a newly authorized mine or mine extension is required to formulate spontaneous combustion management plans (SCMP) to prevent the occurrence of combustion and heating and minimize the potential risk and impacts imposed on workers or normal production (NSW Department of Industry and Investment 2011a). Although SCMP may vary from mine to mine, it primarily includes the essential elements illustrated in Figure 3.2. The SCMP is required to be reviewed regularly and revised where necessary.

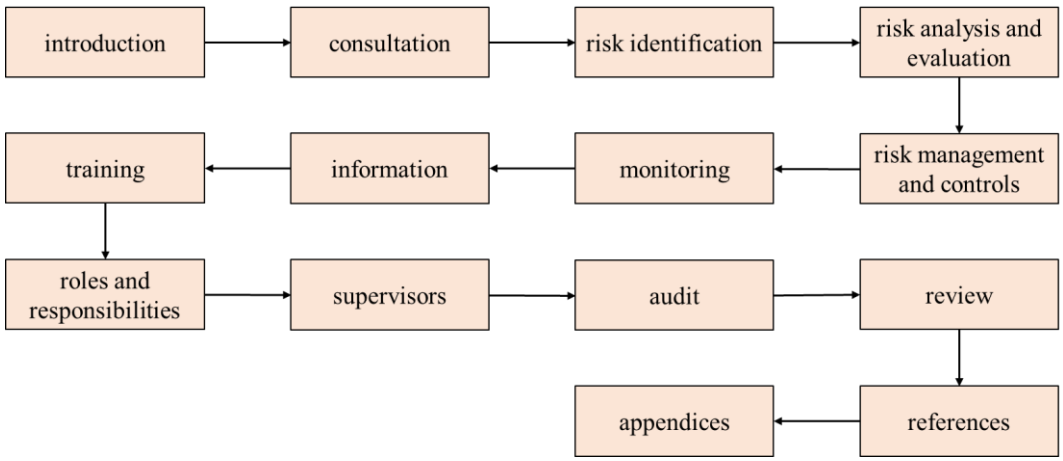

Figure 3.2 Essential elements required in the SCMP (NSW Department of Industry and Investment 2011a)

As an integral part of SCMP, trigger action response plans (TARP) provide clear guidance for workers involved in mining-related activities on reacting correctly and safely when an abnormal condition is encountered. As a result, detailed knowledge of the normal condition and background gas level plays a significant role in determining the trigger alarm values and appropriate actions. Due to different atmospheric conditions in various locations in underground coal mines, the TARP should be defined separately by taking the site-specific conditions into account. According to the severity of the situation and corresponding response, the TARP typically includes at least three levels. Not only should historical data and guidance from experienced experts and industry be considered, but also the latest onsite monitoring data should not be ignored concerning determining trigger values. The gas indicators or ratios commonly used in TARP include, but are not limited to, CO make, Graham's ratio, H_2, O_2, CO concentration, and C_2H_4. An example of a TARP widely used in Australia (Ren 2019) is shown in Figure 3.3.

	Action	Longwall return	Longwall return seals	Longwall intake seals
Normal	Systematic sampling as per schedule from ventilation officer	▪ CO make ≤ 15 l/min; ▪ Graham's ratio < 0.4; ▪ $H_2 \leq 1$ ppm; ▪ $O_2 > 19\%$;	▪ CO < 100 ppm; ▪ Graham's ratio < 0.5; ▪ $H_2 < 10$ ppm;	▪ CO < 100 ppm; ▪ Graham's ratio < 0.5; ▪ $H_2 < 5$ ppm;
Level 1	Precautionary investigation and bag samples taken from underground	▪ 15 l/min < CO make < 35 l/min; ▪ Graham's ratio > 0.4; ▪ 1 ppm < H_2 < 4 ppm; ▪ O_2 >19%;	▪ 100 ppm < CO < 250 ppm and 10 ppm < H_2 < 30 ppm; ▪ Graham's ratio > 0.5;	▪ 100 ppm < CO < 200 ppm and 5 ppm <H_2< 20 ppm; ▪ Graham's ratio>0.5;
Level 2	Thorough investigations and samples taken from neighboring seals	▪ 35 l/min < CO make < 50 l/min and H_2 > 5 ppm; ▪ Graham's ratio > 0.55; ▪ O_2 < 19%;	▪ CO > 250 ppm and 30 ppm < H_2< 50 ppm; ▪ Graham's ratio > 0.75; ▪ Oxygen at K100 seals at cut-through > 4%;	▪ CO > 250 ppm and 20 ppm < H_2 < 50 ppm; ▪ Graham's ratio > 0.75;
Level 3	Confirm results and evacuate personnel	▪ CO make < 50 l/min and H_2 > 5 ppm; ▪ C_2H_4 indicated in bag sample;	▪ CO> 250 ppm and H_2 > 50 ppm; ▪ C_2H_4 indicated in bag sample and flammability trending toward explosive limits; ▪ Oxygen at K 100 seals at cut-through > 8%;	▪ CO > 250 ppm and H_2 > 50 ppm; ▪ C_2H_4 indicated in bag sample and flammability trending toward explosive limits;

Figure 3.3 An example of a typical TARP in Australia (Ren 2019)

3.5 Proactive Spontaneous Combustion Control Technology

In recent years, many underground coal mines in Australia have been increasingly plagued with spontaneous combustion and heating issues, and air leakage is considered the main culprit. There are many potential leakage pathways providing channels for air to ingress into the goaf areas, mainly including leakage at the rear of hydraulic supports, leakage through seals or cracked pillars on the maingate (MG) and tailgate (TG) side, leakage conduits arising from boreholes drilling on the surface, leakage from adjacent goaf areas, ineffective ventilation control devices as well as pre-existing or mining-induced cracks and fractures in the overlying strata, as illustrated in Figure 3.4. If not managed and controlled effectively, those leakage pathways enable oxygen-bearing air to ingress into the goaf area where residual coal are left and increase the likelihood of potential heating. If the rate of heat produced by coal oxidation is higher than the rate of heat dissipated, the accumulated heat is highly likely to lead to spontaneous combustion and even an open fire.

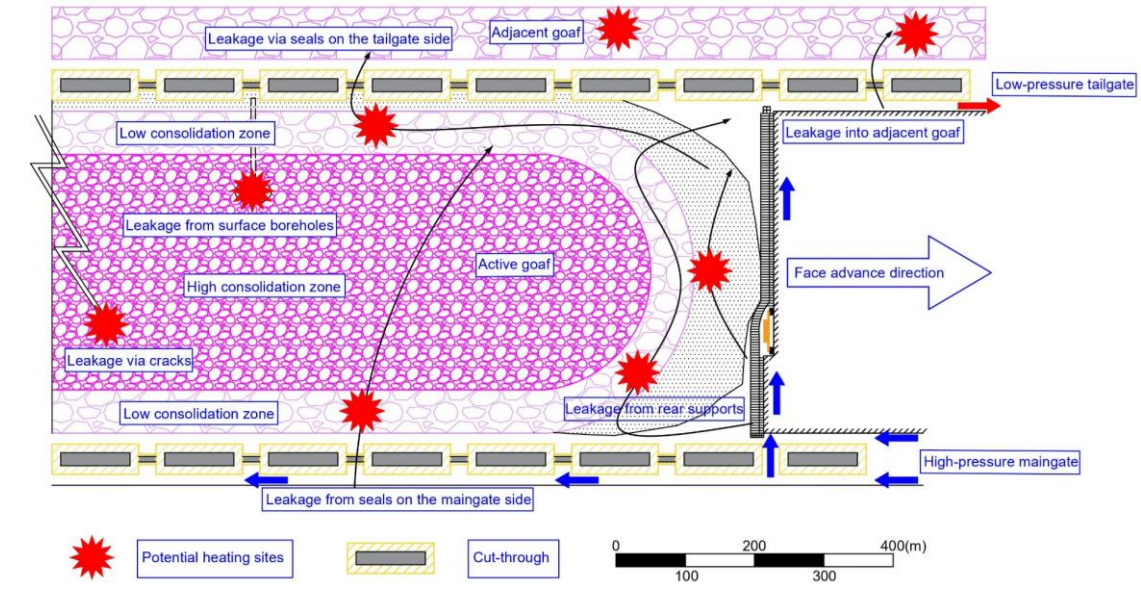

Figure 3.4 Potential air leakage pathways in a retreat LW face

The application of inertisation technology has become overwhelmingly popular in preventing and controlling spontaneous combustion issues commonly arising in LW active goaf by means of injecting inert gas into the goaf area to deplete or reduce oxygen concentration to a safe level. Many types of inertisation gases have been practically used in underground coal mines, such as nitrogen, carbon dioxide as well as boiler gas (usually consisting of 85% nitrogen, 1% oxygen, and 14% carbon dioxide) (Ren et al. 2005).

Although carbon dioxide is more suitable for spontaneous combustion control and fire extinguishment in some circumstances where a favourable gradient presents for dense carbon dioxide to flow and blanket areas of concern or hot atmospheric conditions are found, the usages of carbon dioxide are pretty limited due to its minor constituents of air, the characteristic of becoming noxious in higher concentrations and irritant to people's skin. On the contrary, nitrogen has excellent advantages of being able to be commercially made and transported in large quantities and non-toxic characteristics over other inert gas, thus it has been increasingly employed for the extinction of heating and fire in underground coal mines. With the significant advance in technology, several inert gas generators have been developed and widely used in underground coal mines in Australia, as illustrated in Figure 3.5 (NSW Department of Industry and Investment 2011b). However, many Australian underground coal mines are facing increasing threats from the hazards of spontaneous combustion and heating due to increased production outputs and extraction depth of cover. LW panels are characterized by large panel size (200~400 m), fast advance rate and high ventilation rate (60~100 m^3/s), and less compaction of the caved roof and big pressure difference causes air to easily ingress into the goaf area, thus increasing the risk of spontaneous combustion and heating. In most cases, inert gas is injected into the goaf area via cut-throughs on

the MG side or surface boreholes at an injection rate of approximately 0.5 m^3/s to contain spontaneous combustion. Compared to high ventilation rates, goaf gas emission rates and serious air leakage, the existing practices of goaf inertisation cannot meet the requirement for effectively suppressing spontaneous heating. Therefore, it is necessary to conduct further case studies to optimize goaf inertisation strategies for those underground coal mines with high ventilation rates and goaf gas emission rates.

(a) Mineshield Unit (Liquid N_2 ~2 to 3 m^3/s)

(b) Tomlinson Boiler Unit (85% N_2 and 14% CO_2 ~ 0.5 m^3/s)

(c) Floxal Unit (N_2>99% ~0.15 to 0.5 m^3/s)

(d) GAG Jet Engine Inertisation device (Inert gas ~10 to 20 m^3/s)

Figure 3.5 Inert gas generators used in Australia (NSW Department of Industry and Investment 2011b)

3.6 Case Study of Spontaneous Combustion Prevention and Control

3.6.1 General mine site conditions

In this paper, a typical underground coal mine (Mine A) in New South Wales (NSW) was selected for the simulation study. This mine is located 28 km south of NSW, producing high-quality pulverized coal injection (PCI) coal and low-ash thermal coal. The Hoskissons seam is the primary coal seam mined with a full thickness of 9 m and a depth of cover from 150 m to 380 m. According to the information provided by the mine site, the coal seam is classified as spontaneous combustion prone.

The LW face is ventilated with U-type ventilation with an average airflow rate of 65.2 m^3/s. The seam gas is predominantly composed of CO_2, accounting for approximately 80% of total goaf

gases, with the rest being CH_4, taking up about 20%. The total goaf gas emission rate is approximately 2000 l/s. Both in-seam gas boreholes and surface goaf holes are used for gas drainage. The depth of cover of the LW ranges from 240 m to 320 m, with an average mining height of 4.3 m. The width of the LW panel is 400 m, and the length of the panel is 3600 m. The face has already advanced 2800 m, with an advance rate of 32 m per week. The elevation of the TG side is 8 m higher than that of the MG side, while the elevation of the starting-off line is 18 m higher than that of the LW face. The dimension of the gateroad is 5.4 m in width and 3.7 m in height. The spacing of cut-throughs (CTs) on the MG and TG side is 150 m and 100 m, respectively, while the interval between surface boreholes is 100 m. The layout of the LW panel (part of the goaf area) is shown in Figure 3.6.

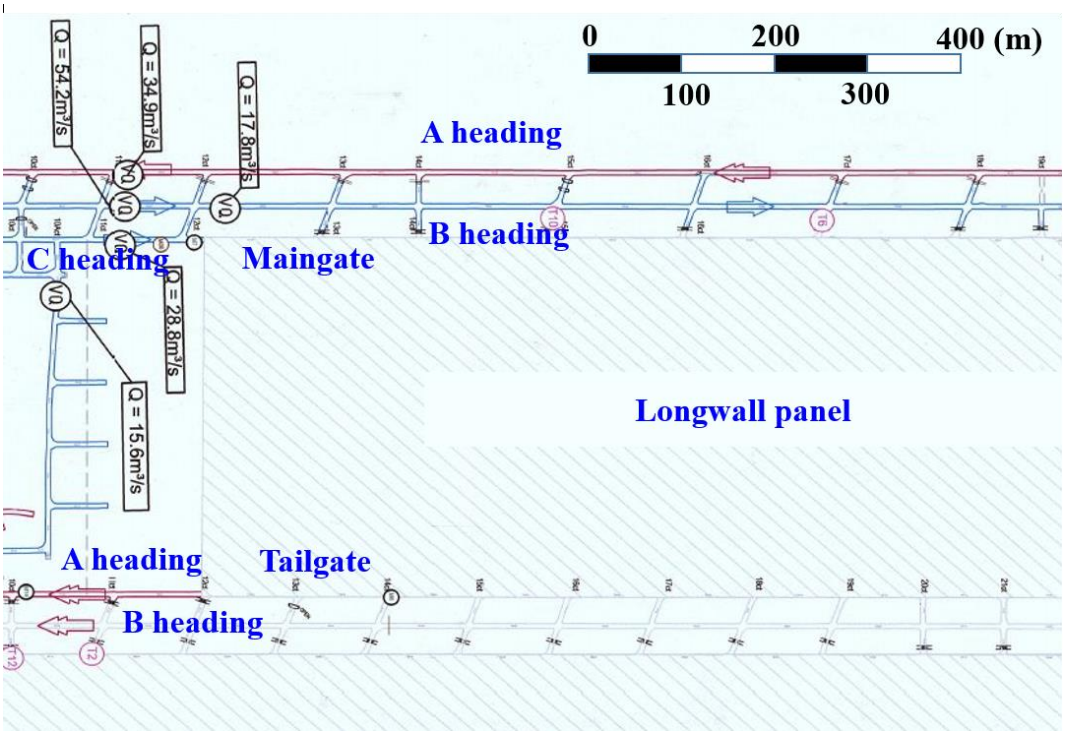

Figure 3.6 Layout of the LW panel

According to the datasets collected from the mine site, the mixed gas (85% CO_2 and 15% CH_4) and pure N_2 were injected into the active goaf area via CT16 and CT15 on the MG side at an injection flowrate of 72 l/s and 150 l/s, respectively, to contain the heating. The goaf gas emission rate, goaf gas composition, gas injection rate and type of gas injected were written in User Defined Function (UDF) and imported into Fluent for calculation. A tube bundle system was used to monitor the gas concentration at areas of concern, and one tube bundle was positioned at each CT on the MG side, with the average gas concentration in each specific tube bundle point. Figure 3.7 shows a partial layout of the LW panel with a length of 1000 m for the CFD model and onsite gas monitoring data from each TB point.

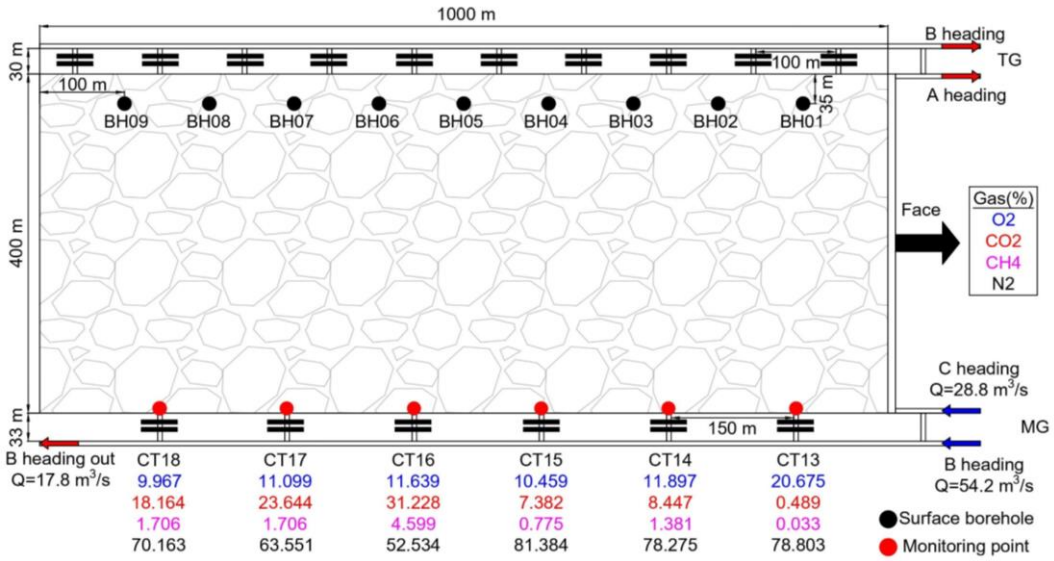

Figure 3.7 Partial LW layout and onsite gas monitoring data

3.6.2 Model development and boundary conditions

Based on site-specific conditions, a 3D model was constructed. In order to reduce the computational time and increase the simulation accuracy, the goaf area 1000 m behind the face was considered in the model. The length of the LW face was 400 m, including the width of MG and TG gateroad. The model was 80 m in height to cover the immediate caving regions with high porosity in the goaf, which included 10 m of the floor strata, 4.3 m of average cutting height and 65.7 m of the roof above the mined seam.

The model was meshed using the hexahedron meshing method for gateroads, LW face, coal seam and floor, and the tetrahedron meshing method for the drainage boreholes to accommodate the complex geometry. The mesh size for the gateroad and drainage borehole was 1 m and 0.25 m, respectively. A mesh independence study was conducted. The mesh sizes for coal seam were 2.5 m, 2.0 m and 1.6 m for coarse, medium, and fine mesh, and the total element for the three scenarios were 782376, 926367 and 1082392, respectively. As shown in Figure 3.8, there were no significant differences in velocity on the MG side along the goaf area and along the working face (behind the face). Therefore, the model with medium mesh was selected for this study. The minimum orthogonal quality and the maximum skewness value were 0.85 and 0.45, respectively, both of which indicated that the meshed model was of very good quality according to ANSYS Meshing Users' Guide (ANSYS 2018b). Then the medium-mesh model was imported into ANSYS Fluent 18.2 and refined with higher density mesh in the areas of interest, such as in the vicinity of the face and gateroads using region adaption, as shown in Figure 3.9. Boundary conditions based on site data were defined for the CFD simulations (Ren et al. 2012; Shen et al. 2020; Zhang et al. 2019b), as detailed in Table 3.2. In addition, an iteration independence study was conducted, and it was found that there was a negligible difference in goaf gas distribution in the goaf area when the

iteration exceeded 4000. Therefore, all simulations were conducted in 4000 iterations.

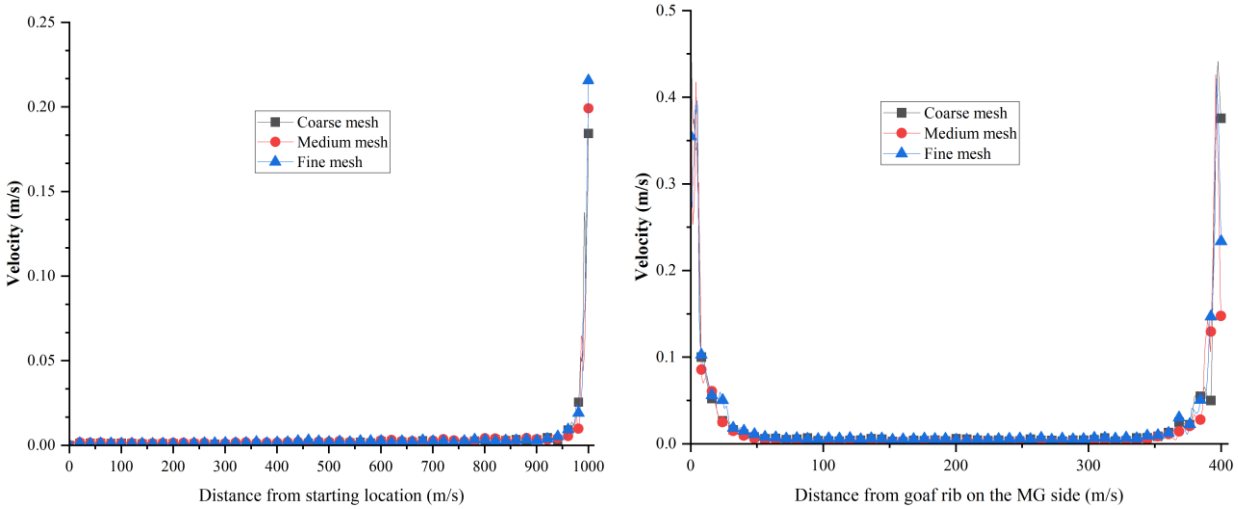

(a) Velocity comparison on the MG side (b) Velocity comparison along the working face (behind the face)

Figure 3.8 Mesh independence study results

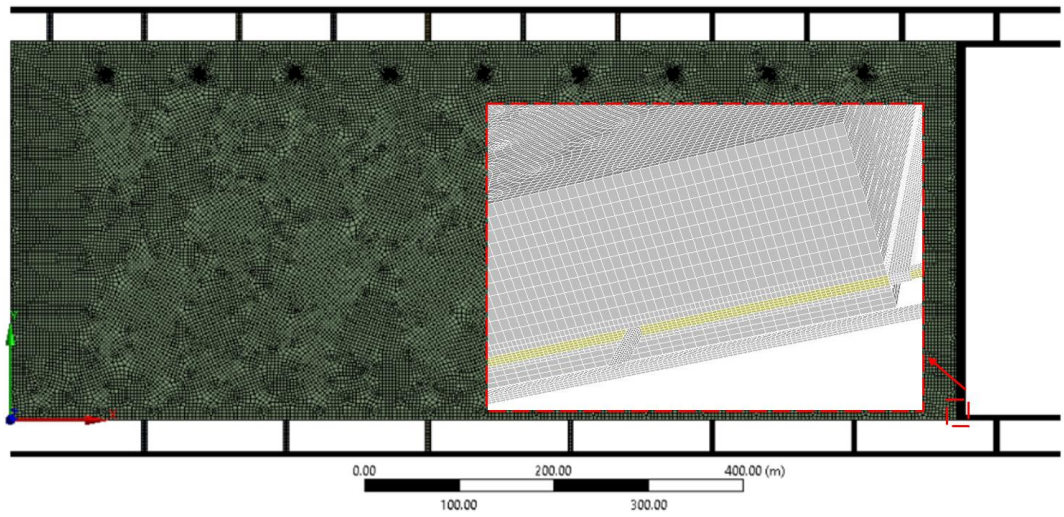

Figure 3.9 Meshed model

Table 3.2 Boundary conditions for the simulations

Name	Boundary type	Value	Name	Boundary type	Value
Solver	Pressure-Based	/	Viscous model	Standard k-ε	/
Near-wall treatment	Standard wall functions	/	Species model	Species transport	Methane-air
B heading (MG)	Velocity inlet	2.713 m/s	C heading (MG)	Velocity inlet	1.441 m/s
A heading (TG)	outflow	/	B heading (TG)	Outflow	/
B heading out (MG)	Velocity inlet	0.891 m/s	Other faces	Standard wall	/
Scheme	SIMPLE	/	Initialization	Standard	/

Table 3.3 permeability distribution in the goaf area

Author	Permeability distribution (m^2)
Whittles et al. (2006)	1×10^{-8}~5×10^{-7}
Esterhuizen and Karacan (2007)	9.87×10^{-11}~9.87×10^{-10}
Karacan (2008)	2.5×10^{-9}~6×10^{-9}
Yuan and Smith (2008)	2.97×10^{-8}~8.42×10^{-7}
Ren et al. (2011)	1.97×10^{-9}~1.97×10^{-12}
Guo et al. (2015)	1×10^{-13}~1×10^{-4}
Qin et al. (2015)	$1\times10^{-9.5}$~$1\times10^{-6.5}$
Ren et al. (2018a)	1×10^{-9}~1×10^{-2}
Zhang et al. (2019a)	4.1×10^{-9}~1.2×10^{-7}

Table 3.3 lists the permeability value defined by other scholars in their work, which indicates that a big difference existed in the permeability value, which could be ascribed to the different geologic and mining conditions. As reported by Guo et al. (2012) and Qin et al. (2015), the permeability distribution was in the shape of an O-ring, with a higher value on the periphery of the goaf area and a lower value in the centre of the goaf area.

Based on the information provided by the mine site and the equations (3-6)-(3-9) (Liu 2019), the permeability distribution ranges from 10^{-3} m^2 to 10^{-10} m^2, as shown in Figure 3.10. In particular, the permeability in the centre of the goaf was the lowest, while it was highest in the periphery of the goaf area. The index in the figure caption is the exponent of the permeability in m^2. A function is defined in the UDF to describe the spatial changes of permeability in the CFD model for computational elements.

$$\left\{\alpha = 10^{-(a_1+a_2*\tanh(\frac{Z_i-Z_0}{a_{z1}}))*(\frac{Y_i-Y_0}{a_y}+0.5+\left(0.5-\frac{Y_i-Y_0}{a_y}\right)*\tanh\left(\frac{X_i-X_0}{a_{x1}}\right)}, Z_i \le \frac{z_0+z_1}{2}, X_i \le \frac{X_0+X_1}{2}\right\} \quad (3-6)$$

$$\left\{\alpha = 10^{-(a_1+a_2*\tanh(\frac{Z_1-Z_i}{a_{z2}}))*(\frac{Y_i-Y_0}{a_y}+0.5+\left(0.5-\frac{Y_i-Y_0}{a_y}\right)*\tanh\left(\frac{X_i-X_0}{a_{x1}}\right)}, Z_i > \frac{z_0+z_1}{2}, X_i \le \frac{X_0+X_1}{2}\right\} \quad (3-7)$$

$$\left\{\alpha = 10^{-(a_1+a_2*\tanh(\frac{Z_i-Z_0}{a_{z1}}))*(\frac{Y_i-Y_0}{a_y}+0.5+\left(0.5-\frac{Y_i-Y_0}{a_y}\right)*\tanh\left(\frac{X_1-X_i}{a_{x2}}\right)}, Z_i \le \frac{z_0+z_1}{2}, X_i > \frac{X_0+X_1}{2}\right\} \quad (3-8)$$

$$\left\{\alpha = 10^{-(a_1+a_2*\tanh(\frac{Z_1-Z_i}{a_{z2}}))*(\frac{Y_i-Y_0}{a_y}+0.5+\left(0.5-\frac{Y_i-Y_0}{a_y}\right)*\tanh\left(\frac{X_1-X_i}{a_{x2}}\right)}, Z_i > \frac{z_0+z_1}{2}, X_i > \frac{X_0+X_1}{2}\right\} \quad (3-9)$$

Where: α stands for the permeability in the goaf area; a_1 and a_2 are the constants; X_i, Y_i and Z_i represent the coordinates of any position in the goaf area in the direction of the face length, face height and face retreat, respectively; X_0, Y_0 and Z_0 stand for the coordinates at the start of the goaf

far away from the LW face; X_1 is the x coordinate at the goaf immediately behind the LW face; Z_1 stands for the z coordinate at the other side of the goaf; a_{x1}, a_{x2}, a_y, a_{z1} and a_{z2} represent the coefficients determining the permeability change in x, y and z direction, respectively.

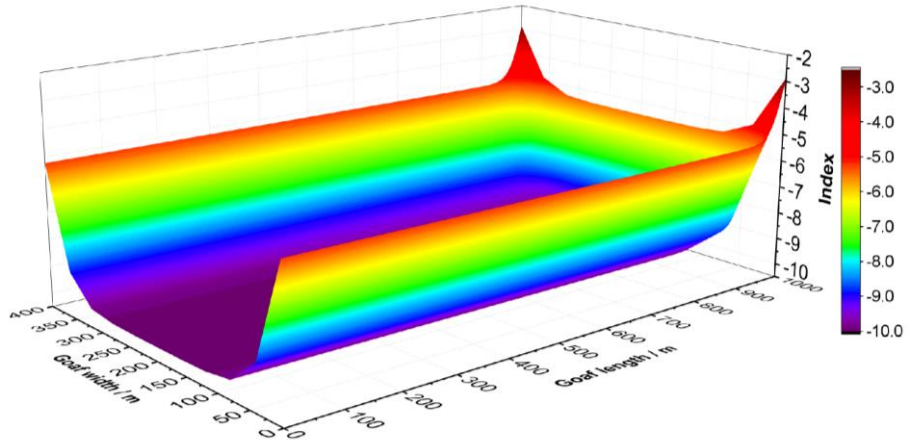

(a) 3D view

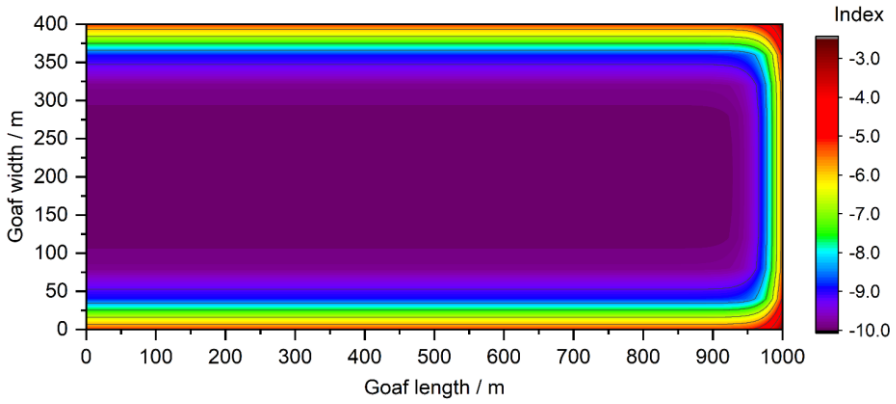

(b) Plane view

Figure 3.10 Permeability index distribution at 2m above the seam floor

3.6.3 Model validation and simulation results

To validate the numerical model, oxygen concentration at each cut-through on the MG side was compared between the base model simulation results and onsite monitoring data, as depicted in Figure 3.11. A good agreement was reached with variation between simulation results and monitoring data lying within 6%, which meant that the CFD model was capable of predicting gas flow dynamics and distribution patterns in the goaf area.

The oxygen distribution in the goaf area is illustrated in Figure 3.12. The results demonstrated that oxygen ingress into the goaf was higher on the MG side and TG side, with oxygen concentration well over 8% at 1000 m behind the face. The gas buoyancy effect could also be noted in gas distribution patterns in the goaf area, resulting in oxygen layering at the higher elevation parts of the goaf and carbon dioxide close to the floor level of the coal seam. This is because that the goaf

gas is predominantly composed of carbon dioxide, whose density is much heavier than oxygen, nitrogen and methane. The apparent oxygen penetration into the goaf area indicated that the existing goaf inertisation strategy did not produce a satisfactory result in dropping oxygen levels that will hinder the development of spontaneous combustion. Obviously, there is a need to optimize goaf inertisation strategies.

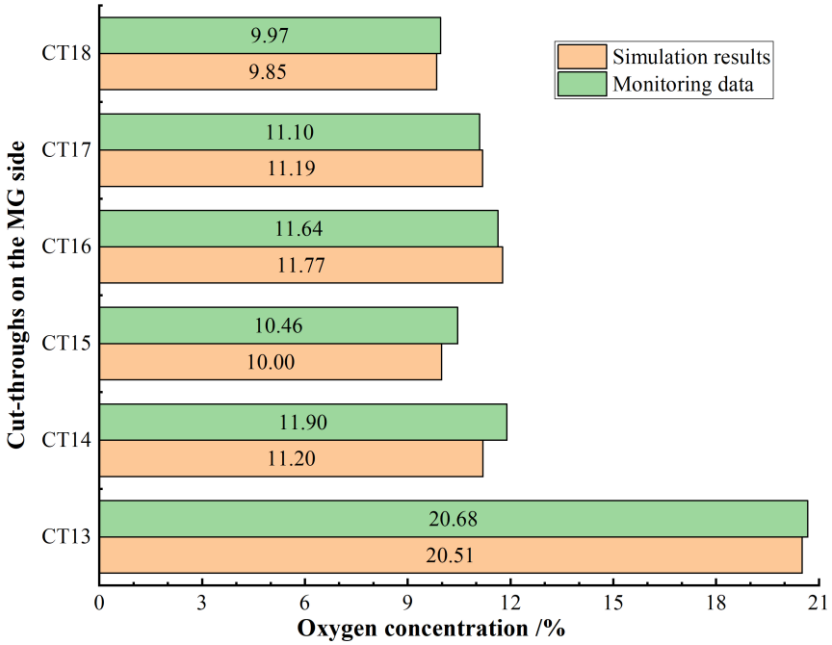

Figure 3.11 Model validation by comparison of oxygen concentration on the MG side

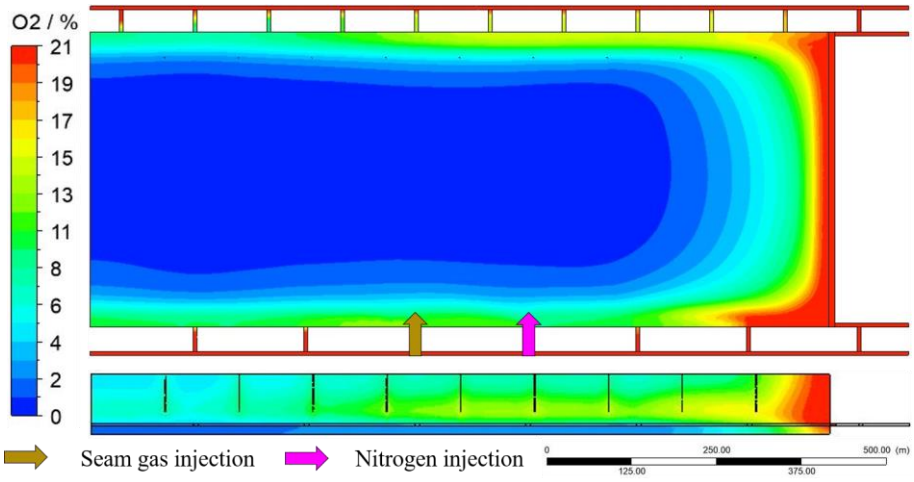

Figure 3.12 Oxygen distribution in the LW goaf (2m from the seam floor)

3.6.4 Optimization of goaf inertisation strategies

Based on the validated model, extensive parametric studies were conducted to understand the influence of different goaf inertisation plans on goaf gas behaviour and spontaneous combustion containment. Three key parameters, including inert gas injection locations, inert gas injection rate and inert gas type, were investigated qualitatively and quantitatively with a view to improving current goaf inertisation practices.

3.6.4.1 Nitrogen injection locations

(A) Nitrogen injection via one location

A base model without nitrogen injection is useful to show the oxygen ingress pattern in the goaf area and identify the potential areas for spontaneous combustion. Goaf inertisation with nitrogen should be targeted in these areas at potential spontaneous combustion risk. As illustrated in Figure 3.13(a) without nitrogen injection, oxygen levels were well over 10% on the MG and TG side at 1000 m behind the face.

Nitrogen can be injected into the goaf area via an underground cut-through on the MG or TG side or through a surface borehole. There are six and ten cut-throughs, respectively, behind the face on the MG and TG side and nine drilling boreholes on the surface. Therefore, twenty-five scenarios were numerically investigated, and several typical results of oxygen distribution in the goaf area are presented in Figure 3.13. Nitrogen injection flowrate was 500 l/s in the simulation based on the recommendations of Ren and Balusu (2009; 2005) for effective goaf inertisation.

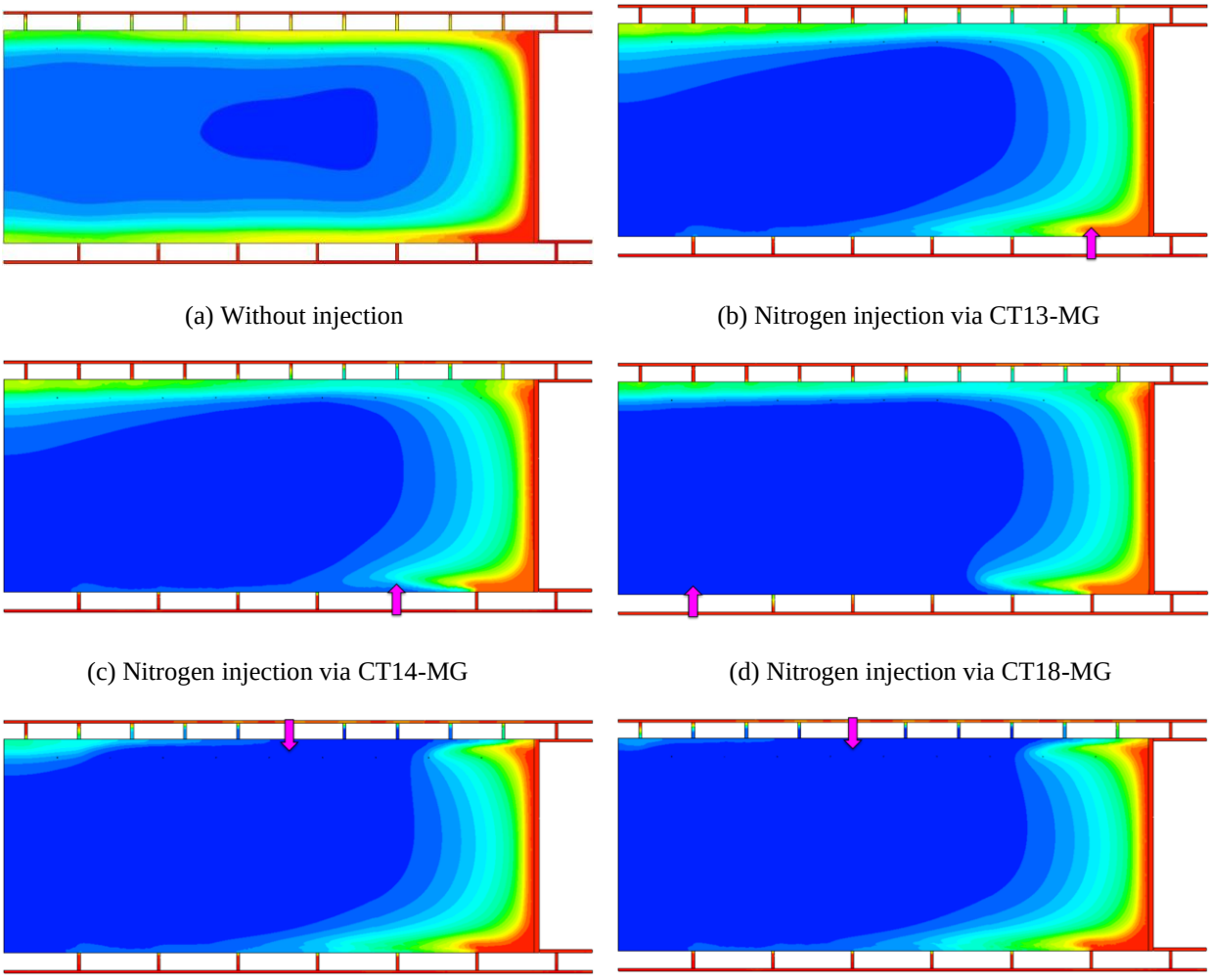

(a) Without injection

(b) Nitrogen injection via CT13-MG

(c) Nitrogen injection via CT14-MG

(d) Nitrogen injection via CT18-MG

(e) Nitrogen injection via CT17-TG

(f) Nitrogen injection via CT18-TG

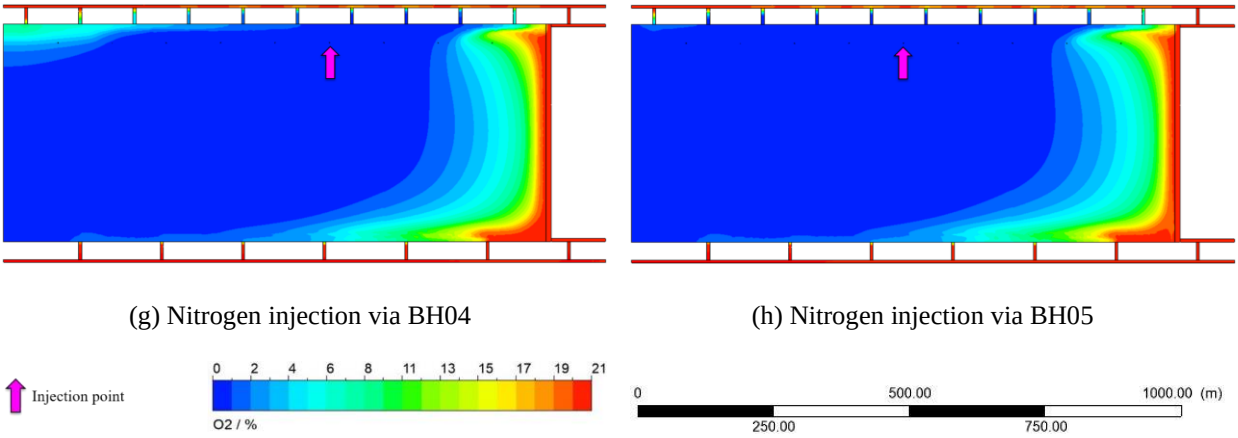

(g) Nitrogen injection via BH04 (h) Nitrogen injection via BH05

Figure 3.13 Oxygen distribution in the goaf area with one nitrogen injection location (2m from the seam floor)

The simulation results indicated that nitrogen injection locations played a significant role in oxygen distribution in the LW goaf. As shown in Figure 3.13(b)-(d), when nitrogen was injected via one cut-through (except CT13) on the MG side, oxygen concentration on the MG side dropped below 5% at a distance of 180 m behind the face. However, nitrogen injection via one cut-through had a marginal impact on preventing oxygen penetration into the goaf area on the TG side with the current injection rate.

Goaf inertisation performance could be improved when nitrogen was injected into the goaf area via a surface borehole or a cut-through on the TG side, as depicted in Figure 3.13(e)-(h). Oxygen levels on the MG side could be reduced to 5% at a distance of 380 m behind the face. When the distance between the injection location and the LW face was shorter than 460 m, a high oxygen concentration on the TG side could be observed in the deep goaf. However, with the nitrogen injection location moving further inbye of the LW panel toward deep goaf, oxygen concentration could be dropped below 5% at approximately 120 m behind the face.

(B) Nitrogen injection via two locations

Extensive simulations were conducted to evaluate the goaf inertisation performance achieved by nitrogen injection via two different locations, such as two cut-throughs on the MG side, two cut-throughs on the TG side, two drilling boreholes on the surface, one cut-through on the MG side and one cut-through on the TG side, one cut-through on the MG side and one drilling borehole on the surface. The nitrogen injection at each location was 250 l/s. The representative simulation results of oxygen distribution in the goaf area are shown in Figure 3.14 and Figure 3.15, respectively.

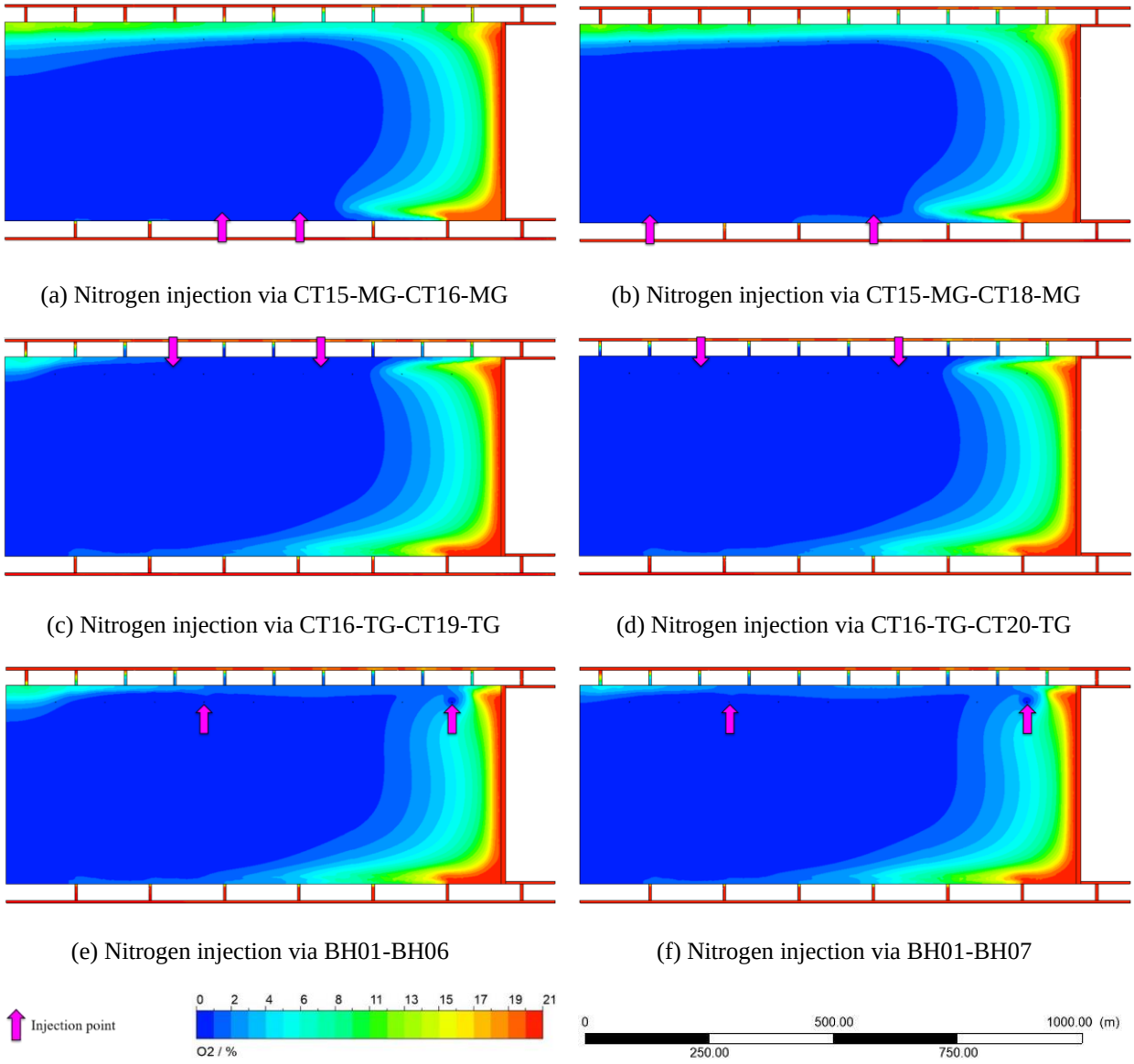

(a) Nitrogen injection via CT15-MG-CT16-MG

(b) Nitrogen injection via CT15-MG-CT18-MG

(c) Nitrogen injection via CT16-TG-CT19-TG

(d) Nitrogen injection via CT16-TG-CT20-TG

(e) Nitrogen injection via BH01-BH06

(f) Nitrogen injection via BH01-BH07

Figure 3.14 Oxygen distribution in the goaf area with nitrogen injected via two locations on the same side

It was noted from Figure 3.14(a)-(b) that nitrogen injection via two cut-throughs on the MG side could reduce oxygen ingress into the goaf area on the MG side, but oxygen levels on the TG side were over 10% even at 1000 m behind the face, producing an unsatisfactory goaf inertisation performance. However, oxygen ingress on both sides could be reduced when nitrogen was properly injected into the goaf via two cut-throughs on the TG side, as shown in Figure 3.14(c)-(d). In particular, to avoid the occurrence of a high-oxygen area (over 5%) on the TG side in the deep goaf, one nitrogen injection location should be set at approximately 750 m (CT20-TG) behind the face. Compared with nitrogen injection via two cut-throughs on the TG side, there were slight differences in oxygen distribution with nitrogen injected via two surface drilling boreholes, as illustrated in Figure 3.14(e)-(f). When nitrogen was injected via BH01 and BH07, oxygen concentration on the TG side could be reduced below 5% at a distance of 75 m behind the face. In order to mitigate air leakage into the goaf area via deep cut-through on the TG side, one of the

nitrogen injection boreholes was required to be located at least 700 m behind the face (BH07).

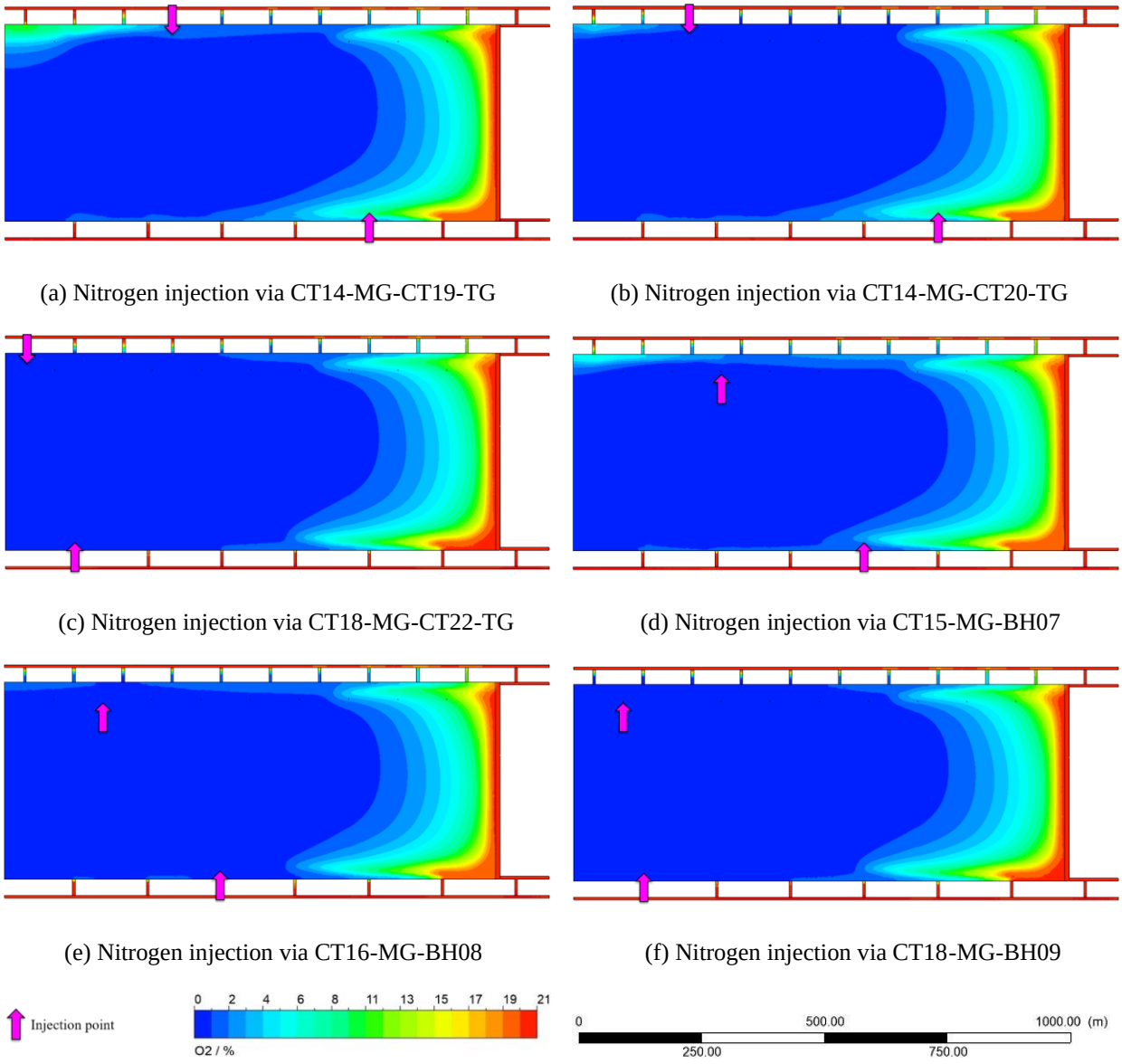

(a) Nitrogen injection via CT14-MG-CT19-TG

(b) Nitrogen injection via CT14-MG-CT20-TG

(c) Nitrogen injection via CT18-MG-CT22-TG

(d) Nitrogen injection via CT15-MG-BH07

(e) Nitrogen injection via CT16-MG-BH08

(f) Nitrogen injection via CT18-MG-BH09

Figure 3.15 Oxygen distribution in the goaf area with nitrogen injected via the surface sites

With regard to scenarios where nitrogen was injected appropriately from both sides, oxygen distribution was quite similar to the scenarios in which nitrogen was injected via two deep cut-throughs on the TG side or two surface boreholes. For the purpose of achieving a better goaf inertisation performance in the deep goaf, it is recommended that the nitrogen injection location on MG and TG side should be set at a distance of approximately 400 m and 700 m behind the face, respectively.

In order to determine the best nitrogen injection locations for goaf inertisation, the area of the oxidation zone where oxygen concentration was in the range of 5% and 18% was calculated and quantitatively compared, with the main results shown in Table 3.4. To evaluate the severity of spontaneous combustion, the oxidation ratio was introduced and defined as the ratio of the oxidation zone area to the goaf area.

Table 3.4 Impact of nitrogen injection locations on the oxidation zone area

Injection scenarios	CT18-MG	CT18-TG	BH05	CT16-CT18-MG
Oxidation zone area (m^2)	66333	49640	47544	67487
Goaf area (m^2)	400000	400000	400000	400000
Oxidation ratio (%)	16.6	12.4	11.9	16.9
Injection scenarios	CT16-CT20-TG	BH01-BH07	CT14-MG-CT20-TG	CT16-MG-BH08
Oxidation zone area (m^2)	50711	44014	51235	50221
Goaf area (m^2)	400000	400000	400000	400000
Oxidation ratio (%)	12.7	11	12.8	12.6

The analysis of the oxidation ratio revealed that simultaneous nitrogen injection via BH01 and BH07 yielded the best goaf inertisation performance, followed by nitrogen injection via BH05.

From the above studies, it was noted that seam orientation and goaf gas composition played a significant role in goaf gas flow dynamic patterns and oxygen distribution in the goaf area, which further influenced the oxidation zone area under the condition of different nitrogen injection locations. Considering specific geological conditions that the elevation of the TG side is higher than that of the MG side and the elevation of the starting-off line is higher than that of the LW face, nitrogen injection via one cut-through or two cut-throughs on the MG side demonstrated undesirable strategies for spontaneous combustion, as the oxygen concentration was high on the TG side of the deep goaf. On the contrary, nitrogen injection should be injected into the goaf area from the TG side or both MG and TG sides at the appropriate distance from the LW face. To avoid high oxygen levels on the TG side of the deep goaf, injection locations on the TG side should be set at approximately 550 m and 750 m behind the LW face when nitrogen was injected via one and two locations, respectively. In addition, nitrogen injection via surface boreholes previously used from gas drainage performed better than cut-throughs on the TG side.

Although the oxidation zone area was significantly narrowed when nitrogen was injected into the goaf area, oxygen concentration higher than 5% could still extend 370 m into the goaf area even under the best inertisation scenarios where nitrogen was injected via BH01 and BH07. As a result, the current nitrogen injection rate is insufficient to effectively hinder the onset of spontaneous combustion, particularly on the MG side, and there is a need to optimize nitrogen injection rates.

3.6.4.2 Nitrogen injection rates

From the above studies, nitrogen injection via BH01 and BH07 performed better in reducing oxygen levels in the goaf area. Considering high oxygen ingress on the MG side, the different nitrogen injection rates ranging from 500 l/s to 2500 l/s were numerically studied, with an

increment of 250 l/s, as shown in Figure 3.16.

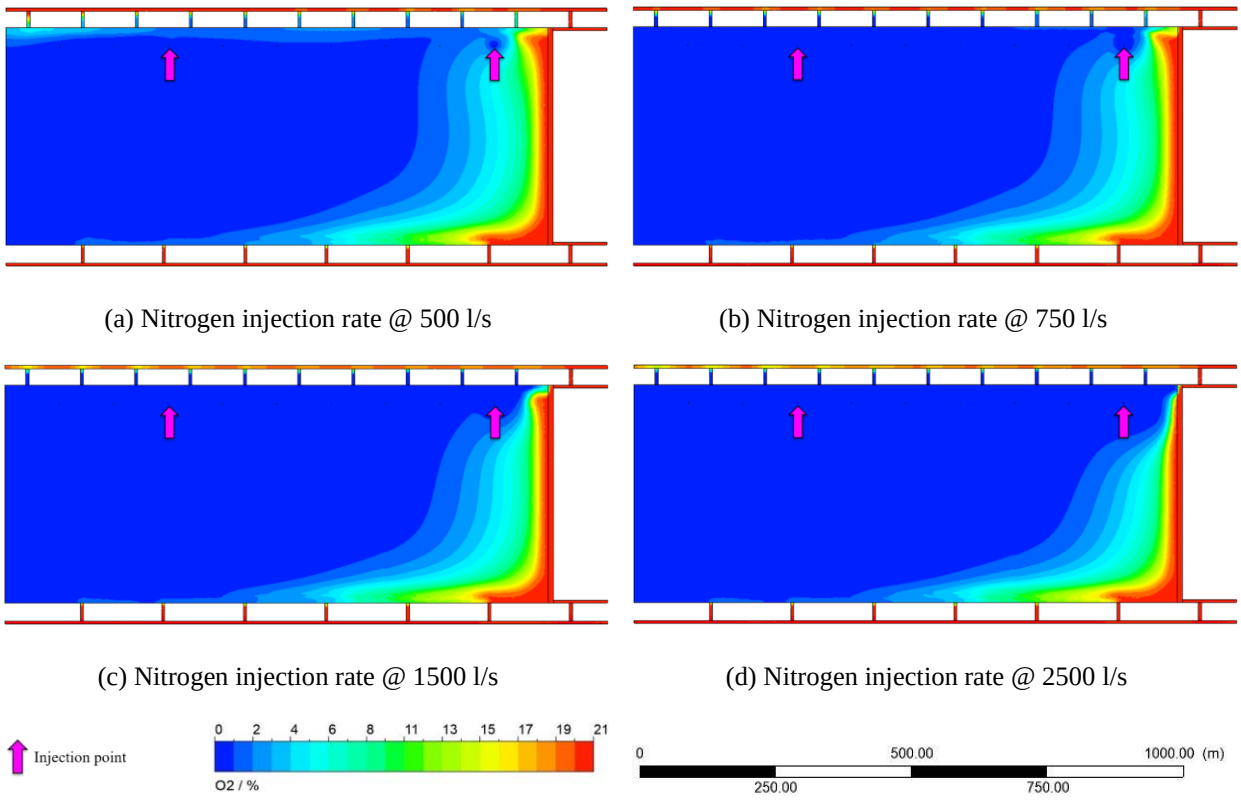

(a) Nitrogen injection rate @ 500 l/s

(b) Nitrogen injection rate @ 750 l/s

(c) Nitrogen injection rate @ 1500 l/s

(d) Nitrogen injection rate @ 2500 l/s

Figure 3.16 Oxygen distribution under different injection rates of nitrogen via BH01 and BH07

It was observed that with the increase in nitrogen injection rates, the area of the oxidation zone decreased. A problem arising with these scenarios was that oxygen concentration would be lower than 19.5% at the tailgate end of the LW face once the nitrogen injection rate was higher than a critical value (750 l/s), which did not comply with the statutory limit regulated by the NSW government. Another problem with nitrogen only being injected from the TG side was that oxygen concentration on the MG side remained above 5% at approximately 350 m behind the face even if the total injection rate hit 2500 l/s.

Considering oxygen concentration on the MG side was higher than 5% at approximately 350 m behind the face and low oxygen levels on the TG end of the LW face, one scenario was proposed and investigated: nitrogen injection via CT14 on the MG side and BH01-BH07. When nitrogen was injected via BH01 and BH07 at an injection rate of 250 l/s and 250 l/s, oxygen concentration dropped below 5% on the TG side at approximately 75 m behind the face, which reduced the spontaneous combustion potential on the TG side. As a result, the injection rate in BH01 and BH07 was constant at 250 l/s, while it increased at CT14 on the MG side with an increment of 250 l/s.

It was observed from Figure 3.17 and Figure 3.18 that with the increase in nitrogen injection rate at CT14 on the MG side, oxygen penetration into the goaf on the MG side was reduced, and the oxidation zone area narrowed. When nitrogen injection at CT14 on the MG side reached 1250 l/s,

the reduction in the oxidation zone area slowed down despite the continued increase in nitrogen injection. Therefore, it was regarded that nitrogen injection via CT14 (MG), BH01 and BH07 with an injection rate of 1250 l/s, 250 l/s, and 250 l/s, respectively, produced the most desirable goaf inertisation results.

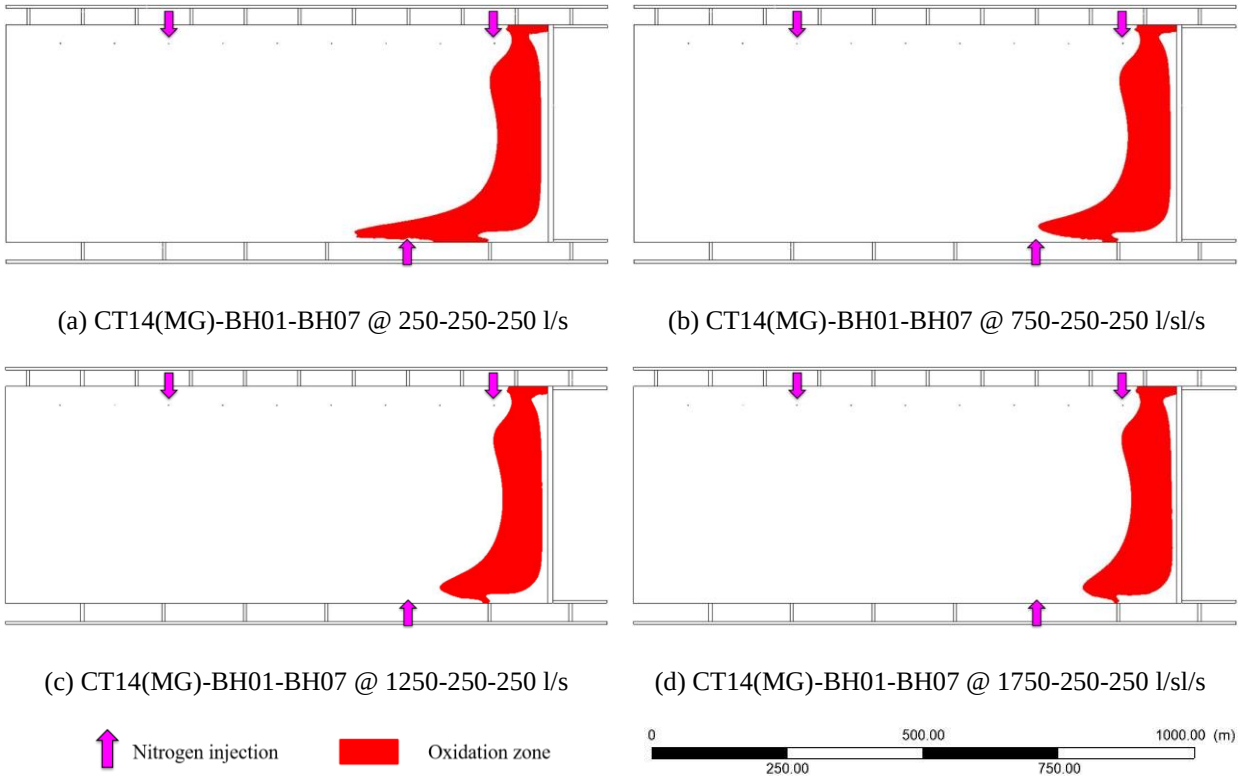

Figure 3.17 Oxidation zone under different injection rates via CT14(MG)-BH01-BH07

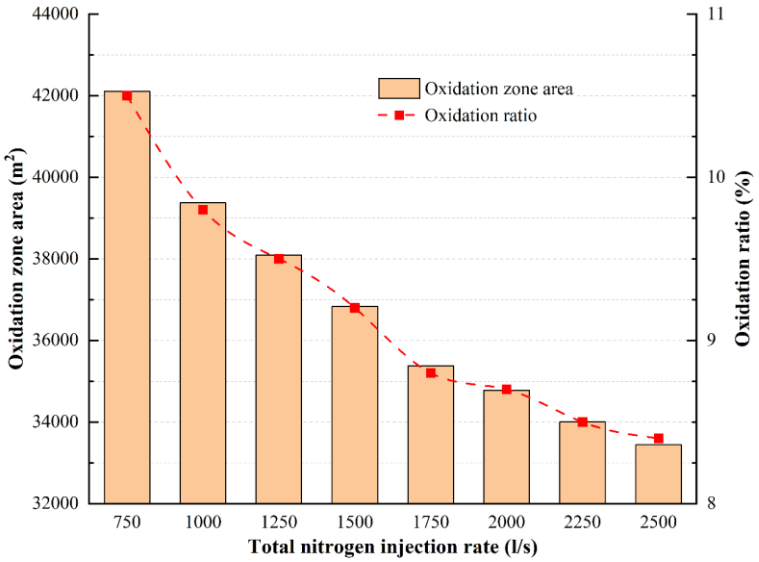

Figure 3.18 Impact of nitrogen injection rate on oxidation zone area and ratio with nitrogen injected via CT14 (MG)-BH01-BH07

To summarise, the desired injection rate was 1750 l/s, and oxygen concentration dropped below 5% on the MG and TG side at 120 m and 75 m behind the face. Many factors are needed to be

considered in determining the optimal injection rates, such as oxygen ingress distance on the MG and TG side, oxygen levels at the tailgate end (higher than 19.5%), and the reduction rate of oxidation zone area and oxidation ratio. In addition, under the condition of a high goaf gas emission rate (approximately 2000 l/s), the existing goaf inertisation practices of 500 l/s could not meet the requirement for containing the onset of spontaneous combustion. The desired nitrogen injection rate should match with the goaf gas emission rate.

3.6.4.3 Inert gas type

Due to the significant impact of gas buoyancy effect on gas distribution in the goaf area, there was a need to investigate the optimal inert gas for containing spontaneous heating in the goaf area. Currently, three different types of inert gas are used in Australia, including nitrogen, carbon dioxide and boiler gas. Figure 3.19 shows oxygen distribution in the goaf area under different inert gases injected via CT14 on the MG side, BH01 and BH07 with an injection rate of 1250, 250 and 250 l/s, respectively. It was evident that an area with a high-oxygen concentration could be found on the TG side of the deep goaf when boiler gas or carbon dioxide was injected, increasing the likelihood of spontaneous heating in this area. Quantitative analysis of the oxidation zone area revealed that it was the largest for carbon dioxide injection (68005 m^2), followed by boiler gas (45606 m^2), while it was the smallest for nitrogen (35375 m^2).

By quantitatively and qualitatively analyzing oxygen distribution patterns in the goaf area, it was concluded that a satisfactory goaf inertisation result could be obtained when nitrogen was injected into the goaf area via CT14 (MG)-BH01-BH07 with an injection rate of 1250, 250 and 250 l/s. Both goaf gas composition and seam orientation had an impact on the choice of inert gas type. Particularly in deep goaf, the buoyancy effect significantly impacted the goaf gas distribution, thus influencing the selection of inert gas for goaf inertisation. These factors are required to take into account when selecting the inertisation gas. Due to the limitation of the simulation, the cooling effect of nitrogen and carbon dioxide was not considered.

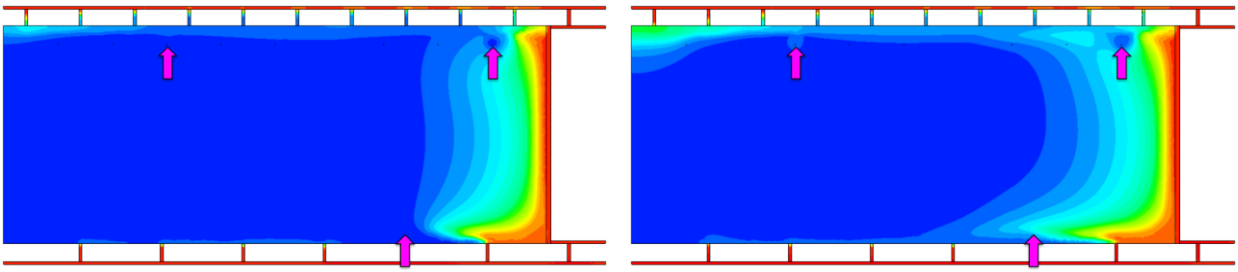

(a) nitrogen injection

(b) Boiler gas injection

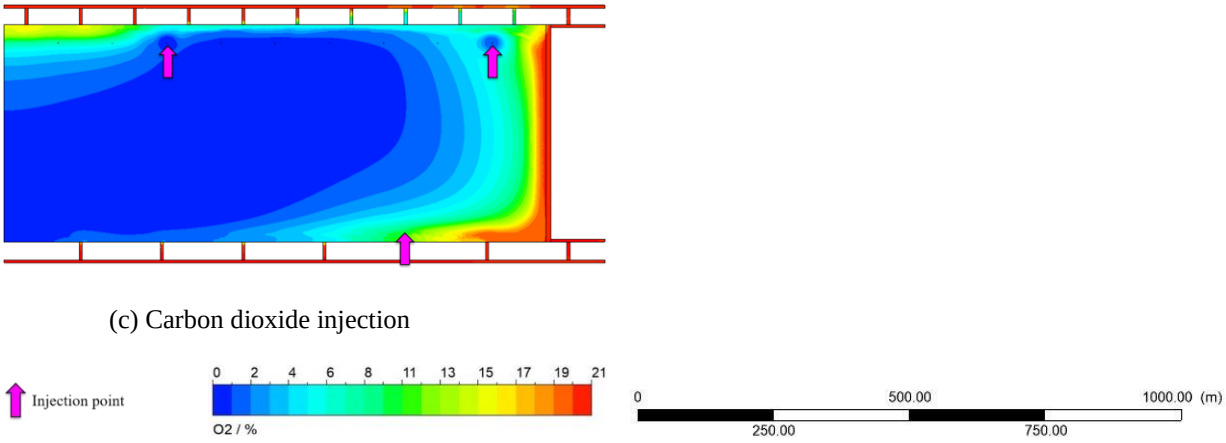

(c) Carbon dioxide injection

Figure 3.19 Oxygen distribution under different inert gas injected into goaf via CT14(MG)-BH01-BH07

3.7. Conclusions

This paper introduced the integrated spontaneous combustion management system that is widely employed in Australian underground coal mines and presented CFD modelling for the simulation of goaf gas flow dynamics and proactive inertisation optimization. The major conclusions are as follows:

(1) The spontaneous combustion propensity is measured and evaluated by the R_{70} method prior to the mining operation. The goaf gas flow dynamics and ventilation migration patterns are systematically monitored during coal extraction. Site-specific Trigger Action Response Plan (TARP) for spontaneous combustion must be established and implemented with gas monitoring and sampling for different locations.

(2) Based on the site-specific conditions of an underground coal mine in New South Wales, a 3D CFD model was built and validated using onsite real-time gas monitoring data. A good agreement between base-model simulation results and onsite monitoring data was reached, which increased the confidence in investigating scenarios outside of the base case and optimizing goaf inertisation strategies.

(3) Due to the fact that the elevation of TG is higher than that of the MG side and the elevation of the starting-off line is higher than the working face, inert gas injection on the TG side performed better in goaf inertisation than the MG side, and nitrogen was superior to boiler gas and carbon dioxide.

(4) The qualitative and quantitative analysis of simulation results showed that the desirable goaf inertisation strategy is to inject nitrogen into the goaf area via cut-through at 250 m on the MG side and surface borehole at 100 m and 700 m on the TG side with a total injection rate higher than 1750 l/s. Oxygen ingress into the goaf area on both sides was reduced significantly with an oxidation zone area of 35375 m^2, which was approximately one-third of the oxidation zone area

of the scenario without any inert gas injection (106666 m^2).

(5) Both geological conditions (e.g., seam orientation, goaf gas composition and emission) and mining parameters (e.g., face layout and ventilation rate, advance rate) have impacts on goaf gas flow dynamics and distribution patterns, which needs to be taken into consideration in determining goaf inertisation strategies.

The following limitations of the study are noted. The coal reaction with oxygen and the cooling effect of nitrogen and carbon dioxide were not considered. In addition, in order to save computational time and cost, only a 1000-m long goaf area was stimulated rather than the entire goaf area (2800 m).

Despite the above limitations, this study will improve current goaf inertisation practices in Australia to effectively contain spontaneous heating in large LW goaf areas with high production rates, high ventilation rates, as well as high gas emission rates, and improve coal mining safety. Due to the fact that the goaf gas is composed of 80% carbon dioxide and 20% methane, the goaf gas distribution was different to those primarily comprised of methane. Therefore, this study can provide guidance for underground coal mines experiencing similar geological conditions to determine proactive goaf inertisation parameters and effectively contain the onset and development of spontaneous heating in the goaf area.

In the future, more work will be performed to investigate the impact of goaf gas composition and seam orientations on goaf gas distribution characteristics and flow patterns in the goaf area and optimize the proactive goaf inertisation parameters to effectively and efficiently suppress spontaneous combustion and heating.

CHAPTER 4 INSIGHT INTO PROACTIVE INERTISATION STRATEGIES FOR SPONTANEOUS COMBUSTION MANAGEMENT DURING LONGWALL MINING OF COAL SEAMS WITH VARIOUS ORIENTATIONS

Summary

This chapter focuses on the impact of coal seam orientations on spatial gas distribution and proactive goaf inertisation strategies for spontaneous combustion management and prevention. The onset and development of spontaneous combustion in the goaf area are dictated by various seam conditions and operational parameters. Field observation and previous studies show that coal seam orientations could impact goaf gas flow dynamics and distribution characteristics, hence the occurrence of spontaneous heating in the goaf area. To fill this knowledge gap, extensive CFD modelling was conducted based on the three-dimensional model established in Chapter three, and nine different scenarios were studied. The coal seam orientations in this modelling study were dictated by the elevation of maingate (MG) and tailgate (TG) and the height of the longwall (LW) face and the start-up line. The impacts of coal seam orientations on spatial distribution characteristics of oxygen in the active LW goaf and the determination of proactive goaf inertisation strategies were investigated qualitatively and quantitatively. The modelling results provide new insight into the gas flow dynamics and spatial gas distribution in the active LW goaf with different coal seam orientations and develop better proactive goaf inertisation strategies, thus reducing the likelihood of spontaneous heating in the active LW goaf and improving health and safety in mining industry.

Citation

M Qiao, T Ren, J Roberts, X Yang, Z Li, & J Wu. Insight into proactive inertisation strategies for spontaneous combustion management during longwall mining of coal seams with various orientations. **Energy Sources, Part A: Recovery, Utilization, and Environmental Effects, 2023**.

https://doi.org/10.1080/15567036.2023.2191062

Abstract

Spontaneous combustion of coal occurs in the longwall (LW) goaf during mining cycles due to coal oxidation at low temperature and air ingress. Coal seam orientations, dictated by the elevation of the maingate (MG) and tailgate (TG) and the height of the working face and starting-up line, significantly impact gas distribution in the goaf. Despite this, there has been limited study on the effects of coal seam orientations on spontaneous heating management. To fill this knowledge gap, extensive computational fluid dynamics (CFD) modelling was conducted based on the actual conditions of an Australian underground coal mine and verified with onsite gas monitoring data, after which extensive parametric studies of how coal seam orientations influenced gas distribution were conducted. Simulation results indicate that coal seam orientations significantly impact spatial gas distribution in the LW goaf and development of proactive goaf inertisation strategies. Regardless of coal seam orientations, nitrogen performs better than carbon dioxide in reducing the oxidation zone area. In addition, at least 1.5 m^3/s of nitrogen is required to effectively prevent spontaneous heating, and the area ratio of oxidation zone to active goaf is approximately 10%, reducing by about 15% compared to scenarios without inertisation. The modelling results shed insight into goaf gas distribution characteristics under various coal seam orientations and provide guidance on developing corresponding proactive inertisation strategies for managing spontaneous heating in the goaf, thus improving mining safety.

Keywords

Spontaneous combustion; CFD modelling; Coal seam orientations; Goaf inertisation strategies; Heating management.

4.1. Introduction

As one of the principal hazards specified by the NSW Resources Regulator (2016), spontaneous combustion of coal is plaguing a large number of Australian underground coal mines, particularly those located in New South Wales and Queensland in which the abundant coal resources are located. Many incidents involving spontaneous combustion were reported in several underground mines in Australia during mining cycles, which posed a severe threat to mining safety. Spontaneous combustion of coal is able to provide sufficient heat to initiate methane explosion where both oxygen and methane levels are in the explosive range and cause devastating consequences, such as production delay and stoppage (Liu et al. 2021), personnel injury and death (Xue et al. 2022), environmental pollution (Tutak & Brodny 2017b) or permanent mine closure (Wang et al. 2018e). In many cases, it is not easy to detect spontaneous combustion and exactly locate the heating locations at the early onset and development of heating (Liu et al. 2022). Therefore, more emphasis should be placed on effectively preventing spontaneous heating from

taking place in the active longwall (LW) goaf area. In Australia, proactive goaf inertisation has been widely applied in underground coal mines during normal mining cycles to deplete or lower oxygen concentration to a safe level, thus preventing the occurrence of spontaneous heating in the active goaf (Qiao et al. 2022a). To develop effective proactive goaf inertisation strategies, there is a need to enhance the knowledge of how different gases are distributed in the LW goaf.

Due to the fact that the LW goaf area is inaccessible, Computational Fluid Dynamics (CFD) has been widely used to solve problems arising in this area, particularly spontaneous heating in the active goaf. Compared to traditional laboratory experiments and field testing, CFD simulations allow users to visualize the distribution of different gases in the hard-to-access goaf area and evaluate different engineering measures, thus providing fundamental knowledge that enables robust control and mitigation strategies for spontaneous-combustion-related problems to be developed (Xue et al. 2023). To shed light on addressing spontaneous combustion issues faced by underground collieries, Yuan et al. (2006) conducted numerical studies pertaining to the impact of ventilation schemes on airflow migration characteristics behind the working face and identified the potential critical velocity areas in which spontaneous heating can occur with a high probability. A three-dimensional model was constructed by Taraba and Michalec (2011) to better understand how the face advance rate impacted the occurrence of spontaneous combustion in the active LW goaf, and a critical advance rate at which spontaneous heating would progress into flaming was verified. More emphasis was placed by Morla et al. (2013) on spontaneous heating in the LW panel with thick mining seams, and the performance of different ventilation systems and the number of gas injection locations in containing spontaneous combustion were evaluated. Xia et al. (2014) carried out numerical simulations to understand the heating evolution in the active LW goaf and evaluated the impact of various operational parameters, including ventilation flow rate and resistance, face advance rate, and coal deformation caused by methane desorption, on the progress of spontaneous combustion. Tanguturi and Balusu (2015) analyzed the displacement characteristics of goaf gases under the condition of different panel orientations, while no discussions about goaf inertisation strategies were provided. Huang et al. (2018) investigated the influence of periodic weighting on spontaneous heating in the active LW goaf. Focusing on goaf inertisation in a 3-km-long panel, Balusu et al. (2019) found that a minimum of 1500 l/s was required to render the goaf atmosphere inert with multi-point injection preferred. Three-dimensional CFD models were constructed by Zhang et al. (2019a) to investigate the proactive and reactive inertisation strategies for the management of spontaneous heating, and an inertisation strategy exchange from the proactive case to the reactive case was identified. Based on specific geological conditions of shallowly buried coal seams, Zhuo et al. (2019) studied the distribution patterns of oxygen and carbon monoxide in the lower and upper parts of the goaf and identified

the major sources of carbon dioxide. In combination with laboratory experiments, field study and numerical simulations, Liu et al. (2020b) explored the gas distribution and spontaneous combustion development in triple goafs and proposed the optimal nitrogen injection location in the goaf area to effectively contain the spontaneous combustion. Li et al. (2020a) investigated the influence of air leakage on methane concentration in the LW goaf, and they found that stronger air leakage resulted in low methane concentration in the leakage locations. Efforts were made by Lu et al. (2020a) to numerically study the impact of gas drainage on spontaneous combustion, and the simulation results indicated that gas drainage could lower gas levels at the tailgate end but enlarge the area of spontaneous heating. Yang et al. (2021) conducted numerical simulations to study the impact of the air volume on gas distribution in the goaf using Y-type ventilation, and it was revealed that air quantity significantly impacted the area where the gas explosion and spontaneous combustion may occur. CFD modelling was applied by Li et al. (2021b) to research the impacts of ventilation flowrates and face advancing rates on the distribution of oxygen and methane in the goaf, and the simulation results showed the potential area where gas explosion and spontaneous heating could take place simultaneously. An investigation into the impact of air leakage from surface cracks on oxygen distribution in the goaf area was conducted by Zhuo et al. (2021), and the results indicated that a rise in air leakage volume could cause the width of spontaneous combustion zone gradually rose. Hou et al. (2022) explored the influence of the porosity of the adjacent goafs and active goaf pillars on oxygen distribution in the goaf, and they found that a reduction in the porosity of adjacent goafs and active goaf pillars assisted in managing spontaneous heating. Cheng et al. (2022) numerically studied the evolution of oxygen in the goaf area and carbon monoxide at the return corner, and a prediction method of spontaneous combustion status was proposed by considering the evolution of carbon monoxide.

From the above literature review, it is evident that previous studies mainly focus on the influence of many geological and mining conditions on gas flow dynamics in the active goaf area, mainly including goaf gas composition, goaf gas emission rate, thick mining seams, shallowly buried coal seams, ventilation patterns, face advance rate, coal deformation induced by methane desorption, ventilation resistance, periodic weighting, the length of LW panel, adjacent goafs, air leakage, gas drainage, airflow rate provided to the LW face, and the porosity of active goaf pillars. However, the impact of coal seam orientations on spatial gas distribution in the LW goaf and proactive goaf inertisation strategies for spontaneous heating management has had limited investigation. The research findings from Balusu et al. (2005a) and Tanguturi and Balusu (2015) revealed that coal seam orientations, dictated by the elevation of maingate (MG) and tailgate (TG) and the height of the LW face and the start-up line in mining operation, significantly impacted the as distribution in the LW goaf. However, they only considered four simple scenarios of coal seam orientations in

the goaf where goaf gas was primarily composed of methane, and the optimization of proactive goaf inertisation strategies was insufficiently investigated. In addition, the gas distribution patterns in the active goaf, where goaf gas mainly comprises carbon dioxide, under various coal seam orientations have not been studied in detail. Therefore, there is a need to conduct extensive CFD modelling simulations to bridge this knowledge gap to effectively manage and control spontaneous heating in the active goaf. In this chapter, the three-dimensional CFD model used in Section 3.6.2 was used. Nine typical scenarios of coal seam orientations were simulated, and gas distribution characteristics, particularly oxygen, were analyzed, after which the proactive goaf inertisation strategy for each scenario was optimized to prevent spontaneous combustion. In mining practice, it is impossible to choose the seam orientations, but this study is carried out for cases of what would happen if the coal seam and active goaf are inclined differently. In addition, the purpose of modelling concerns the selection of the technique for proactive goaf inertisation of the goaf atmosphere depending on the type of coal seams planned to be mined. Results from CFD modelling will enhance the knowledge of spatial gas distribution characteristics in the active goaf under different coal seam orientations, and provide guidance on developing effective proactive goaf inertisation strategies for preventing and managing spontaneous combustion, thus improving mining safety.

4.2. Results and Discussion

In order to gain a better insight into the influence of coal seam orientations on the spatial distribution of goaf gas and proactive goaf inertisation strategies, nine scenarios listed in Table 4.1 were numerically studied. Considering the angle of the coal seam in the dip and strike direction was approximately 1°, the difference in MG and TG elevation was set to be 15 m for the proposed scenarios (The dip angle was approximately 2°) for the sake of investigating the impact of seam orientations on the spatial distribution of goaf gas. Except for the change in the coal seam orientations, other parameters were kept unchanged, such as the ventilation scheme, goaf permeability distribution, goaf gas composition, emission rate, and other boundary conditions. Simulation results by Ren and Balusu (2009) indicated that an injection rate of 0.5 m^3/s was required to achieve a desirable goaf inertisation performance, and thus the inert gas injection rate was kept constant at 0.5 m^3/s. In addition, steady-state simulations were conducted, considering the easy comparison of the final state of O_2 distribution in the LW goaf for each scenario and saving computational time.

According to the difference in oxygen concentration, the goaf area could be classified into three different zones, including the consolidation zone (0%~5%), oxidation zone (5%~18%) and dissipation zone (18%~21%) (Qiao et al. 2022a). In the oxidation zone, spontaneous heating can

potentially occur due to sufficient oxygen and heat build-up. To quantitatively analyze the influence of coal seam orientations on oxygen distribution and proactive goaf inertisation strategies, the area ratio of oxidation zone to active goaf (ratio of OZA to GA) is calculated for further comparison.

Table 4.1 Different cases proposed and simulated

Case	The elevation of working face and starting-up line	The elevation of MG and TG side
1	Same elevation	Same elevation
2	The working face was 18m lower	Same elevation
3	The working face was 18m higher	Same elevation
4	Same elevation	MG side was 15m higher
5	Same elevation	MG side was 15 m lower
6	The working face was 18m lower	MG side was 15 m lower
7	The working face was 18m higher	MG side was 15 m lower
8	The working face was 18m lower	MG side was 15 m higher
9	The working face was 18m higher	MG side was 15 m higher

The simulation results of models without inert gas injection for the proposed scenarios are illustrated in Figure 4.1 and Figure 4.2. It could be observed that air ingress occurred at both sides of the active LW goaf, with oxygen levels higher than 5% at approximately 850 m behind the LW face for all cases. Oxygen levels at the MG of the active goaf were generally lower when the MG elevation was lower than the TG counterpart, compared to the case 1 where the coal seam was flat. Conversely, oxygen concentration at the TG of the active goaf was generally lower when the MG elevation exceeded the TG elevation in comparison to the case 1. In the vertical direction, it was noted that oxygen was mainly distributed above the coal seam and the air ingress distance at the MG of the active goaf (y=35 m) was longer than at the TG of the goaf (y=365 m) regardless of the coal seam orientations. The area ratios of the oxidation zone and active goaf for proposed cases are detailed in Table 4.2. It was evident that the area ratio of the oxidation zone to active goaf was always larger when the MG elevation was higher than the TG counterpart. It was indicated from the base-case simulations that the oxidation zone area was still large in the active LW goaf, thus inert gas injection was required for the purpose of effectively lowering the oxygen levels at which spontaneous combustion could be prevented.

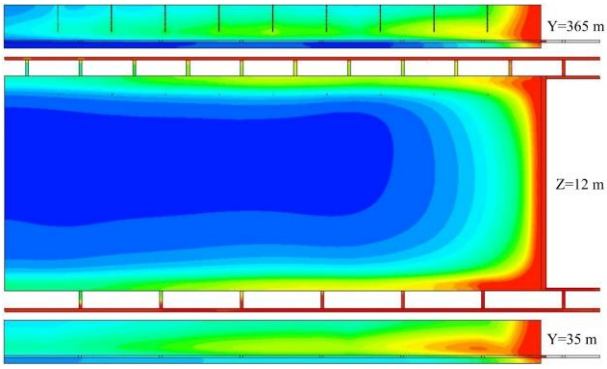

(a) Case1

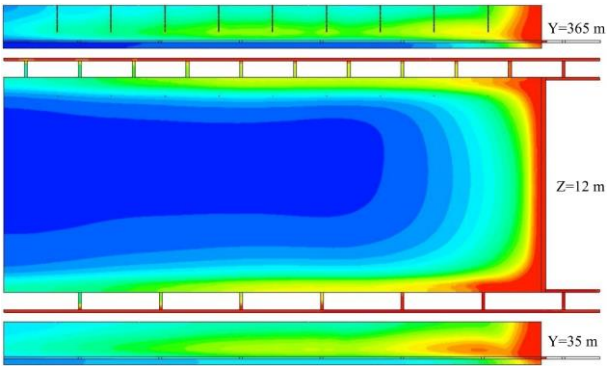

(b) Case2

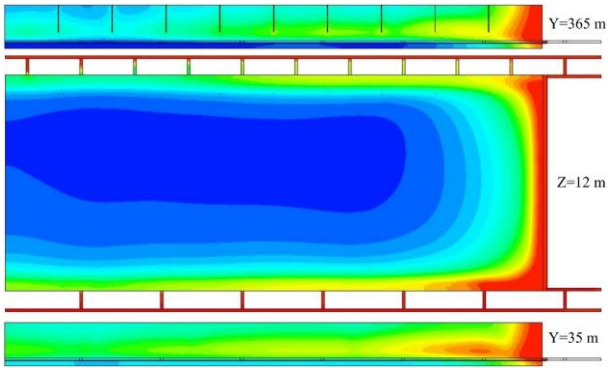

(c) Case3

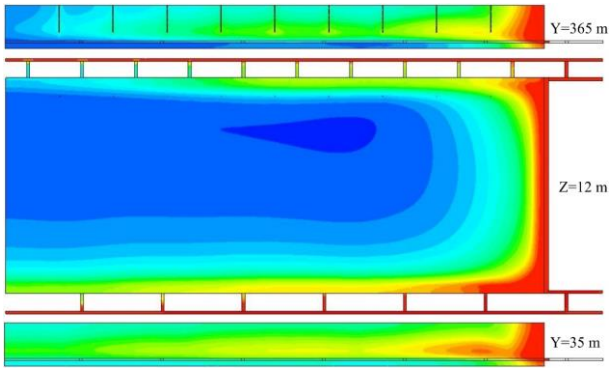

(d) Case4

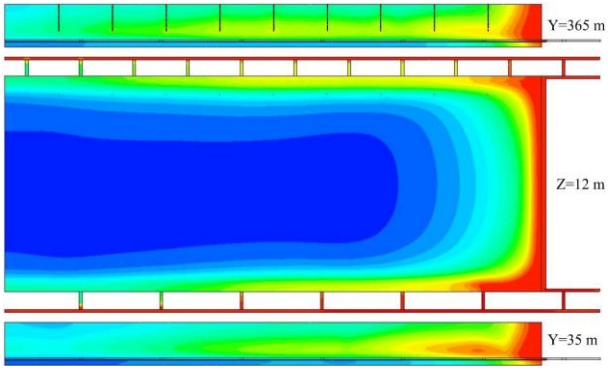

(e) Case5

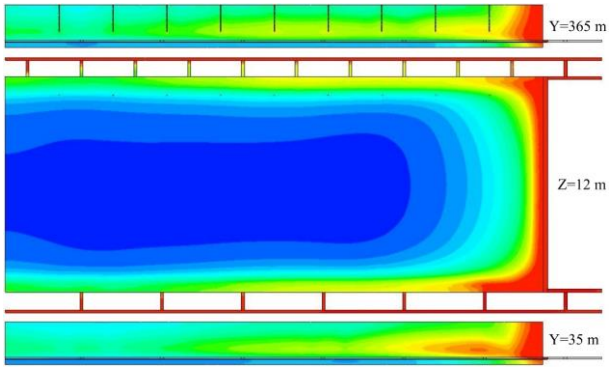

(f) Case6

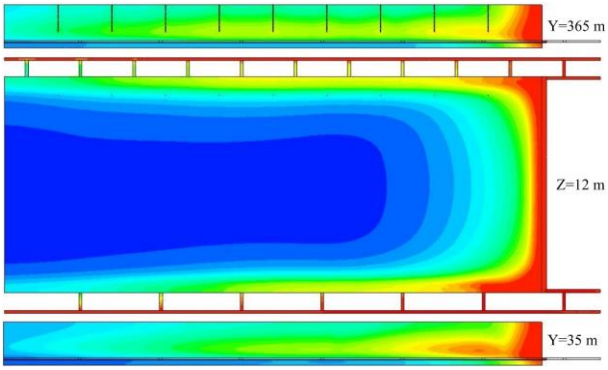

(g) Case7

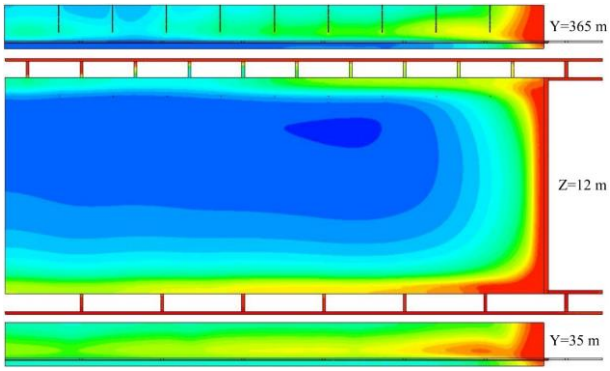

(h) Case8

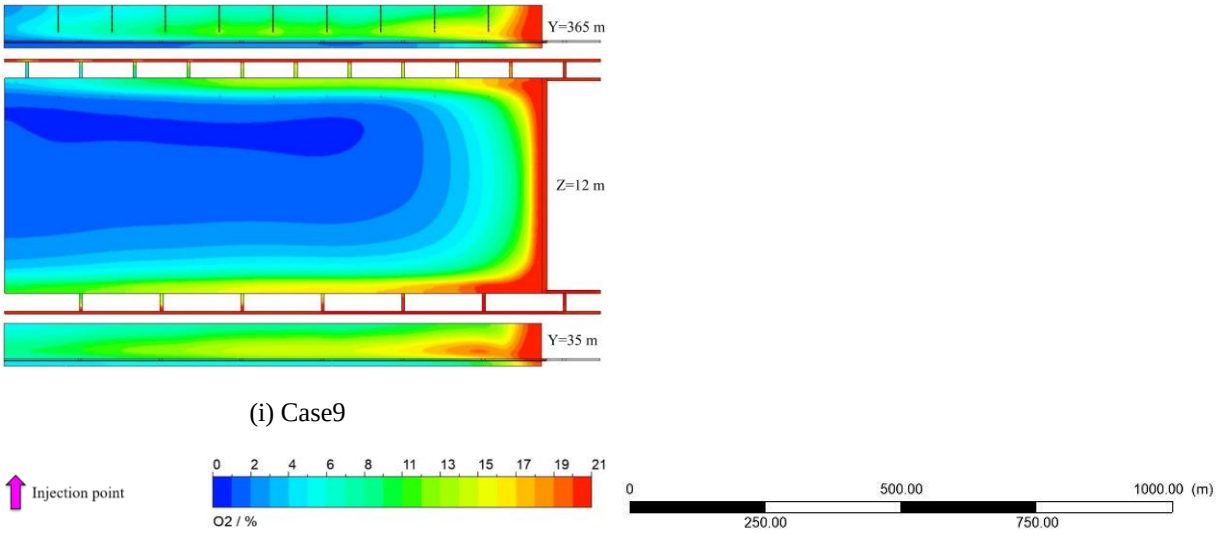

(i) Case9

Figure 4.1 Oxygen distribution in the LW panel for different scenarios

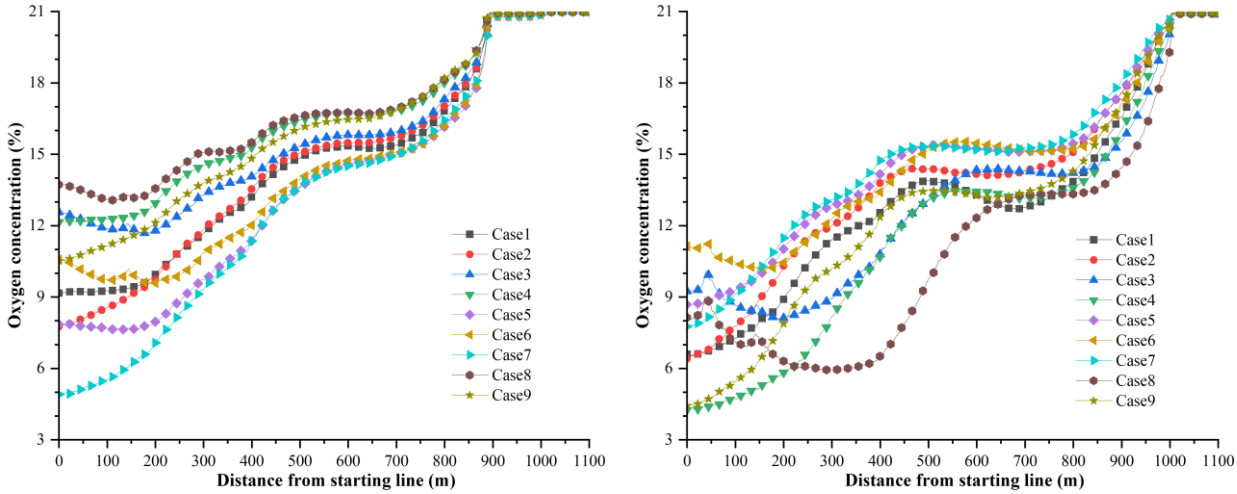

(a) MG (b) TG

Figure 4.2 Oxygen concentration at the MG and TG of the active goaf for different scenarios

Table 4.2 The area ratio of oxidation zone and active goaf for proposed scenarios

Scenario	Case1	Case2	Case3	Case4	Case5	Case6	Case7	Case8	Case9
Oxidation zone area (m^2)	101759	104468	103103	110627	100665	100860	100651	114957	111436
Ratio of OZA to GA (%)	25.4	26.1	25.8	27.7	25.2	25.2	25.2	28.7	27.9

4.2.1 Different inert gas injection locations

The inert gas injection locations exert a strong influence upon spatial gas distribution patterns in the active LW goaf, thus indicating the goaf inertisation performance. Typical injection locations include cut-throughs at the MG or TG of the active LW goaf or vertical surface drainage boreholes previously used for pre-drainage. It is recommended from the simulation results (Ren & Balusu 2009) that a flow rate of 0.5 m^3/s be required for inert gas injection to substantially limit air ingress

into the active LW goaf and effectively contain spontaneous heating. Therefore, a total nitrogen flow rate of 0.5 m^3/s was applied in this section. Only the oxygen distribution at 2 m from the seam floor (Z=12 m) in the active goaf was presented for comparison.

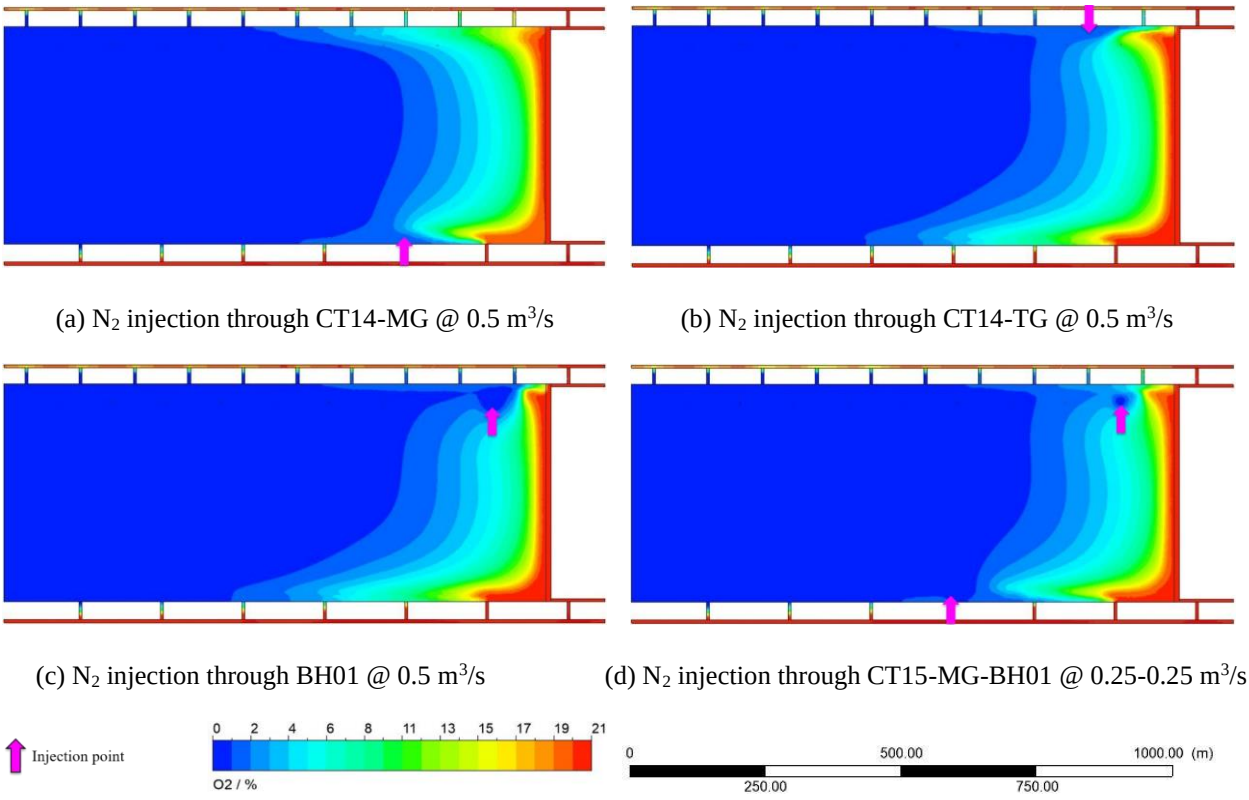

(a) N_2 injection through CT14-MG @ 0.5 m^3/s (b) N_2 injection through CT14-TG @ 0.5 m^3/s

(c) N_2 injection through BH01 @ 0.5 m^3/s (d) N_2 injection through CT15-MG-BH01 @ 0.25-0.25 m^3/s

Figure 4.3 Oxygen distribution in the LW panel for case 1 with different nitrogen injection locations

Figure 4.3 shows oxygen distribution in the LW panel for case 1 where the coal seam was flat. As shown in Figure 4.3(a), air ingress at the MG of the active goaf was considerably reduced with nitrogen being injected via CT14, whereas oxygen at the return side could still flow deep into the active goaf with a distance of approximately 250 m. In contrast, nitrogen injection at the TG of the active LW goaf at a close distance behind the LW face (e.g., CT14-TG in Figure 4.3(b) or BH01 in Figure 4.3(c)) could evidently limit air ingress at the same side, but low oxygen levels could be observed at the goaf stream, which could not meet the requirements for mining safety. Since oxygen ingress was noticeable on one side when nitrogen injection was operated on the other side, nitrogen injection on both sides of the active LW was numerically simulated and evaluated for the reduction in oxidation zone area and goaf inertisation performance. Simulation results indicated that optimal goaf inertisation was gained by pumping nitrogen into the active LW goaf via CT14-MG and BH01 at a flow rate of 0.25 and 0.25 m^3/s, as demonstrated in Figure 4.3(d). The oxidation zone area was approximately 42816 m^2, which was reduced by approximately 57.9% in comparison to the non-injection base case.

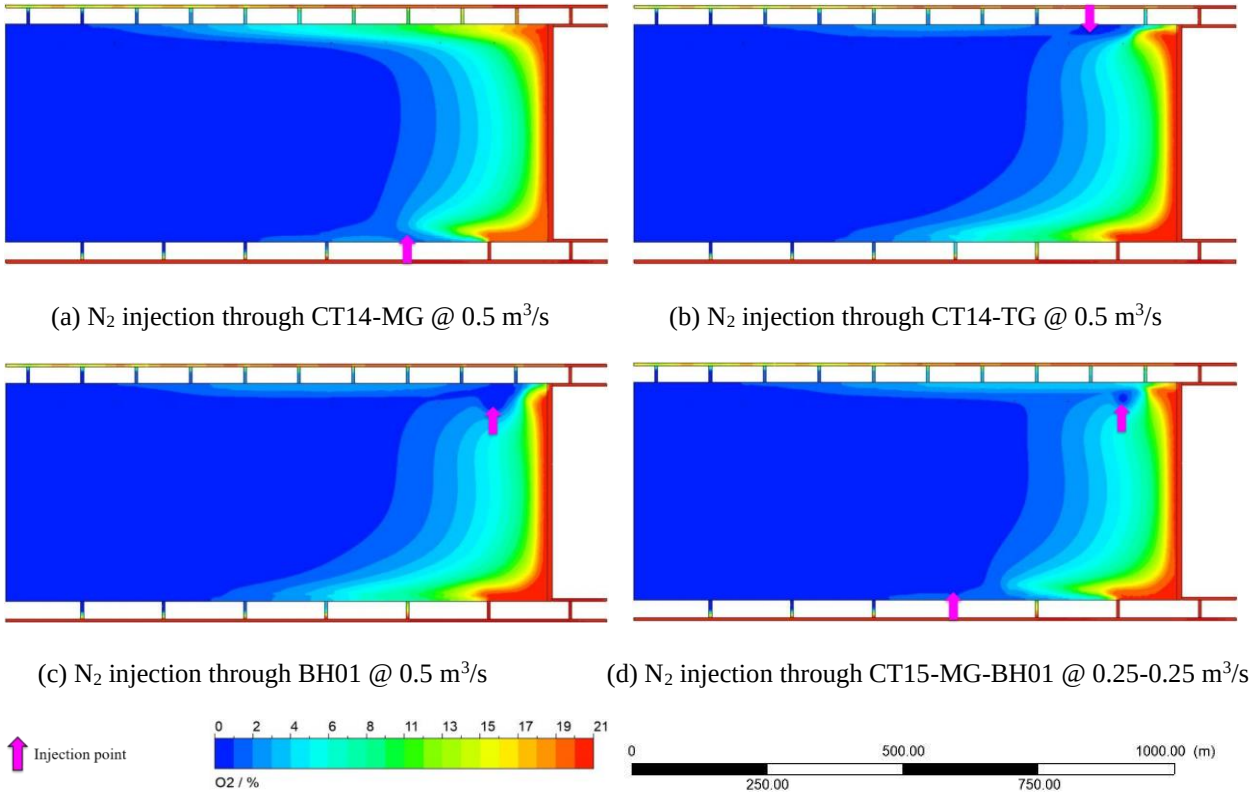

(a) N_2 injection through CT14-MG @ 0.5 m^3/s (b) N_2 injection through CT14-TG @ 0.5 m^3/s

(c) N_2 injection through BH01 @ 0.5 m^3/s (d) N_2 injection through CT15-MG-BH01 @ 0.25-0.25 m^3/s

Figure 4.4 Oxygen distribution in the LW panel for case 2 with different nitrogen injection locations

Figure 4.4 illustrates oxygen distribution in the LW panel with different nitrogen injection locations for case 2. It was observed in Figure 4.4(a) that air ingress at the MG of the active goaf was limited inbye of CT14-MG where nitrogen was injected, whilst oxygen flowed about 450 m deep into the TG side of active goaf. As for the scenarios where nitrogen was pumped at the return side of the active goaf at a close distance behind the LW face (e.g., CT14-TG in Figure 4.4(b) or BH01 in Figure 4.4(c)), although oxygen penetration at the same side was effectively limited, oxygen levels at the goaf stream were lower than the safety limit of 19.5% and oxygen migration at the MG of the active goaf was evident with oxygen volume fraction exceeding 5% at 350 m behind the LW face. With the injection point moving deep inside the TG of the active goaf, goaf inertisation performance became worse. Nitrogen injection at both sides of the LW goaf was simulated and analyzed, with typical results demonstrated in Figure 4.4(d) in which oxygen ingress on both sides of the LW goaf was limited. A desired spontaneous heating management performance was yielded by injecting nitrogen through CT15-MG and BH01 at a flow rate of 0.25 and 0.25 m^3/s, respectively. Its oxidation zone (43109 m^2) narrowed down by approximately 58.7% compared to the base scenario without injection.

Figure 4.5 depicts oxygen distribution in the LW panel with different nitrogen injection locations for case 3. As illustrated in Figure 4.5(a), air ingress at the MG of the LW goaf was reduced with nitrogen being pumping through CT14-MG, but oxygen at the return side was observed to flow into the deep goaf, with an oxygen volume fraction higher than 12% in the deep goaf. As the intake

injection point was relocated at a cut-through far away from the LW face, high-concentration oxygen could still be found at the TG of the active LW goaf, where spontaneous heating could occur with a higher probability. To prevent the occurrence of high oxygen zone at the TG of the deeper goaf, nitrogen should be pumped at the TG of the LW goaf at an appropriate location. The simulation results indicated that the injection point should be located at least 600 m behind the LW face, as shown in Figure 4.5(b) and (c). For scenarios with nitrogen injected at both sides of the LW goaf or through two locations at the return side, the nitrogen injection point at the TG of the LW goaf should be placed at least 800 m behind the LW face with a view to avoiding high-concentration oxygen at the TG of the deeper goaf, as illustrated in Figure 4.5(d). Modelling results indicated that nitrogen injection through BH06 (oxidation zone area: 50243 m^2) performed slightly better than CT16-MG-BH08 (oxidation zone area: 51534 m^2), which enabled the oxidation zone area to be reduced by approximately 51.3% in comparison to the scenario without inert gas injection.

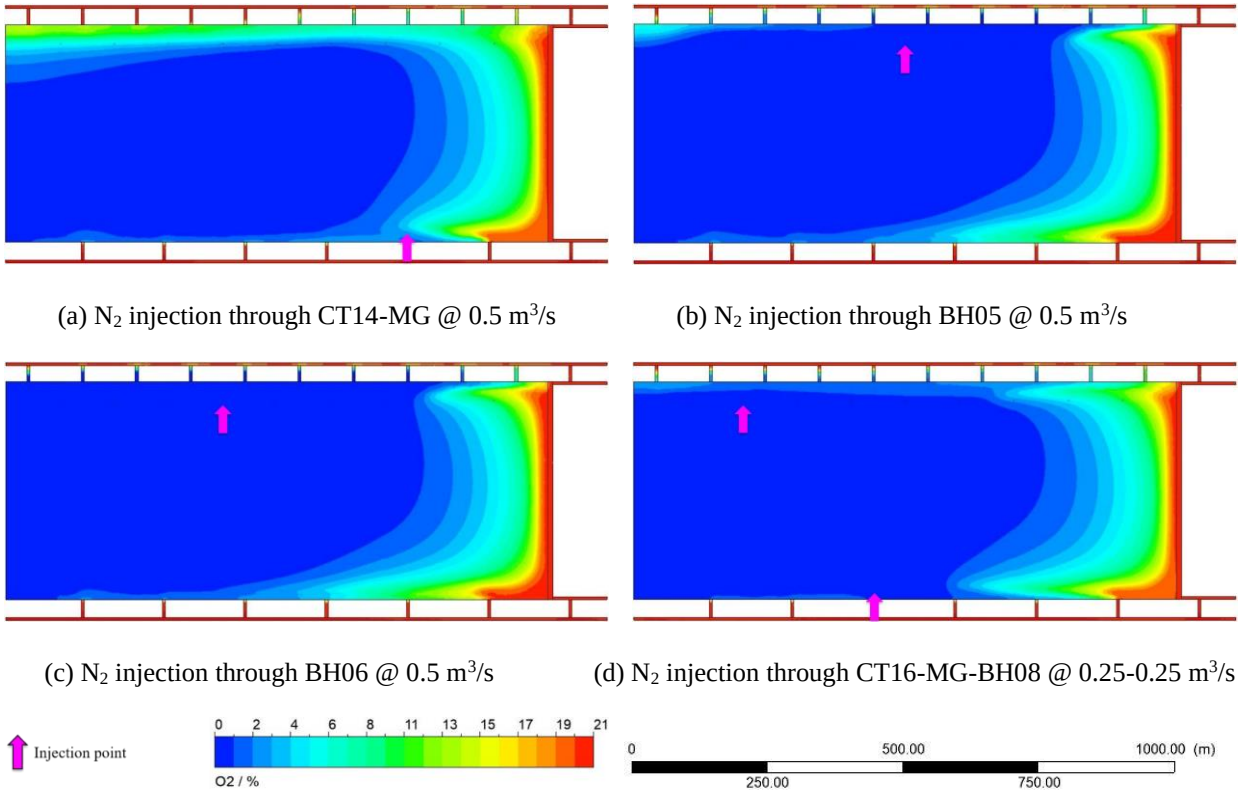

(a) N_2 injection through CT14-MG @ 0.5 m^3/s (b) N_2 injection through BH05 @ 0.5 m^3/s

(c) N_2 injection through BH06 @ 0.5 m^3/s (d) N_2 injection through CT16-MG-BH08 @ 0.25-0.25 m^3/s

Figure 4.5 Oxygen distribution in the LW panel for case 3 with different nitrogen injection locations

Figure 4.6 presents oxygen distribution in the LW panel with different nitrogen injection locations for case 4. As shown in Figure 4.6(a), a high-oxygen zone with a concentration higher than 5% could be found in the vicinity of CT15 and CT16 at the intake side of the LW goaf with nitrogen injection being performed through CT14-MG. This high-oxygen zone disappeared as the injection location moved from CT14-MG to CT15-MG, as shown in Figure 4.6(b). Although air ingress distance at the MG of the active LW goaf could be dramatically decreased with nitrogen being

pumped through BH01 shown in Figure 4.6(c), some nitrogen could flush onto the LW face, resulting in oxygen levels lower than 19.5% at the localized TG end. The modelling results showed that nitrogen injection at both sides of the LW goaf could mitigate air ingress on both sides. A decent goaf inertisation results could be produced when nitrogen was pumped through CT16-MG and BH01 at a flow rate of 0.333 and 0.167 m^3/s, respectively, and its oxidation zone area (44981 m^2) was reduced by approximately 59.3% when compared to the non-injection base case (110627 m^2).

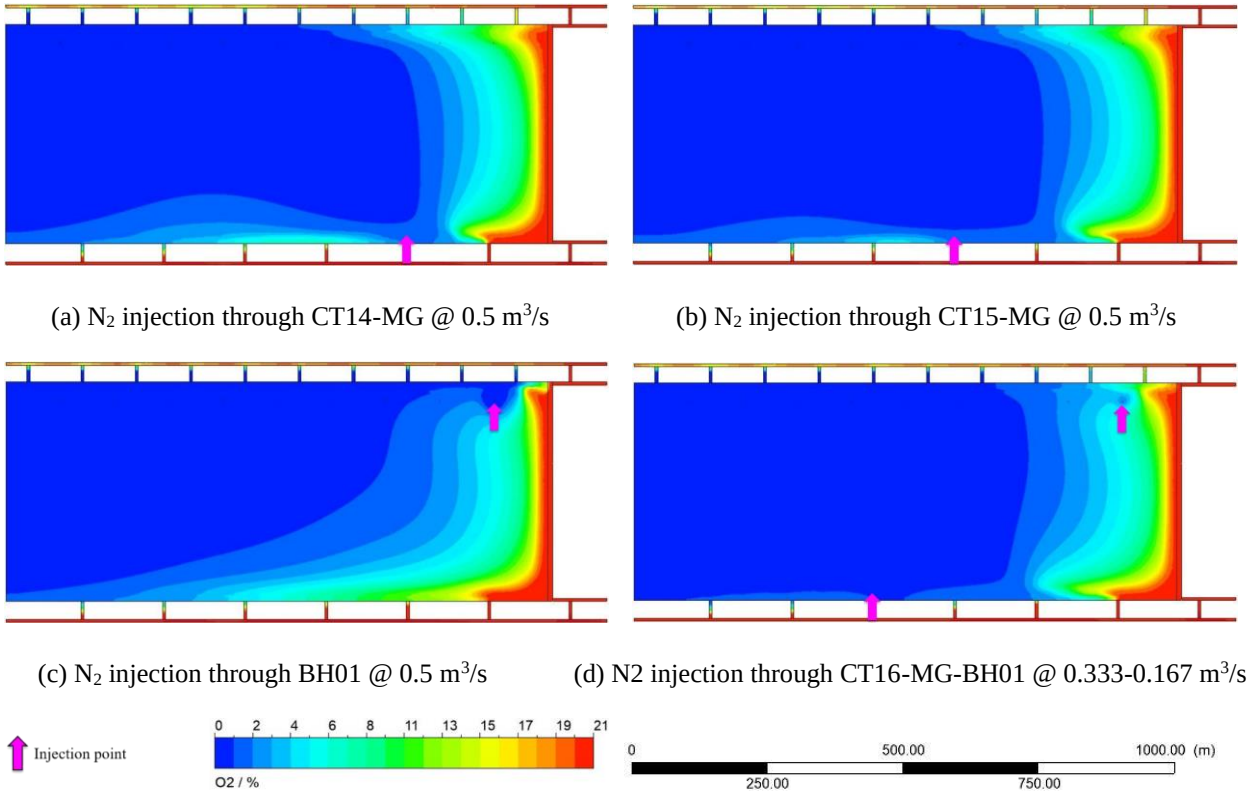

(a) N_2 injection through CT14-MG @ 0.5 m^3/s

(b) N_2 injection through CT15-MG @ 0.5 m^3/s

(c) N_2 injection through BH01 @ 0.5 m^3/s

(d) N2 injection through CT16-MG-BH01 @ 0.333-0.167 m^3/s

Figure 4.6 Oxygen distribution in the LW panel for case 4 with different nitrogen injection locations

Figure 4.7 demonstrates oxygen distribution in the LW panel with different nitrogen injection locations for case 5. As depicted in Figure 4.7(a) and (b), sole nitrogen injection at one side of the active LW goaf could limit air ingress at the same side, but oxygen at the other side still penetrated a longer distance into the LW goaf. Nitrogen pumping at both sides of the LW goaf was further simulated and analyzed, with typical results shown in Figure 4.7(c) and (d). Compared to case (c) where a stream of oxygen with a volume fraction exceeding 5% could leak about 550 m into the LW goaf (return side), air ingress at the TG of the active LW goaf was limited in case (d), with oxygen levels lowering to 5% at about 100 m behind the LW face. The optimal inertisation plan was to pump nitrogen through CT16-MG and BH01 at a flow rate of 0.25 and 0.25 m^3/s, which could reduce the oxidation zone area by approximately 58.7% compared to the base-case scenario without nitrogen injection.

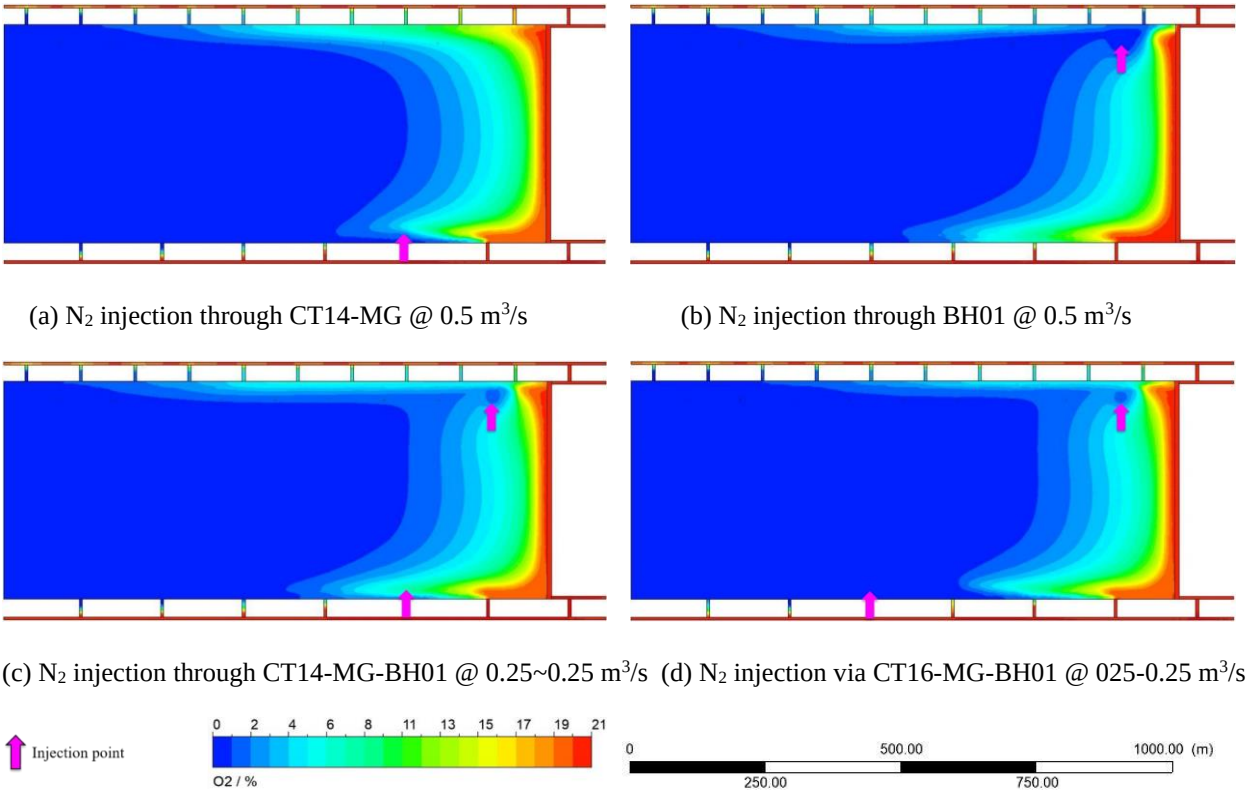

(a) N_2 injection through CT14-MG @ 0.5 m^3/s (b) N_2 injection through BH01 @ 0.5 m^3/s

(c) N_2 injection through CT14-MG-BH01 @ 0.25~0.25 m^3/s (d) N_2 injection via CT16-MG-BH01 @ 025-0.25 m^3/s

Figure 4.7 Oxygen distribution in the LW panel for case 5 with different nitrogen injection locations

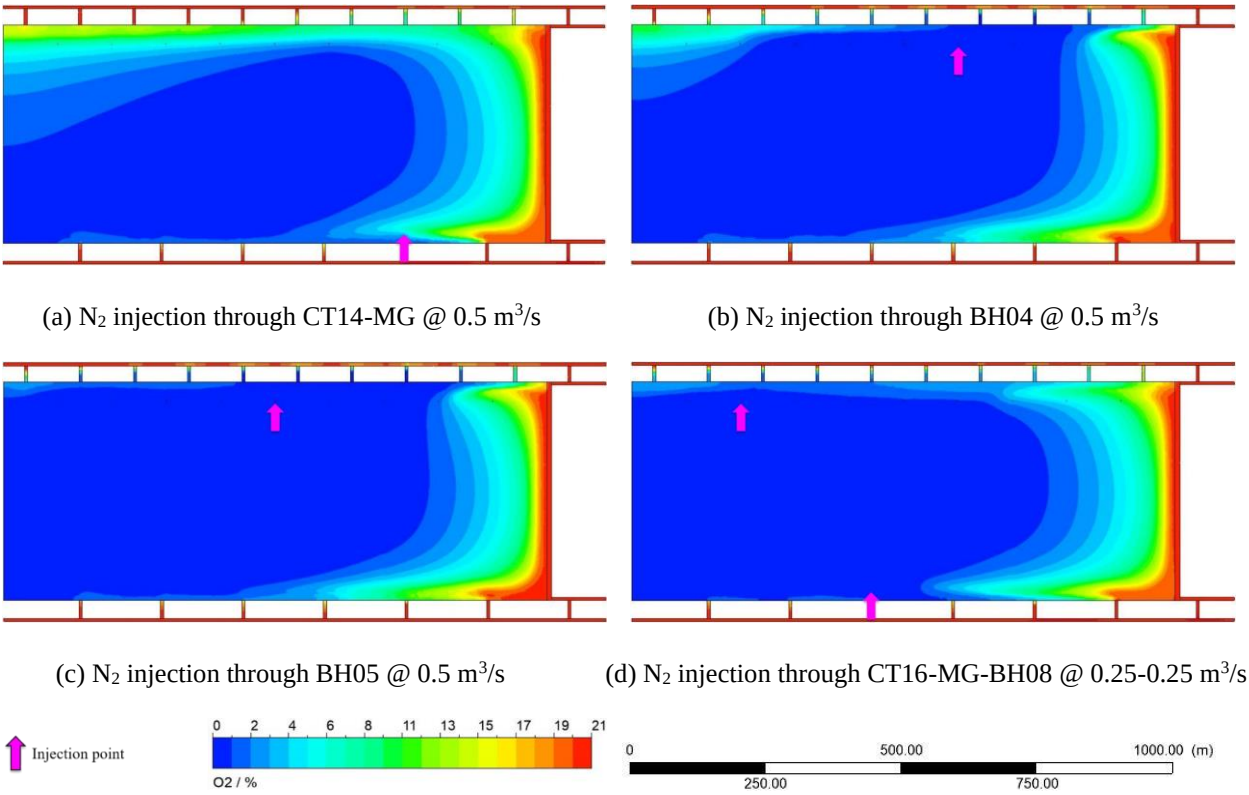

(a) N_2 injection through CT14-MG @ 0.5 m^3/s (b) N_2 injection through BH04 @ 0.5 m^3/s

(c) N_2 injection through BH05 @ 0.5 m^3/s (d) N_2 injection through CT16-MG-BH08 @ 0.25-0.25 m^3/s

Figure 4.8 Oxygen distribution in the LW panel for case 6 with different nitrogen injection locations

Figure 4.8 shows oxygen distribution in the LW panel with different nitrogen injection locations for case 6. It is noted from Figure 4.8(a) that although nitrogen injection through CT14-MG could limit air ingress at the MG of the active LW goaf, oxygen levels at the TG of the deeper LW goaf

were quite high, which was similar to case 3. However, nitrogen injection performed at appropriate locations at the TG of the LW goaf could mitigate air ingress at both sides of the LW goaf. Regarding the scenarios where nitrogen was solely pumped through one location at the TG of the active goaf, the injection point was best located at least 500 m behind the LW face to avoid the occurrence of potential heating at the TG of the deeper LW goaf, as illustrated in Figure 4.8(b) and (c). As for the cases where nitrogen injection was operated at both sides of the LW goaf or through two different sites at the TG of the LW goaf, the injection point at the return side should be located at least 800 m behind the LW face for the purpose of preventing oxygen from accumulating at the TG of the deeper LW goaf. The analysis of modelling results indicated that nitrogen injection through BH05 (oxidation zone area: 46875 m^2) performed better than injection through CT16-MG and BH08 (oxidation zone area: 51123 m^2), which caused the oxidation zone area to reduce by approximately 53.5%.

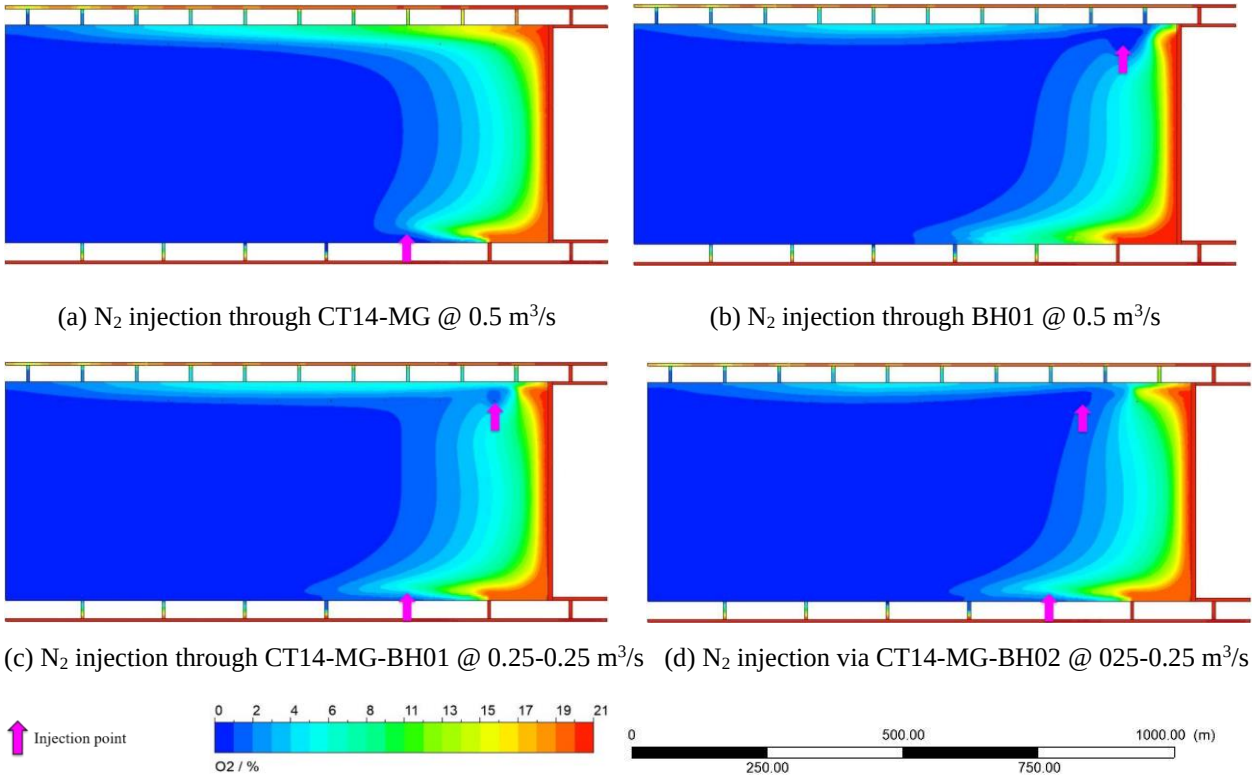

(a) N_2 injection through CT14-MG @ 0.5 m^3/s

(b) N_2 injection through BH01 @ 0.5 m^3/s

(c) N_2 injection through CT14-MG-BH01 @ 0.25-0.25 m^3/s

(d) N_2 injection via CT14-MG-BH02 @ 025-0.25 m^3/s

Figure 4.9 Oxygen distribution in the LW panel for case 7 with different nitrogen injection locations

Figure 4.9 illustrates oxygen distribution in the LW panel with different nitrogen injection locations for case 7, which was similar to case 5. Nitrogen injection on one side of the goaf could reduce air ingress on the same side, while high-concentration oxygen could still flow deeply into the active LW goaf on the other side, as illustrated in Figure 4.9(a) and (b). When nitrogen was pumped at both sides of the LW goaf through proper locations, air leakage on both sides could be reduced. When nitrogen injection was performed through CT14-MG-BH01, it was noticeable that oxygen at the return side could migrate deeply into the active LW goaf, which increased the

potential of spontaneous heating. To prevent oxygen from flowing deep into the TG goaf, the nitrogen injection point at the TG of the active LW goaf was required to be set at least 200 m behind the LW face. The optimal inertisation strategy was to pump nitrogen through CT14-MG and BH02 at a flow rate of 0.25 and 0.25 m^3/s, resulting in the oxidation zone area decreasing by 56.4% in comparison to the scenario without nitrogen injection.

Figure 4.10 depicts oxygen distribution in the LW panel with different nitrogen injection locations for case 8, which was similar to case 2 and case 5. As demonstrated in Figure 4.10(a), nitrogen injection solely performed at the MG of the active LW goaf could stop air from flowing deep into the LW goaf at the intake side, but air ingress at the return side was still evident at the TG of the deeper LW goaf, resulting in spontaneous heating potentially occurring at this area. In order to effectively limit air leakage at the TG of the deep LW goaf and decrease the oxidation zone area, it would be better to locate nitrogen injection at the TG of the LW goaf at least 500 m and 800 m behind the LW face for the case of sole nitrogen injection at one TG location and two nitrogen injection locations (either at both sides of the LW goaf or only at the TG of LW goaf), respectively. The analysis of modelling results indicated that nitrogen injection through CT16-MG and BH08 (oxidation zone area: 52740 m^2) performed slightly better than injection through BH05 (oxidation zone area: 52997 m^2), and reduced the oxidation zone area by approximately 54.1% in comparison to the scenario without nitrogen injection.

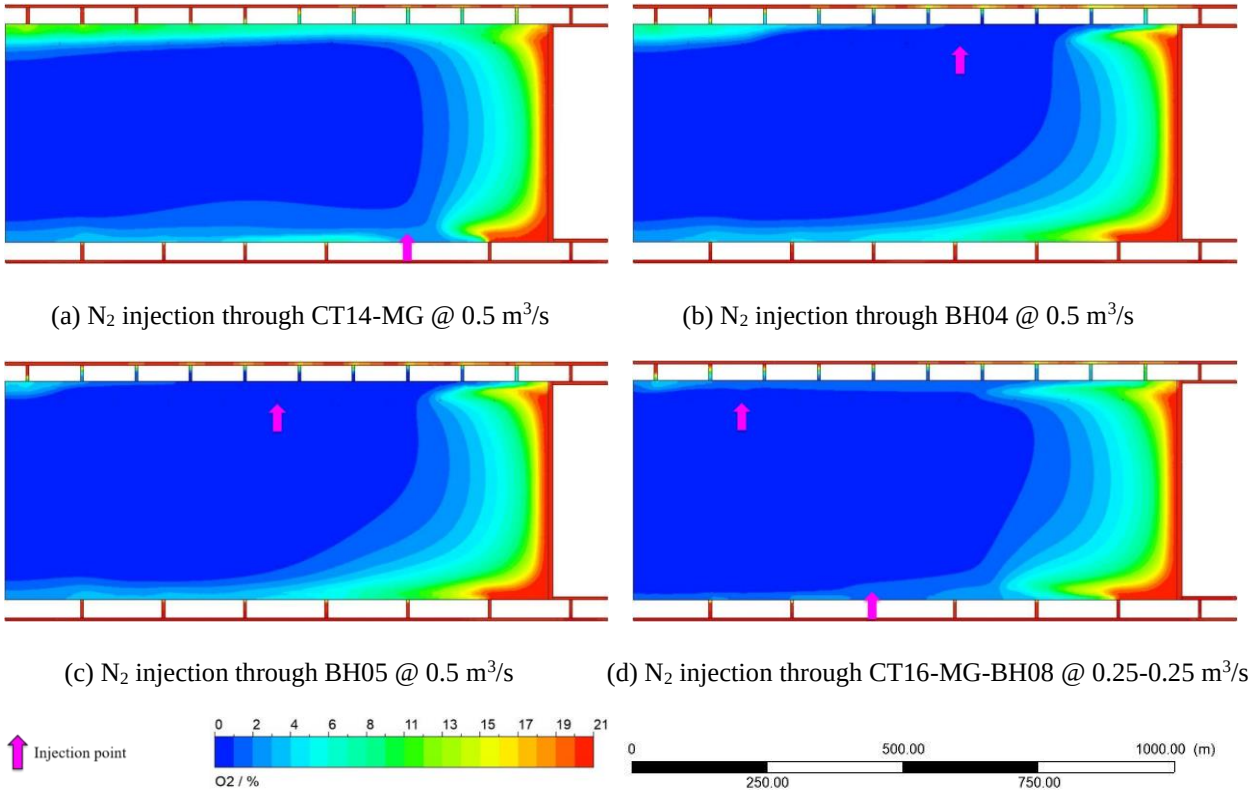

(a) N_2 injection through CT14-MG @ 0.5 m^3/s

(b) N_2 injection through BH04 @ 0.5 m^3/s

(c) N_2 injection through BH05 @ 0.5 m^3/s

(d) N_2 injection through CT16-MG-BH08 @ 0.25-0.25 m^3/s

Figure 4.10 Oxygen distribution in the LW panel for case 8 with different nitrogen injection locations

Figure 4.11 demonstrates oxygen distribution in the LW panel with different nitrogen injection locations for case 9, which was similar to case 4. As depicted in Figure 4.11(a), when nitrogen was pumped through CT14-MG, a stream of oxygen with a volume fraction exceeding 5% occurred in the vicinity of CT15 and CT16 at the MG of the active goaf. To prevent high-level oxygen from accumulating in this specific area, the nitrogen injection point at the MG of the active LW goaf was required to locate at least 400 m behind the LW face, as illustrated in Figure 4.11(b). As for the scenario of nitrogen injection at the TG of the LW goaf, the results showed that air migration at the MG of the LW goaf was evident, with oxygen levels exceeding 5% even at 500 m behind the LW face. Conversely, air leakage was mitigated at both sides of the LW goaf when nitrogen was pumped on both sides. A better goaf inertisation performance was obtained by pumping nitrogen through CT15-MG and BH01 at a flow rate of 0.25 and 0.25 m^3/s. and the oxidation zone area was 45063 m^2, which dropped by 59.6% compared to the base-case scenario without nitrogen injection.

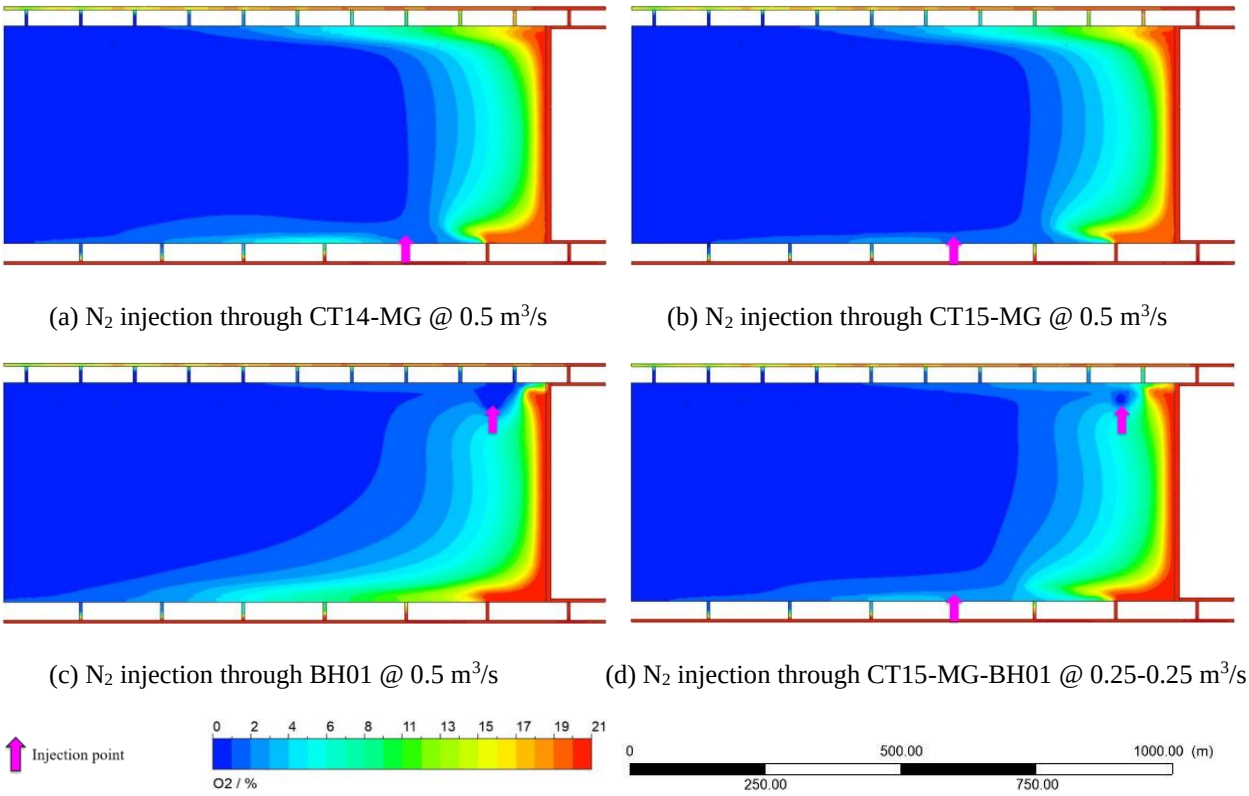

(a) N_2 injection through CT14-MG @ 0.5 m^3/s

(b) N_2 injection through CT15-MG @ 0.5 m^3/s

(c) N_2 injection through BH01 @ 0.5 m^3/s

(d) N_2 injection through CT15-MG-BH01 @ 0.25-0.25 m^3/s

Figure 4.11 Oxygen distribution in the LW panel for case 9 with different nitrogen injection locations

Considering the chainage of CT15-MG was almost the same as that of BH04 in the strike direction, and the distance between CT16-MG and the LW face was the same as that between CT18-TG and the LW face, the oxidation zone area under these four nitrogen strategies is listed in Table 4.3. It was evident that nitrogen injection at the MG of the active LW goaf yielded a better result in goaf inertisation for case 4 and case 9, whereas nitrogen injection at the TG of the LW goaf performed better for all other scenarios except for case 1.

When the elevation of MG was the same as that of the TG (case 1, case 2 and case 3), better goaf inertisation performance was generated with nitrogen injected at the TG of the active LW goaf, particularly via the surface borehole. If the starting-up line was 18 m higher than the working face in terms of elevation, nitrogen injection locations should be set at a distance of 500~600 m behind the LW face for the purpose of avoiding high-level oxygen at the TG of the deeper LW goaf. However, if the starting-up line was 18 m lower than or at the same height as the working face, the nitrogen injection location at the TG of the LW goaf could be at about 100 m behind the LW face with an appropriate injection rate to avoid a low oxygen level at the goaf stream. This goaf inertisation strategy was also applicable to the condition where the MG was 15 m lower than the TG in elevation (case 5, case 6, and case 7). However, when the MG was 15 m higher than the TG, it would be better to pump nitrogen at the MG of the active LW goaf if the working face was 18 m higher than or at the same elevation as the starting-up line (case 4 and case 9). If the starting-up line was 18 m higher than the LW face, nitrogen should be injected at the TG of the LW goaf even though the MG side was 15 m higher than the TG side (case 8).

Table 4.3 Comparison of the oxidation zone area for different scenarios

Scenario	Oxidation zone area (m^2)			
	CT15-MG	**BH04**	**CT16-MG**	**CT18-TG**
1	49311	48278	49252	51441
2	54976	49836	54701	52890
3	68724	54391	67181	54651
4	47522	52096	49205	56331
5	52567	46281	50591	49823
6	74700	52603	71400	49833
7	58208	47584	58259	50899
8	63232	57522	64019	60274
9	52718	56392	53752	58863

To summarise, when the working face was at the same elevation as (case 1, case 4 and case 5) or 18 m higher than (case 3, case 7 and case 9) the starting-up line, it would be better to inject nitrogen at the MG of the active LW goaf if the MG was 15 m higher than the TG, otherwise nitrogen should be injected on the TG side. However, for scenarios where the working face was 18 m lower than the starting-up line (case 2, case 6 and case 8), nitrogen should be injected at the TG of the LW goaf regardless of the difference in the elevation of the MG and TG.

4.2.2 Different types of inert gas

Three kinds of inert gas have been widely applied in Australian underground coal mines with a view to reducing oxygen volume fraction to a safer level at which spontaneous heating could be effectively contained, including nitrogen, boiler gas (85% N_2, 14% CO_2, and 1% O_2), and carbon dioxide (Balusu et al. 2005b; Ren & Balusu 2009). Considering the majority of component of boiler gas is nitrogen, only pure nitrogen and carbon dioxide injection was compared. To study the influence of different inert gas on oxygen distribution and goaf inertisation performance under different coal seam orientations, numerical simulations were conducted for the nine proposed scenarios. Only representative simulation results are shown below.

Figure 4.12 shows the distribution of the oxidation zone in the active LW goaf for case 2, in which different inert gas was pumped through CT15-MG and BH01 at a flow rate of 0.25 and 0.25 m^3/s, respectively. The oxidation zone area was smaller with nitrogen injection (43109 m^2) in comparison to carbon dioxide injection (77255 m^2). When carbon dioxide was pumped into the LW goaf, high-concentration oxygen could flow deep into the active LW goaf at the return side, which would increase the likelihood of spontaneous heating.

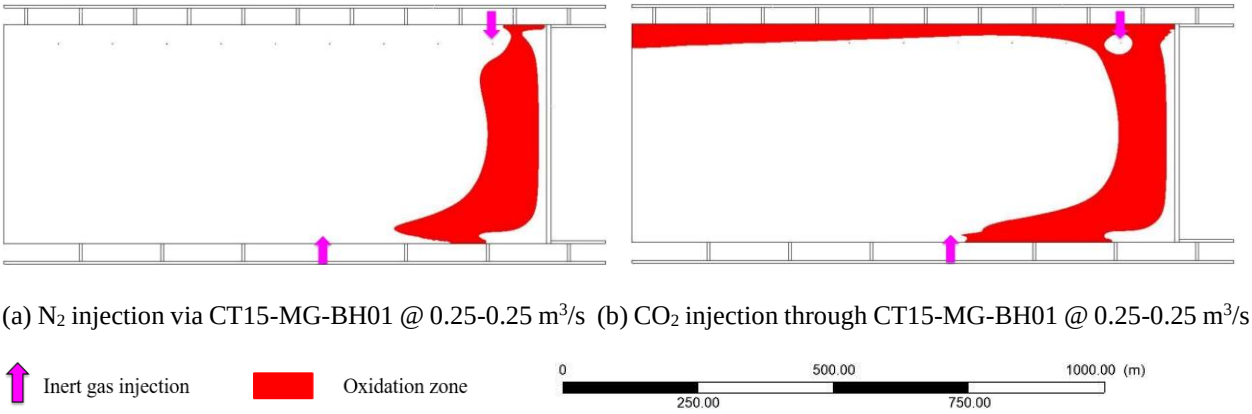

(a) N_2 injection via CT15-MG-BH01 @ 0.25-0.25 m^3/s (b) CO_2 injection through CT15-MG-BH01 @ 0.25-0.25 m^3/s

Figure 4.12 Oxidation zone distribution of case 2 with inert gas injected via CT15 -MG and BH01 at a rate of 0.25 and 0.25 m^3/s

Figure 4.13 presents the distribution of the oxidation zone in the active LW goaf for case 6, in which different inert gas was pumped into the active LW goaf through BH05 at a flow rate of 0.5 m^3/s. It was also evident that nitrogen performed better in reducing the oxidation zone area in the active LW goaf than carbon dioxide. Oxygen accumulation was found at the TG of the deeper LW goaf when Carbon dioxide was pumped into the active LW goaf through BH05, which could increase the propensity for spontaneous heating in this area.

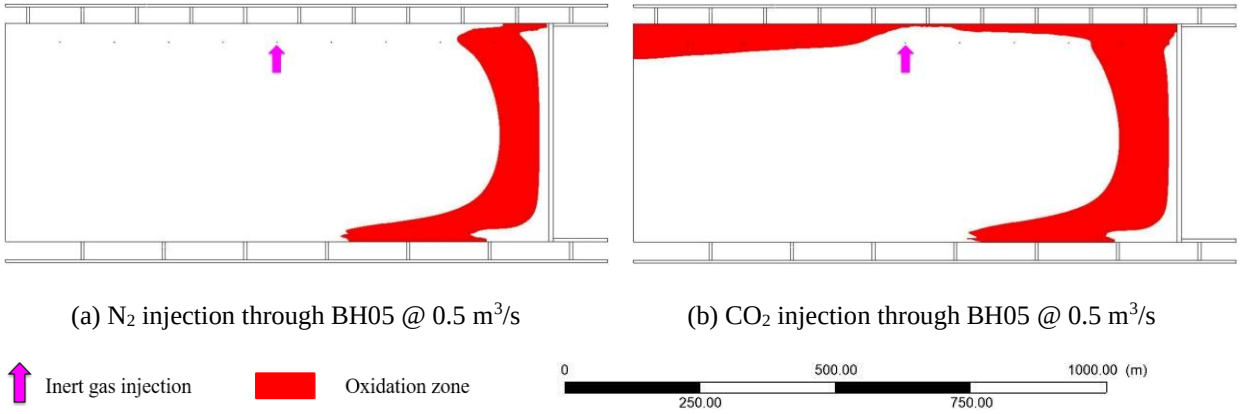

(a) N_2 injection through BH05 @ 0.5 m^3/s (b) CO_2 injection through BH05 @ 0.5 m^3/s

Figure 4.13 Oxidation zone distribution of case 6 with inert gas injected via BH05 at a flow rate of 0.5 m^3/s

Table 4.4 Comparison of oxidation zone area for different gas inertisation strategies

Case	Inert gas injection locations	Oxidation zone area (m^2)	
		N_2	CO_2
1	CT15-MG-BH01 @ 0.25-0.25 m^3/s	42816	54390
2	CT15-MG-BH01 @ 0.25-0.25 m^3/s	43109	77255
3	BH06 @ 0.5 m^3/s	50243	73523
4	CT16-MG-BH01 @ 0.333-0.167 m^3/s	44981	58168
5	CT16-MG-BH01 @ 0.25-0.25 m^3/s	41594	57439
6	BH05 @ 0.5 m^3/s	46875	80878
7	CT14-MG-BH02 @ 0.25-0.25 m^3/s	43877	53113
8	CT16-MG-BH08 @ 0.25-0.25 m^3/s	52740	77748
9	CT15-MG-BH01 @ 0.25-0.25 m^3/s	45063	59673

Table 4.4 lists the oxidation zone area based on the optimal inert gas injection locations for different proposed scenarios. Regardless of the coal seam orientations, proactive goaf inertisation with nitrogen could produce better results than carbon dioxide in limiting air ingress at both sides of the active LW goaf and minimizing the oxidation zone area. Therefore, it is recommended that nitrogen should be used for goaf inertisation when the seam gas is predominantly comprised of carbon dioxide and less methane.

4.2.3 Injection flow rates

When nitrogen was pumped into the active LW goaf through optimal locations, the decrease in the oxidation zone area for the nine proposed scenarios ranged from 51.3% to 60.4%. However, there was still a big oxidation zone in the goaf area. Therefore, there is a need to optimize nitrogen injection flow rates to suppress spontaneous combustion and heating. With regard to case 3 and case 6, oxygen concentration at the goaf stream would be lower than the statutory limit as nitrogen

flow rates at the surface borehole continued to increase. As a result, to study the influence of nitrogen flow rate on spontaneous heating control for case 3 and case 6, the nitrogen injection rate at the surface borehole was kept constant at 0.5 m^3/s, and nitrogen was simultaneously pumped into the active LW goaf through CT14-MG with gradually increasing flow rate. As for the other cases where nitrogen was pumped at both sides of the LW goaf, the continued rise in nitrogen flow rate at the TG injection locations could cause nitrogen to flow onto the LW face and decrease the oxygen volume fraction at the goaf stream. Therefore, the nitrogen flow rate at the TG injection location was kept constant, but the rate at the MG injection location gradually increased for these scenarios. The increment of the nitrogen flow rate was set as 0.25 m^3/s. Numerical simulations were conducted for nine scenarios, but only representative simulation results are presented below.

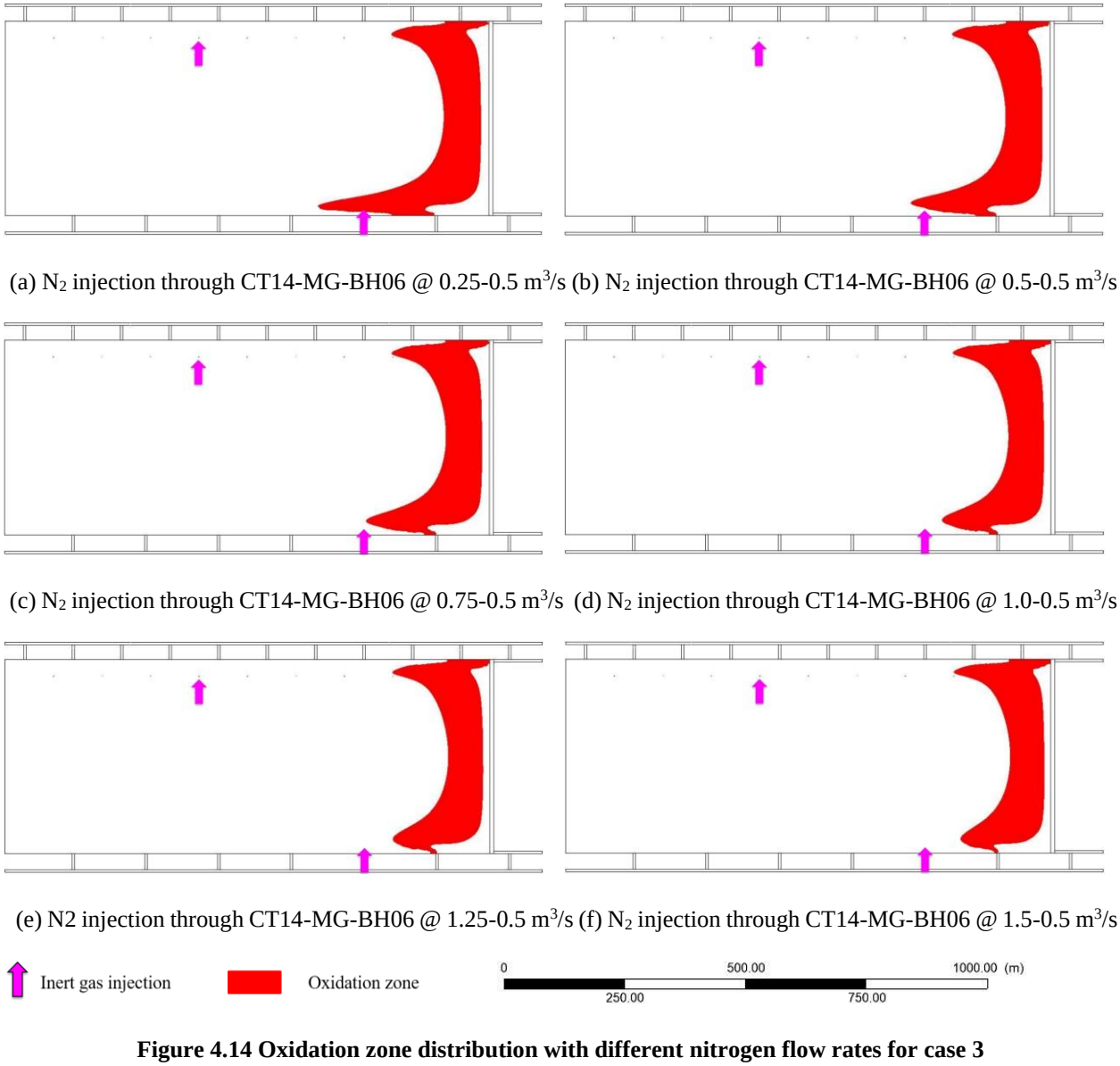

Figure 4.14 Oxidation zone distribution with different nitrogen flow rates for case 3

With regard to case 3, it was evident from Figure 4.14 that the oxidation zone area reduced with an increase in the nitrogen injection rate. The reduction rate of the oxidation zone area decreased

gradually with increasing injection rate, and it is suggested that 1.5 m^3/s could be an optimum value based on these results, as depicted in Figure 4.15.

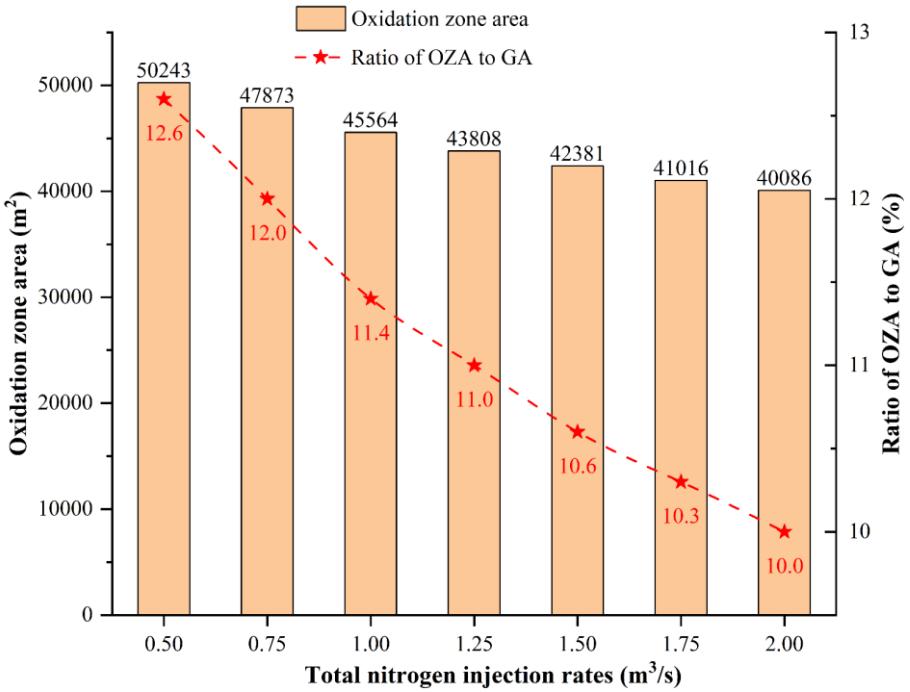

Figure 4.15 Oxidation zone area with different nitrogen flow rates for case 3

Figure 4.16 illustrates oxidation zone distribution in the active LW goaf with different nitrogen injection rates for case 7. It was noted from Figure 4.16 that the oxidation zone area narrowed down as total nitrogen flow rates rose. When the total nitrogen injection rate hit 1.5 m^3/s, the reduction rate of the ratio of OZA to GA decreased as the nitrogen flow rate continued to rise, as depicted in Figure 4.17. The oxygen volume fraction at about 200 m behind the LW face dropped below 5% with a nitrogen flow rate of 1.5 m^3/s.

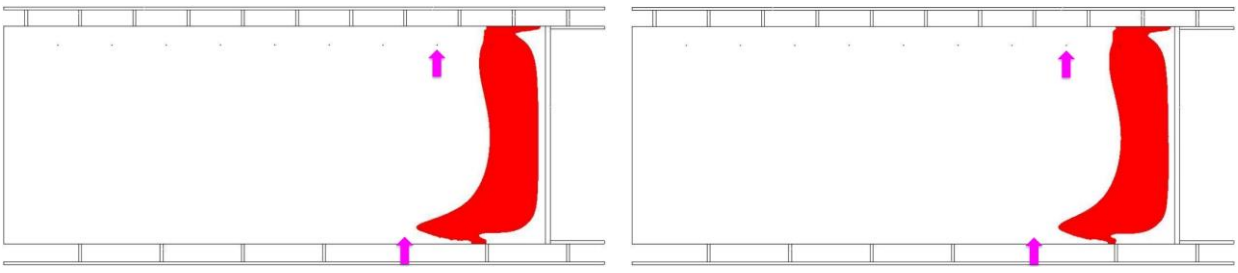

(a) N_2 injection through CT14-MG-BH02 @ 0.5-0.25 m^3/s (b) N_2 injection via CT14-MG-BH02 @ 0.75-0.25 m^3/s

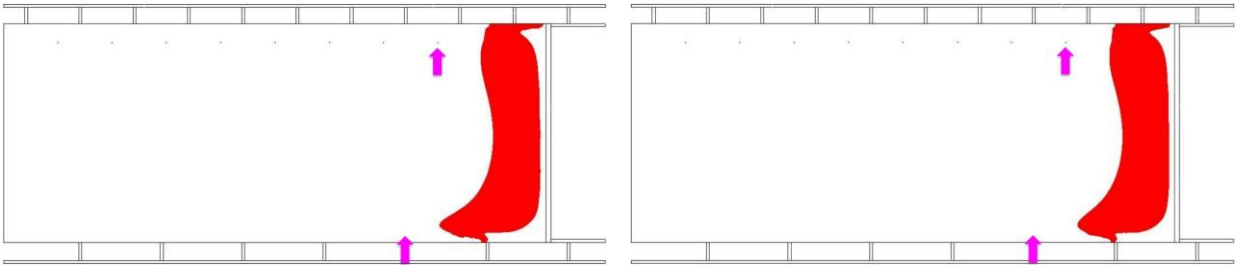

(c) N2 injection through CT14-MG-BH02 @ 1.0-0.25 m^3/s (d) N_2 injection via CT14-MG-BH02 @ 1.25-0.25 m^3/s

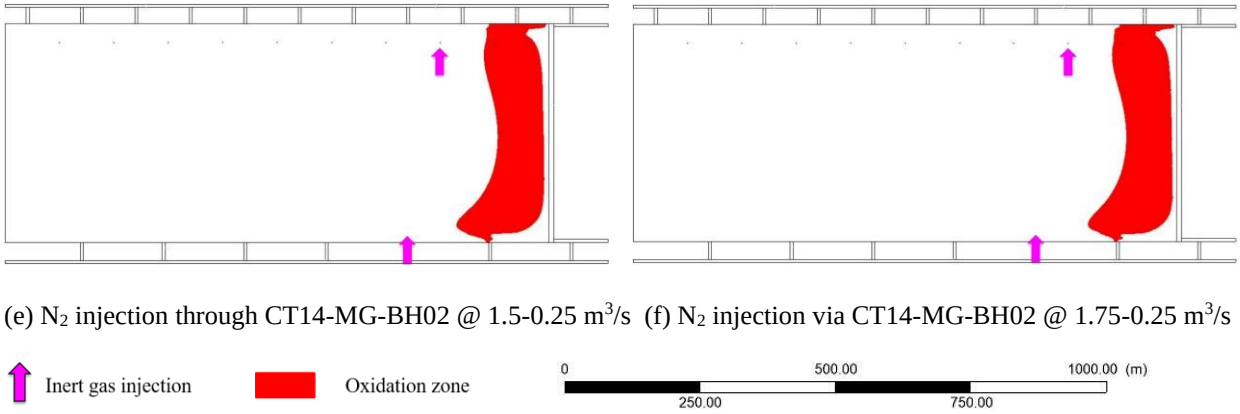

(e) N_2 injection through CT14-MG-BH02 @ 1.5-0.25 m^3/s (f) N_2 injection via CT14-MG-BH02 @ 1.75-0.25 m^3/s

Figure 4.16 Oxidation zone distribution with different nitrogen flow rates for case 7

For other cases proposed, the variation of the oxidation zone area in the active LW goaf area with different nitrogen injection rates presented a similar trend. When the total nitrogen injection rate increased to 1.5 m^3/s, the reduction rate of the oxidation zone area slowed down. Considering goaf inertisation performance and operational cost, a minimum injection rate of 1.5 m^3/s is recommended.

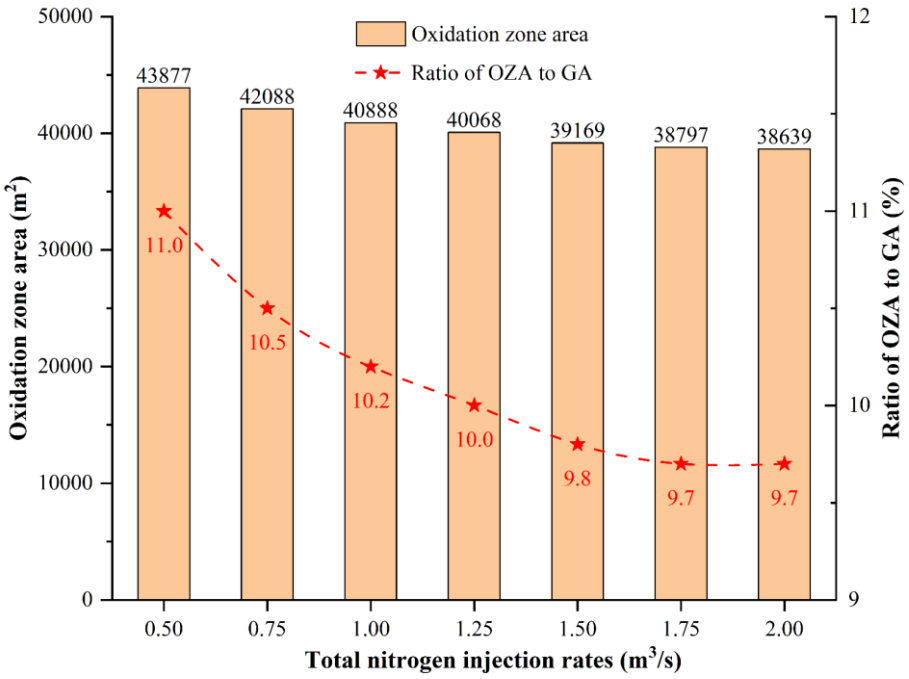

Figure 4.17 Oxidation zone area with different nitrogen flow rates for case 7

4.3 Conclusions

Considering the variation of coal seam orientations dictated by the elevation of the MG and the TG and the height of the LW face and the starting-up line, extensive numerical simulations were conducted.

(1) Nine scenarios of different coal seam orientations were studied. For the base model without inert gas injection, air ingress at both sides of the active LW goaf was evident, and the area ratio of oxidation zone to active LW goaf ranged between 25.2% and 28.7%.

(2) For cases where the MG was higher than the TG and at the same time the starting-up line was lower than or at the same elevation as the LW face, it would be better to inject nitrogen at the MG of the active LW goaf, otherwise nitrogen injection was the best option at the TG of the LW goaf.

(3) If the LW face was lower than the start-up line, the nitrogen injection point at the TG of the active LW goaf should be located at least 500~600 m behind the LW face to prevent oxygen accumulation at the TG of the deeper LW goaf. Conversely, if the LW face was higher than or at the same elevation as the starting-up line, the nitrogen injection point at the TG of the LW goaf could be set about100~200 m behind the LW face with an appropriate injection rate to avoid low oxygen volume fraction at the goaf stream.

(4) Regardless of the coal seam orientations, nitrogen was superior to carbon dioxide in reducing the oxidation zone area and containing spontaneous heating under the condition that seam gas was primarily comprised of 80% carbon dioxide with a total gas emission rate of 2 m^3/s.

(5) A total nitrogen flow rate of 1.5 m^3/s was required to contain spontaneous heating, and the ratio of OZA to GA is about 10%, lowering by about 15% compared to non-injection scenarios.

The following limitations of this research are noted. The reaction of residual coal in the active goaf and the impact of temperature evolution on goaf gas distribution patterns were not considered in the simulation. In addition, only the goaf area at 1000 m behind the LW face was considered in the simulation rather than the whole LW panel. Future research on these limitations should be pursued. Despite the above limitations, this research provides new insight into the influence of coal seam orientations on spatial gas distribution in the LW panel and inertisation strategies for preventing spontaneous heating in LW goaf with higher ventilation flow rates and seam gas emission rates, thus reducing the likelihood of spontaneous heating and improving safety in mining industry.

CHAPTER 5 VENTILATION FLOW DYNAMICS AND PROACTIVE INERTISATION STRATEGIES FOR SPONTANEOUS HEATING MANAGEMENT IN ACTIVE GOAF WITH VARIOUS SEAM GAS COMPOSITION

Summary

This chapter focuses on the impact of seam gas composition on ventilation dynamics in the active goaf area and proactive inertisation strategies for spontaneous combustion prevention and control. In Australia, seam gas composition varies in different coalfield locations. In Bowen Basin in Queensland, methane is the predominant coal seam gas, while carbon dioxide is the dominant coal seam gas in the Gunnedah Basin in New South Wales. In particular, the gas components in the Bulli coal seam of Illawarra coalfield in New South Wales can vary from 95% methane (CH_4) and 90% carbon dioxide (CO_2) across the coal seam. However, there is a lack of detailed understanding of ventilation dynamics and gas distribution patterns in the active goaf area with different seam gas composition and the determination of fit-for-purpose goaf inertisation strategies. To fill this knowledge gap, extensive CFD modelling has been carried out using the three-dimensional model established in Chapter three, and the oxidation zone area (where oxygen concentration lies in the range of 5%~18%) and oxidation ratio (the ratio of the oxidation zone area to the goaf area) have been introduced and calculated to qualitatively and quantitatively evaluate the status of spontaneous heating and the effectiveness of goaf inertisation strategies. The modelling results provide new knowledge of the gas flow dynamics in the goaf area with different goaf gas composition and aid the development of better proactive goaf inertisation strategies, thus effectively containing spontaneous combustion in the active goaf area and improving coal mining safety.

Citation

This paper has been submitted to **Mining, Metallurgy & Exploration** and is currently under review.

Abstract

Spontaneous heating of coal continues to present a health and safety hazard in underground coal mines. The influence of seam gas composition on ventilation behaviour and gas flow dynamics in the active longwall goaf has not been studied in-depth, and corresponding effective proactive goaf inertisation strategies for preventing potential spontaneous heating from occurring have limited investigation. To advance this knowledge, extensive computational modelling was developed and conducted based on specific conditions of an Australian underground coal mine, and onsite gas monitoring data was collated to verify simulation results, which allowed for various scenarios of seam gas composition to be simulated with confidence. Simulation results showed that oxygen (O_2) was primarily distributed at the middle and upper sections of the CO_2-dominant goaf, whilst it was mainly layered at the floor level of the CH_4-dominant goaf. N_2 was preferred over CO_2 in goaf inertisation for CO_2-dominant goaf, whereas CO_2 performed better than N_2 for the CH_4-dominant goaf. The optimal inert gas injection rates for the scenario of 100% CO_2, 80% CO_2 and 20% CH_4, 50% CO_2 and 50% CH_4, 20% CO_2 and 80% CH_4 and 100% CH_4 were 1.5, 1.75, 0.75, 0.5 and 1.0 m^3/s, and the oxidation zone area reduced by 55.8%, 67.2%, 58.0%, 78.2% and 81.8%, respectively. The simulation results allow for increased insight and understanding of the gas and ventilation behaviour in the active longwall goaf with different goaf gas composition and the development of corresponding proactive goaf practices, thus minimising potential spontaneous-heating-related hazards and improving mining safety.

Keywords

CFD modelling; Goaf gas composition; Oxidation zone area; Proactive goaf inertisation; Spontaneous heating management.

5.1 Introduction

As production outputs and the depth of cover increase, spontaneous combustion and self-heating of coal are increasingly presenting significant threats to safety in the mining industry in Australia, as evidenced in recent heating incidents. If not managed timely and controlled effectively, spontaneous heating can cause serious consequences, such as production stagnation, toxic-gas-induced environmental pollution, miner injury and death, and temporary or permanent mine closure. Early in September 2018, a heating event occurred behind one longwall (LW) face of the North Goonyella mine with elevated carbon monoxide levels, and all miners were withdrawn from the underground workings as a result of carbon monoxide readings exceeding trigger values stipulated in the Trigger Action Response Plan (TARP) (Queensland Mines Inspectorate 2019), culminating in an LW production stoppage for several months. A serious accident involving two forceful pressure waves took place at the Grosvenor mine on 6 May 2020, which caused 5 miners

to be seriously injured (NEWS 2020). The subsequent report (Terry Martin SC & Clough 2021) revealed that one of the pressure waves was highly likely triggered by spontaneous heating. To address this dynamic hazard arising from spontaneous heating in the active LW goaf, many measures have been applied in Australia, including proactive goaf inertisation, firefighting foam injection, flyash or carbofill plugs, and water injection (Salisbury et al. 2022), among which proactive goaf inertisation is widely used as prevention is better than cure. The purpose of proactive goaf inertisation is to prevent and manage the onset of spontaneous heating in the LW goaf by injecting inert gas into the active goaf during normal mining production to effectively lower oxygen concentration to a safe level at which coal oxidation progresses very slowly and even is smothered.

Active LW goaf is commonly characterized by a restricted area, making it considerably difficult to understand the distribution characteristics of goaf gas and take corrective actions to prevent and control potential spontaneous heating in the active goaf by traditional field measurements and laboratory experiments. To overcome the above difficulties, Computational Fluid Dynamics (CFD) modelling has been increasingly used due to its considerable advantages of saving time, saving cost and visualizing gas distribution. Ren et al. (2005) performed CFD simulations to study the effect of inert gas injection locations, types and flow rates of inert gas on the gas distribution characteristics in the LW goaf. Yuan et al. (2006) investigated the impact of ventilation systems on spontaneous heating in the goaf, and the injection locations and rates of nitrogen for suppressing spontaneous combustion in an active and sealed LW goaf were also studied (Yuan & Smith 2014). Taraba and Michalec (2011) researched the impact of face advancing rates on spontaneous heating in the active goaf, and figured out the critical advancing rate based on simulation results. Considering the thermo-mechanical effects of coal, Xia et al. (2014) investigated the effect of ventilation flux, ventilation resistance and LW face advancing rate on coal self-heating, and it was revealed that ventilation flux and resistance were positively correlated to self-heating zone, whereas face advancing rate showed a negative relationship with the self-heating zone. Three-dimensional (3D) models were constructed by Liu et al. (2016a) to understand the oxygen distribution in the active LW goaf with nitrogen or carbon dioxide injection, and the optimal injection location was identified. Qin et al. (2016b) numerically conducted research on oxygen and temperature distribution in the active goaf with nitrogen injection, and simulation results were proved to be reliable by field tests with liquid nitrogen injected into the goaf. Huang et al. (2018) performed numerical simulations to improve the understanding of the impact of periodic weighting on spontaneous combustion in the active LW goaf, and revealed that the width of the spontaneous combustion zone reduced with an increase in weighting interval. Focusing on appropriate strategies for managing and controlling gas and spontaneous heating in long panels with a length

of 1000 m and 3000 m, Balusu et al. (2019) carried out extensive CFD modelling, and the results suggested that nitrogen should be injected into the 3000-m-long goaf through multi points with a minimum injection rate of 1.5 m^3/s to effectively manage and control spontaneous combustion. Liu et al. (2019d) investigated the evolution of oxygen and temperature in the active goaf amid mining stoppage, and mining countermeasures for spontaneous combustion control were proposed during this period. Shi et al. (2019) investigated temperature distribution in the active goaf area and the impact of liquid nitrogen injection locations and rates on cooling hot zones, which guided the usage of liquid nitrogen for coal oxidation prevention. In combination with an orthogonal test and CFD modelling, Si et al. (2019) investigated the effect of face advancing rate, carbon dioxide injection location and flowrate, injection pipeline position on oxygen distribution in the active goaf area, and optimal parameters for spontaneous combustion control were also determined. A 3D CFD model was built by Zhang et al. (2020) to study the time factor for proactive and reactive inertisation for spontaneous heating management in the LW goaf, and optimal inertisation strategies for suppressing goaf heating were developed. Focusing on coals seam with a shallow buried depth, Zhuo et al. (2019) numerically researched goaf gas distribution characteristics in two adjacent gob areas, and the primary source of carbon monoxide was identified. With the aid of numerical simulation and laboratory experiments, Liu et al. (2020b) studied oxygen distribution characteristics in three adjacent goafs, and an optimal nitrogen injection location for spontaneous heating management was established. The influence of air leakage on spontaneous combustion zone in the active LW goaf with a shallow buried depth was evaluated by Zhuo et al. (2021) and it was found that the spontaneous heating zone moved towards the intake side and deep goaf as the air leakage rose. Qiao et al. (2022b) conducted extensive CFD simulations on gas distribution characteristics in the active LW goaf area where seam gas was mainly composed of carbon dioxide (80%), and influencing factors of goaf inertisation parameters were discussed.

From the above literature reviews, it was found that the influence of many geologic and mining factors (e.g., ventilation systems, face advancing rate, ventilation flux, ventilation resistance, periodic weighting, super-long panel, air leakage, the porosity of adjacent goafs and coal pillars) on spontaneous combustion management and control has been thoroughly discussed and evaluated, and gas atmosphere in the goaf area was mainly comprised of CH_4 in the vast majority of studies. However, the impact of seam gas composition on ventilation behaviour and corresponding proactive goaf inertisation for spontaneous heating prevention are under-researched. In addition, it was reported that the gas components in the Bulli coal seam of Illawarra coalfield in Australia can vary from 95% CH_4 to 90% CO_2 (Ren et al. 2018a), which would bring challenges to proactively managing and controlling spontaneous combustion by proactively injecting inert gas into the LW goaf. Therefore, it is necessary to advance the knowledge of ventilation behaviour

and gas flow dynamics in the active goaf with different goaf gas composition during the normal mining process, and correspondingly develop proactive goaf inertisation to manage the onset and development of spontaneous heating. The simulation results allow for increased insight and understanding of ventilation behaviour and gas flow dynamics in the active LW goaf with different seam gas composition, and guide the development of corresponding proactive goaf inertisation for preventing and managing spontaneous heating.

5.2 Parametric Studies

The CFD model in Section 3.6.2 was used in this study.

To investigate the effect of seam gas composition on oxygen distribution characteristics in the LW active goaf and proactive goaf inertisation strategies, five different scenarios were proposed, as listed below. The other parameters were kept constant, such as ventilation schemes, coal seam orientation and dip angle, total goaf gas emission rates, permeability distribution and boundary conditions. Five scenarios of seam gas composition are listed:

(a) 100% CO_2;

(b) 80% CO_2 and 20% CH_4;

(c) 50% CO_2 and 50% CH_4;

(d) 20% CO_2 and 80% CH_4;

(e) 100% CH_4.

Ren and Balusu (2009) suggested that a desired goaf inertisation result could be yielded by pumping inert gas at a flow rate of 0.5 m^3/s for most cases. As a result, the inert gas injection rate of 0.5 m^3/s was applied to study the optimal goaf inertisation strategies under different goaf gas composition. For the sake of quantitative analysis of the effectiveness of different goaf inertisation strategies, the upper and lower limits of oxygen level in the oxidation zone were 18% and 5%, and the area ratio of the oxidation zone (OZA) to the active goaf (GA) was calculated for comparison and termed as oxidation ratio in this study.

5.3 Results and Discussion

5.3.1 Oxygen distribution in the active LW goaf

For the proposed scenarios, oxygen distribution characteristics in the active LW goaf without injection are shown in Figure 5.1. Only the horizontal plan view of Z=12 m (2m from the coal seam floor) and the elevation view of Y= 365 m (crossing the surface boreholes) are presented. It is evident in Figure 5.1(a), (b), (d), and (e) that air ingress occurred at both sides of the LW goaf, with oxygen levels higher than 10% in the deep goaf, whereas air ingress at both sides of the LW

goaf was alleviated for scenario(c) where the goaf gas was composed of 50% CO_2 and 50% CH_4, with oxygen concentration dropping below 5% at about 550 m behind the LW face. At the elevation view of Y= 365 m, it was observed that oxygen was mainly distributed at the middle of the active goaf in Figure 5.1(a) and (b) in which the goaf gas was primarily composed of CO_2, whereas oxygen was mainly distributed at the bottom of the goaf area in Figure 5.1(d) and (e) where CH_4 accounted for the majority of the goaf gas. When the goaf gas was composed of 50% CO_2 and 50% CH_4, oxygen was mainly layered at the middle of the goaf, which was similar to scenarios where the goaf gas was primarily comprised of CO_2. As shown in Figure 5.2(a) and (b), it was noted that oxygen concentration at the TG and MG side of the LW goaf generally showed a downward trend as the composition of CH_4 reduced from 100% to 50%. However, with the composition of CH_4 reduced from 50% to 20%, oxygen levels at the TG and MG of the active goaf increased again. As the composition of CH_4 dropped from 20% to 0%, oxygen levels at the TG and MG of the active goaf reduced slightly in general.

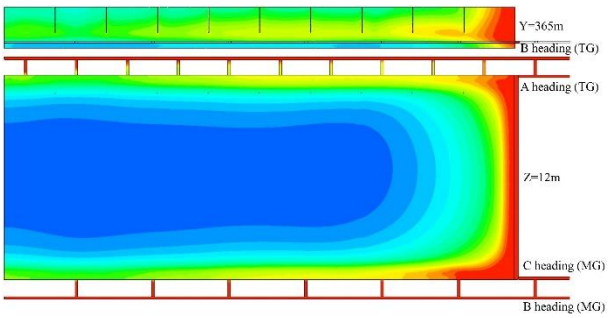

(a) 100% CO_2

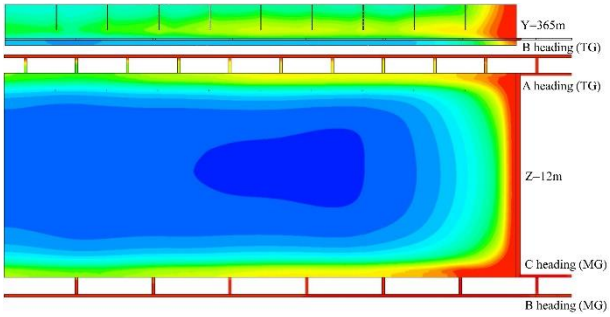

(b) 80% CO_2 and 20% CH_4

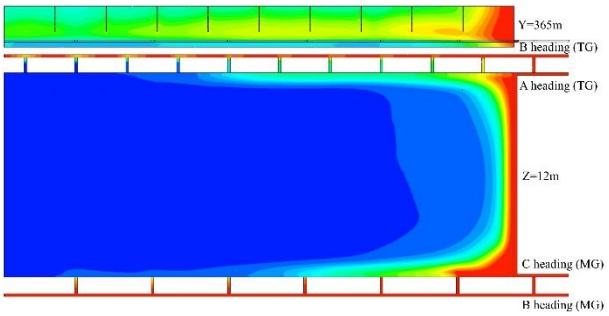

(c) 50% CO_2 and 50% CH_4

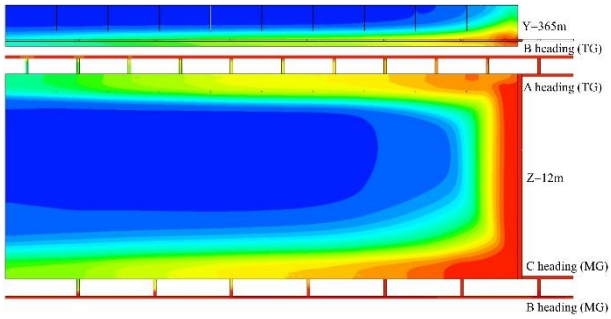

(d) 20% CO_2 and 80% CH_4

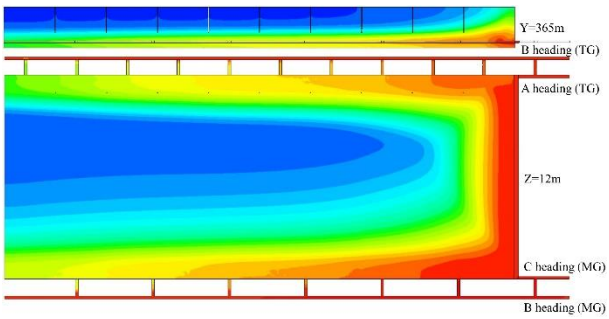

(e) 100% CH_4

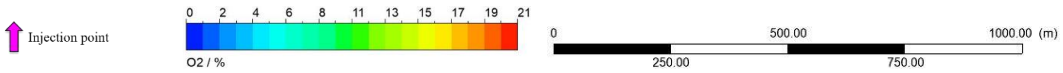

Figure 5.1 Oxygen distribution patterns in the LW goaf for different scenarios of seam gas composition

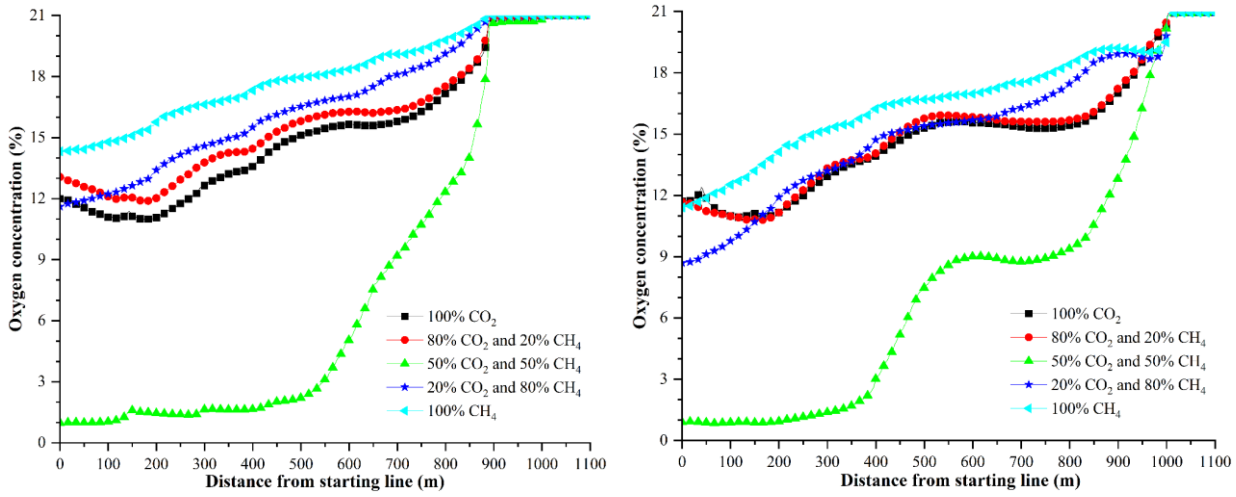

(a) MG (b) TG

Figure 5.2 Oxygen concentration along the LW goaf under different goaf gas composition

The oxidation zone area and oxidation ratio of the five proposed scenarios are listed in Table 5.1. The goaf area kept constant at 400000 m^2. It is noted that the oxidation ratio showed a decreasing trend as the composition of CH_4 rose from 0% to 50%; however, with the increase in CH_4 composition from 50% to 100%, the oxidation ratio increased. Except for the scenario where the goaf gas was composed of 50% CO_2 and 50% CH_4, the oxidation ratio was higher than 20%. As a result, there is a need to numerically study the influence of seam gas composition on goaf inertisation strategies to proactively manage and control spontaneous heating in the active LW goaf.

Table 5.1 Oxidation ratios for scenarios of different goaf gas composition

	100% CO_2	80% CO_2 and 20% CH_4	50% CO_2 and 50% CH_4	20% CO_2 and 80% CH_4	100% CH_4
Oxidation zone area (m^2)	126027	106666	28624	132684	197312
Oxidation ratio (%)	31.51	26.70	7.16	33.17	49.33

5.3.2 Proactive goaf inertisation strategies

5.3.2.1 Inert gas types

Three different types of inert gases have been widely used in Australia to proactively inert goaf atmosphere to suppress spontaneous combustion, such as nitrogen, carbon dioxide and boiler gas (85% N_2, 1% O_2 and 14% CO_2) (Ren & Balusu 2005; Ren & Balusu 2009). To study the effect of inert gas types on oxygen distribution characteristics and goaf inertisation performance under

different seam gas composition, three different types of inert gas were pumped into the LW goaf through CT18 (MG) and BH09 with an injection flowrate of 0.25 and 0.25 m^3/s, respectively, with results depicted in Figure 5.3. Only oxygen distribution results at Z=12 m (2 m above the floor strata) under nitrogen and carbon dioxide injection were presented. Table 5.2 details the oxidation ratios under different types of inert gas injected through CT18 (MG) and surface BH09 at a flow rate of 0.25 and 0.25 m^3/s, respectively, for the proposed scenarios.

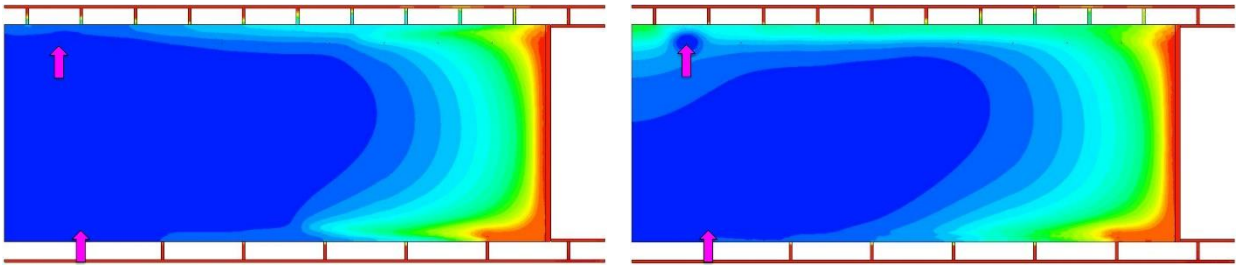

(a1) N_2 injection (a2) CO_2 injection

(a) 100% CO_2

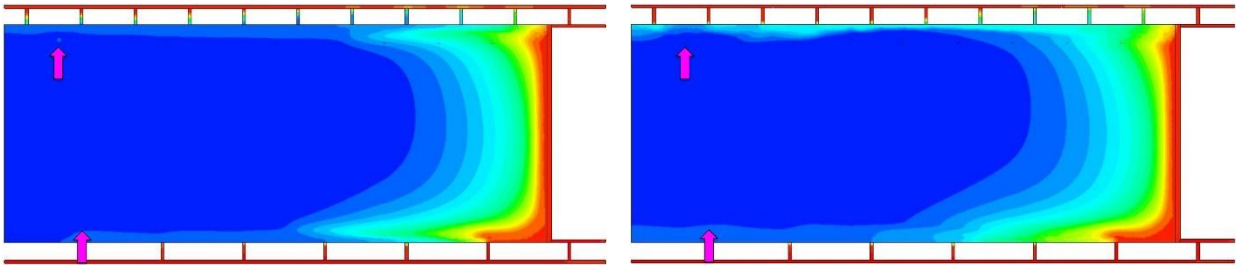

(b1) N_2 injection (b2) CO_2 injection

(b) 80% CO_2 and 20% CH_4

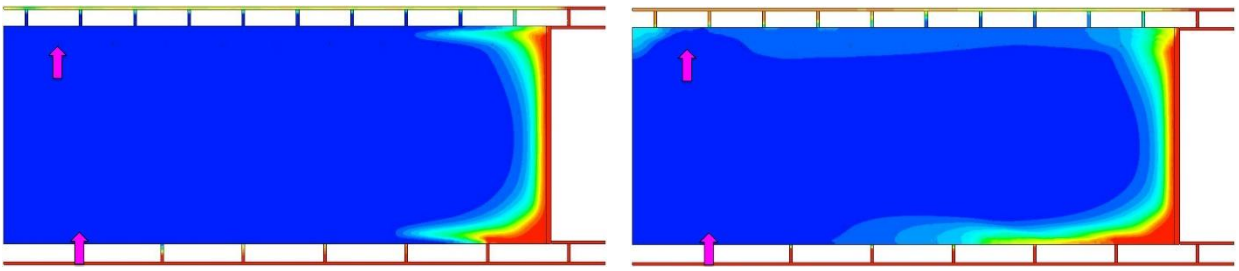

(c1) N_2 injection (c2) CO_2 injection

(c) 50% CO_2 and 50% CH_4

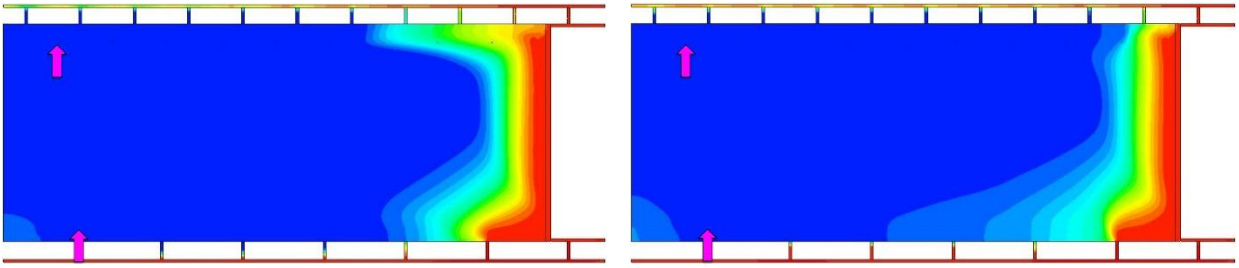

(d1) N_2 injection (d2) CO_2 injection

(d) 20% CO_2 and 80% CH_4

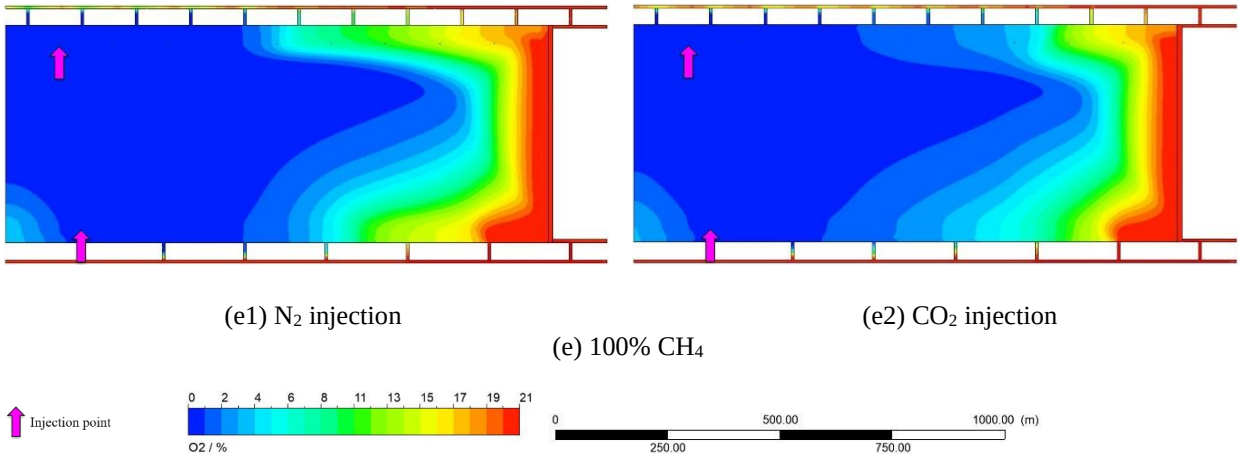

(e1) N_2 injection (e2) CO_2 injection

(e) 100% CH_4

Figure 5.3 Oxygen distribution in the LW goaf with nitrogen and carbon dioxide injection through CT18-MG-BH09

Table 5.2 Oxidation ratio under different types of inert gas injected at CT18-MG-BH09

		N_2	Boiler gas	CO_2
100% CO_2	Oxidation zone area (m^2)	70090	73370	89054
	Oxidation ratio (%)	17.52	18.34	22.26
80% CO_2 and 20% CH_4	Oxidation zone area (m^2)	51262	52475	58817
	Oxidation ratio (%)	12.82	13.12	14.70
50% CO_2 and 50% CH_4	Oxidation zone area (m^2)	17044	18543	20782
	Oxidation ratio (%)	4.26	4.64	5.20
20% CO_2 and 80% CH_4	Oxidation zone area (m^2)	39557	38504	31804
	Oxidation ratio (%)	9.89	9.63	7.95
100% CH_4	Oxidation zone area (m^2)	83839	80107	65326
	Oxidation ratio (%)	20.96	20.03	16.33

As illustrated in Figure 5.3(a) and (b) where the goaf gas was composed of 100% CO_2 and 80% CO_2, nitrogen yielded better goaf inertisation results than carbon dioxide. Air ingress at the TG of the LW goaf was more severe for carbon dioxide injection than nitrogen injection, as oxygen concentration still exceeded 5% at about 750 m behind the working face. The oxidation ratio was 17.52% and 12.82% with nitrogen injected through CT18 (MG) and BH09 for the scenario (a) and (b), in comparison to 18.34% and 13.12% with boiler gas injection, and 22.26% and 14.70% with carbon dioxide injection, which meant that nitrogen was better than boiler gas and carbon dioxide in controlling spontaneous heating for the scenarios where the goaf gas was dominantly composed of CO_2.

When the seam gas was comprised of 50% CO_2 and 50% CH_4, although air ingress at the TG of the LW goaf was reduced with carbon dioxide being injected, air ingress at the MG of the LW goaf was evident, with oxygen concentration exceeding 5% at about 380 m behind the working face. On the contrary, air ingress on both sides of the LW goaf was reduced, with oxygen levels lower than 5% at about 250 m behind the working face. The oxidation ratio was 4.26%, 4.64% and 5.20% for nitrogen, boiler gas and carbon dioxide injection, respectively, meaning that nitrogen performed marginally better than boiler gas and carbon dioxide in goaf inertisation when the goaf gas was comprised of 50% CO_2 and 50% CH_4.

With regard to scenarios (d) and (e) depicted in Figure 5.3(d) and (e), it was noted that air ingress on both sides of the goaf was reduced with carbon dioxide being injected when compared to nitrogen injection. Oxygen levels at the MG and TG of the LW goaf were lower than 5% at about 200 m and 80 m behind the working face, respectively, for scenario (d) with carbon dioxide injection. Similarly, oxygen levels at the TG and MG of the LW goaf were reduced below 5% at about 250 m and 340 m behind the working face for scenario (e) with carbon dioxide injection. The results also indicated that carbon dioxide performed better in managing spontaneous heating than nitrogen and boiler gas, with oxidation ratios being 7.95% and 16.33% for scenarios (d) and (e), respectively, under the condition of carbon dioxide injection.

In addition, as the composition of CO_2 or CH_4 in the goaf gas increased from 50% to 100%, the oxidation ratio rose, regardless of the types of inert gas injected. For the goaf gas that is primarily constituent of CO_2, nitrogen is recommended for goaf inertisation; Conversely, carbon dioxide is suggested for spontaneous combustion management in the LW goaf where the goaf gas is dominantly composed of CH_4.

5.3.2.2 Injection locations

To reduce oxygen levels in the active LW goaf, the inert gas injection could be operated via cut-throughs at both sides of the LW goaf or via surface boreholes previously used for gas drainage. For scenarios (a), (b) and (c), nitrogen was selected as the inert gas for goaf inertisation, whereas carbon dioxide was chosen as the inert gas for scenarios (d) and (e). The total inert gas injection rate was kept constant at 0.5 m^3/s. Extensive numerical simulations were conducted, and only representative oxygen distribution results at Z=12 m are shown in Figure 5.4-5.8.

Figure 5.4 shows oxygen concentration distribution patterns for nitrogen injection through different locations in the active goaf area in which the seam gas was composed of 100% CO_2. As shown in Figure 5.4(a), oxygen levels at the MG of the LW goaf could drop below 5% at about 350 m behind the working face when nitrogen was pumped through CT14 (MG), while they were still higher than 5% at the TG of the deep goaf, resulting in unsatisfactory goaf inertisation

performance. With nitrogen injection locations moving forward to the cut-through at the MG of the deep goaf, oxygen concentration at the TG of the LW goaf was still high, demonstrating that nitrogen injection solely at the MG of the LW goaf was not a good option for spontaneous heating control. When nitrogen was injected on the TG side via CT20 or BH07, oxygen levels at the MG and TG of the LW goaf could reduce below 5% at about 400 m and 250 m behind the working face, which produced better goaf inertisation results than nitrogen injected on the MG side. In order to avoid high oxygen concentration at the TG of the deep goaf shown in Figure 5.4(b), the nitrogen injection location at the TG of the goaf should be placed at least 700 m behind the working face. For scenarios of nitrogen injection through two TG cut-throughs or two drainage boreholes, there was no significant difference in oxygen distribution patterns in the active LW goaf. For nitrogen injection via an MG cut-through and a TG location (a drainage borehole or a cut-through), there was no noticeable difference in air ingress distance at the MG of the LW goaf, but air ingress distance at the TG was longer than in scenarios where nitrogen was only injected on the TG side. In order to prevent high-concentration oxygen from occurring at the TG of the deep LW goaf, the nitrogen injection location at the TG of the active goaf should be placed at least 900 m behind the working face for the cases where nitrogen injection was performed at both sides of the LW goaf, as illustrated in Figure 5.4(f). The results showed that desired goaf inertisation results were yielded by nitrogen injection through BH03 and BH09 at a flow rate of 0.25 and 0.25 m^3/s, and its oxidation ratio was 16.22%, which is approximately half of the scenario without injection.

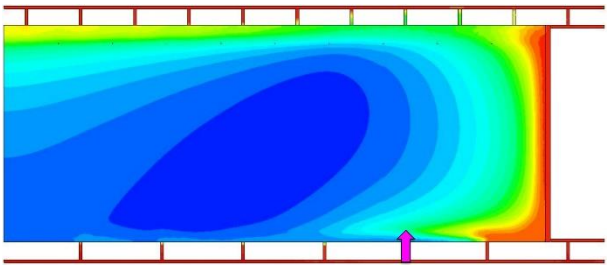

(a) N_2 injection via CT14-MG @ 0.5 m^3/s

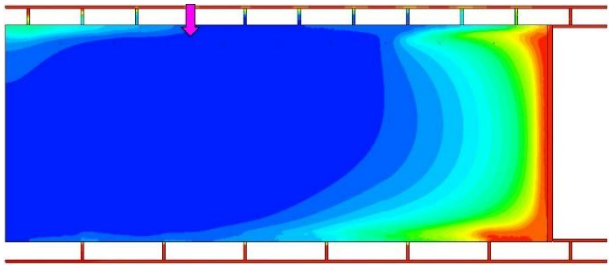

(b) N_2 injection via CT19-TG @ 0.5 m^3/s

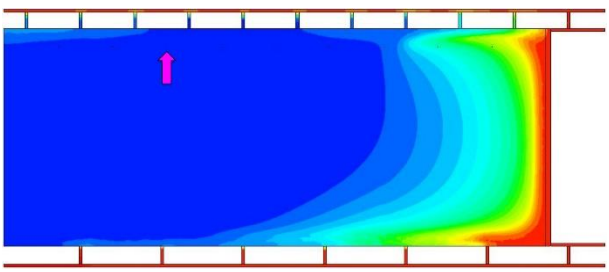

(c) N_2 injection via BH07 @ 0.5 m^3/s

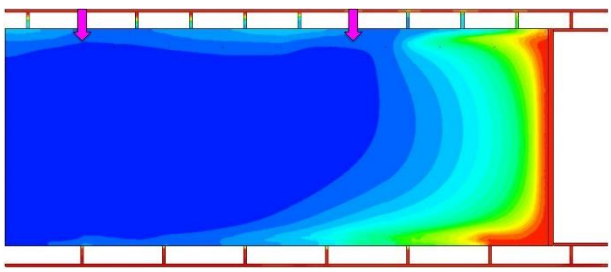

(d) N_2 injection via CT16-CT21-TG @ 0.25-0.25 m^3/s

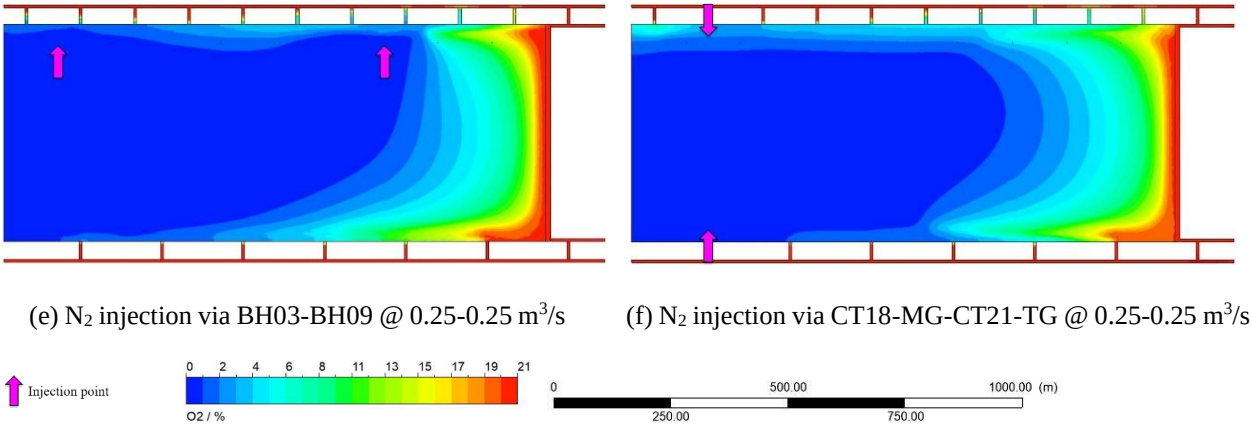

(e) N_2 injection via BH03-BH09 @ 0.25-0.25 m^3/s (f) N_2 injection via CT18-MG-CT21-TG @ 0.25-0.25 m^3/s

Figure 5.4 Oxygen distribution at Z=12 m with different nitrogen injection locations for 100% CO_2 goaf

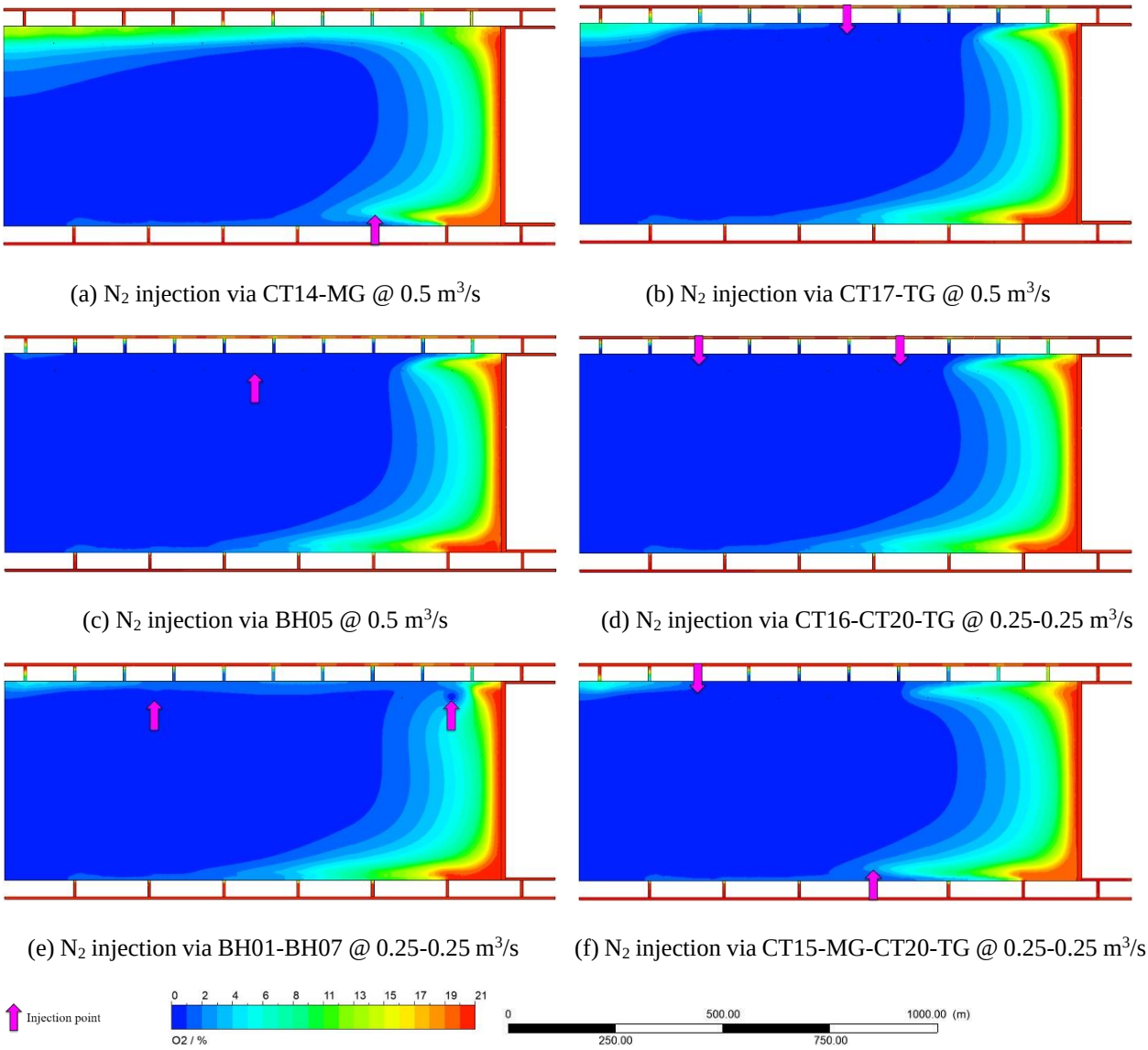

(a) N_2 injection via CT14-MG @ 0.5 m^3/s (b) N_2 injection via CT17-TG @ 0.5 m^3/s

(c) N_2 injection via BH05 @ 0.5 m^3/s (d) N_2 injection via CT16-CT20-TG @ 0.25-0.25 m^3/s

(e) N_2 injection via BH01-BH07 @ 0.25-0.25 m^3/s (f) N_2 injection via CT15-MG-CT20-TG @ 0.25-0.25 m^3/s

Figure 5.5 Oxygen distribution at Z=12 m with different nitrogen injection locations for 80% CO_2 and 20% CH_4 goaf

Figure 5.5 depicts oxygen distribution at Z=12 m with nitrogen injected through different locations in the active goaf area in which the seam gas was comprised of 80% CO_2 and 20% CH_4. The oxygen distribution patterns under different nitrogen injection strategies were similar to the

scenario where the seam gas was comprised of 100% CO_2. Specifically, Figure 5.5(a) shows that nitrogen injection at the MG of the LW goaf could only help reduce oxygen levels at the MG of the active goaf, while air ingress at the TG of the LW goaf was still evident, with oxygen concentration higher than 13% at the deep goaf. Conversely, nitrogen injection through an appropriate TG location (e.g., a drainage borehole or a TG cut-through) could reduce oxygen levels at both sides of the LW goaf to a certain extent, as shown in Figure 5.5(c). To avoid high-concentration oxygen at the TG of the deep goaf illustrated in Figure 5.5(b), the nitrogen injection at the TG of the active goaf should be performed at a minimum distance of 500 m behind the working face. Compared with nitrogen injection through a TG location (a drainage borehole or a TG cut-through), there was no significant difference in oxygen levels in the LW goaf with nitrogen injection through two TG sites. However, when nitrogen injection was performed at both sides of the active goaf illustrated in Figure 5.5(f), air ingress distance at the TG of the LW goaf was longer than the scenarios where nitrogen was solely injected on the TG side, suggesting it is not a good option for goaf inertisation under current nitrogen injection rates. The results indicated that nitrogen injection through BH01 and BH07 at a flow rate of 0.25 and 0.25 m^3/s could produce the best goaf inertisation results, and the oxidation zone area is reduced by about 58.74% compared to the scenario without injection.

Figure 5.6 shows oxygen distribution at Z=12 m with nitrogen injection through different locations of the LW goaf where the seam gas was composed of 50% CO_2 and 50% CH_4. When nitrogen was injected through CT14 (MG), air ingress at the MG of the LW goaf could be limited, with oxygen levels at the MG of the LW goaf being lower than 5% at about 150 m behind the LW face. As demonstrated in Figure 5.6(b) and (c) in which nitrogen was injected at the TG of the LW goaf, although oxygen levels on the injection side were significantly reduced, oxygen levels at the goaf stream were also low, and air ingress at the MG of the LW goaf was evident. In comparison with the oxygen distribution in Figure 5.6(d) and (e), it was apparent that an improvement in reducing oxidation zone area could be observed with the TG injection location being closer to the LW face. However, oxygen levels at the TG end were below 19.5% when the nitrogen injection location was too close to the LW face with a relatively high flow rate, which would not meet the statutory limits of the NSW government. Therefore, the flow rate of nitrogen injected at the TG of the active goaf should be controlled within an appropriate value. The flow rate of nitrogen injected at the TG of the LW goaf could not exceed 0.1 m^3/s to avoid low oxygen concentration at the goaf stream. In addition, a better goaf inertisation performance was produced with nitrogen injection through CT14 (MG) and BH01 at a flow rate of 0.45 and 0.05 m^3/s, and the oxidation ratio was 3.39%, which is approximately 52% of the scenario without injection.

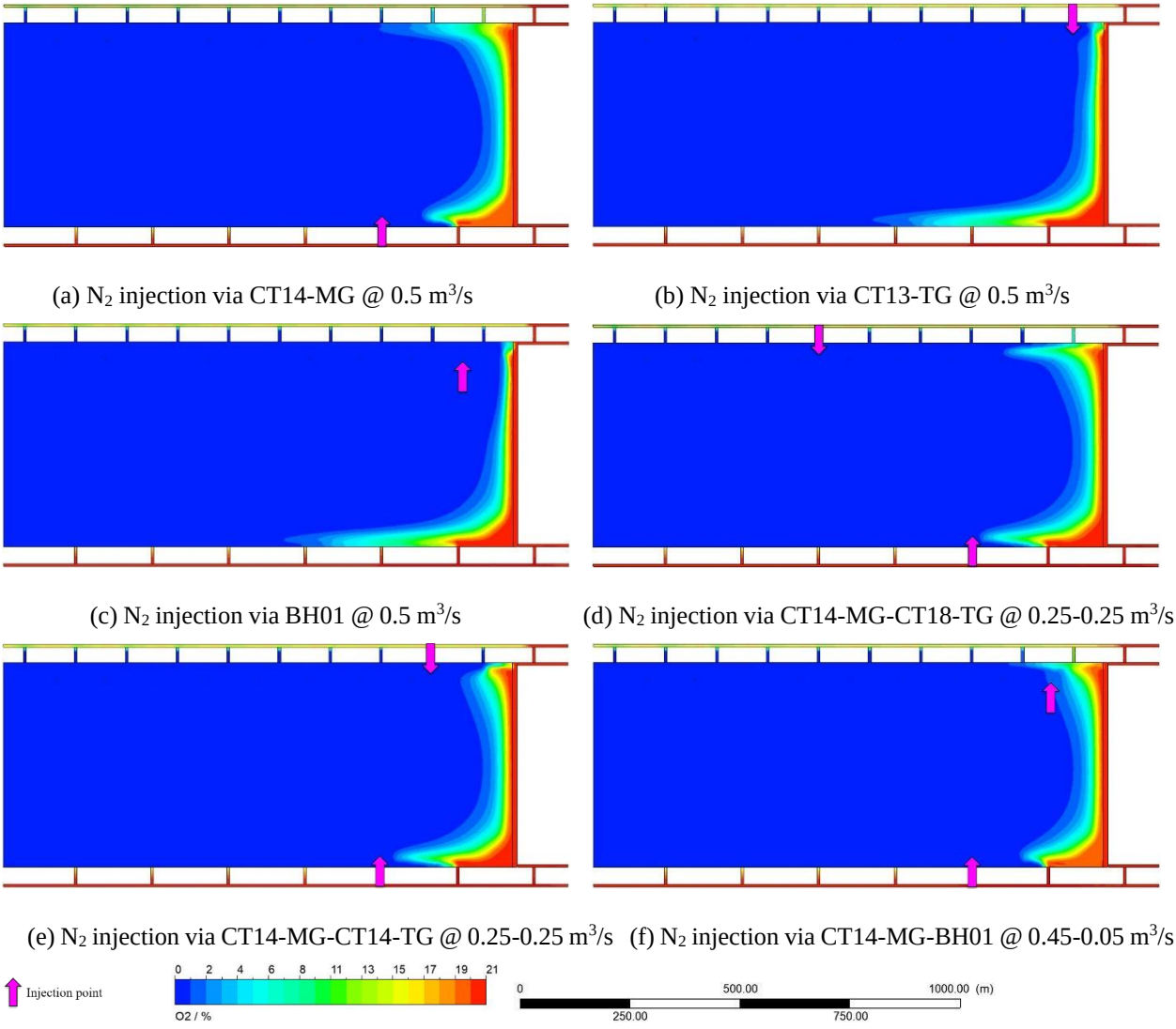

Figure 5.6 Oxygen distribution at Z=12 m with different nitrogen injection locations for 50% CO_2 and 50% CH_4 goaf

Figure 5.7 indicates that the injection locations of carbon dioxide significantly impacted oxygen distribution patterns in the active LW goaf composed of 20% CO_2 and 80% CH_4. When carbon dioxide was injected through CT17 (MG), air ingress at the TG of the LW goaf was noticeable, and high-concentration oxygen was observed at the MG of the deep LW goaf. In order to prevent high-level oxygen from occurring in this area, the carbon dioxide injection location at the MG of the LW goaf should be placed at around 850 m behind the working face (e.g., CT18-MG). As depicted in Figure 5.7 (b) and (c) where carbon dioxide was injected at the TG of the LW goaf, air ingress at the injection site was significantly reduced, but air ingress at the other side was high, with oxygen levels exceeding 5% at around 700 m behind the working face. Another problem associated with the sole injection of carbon dioxide on the TG side at a flow rate of 0.5 m^3/s was low oxygen levels at the goaf stream. In order to effectively reduce air ingress at both sides of the goaf, carbon dioxide injection should be performed at both sides of the LW goaf, with results shown in Figure 5.7(d), (e) and (f). The results showed that a flow rate of 0.25 m^3/s at the TG

injection location was excessive to limit air ingress at the injection site, as evidenced by low oxygen levels at the goaf stream. Conversely, a flow rate of 0.167 m^3/s was sufficient to limit oxygen penetration on the TG side. The modelling results showed that desired goaf inertisation performance was produced by injecting carbon dioxide through CT18 (MG) and BH05 with a flow rate of 0.333 and 0.167 m^3/s, respectively, and oxygen concentration was lower than 5% at about 170 m behind the face. The oxidation area was 28958 m^2, which is reduced by 78.18% compared to the scenario without carbon dioxide injection (132684 m^2).

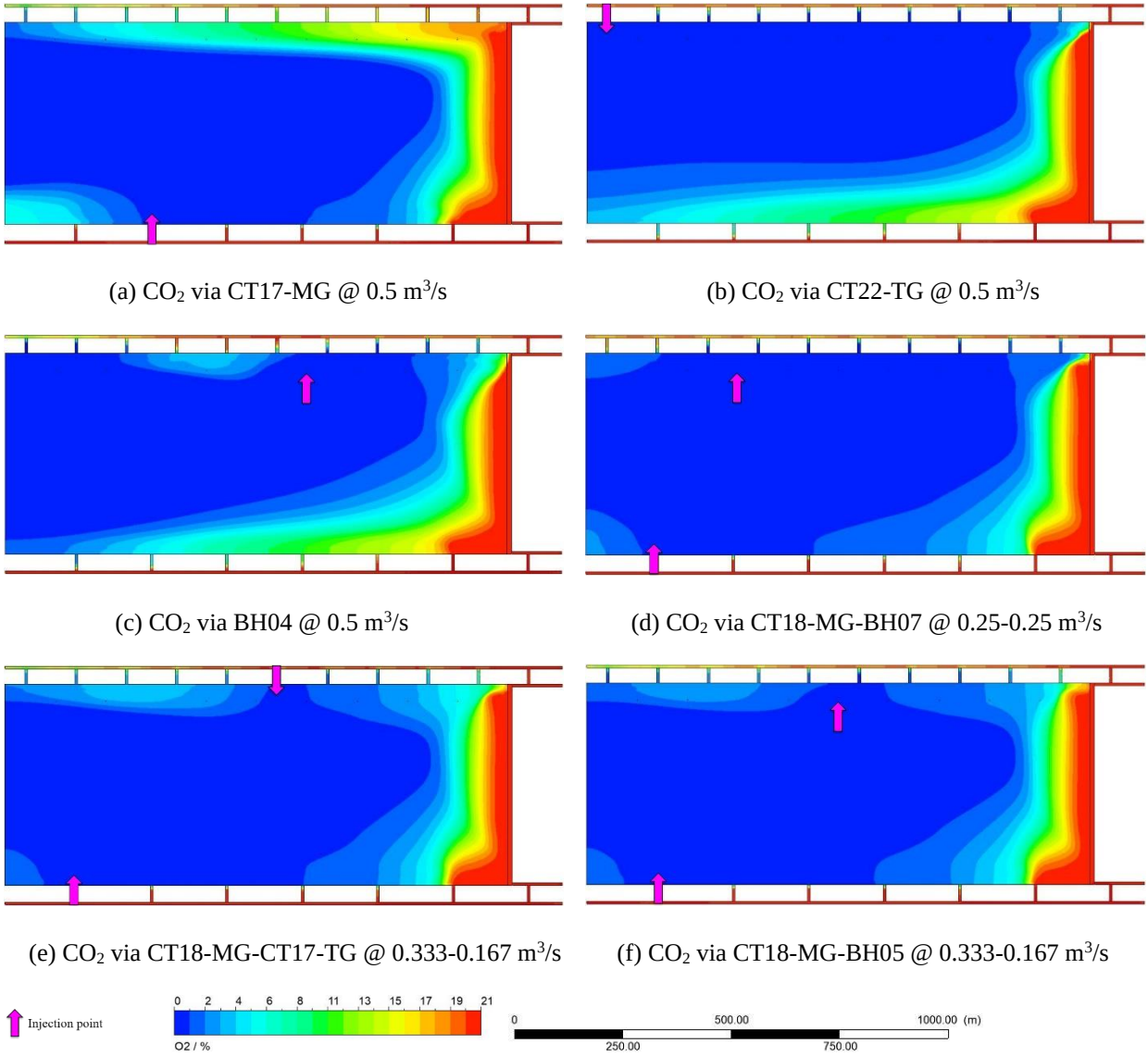

(a) CO_2 via CT17-MG @ 0.5 m^3/s

(b) CO_2 via CT22-TG @ 0.5 m^3/s

(c) CO_2 via BH04 @ 0.5 m^3/s

(d) CO_2 via CT18-MG-BH07 @ 0.25-0.25 m^3/s

(e) CO_2 via CT18-MG-CT17-TG @ 0.333-0.167 m^3/s

(f) CO_2 via CT18-MG-BH05 @ 0.333-0.167 m^3/s

Figure 5.7 Oxygen distribution at Z=12 m with different carbon dioxide injection locations for 20% CO_2 and 80% CH_4 goaf

Figure 5.8 demonstrates oxygen distribution at Z=12 m with carbon dioxide injected through different locations of the goaf area where the goaf gas was comprised of 100% CH_4. As illustrated in Figure 5.8(a), (b) and (c), carbon dioxide injection at one goaf side could only reduce air ingress at the same side of the active goaf area, whereas oxygen penetration at the other side of the active goaf area was apparent, which was similar to the scenario where the goaf gas was composed of

20% CO_2 and 80% CH_4. Therefore, carbon dioxide injection should be performed at both sides of the active goaf area at appropriate locations. In addition, to prevent high-concentration oxygen from occurring at the TG of the deep LW goaf, the TG injection location should be placed at least 500 m behind the working face. Better goaf inertisation results were yielded by injected carbon dioxide via CT18 (MG) and BH05 with a flow rate of 0.25 and 0.25 m^3/s, respectively. The oxidation ratio was 14.29%, which dropped by 71.03% compared to the scenario without injection (49.33%).

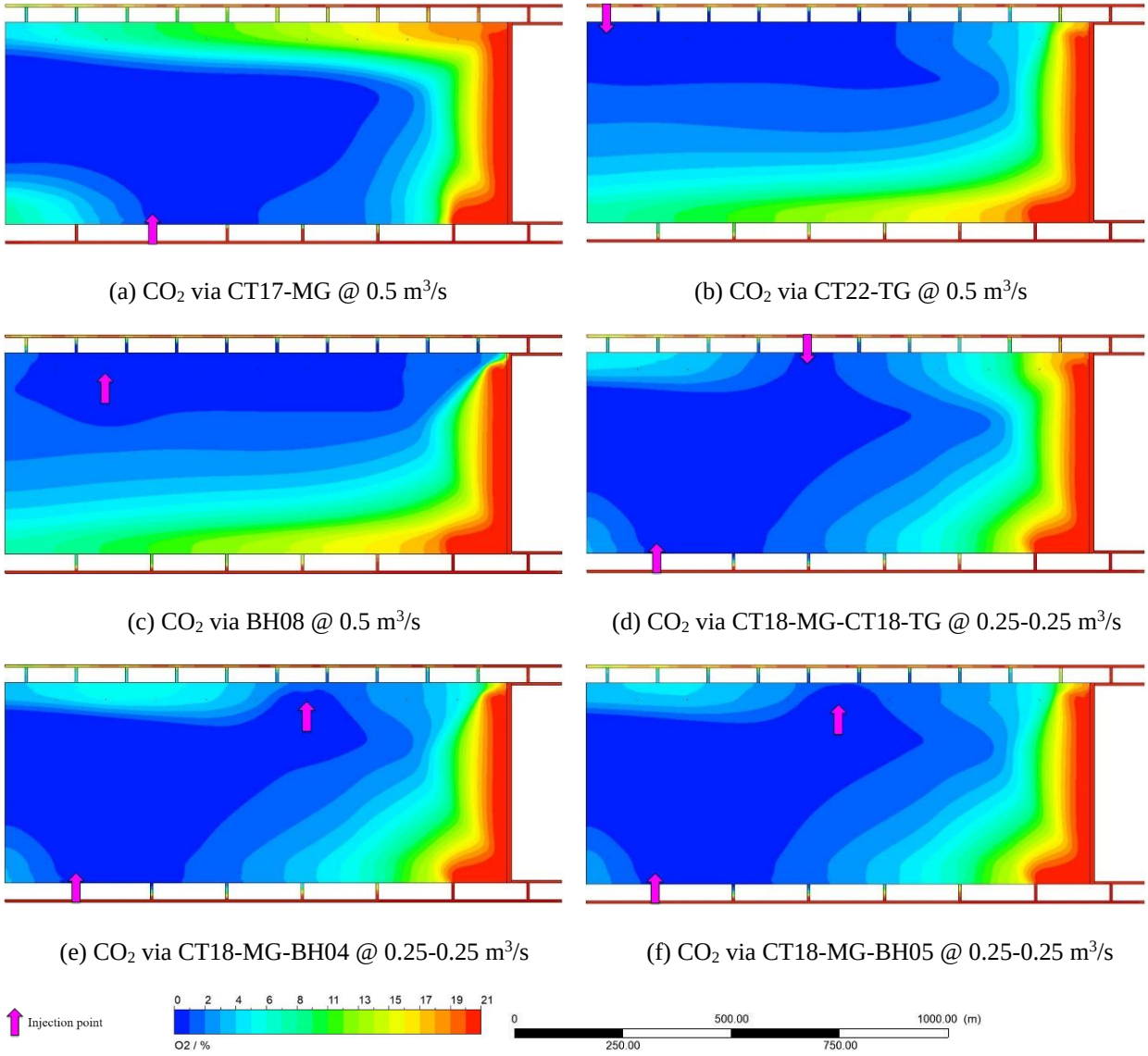

(a) CO_2 via CT17-MG @ 0.5 m^3/s

(b) CO_2 via CT22-TG @ 0.5 m^3/s

(c) CO_2 via BH08 @ 0.5 m^3/s

(d) CO_2 via CT18-MG-CT18-TG @ 0.25-0.25 m^3/s

(e) CO_2 via CT18-MG-BH04 @ 0.25-0.25 m^3/s

(f) CO_2 via CT18-MG-BH05 @ 0.25-0.25 m^3/s

Figure 5.8 Oxygen distribution at Z=12 m with different carbon dioxide injection locations for 100% CH_4 goaf

In summary, injection locations significantly influenced the oxygen distribution in the active goaf. For the scenario where the goaf gas was dominantly comprised of CO_2 (e.g., scenarios (a) and (b)), inert gas injection at the TG of the goaf produced better results in limiting air ingress than the MG injection; Conversely, for the scenario where the goaf gas was dominantly comprised of CH_4, the inert gas injection should be operated at both sides of the LW goaf with appropriate injection rates

to effectively limit air ingress on both sides of the goaf. Regarding the scenario where the goaf gas was equally composed of CO_2 and CH_4, inert gas should be pumped at both sides of the LW goaf, but the injection rate on the TG side should be controlled strictly to avoid low oxygen levels at the goaf stream.

In comparison to oxygen distribution patterns in the active goaf in which the seam gas was comprised of 80% CO_2 and 20% CH_4, the optimal nitrogen injection location on the TG side was further away from the LW face for the goaf composed of 100% CO_2. However, compared to the scenario where the goaf gas was comprised of 100% CH_4, the injection rate of carbon dioxide on the TG side should be reduced to avoid low oxygen levels at the goaf stream when the goaf gas was composed of 20% CO_2 and 80% CH_4.

5.3.2.3 Injection flow rates

For scenarios (a) and (b) where the goaf gas was predominantly composed of CO_2, a continued rise in nitrogen flow rate at the TG of the active goaf could result in low oxygen levels at the goaf stream and had a minor impact on limiting air ingress at the MG of the active goaf. Therefore, to research the influence of inert gas flow rates on goaf inertisation performance, the flow rate of nitrogen through CT14 (MG) was increased at an increment of 0.25 m^3/s, while the flow rate on the other side was kept constant. However, for scenarios (c), (d) and (e) in which inert gas injection should be performed at both sides of the LW goaf, the injection rate at the MG of the goaf gradually increased by 0.25 m^3/s, but the injection rate on the other side was kept constant to avoid low oxygen concentration at the goaf stream.

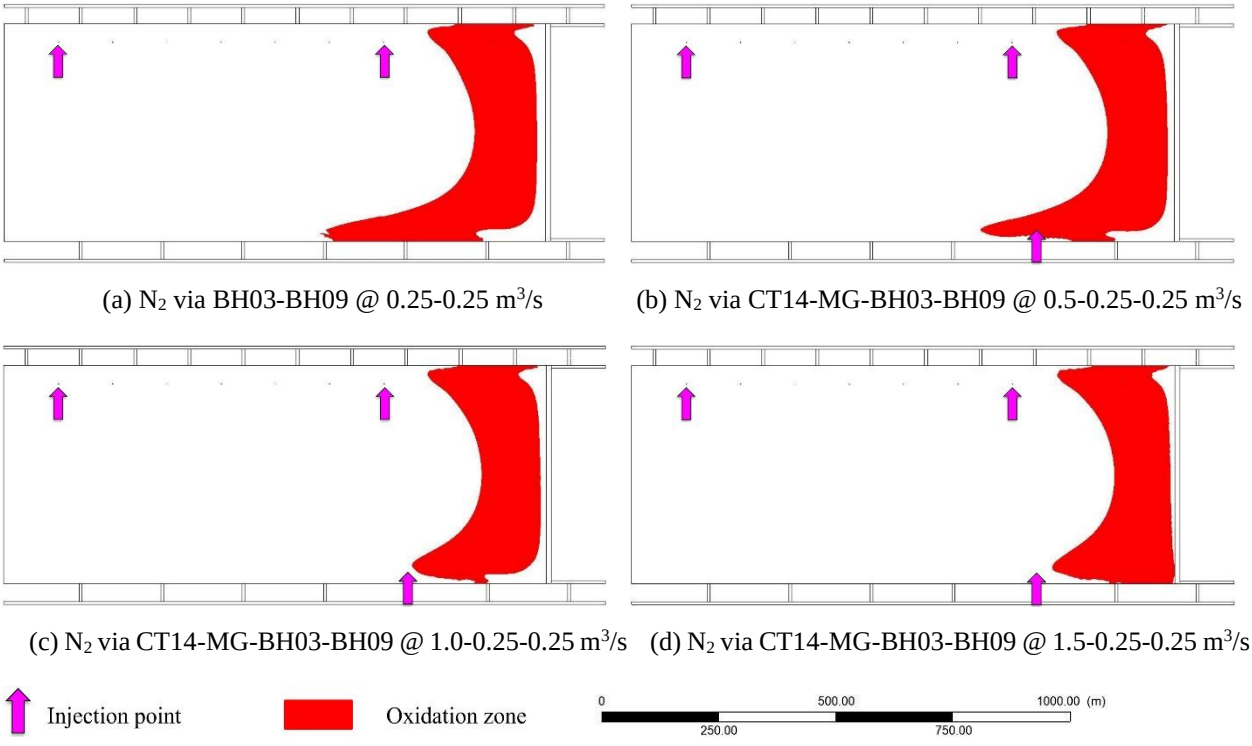

Figure 5.9 Oxidation zone area at different flow rates for 100% CO_2 goaf

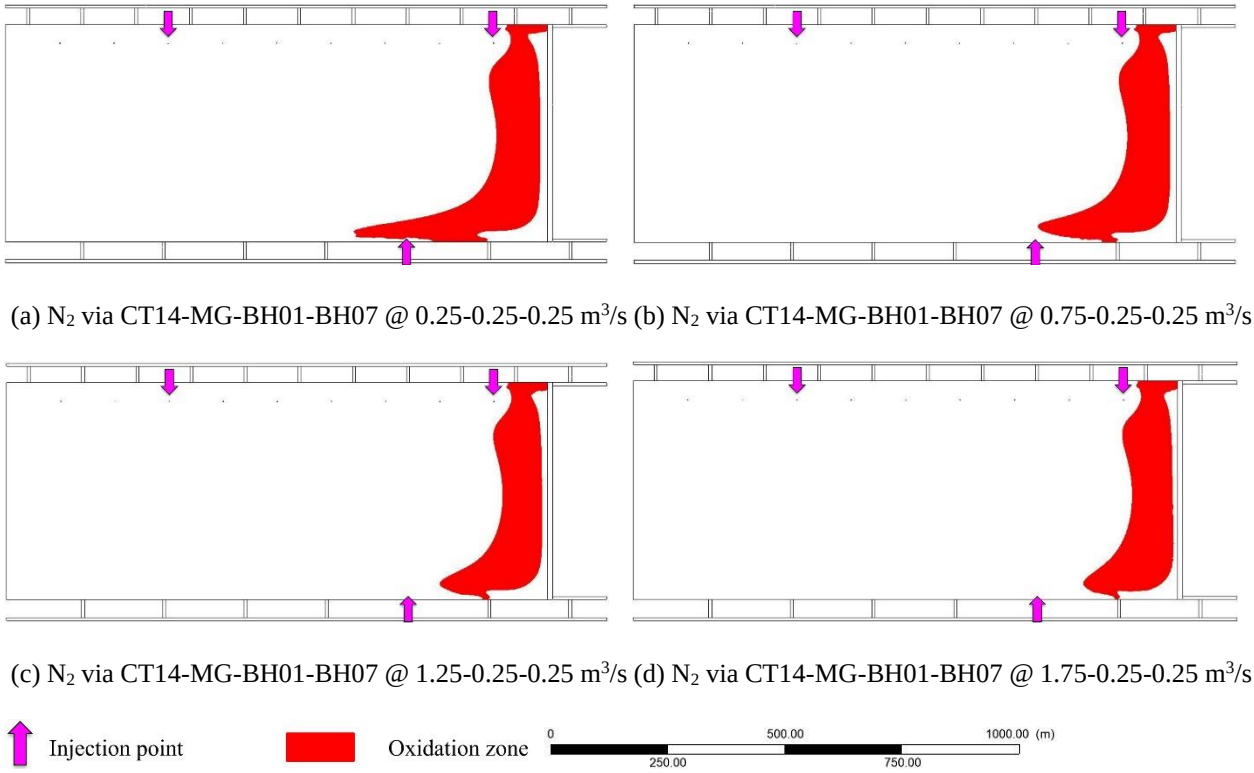

Figure 5.10 Oxidation zone area at different flow rates for 80% CO_2 and 20% CH_4 goaf

Figure 5.9 and Figure 5.10 show the oxidation zone area at different nitrogen flow rates for the goaf composed of 100% CO_2 (scenario (a)), and 80% CO_2 and 20% CH_4 (scenario (b)). As the flow rate increased, the oxidation zone area narrowed, and air ingress via MG goaf was reduced significantly. When the total nitrogen injection rate reached 1.5 and 1.75 m^3/s, the reduction rate of the oxidation zone area slowed down for scenarios (a) and (b), respectively.

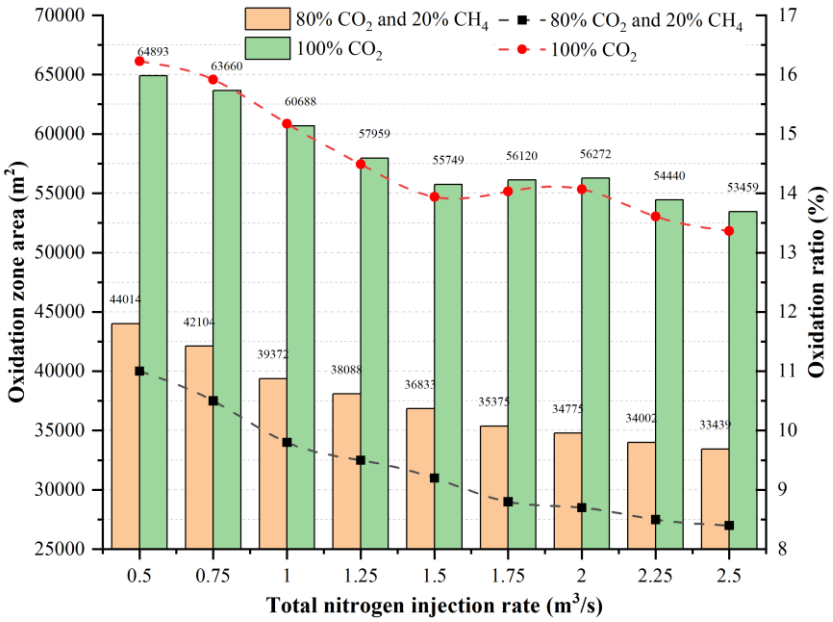

Figure 5.11 Oxidation ratios at different nitrogen flow rates for the scenario (a) and (b)

As demonstrated in Figure 5.11, simulation results indicated that the oxidation zone area was consistently higher for scenario (a) than scenario (b) at the same nitrogen injection rate. The oxidation ratio for scenario (a) was approximately 1.5 times that of scenario (b) under the same nitrogen flow rate.

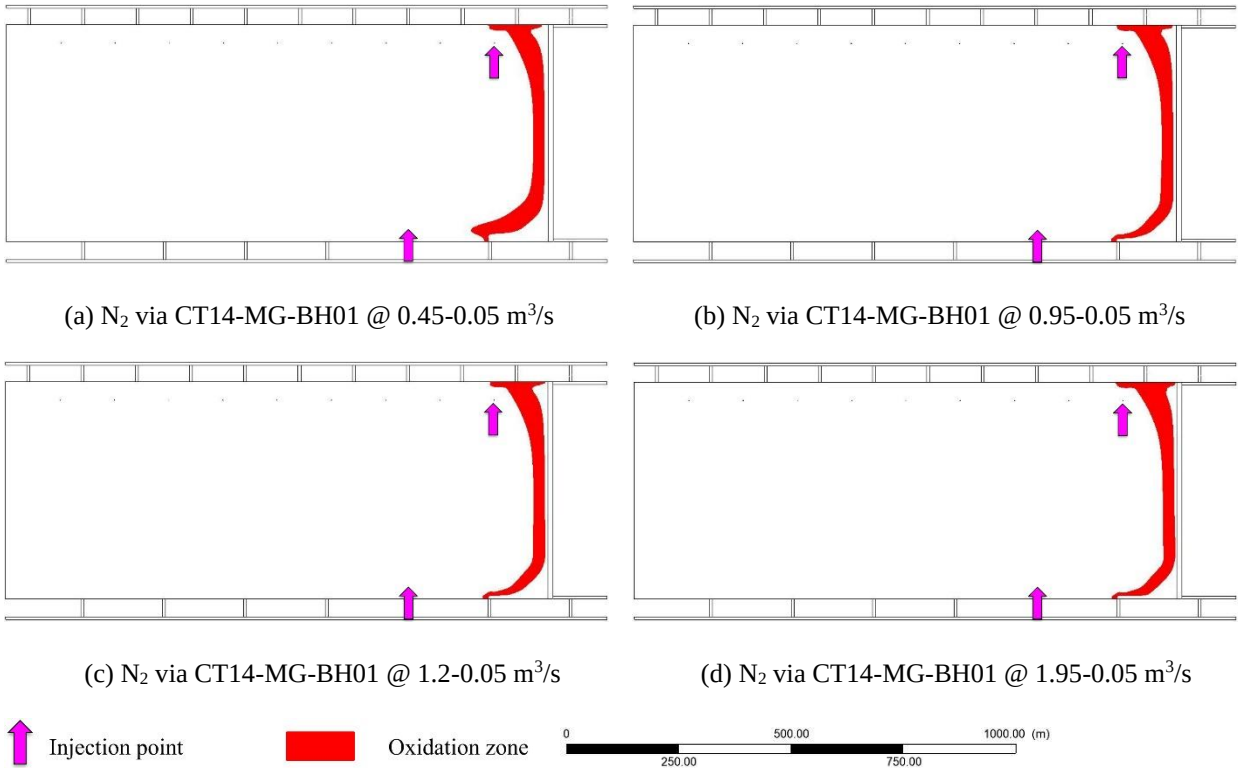

Figure 5.12 Oxidation zone area at different flow rates for 50% CO_2 and 50% CH_4 goaf

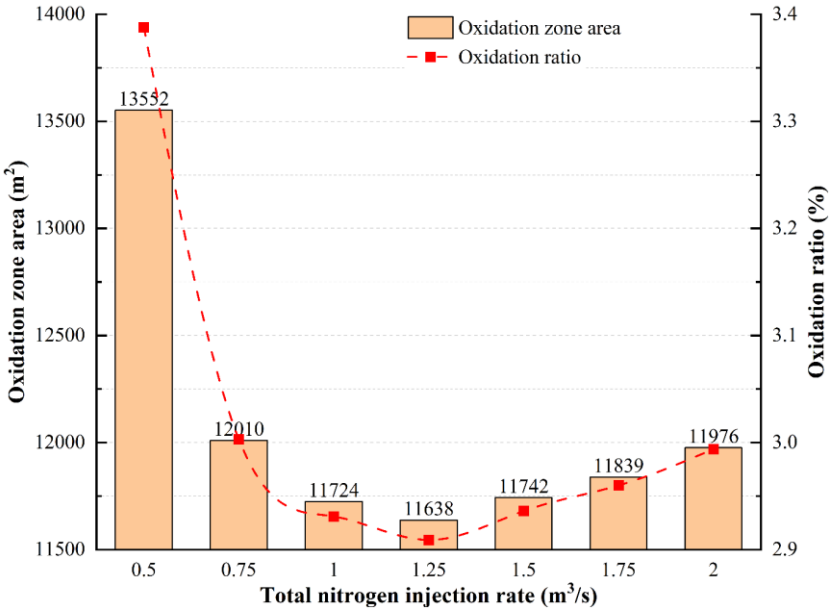

Figure 5.13 Oxidation ratios at different flow rates for 50% CO_2 and 50% CH_4 goaf

As depicted in Figure 5.12 and Figure 5.13, the oxidation zone area reduced gradually as the nitrogen flow rate rose from 0.5 to 1.25 m^3/s. However, as the nitrogen flow rate increased from

1.25 to 2.0 m^3/s, the oxidation zone area increased marginally. This is because the partial dissipation zone (oxygen concentration higher than 18%) at the MG corner was changed into the oxidation zone with the reduction in oxygen concentration in this zone. The results demonstrated that a flow rate of 0.75 m^3/s is better for goaf inertisation, with the oxygen levels lower than 5% at about 100 m behind the face.

Figure 5.14 and Figure 5.15 show the oxidation zone area at different carbon dioxide flow rates for the goaf composed of 20% CO_2 and 80% CH_4 (scenario (d)) and 100% CH_4 (scenario (e)). As for the goaf gas composed of 20% CO_2 and 80% CH_4, it was observed that the oxidation ratio rose with the increase in the carbon dioxide injection rate. This was because that carbon dioxide mixed with oxygen and reduced oxygen concentration at the MG corner, resulting in the dissipation zone being converted to the oxidation zone. Therefore, the optimal carbon dioxide injection rate was 0.5 m^3/s for the goaf gas composition of 20% CO_2 and 80% CH_4. With regard to scenario(e) where the goaf gas was comprised of 100% CH_4, the oxidation ratio reduced as the carbon dioxide flow rate rose from 0.5 to 1.0 m^3/s. However, with the continued increase in carbon dioxide flow rate, the oxidation ratio rose, which was attributed to the fact that the carbon dioxide diluted the oxygen levels in the dissipation zone at the MG corner and converted the dissipation zone to the oxidation zone. As a result, the optimal carbon dioxide injection rate was 1.0 m^3/s for the goaf composed of 100% CH_4.

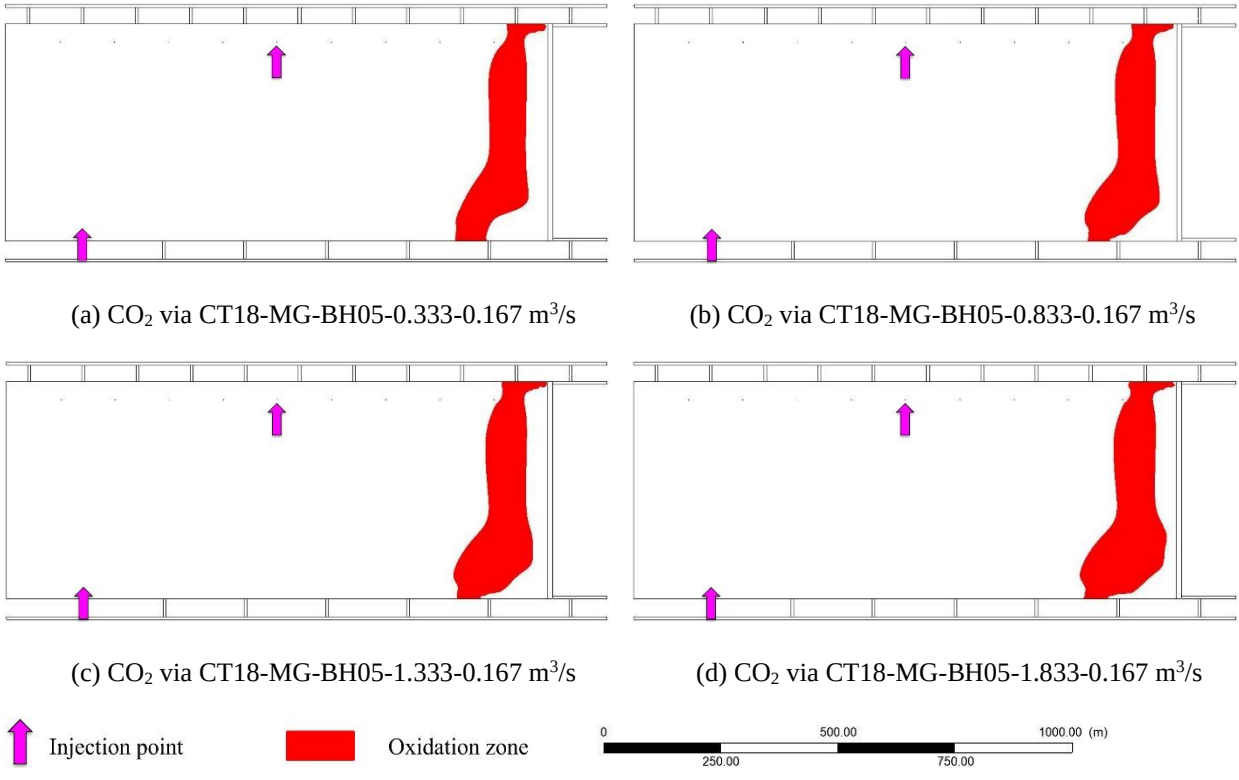

(a) CO_2 via CT18-MG-BH05-0.333-0.167 m^3/s

(b) CO_2 via CT18-MG-BH05-0.833-0.167 m^3/s

(c) CO_2 via CT18-MG-BH05-1.333-0.167 m^3/s

(d) CO_2 via CT18-MG-BH05-1.833-0.167 m^3/s

Figure 5.14 Oxidation zone area at different flow rates for 20% CO_2 and 80% CH_4 goaf

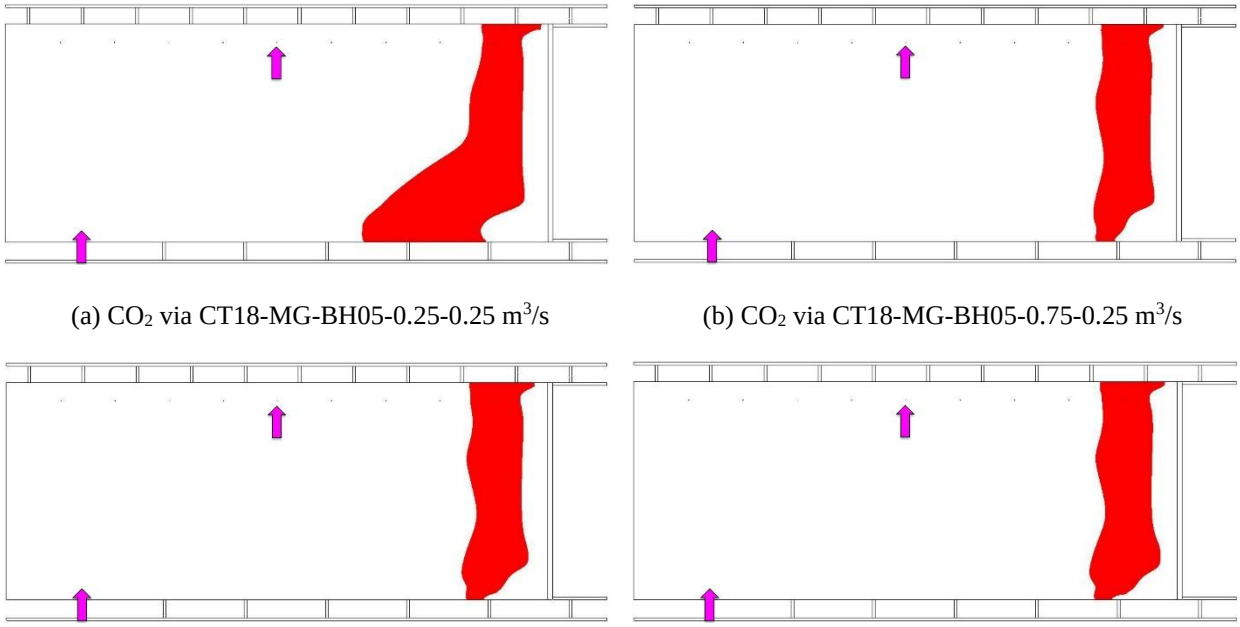

(a) CO_2 via CT18-MG-BH05-0.25-0.25 m^3/s (b) CO_2 via CT18-MG-BH05-0.75-0.25 m^3/s

(c) CO_2 via CT18-MG-BH05-1.25-0.25 m^3/s (d) CO_2 via CT18-MG-BH05-1.75-0.25 m^3/s

Figure 5.15 Oxidation zone area at different flow rates for 100% CH_4 goaf

As shown in Figure 5.16, it was clear that both oxidation zone area and oxidation ratio were higher for 100% CH_4 than 20%CO_2 and 80% CH_4 under the same carbon dioxide injection rate. As the CH_4 composition in the goaf gas rose from 80% to 100%, the optimal carbon dioxide flow rate increased accordingly for effective goaf inertisation. Under the condition of optimal flow rate, the oxidation ratio was lower than 10% for scenarios (d) and (e).

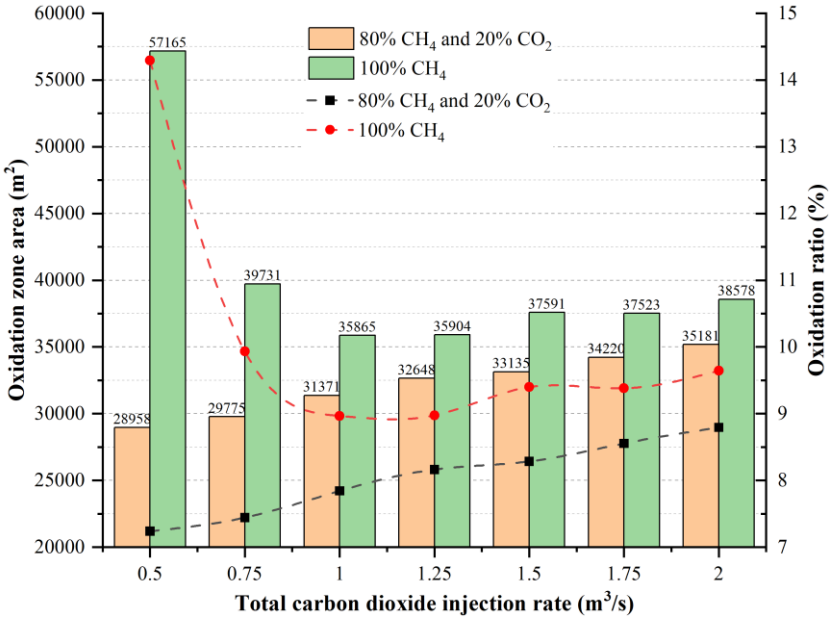

Figure 5.16 Oxidation ratios at different carbon dioxide flow rates for the scenario (d) and (e)

In summary, the optimal inert gas injection rates for scenarios (a), (b), (c), (d) and (e) were 1.5, 1.75, 0.75, 0.5 and 1.0 m^3/s, and the oxidation zone area reduced by 55.76%, 67.21%, 58.04%, 78.17% and 81.82% for the five scenarios, respectively. The nitrogen flow rate required for goaf

inertisation in 100% CO_2 and 80% CO_2 goaf was higher than the carbon dioxide flow rate for the goaf composed of 100% CH_4 and 80% CH_4. In addition, the reduction rate of the oxidation zone area for goaf composed of 100% CH_4 and 80% CH_4 was higher than the goaf comprised of 100% CO_2 and 80% CO_2.

5.4 Conclusions

To enhance the knowledge of ventilation behaviour and gas flow dynamics in the active goaf with different seam gas composition and develop the corresponding proactive goaf inertisation strategies, extensive CFD modelling was performed. Five typical scenarios of goaf gas composition were proposed, and the simulation results were analyzed quantitatively and qualitatively. Scenarios (a), (b), (c), (d) and (e) represent that the goaf gas is composed of 100% CO_2, 80% CO_2 and 20% CH_4, 50% CO_2 and 50% CH_4, 20% CO_2 and 80% CH_4 and 100% CH_4, respectively. The conclusions are summarised below:

(1) Seam gas composition significantly impacted gas flow dynamics in the LW goaf. The simulation results demonstrated that (i) air ingress on both sides of the goaf was evident for scenarios (a), (b),(d) and (e), with oxygen concentration higher than 10% in the deep goaf, while oxygen penetration on both sides of the goaf was limited at 550 m behind the face for scenario (c), with oxygen concentration dropping below 5%; (ii) oxygen was primarily distributed at the middle and upper of the goaf for the scenario (a), (b) and (c), whereas it was mainly layered at the bottom of the goaf area for scenario (d) and (e), which was attributed to buoyancy effect and density difference among goaf gases; (iii) the oxidation ratio showed a decreasing trend as the CH_4 composition rose from 0% to 50%, conversely, the oxidation ratio increased with the continued increase in CH_4 composition from 50% to 100%.

(2) Goaf inertisation strategies were studied to proactively prevent the occurrence of spontaneous combustion in the goaf under different seam gas composition. The results showed that (i) Nitrogen produced a better goaf inertisation result than carbon dioxide for scenarios (a), (b) and (c) where the CO_2 composition was higher than CH_4 composition, while carbon dioxide was superior to nitrogen in rendering goaf atmosphere inert for scenario (d) and (e) where CH_4 composition exceeded CO_2 composition; (ii) Under the condition of total injection rate of 0.5 m^3/s, nitrogen injection at the TG of the goaf performed better in managing spontaneous heating than MG injection for scenarios (a) and (b) where the goaf gas was composed of 100% CO_2 and 80% CO_2, whereas an acceptable goaf inertisation result could be produced by pumping inert gas at both sides of the goaf area for scenario(c), (d) and (e); (iii) the optimal inert gas injection rates for scenarios (a), (b), (c), (d) and (e) were 1.5, 1.75, 0.75, 0.5 and 1.0 m^3/s, and the oxidation zone area reduced by 55.76%, 67.21%, 58.04%, 78.17% and 81.82% for five scenarios, respectively.

The study thoroughly investigated the ventilation behaviour and gas flow dynamics in the LW goaf under different seam gas composition and developed proactive goaf inertisation strategies for each goaf gas scenario. The simulation results shed light on improvements that can be made to current goaf inertisation practice in underground coal mines that experience different seam gas composition, thus containing spontaneous combustion in the active goaf and improving mining safety.

CHAPTER 6 IMPROVED COMPUTATIONAL FLUID DYNAMICS MODELLING OF COAL SPONTANEOUS COMBUSTION CONTROL AND GAS MANAGEMENT

Summary

Underground coal mining is facing increased threats from the hazards of spontaneous combustion and abnormal high mine gas emissions, as a result of increased production outputs and depth of cover. However, most previous Computational Fluid Dynamics (CFD) modelling studies have focused on qualitative rather than quantitative analysis, and the factors influencing spontaneous combustion control and gas management are numerically under-researched. In this chapter, extensive CFD simulations were conducted to investigate the impact of ventilation design and operational measures (e.g., goaf gas tightness, ventilation layouts, proactive goaf inertisation strategies) on spontaneous combustion control, and to study the installation location of brattice and curtains on the longwall (LW) face and tailgate for mitigating high gas levels at the localized tailgate end. Onsite monitoring data was collected for model validation, thus increasing the confidence in study scenarios outside of the base model. The ratio of oxidation zone area (where oxygen concentration lies in 5%~18%) and goaf area were numerically calculated and used for comparison of the potential risk of spontaneous combustion and heating. The modelling results will contribute to the improvement of current practices to effectively suppress spontaneous heating in the LW goaf areas and mitigate methane exceedance at the localized tailgate end.

Citation

M Qiao, T Ren, J Roberts, H Liu, X Yang, L Tan, & J Wu. Improved computational fluid dynamics modelling of coal spontaneous combustion control and gas management. **Fuel**, 2022, 324, 124456.

https://doi.org/10.1016/j.fuel.2022.124456

Abstract

Computational Fluid Dynamics (CFD) is an effective methodology that has been widely used for decades to solve engineering problems involving spontaneous combustion and abnormal gas emissions. However, most of the previous CFD modelling focused on qualitative rather than quantitative analysis, and the factors influencing spontaneous combustion control and gas management are numerically under-researched. The onset of spontaneous heating in the goaf area is dictated by many operational and environmental parameters, including mining method, ventilation and geology. Based on field data from a real mine site, extensive CFD modelling was conducted and analyzed qualitatively and quantitatively to investigate the impact of ventilation design and operational measures on the management and control of spontaneous combustion and gas exceedance. Real-time gas monitoring data was utilized for model validation, and a good agreement between simulation results and monitoring data was reached. The tightness of goaf seals described by permeability was quantitatively investigated, revealing that the permeability should be smaller than 10^{-9} m^2 to prevent air leakage effectively. Goaf inertisation parameter optimization is crucial to minimize the risk of spontaneous combustion. The systematic study revealed that the oxidation zone area (OZA) was the largest for nitrogen injection (29706 m^2), followed by boiler gas (28396 m^2), while it was the smallest for carbon dioxide (11902 m^2), which produced the best goaf inertisation performance. Injection flow rate is another significant factor influencing the effectiveness of heating prevention. The simulation results indicated that a critical injection rate of 1750 m^3/h was determined, and the ratio of the OZA to the goaf area (GA) fluctuated around 7% once the injection rate was beyond this critical value. The installation location of curtains and brattices both on the longwall (LW) face and tailgate end was also simulated and optimized. Noticeable methane reduction at the tailgate end was observed with optimal configurations of brattices and curtains. Results from the modelling will shed light on improving current practices to effectively contain goaf heating in the LW goaf areas and mitigate methane exceedance on the LW face.

Keywords

Spontaneous combustion; Abnormal gas emission; Improved CFD modelling; Tailgate end; Proactive goaf inertisation.

6.1 Introduction

As the fifth-largest coal producer, Australia can yield approximately 500 Mt coal annually, accounting for about 6% of the global coal production (International Energy Agency 2020). Coal mining technology is driven by the need for high-yield and high-efficiency production in Australia, and this is achieved by enlarging longwall (LW) panel width and advancing distance which results

in new challenges for the industry. Two significant challenges faced by underground coal mining are spontaneous combustion and abnormal gas emissions that can threaten safe and high-efficient production (Shi et al. 2021; Tutak et al. 2020; Zhang & Zou 2022).

Spontaneous combustion and heating are deemed to be a longstanding thermal dynamic hazard plagued by many underground coal mines worldwide, particularly those extracting coal with high spontaneous combustion propensity or having left significant quantities of remnant coal in the goaf. The goaf area is characterized by a permeable zone, and air can migrate towards goaf areas via various air leakage pathways and react with residual coal (Szurgacz et al. 2020). When the rate of heat generated by coal oxidation is higher than that of heat dissipated, spontaneous combustion of coal can occur.

If not detected early and managed adequately, spontaneous combustion could cause loss of coal resources, production delay and stoppage, and environmental implications (Ma et al. 2019; Xia et al. 2016; Zhang et al. 2021). In the worst scenario, heating is likely to be escalated into an open fire or initiate a methane explosion when the mixture of methane and oxygen in explosive concentrations is present in the vicinity of the heating site, posing great threats to the health and safety of coal workers. In the last 50 years in Australia, many severe accidents related to spontaneous combustion have already occurred, bringing about catastrophic consequences, and several examples are listed in Table6.1 (Bob 2004; Gluyas 2019; Loane et al. 1975; Terry Martin SC & Clough 2021; Tim & Jennie 2012; Windridge et al. 1994). However, Cliff (2015) predicted that at least one incident associated with spontaneous combustion would occur on average each year, causing coal miners to be withdrawn and evacuated from the mine and even mine closure in some cases. It should also be noted that spontaneous combustion events have occurred in many major coal-producing countries, such as America, China, India, Indonesia, Poland, and South Africa, demonstrating that it is an issue wherever coal is being handled (Brodny & Tutak 2016; Onifade & Genc 2020; Said et al. 2021; Song & Kuenzer 2014).

In addition to spontaneous combustion and heating, concerningly high levels of methane (CH_4) in the return tailgate of the LW panel are becoming prevalent within underground coal mines with higher production rates and deeper mining depth (Tanguturi & Balusu 2014; Tanguturi et al. 2013). To achieve an acceptable level of risk associated with mining activities, both New South Wales and Queensland, as the two largest coal producers in Australia, enacted regulations and acts. Specifically, Coal Mining Safety and Health Regulation 2017 (Queensland Government 2017) by Queensland Government stipulates that the power to the LW shearer, armoured face conveyor, and other machines equipped with automatic methane detectors on the LW face must be tripped off when the methane concentration by volume exceeds 2%. Similarly, Work Health and Safety

(Mines and Petroleum Sites) Regulation 2014 (NSW South Wales 2021) by New South Wales Government specifies that the methane levels by volume in the general body of air in areas where miners work or travel must be controlled below 2%. However, a recent report released by the Queensland Government (Inspectorate 2019) revealed numerous occasions when the methane concentration by volume in the general body of air reached and even exceeded 2.5%, causing power to LW equipment to be cut off and normal operations to be stopped. The gas monitoring data collected from eight underground coal mines operating with LW methods over the course of two years were analyzed, and it was found that the number of gas exceedance incidents was higher than 72 in four of the eight mines, with the most severe one occurrence lasting 600 minutes (Inspectorate 2019).

Table 6.1 Examples of spontaneous heating induced events in Australian coal mines (Bob 2004; Gluyas 2019; Loane et al. 1975; Terry Martin SC & Clough 2021; Tim & Jennie 2012; Windridge et al. 1994)

Time	Mines	Hazard characteristic	Consequence
September 20 1975	Kianga No1. Coal Mine	Explosion initiated by spontaneous combustion	13 miners died, and the mine was sealed
August 7 1994	Moura No.2 Coal Mine	Methane explosion ignited by a heating	11 miners died, and the mine was sealed and closed
December 2003	Southland Colliery	A heating event escalated to an open fire	The mine was closed, and the LW equipment was completely lost
5 January 2011	Blakefield South Mine	Methane explosion highly likely to be ignited by spontaneous combustion	The LW equipment was not recovered
1 September 2018	North Goonyella Mine	A spontaneous combustion event developed into a fire	The mining operation was suspended for 10 months
6 May 2020	Grosvenor Mine	Methane explosion highly likely to be initiated by spontaneous combustion	5 coal miner workers were seriously injured

Recently, Computational Fluid Dynamics (CFD) has been widely used in mining-related research on account of its significant advantages in three-dimensional visualization of results, quick assessment of engineering design, low computational costs as well as solving problems that are difficult or unavailable to be solved by means of traditional laboratory experiments or frequent labour-consuming fieldwork. After calibrating the base model with onsite gas monitoring data from available Tube-Bundle points, Ren et al. (2005; 2009; 2005) and Balusu et al.(2005b) conducted extensive parametric studies with the aim of better understanding the gas flow dynamics and patterns within the goaf and the impact of proactive goaf inertisation on spontaneous

combustion management. Yuan et al. (2008; 2009; 2014) numerically investigate the influence of different ventilation systems (one-entry and two-entry bleederless system and three-entry bleeder system) on airflow patterns and heating distribution in the goaf area and the inertisation performance of different nitrogen strategies. With the aid of CFD simulations, Taraba and Michalec (2011) focused on the influence of the LW advance rate on spontaneous heating within the goaf area and found that the slower the LW advance rate, the higher the peak temperature and shallower the depth of the favourable zone susceptible to spontaneous combustion in the goaf area. The hazardous zone of endogenous fires in the LW goaf was numerically determined by Tutak and Brodny (2017b; 2019) based on oxygen concentration and velocity distribution in the LW goaf where the Y-ventilation system was applied, which provided guidance for taking preventive actions to control the endogenous fires. Given the influence of drainage parameters on the management of spontaneous combustion and gas explosion within the goaf area, Qin et al. (2016a) carried out thorough numerical simulations and reached a conclusion that a reasonable balance between gas drainage efficiency and spontaneous combustion area should be reached in terms of optimizing gas drainage efficiency, particularly drainage pressure. Liu and Qin (2017a; 2017b) modelled both oxygen and carbon monoxide distribution within the goaf area and investigated the influence of advancing rate on spontaneous combustion control. Particular attention was paid by Wang et al. (2018a) and Chu et al. (2018) to studying the influence of various gas drainage parameters on gas control and spontaneous combustion management. Based on site-specific conditions of LW face with a U-type ventilation system, a 3D CFD model was constructed by Brodny and Tutak (2018) to determine the hazardous zone where endogenous fires were highly likely to occur with air velocity ranging from 0.02 to 0.0015 m/s and oxygen concentration higher than 8%. Zhang et al. (2019a; 2020; 2019b) thoroughly undertook scenario-based research on the goaf inertisation method for coal self-heating control, proactively or reactively. Based on specific mining conditions of three adjacent goafs, Liu et al. (2020b) built 3D models and studied the air leakage patterns and nitrogen injection performance for spontaneous combustion control. After calibrating and verifying numerical model results with onsite experiment data, Yang et al. (2021) analyzed the impact of air volume provided to the LW face on the hazardous zone where both spontaneous combustion and gas explosion may simultaneously occur under the condition of a Y-type ventilation system and a high-level roadway serving for gas drainage.

With regard to gas management on the LW face, Mishra et al. (2016; 2018) built 3D simulation models and studied how air velocity on the LW face impacted the methane concentration in the tailgate. The simulation results showed that an increase in air velocity could assist in dispersing methane in the tailgate end and methane concentration was below 1% when the air velocity reached 3 m/s. Brattice curtains or wings are employed in some coal mines in Australia to divert the airflow

and reduce the methane concentration in areas of concern. Ren et al. (2018a) conducted CFD simulations to shed light on the carbon dioxide (CO_2) fringe behaviour on an LW face, and it was observed that the use of brattice in the tailgate could enable CO_2 concentration at the goaf stream of the tailgate end to reduce by 0.5%. A similar study was conducted by Tanguturi et al. (2020) who numerically investigated the impact of various curtain configurations on methane mitigation on the LW face. It was revealed that a combination of curtain installation in the walkway and translational shield could divert face airflow towards the goaf and push methane far away from the motor area in the tailgate, thus resulting in effective methane mitigation performance in this localized area.

From the literature reviewed, it is found that limited numerical simulation work has been done in regards to the impact of hazard control factors (e.g., different ventilation patterns with progressively sealed goaf, the tightness of goaf seals built in the cut-throughs, proactive goaf inertisation, the configurations of ventilation control devices) on gas flow patterns and distribution characteristics in the goaf area and at the tailgate end. The majority of spontaneous combustion-related problems are investigated qualitatively rather than quantitatively. In addition, the impact of the configurations of curtains and brattices (the distance between curtains and goaf ribs, the distance between face brattices and goaf ribs, and the length of the curtains) on the LW face and in the tailgate end on methane mitigation at the goaf fringe are under-researched. Based on the specific geological condition of an Australian underground coal mine experiencing severe coal spontaneous heating problem, extensive CFD modelling simulations were conducted to provide improved insight into the impact of mining factors on gas flow dynamics and patterns in the goaf area and goaf fringe, and help mine operators to design the most effective control measures for both spontaneous combustion and heating in the goaf and methane exceedance in the tailgate end, thus improving coal mining safety and high-efficiency production.

6.2 Geological and Mining Conditions

In this paper, a typical coal mine (Mine B) in Queensland was selected for the simulation study. This mine is located 34 km north of Moranbah in the Central Queensland Coalfields in Australia. There are four coal seams in the mining area: Goonyella Upper Seam (GUS), P Seam, Goonyella Middle Seam (GMS), and Goonyella Lower Seam (GLS). The measured coal seam gas contents lie in the range of 0~10 m^3/t. The gas content level increases as the depth of cover rises, or the seam dips to the east. The coal seam gas in the area of interest is primarily composed of methane (higher than 95%).

This mine utilizes a retreat LW mining method that extracts the Goonyella Middle Seam (GMS) using Longwall-Top-Coal-Caving (LTCC) equipment. The thickness of GMS ranges from 6.5 m

to 7.5 m, and the seam dips almost uniformly at 4° to the east. The LW face is typically 320 m wide, with extraction height varying from 3.9 m to 7.5 m. Continuous miners are developing gateroads with typical roadways at 5.6 m x 3.4 m and 120 m pillar spacing. With the advancement of LW panels, part of coal resources were left in the goaf area, which could provide fuels for heating and combustion. If the heat generated by spontaneous combustion could not be dissipated timely, a spontaneous combustion event was highly likely to occur, leading to production delay and stoppage, and environmental pollution from toxic or suffocating gas emissions.

A U-Type ventilation pattern is applied at this mine, which typically involves air flowing towards and across the LW face, then returning out the tailgate. For the Top Coal Caving Longwall Face, the target LW face quantity is 66 m^3/s.

As coal resources continued to be extracted from LW panel 13 (LW13), high gas emission incidents occurred multiple times, significantly plaguing everyday operations. In addition, massive oxygen ingress into the goaf area was measured, which increased the potential risk of spontaneous heating. The main complexity of spontaneous combustion and gas control optimization in the goaf is the lack of understanding of gas flow patterns in LW goaf and the influence of various hazard control factors (e.g., the tightness of goaf seals at the cut-throughs, ventilation patterns, goaf inertisation parameters, the configurations of brattices and curtains) on goaf gas flow behaviour.

Therefore, a basic understanding of the gas flow dynamics of LW goaf under various conditions is essential. This knowledge is helpful to identify the gas flow dynamics and patterns in the goaf and develop the optimal goaf inertisation strategy and gas control system for underground coal mines.

6.3 CFD Model

6.3.1 Mathematical model

The gases on the LW face and in the goaf area must comply with several governing equations, mainly including the mass conservation equation, momentum conservation equation, and species transport equation (ANSYS 2018a).

(1) Mass conservation equation

$$\frac{\partial \rho}{\partial t} + \nabla(\rho \vec{\boldsymbol{u}}) = S_m \qquad (6-1)$$

Where: ρ is the fluid density; t is the time; $\vec{\boldsymbol{u}}$ is the velocity component in three different directions; S_m stands for the mass added to the continuous phase from the dispersed second phase. If the dispersed second phase does not exist, then S_m=0.

In three dimensions using Cartesian coordinates:

$$\vec{\boldsymbol{u}} = \frac{\partial u}{\partial x} + \frac{\partial v}{\partial y} + \frac{\partial w}{\partial z} \qquad (6-2)$$

(2) Momentum conservation equation

$$\rho\left(\frac{\partial \vec{\boldsymbol{u}}}{\partial t} + \vec{\boldsymbol{u}} \cdot \nabla \vec{\boldsymbol{u}}\right) = -\nabla \boldsymbol{p} + \mu \nabla^2 \vec{\boldsymbol{u}} + F \qquad (6-3)$$

Where: $\nabla \boldsymbol{p}$ represents the pressure gradient; μ denotes the fluid viscosity; F is the body force vector. In particular, $\rho \frac{\partial \vec{\boldsymbol{u}}}{\partial t}$ and $\rho \vec{\boldsymbol{u}} \cdot \nabla \vec{\boldsymbol{u}}$ denote the force component as a result of momentum change and convective acceleration, respectively. $\mu \nabla^2 \vec{u}$ stands for the viscous force.

(3) Species equation

$$\frac{\partial}{\partial t}(\rho Y_i) + \nabla \cdot (\rho \cdot \vec{\boldsymbol{u}} \cdot Y_i) = -\nabla J_i + R_i + S_i \qquad (6-4)$$

Where: Y_i represents the local mass fraction of the specific species i; J_i is the diffusion flux of the species i; R_i stands for the net rate of production of species i by chemical reaction; S_i denotes the rate of creation by addition from the dispersed phase plus any user-defined sources. An equation of this form will be solved for $N-1$ species where N is the total number of fluid phase chemical species present in the numerical modelling.

(4)Turbulence model

Besides the above governing equations, the selection of the turbulence model plays a determining role in simulation results. There are many built-in turbulence models in Fluent, among which the standard k-epsilon (k-ε) model has been widely used in gas-related simulations due to its simplicity and reliability for free-shear layer flows where only small pressure gradients occur (Mishra et al. 2016; Song et al. 2021a; Tutak & Brodny 2018; Wang et al. 2018e).

The standard k-ε model is a two-equation turbulence model, comprising two significant parameters: turbulent kinetic energy (k) and turbulent dissipation rate (ε).

$$\frac{\partial}{\partial t}(\rho k) + \frac{\partial}{\partial x_i}(\rho k u_i) = \frac{\partial}{\partial x_j}\left[\left(\mu + \frac{\mu_t}{\sigma_k}\right)\frac{\partial k}{\partial x_j}\right] + G_k + G_b - p\varepsilon - Y_M + S_k \qquad (6-5)$$

$$\frac{\partial}{\partial t}(\rho \varepsilon) + \frac{\partial}{\partial x_i}(\rho \varepsilon u_i) = \frac{\partial}{\partial x_j}\left[\left(\mu + \frac{\mu_t}{\sigma_\varepsilon}\right)\frac{\partial \varepsilon}{\partial x_j}\right] + C_{1\varepsilon}\frac{\varepsilon}{k}(G_k + C_{3\varepsilon}G_b) - C_{2\varepsilon}\rho\frac{\varepsilon^2}{k} + S_\varepsilon \qquad (6-6)$$

Where: G_k and G_b denote the generation of turbulence kinetic energy due to the mean velocity gradients and buoyancy, respectively; Y_M stands for the contribution of the fluctuating dilatation in compressible turbulence to the overall dissipation rate; σ_k and σ_ε are the turbulent Prandtl numbers for k and ε with a default value of 1.0 and 1.3, respectively; S_k and S_ε are user-defined

source terms. $C_{1\varepsilon}$, $C_{2\varepsilon}$, and $C_{3\varepsilon}$ are constants. The default values for $C_{1\varepsilon}$ and $C_{2\varepsilon}$ are 1.44 and 1.92, respectively.

$$\mu_t = \rho C_\mu \frac{k^2}{\varepsilon} \qquad (6-7)$$

Where: μ_t is a constant with a default value of 0.09.

6.3.2 Numerical model

6.3.2.1 Model construction

Necessary information was collected, and a field dataset was built, mainly including the basic geometric information of the LW goaf, goaf gas composition and emission rate, ventilation systems, gas drainage system, and onsite monitoring gas data of LW operations.

Based on the field dataset, a full-scale 3D model representing the case of a 500-meter-deep goaf was developed using Design Modeller within ANSYS Workbench 18.2, which is referred to as the base model in the following sections. The plan view of the base model is illustrated in Figure 6.1, where the green arrows denote the direction of fresh air, and the red arrows represent the direction of dirty air. The LW face is 320 m long, including the width of maingate (MG) and tailgate (TG), and the width and height of the face are 9 m and 4 m, respectively. The intake and return gateroads are all in the shape of a rectangle, with the dimension of 5.6 m×3.4 m (width×height). In Figure 6.1, TB stands for Tube Bundle that is employed to monitor the concentration of major goaf gases (methane, oxygen, carbon dioxide, carbon monoxide) in a long-term manner. CT represents the cut-throughs connecting the goaf area and gateroads. GD denotes the surface boreholes which serve as post-drainage to reduce methane levels below the statutory limits during mining operations, and the position of each surface borehole is listed in Table 6.2.

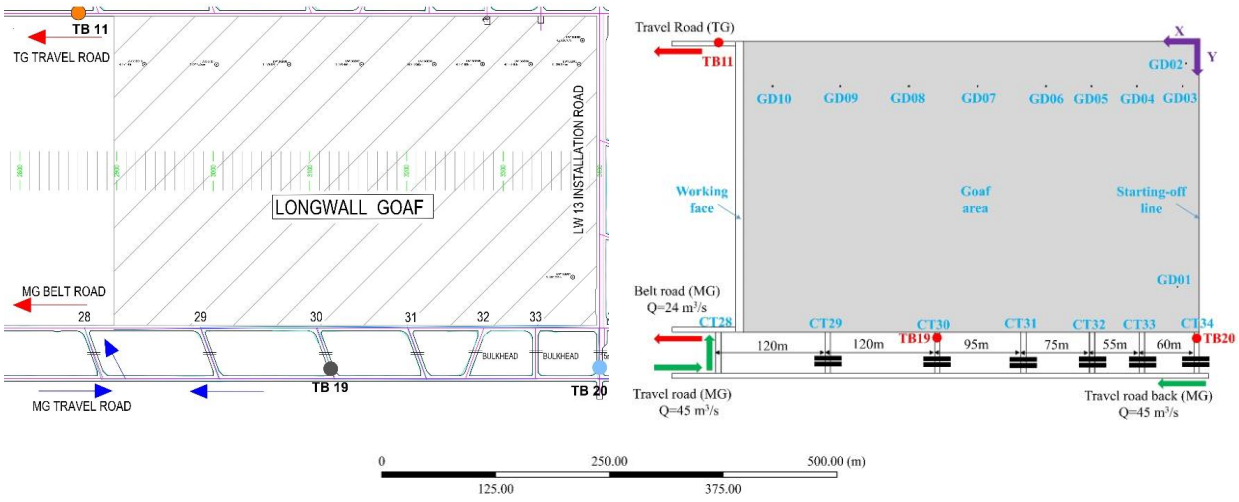

(a) LW layout (b) CFD model layout

Figure 6.1 Model geometry for LW retreating stages-plan view

Table 6.2 Surface borehole coordinates

	GD01	GD02	GD03	GD04	GD05	GD06	GD07	GD08	GD09	GD10
X (m)	25	15	18.4	68.6	118.5	168.4	243.5	318.9	393.9	468.5
Y (m)	270	25	50	50	50	50	50	50	50	50
Z (m)	24	24	24	24	24	24	24	24	24	24

The physical model was meshed using the hexahedron meshing method for gateroads, LW face, coal seam and floor, and the tetrahedron meshing method for the drainage borehole to accommodate the complex geometry. The mesh size for the gateroads and drainage boreholes was 1 m and 0.25 m, respectively. A mesh independence study was conducted. The mesh sizes for the coal seam were 2.5 m. 1.5 m and 1.0 m for coarse, medium and fine mesh, and the total element for the three scenarios were 789375, 881322 and 1235418, respectively. As shown in Figure 6.2, there were no significant differences in velocity on the MG and TG side along the goaf. As a result, the medium-mesh model was chosen for the following numerical study. The minimum orthogonal quality and the maximum skewness value were 0.85 and 0.47, respectively, both of which indicated that the meshed model was of very good quality according to ANSYS meshing users' guide (ANSYS 2018b). The medium-mesh model was imported into Ansys Fluent for flow dynamics calculation. The model was refined with higher density mesh in the areas of interest, such as in the vicinity of the face and airways in ANSYS Fluent by using the region adaption function, as illustrated in Figure 6.3.

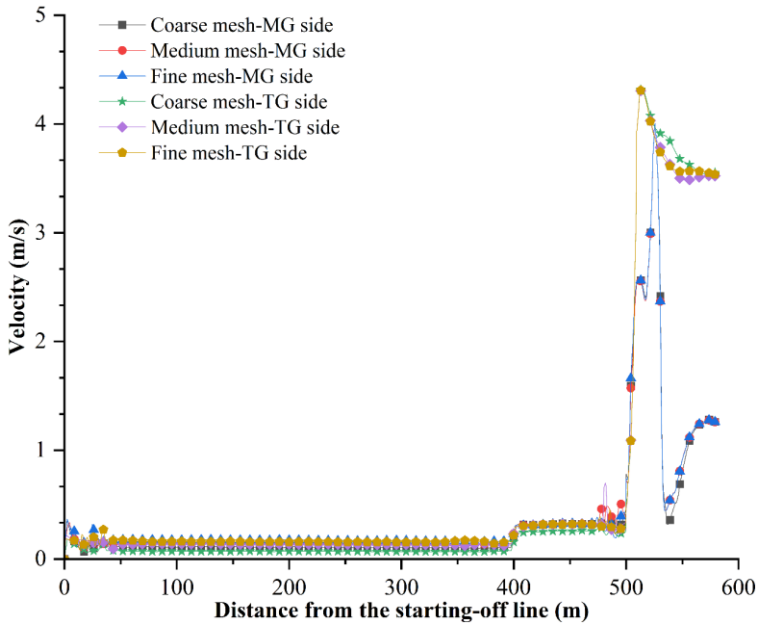

Figure 6.2 Velocity comparison on the MG and TG side for different meshed models

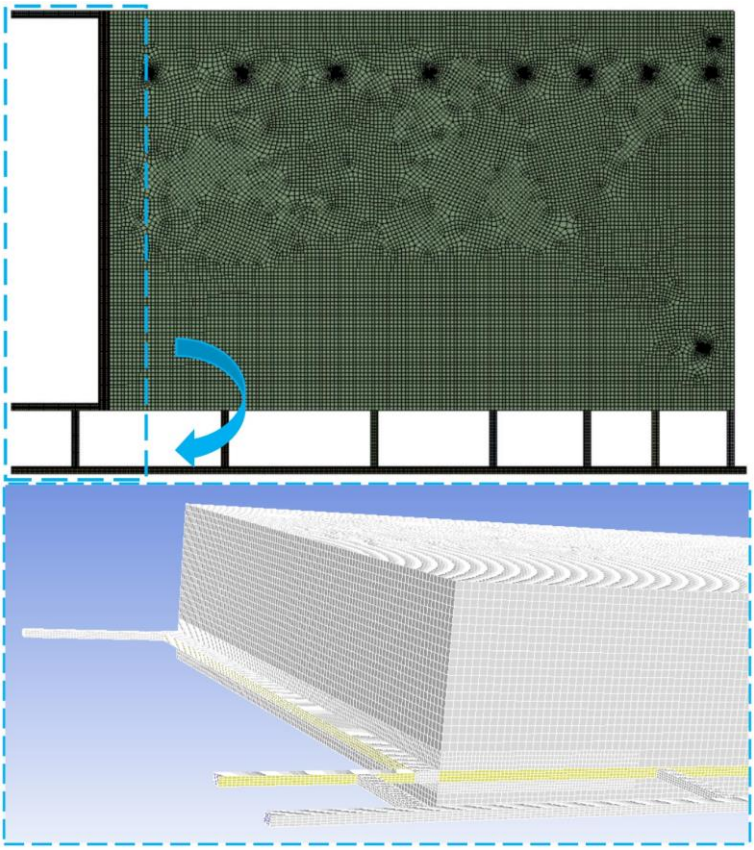

Figure 6.3 CFD meshed model

6.3.2.2 Boundary condition determination

Based on the field dataset, boundary conditions and corresponding parameters have been established for the CFD simulations, as listed in Table 6.3.

Table 6.3 Boundary conditions for the numerical model

Name	Boundary type	Value	Name	Boundary type	Value
Viscous model	Standard k-ε	/	Species model	Species transport	Methane-air
Travel road (MG)	Velocity inlet	2.4 m/s	Travel road back (MG)	Velocity inlet	2.4 m/s
Belt road (MG)	Velocity inlet	-1.3 m/s	Travel road (TG)	Outflow	/
GD09	Velocity inlet	-0.7 m/s	Gravity	X-direction	-0.6843 m/s^2
Gravity	Y-direction	0 m/s^2	Gravity	Z-direction	-9.7864 m/s^2

The standard k-epsilon (k-ε) turbulence model was applied to predict the turbulent transport through the flow region (Mishra et al. 2016; Ren & Balusu 2005; Tanguturi & Balusu 2014; Tanguturi & Balusu 2015; Tutak & Brodny 2017b). The velocity inlet was assigned to the belt road, travel road and travel road back on the MG side, while an outflow condition was assigned to the travel road on the TG side. Coal ribs, floors, and roofs were considered no-slip standard walls to estimate the flow near the boundaries. The model was set up to reflect the laminar flow in the

goaf area as a result of the small velocity within this region and the turbulent flow in the LW gateroads (Ma et al. 2020a; Taraba & Michalec 2011; Yuan & Smith 2014; Zhu & Liu 2012).

The elevation of the LW face is higher than that of the start-off line with a dip angle of 4°, while MG and TG sides are at the seam height. In Fluent, the gravity was activated and decomposed accordingly due to the consideration of the buoyancy effect of goaf gases.

As reported by Guo et al. (2012) and Qin et al. (2015), the permeability distribution in the goaf area was in the shape of an O-ring, with a higher value on the edge of the goaf area and a lower value in the centre of the goaf area. Based on the information provided by the mine site and the equations (6-8)-(6-11) (Liu 2019), the permeability distribution in the goaf ranged from 10^{-3} m^2 to 10^{-10} m^2, as shown in Figure 6.4. The model was set up to simulate both turbulent flow conditions near the face and laminar flow inside the goaf region.

$$\left\{\alpha = 10^{-(a_1+a_2*\tanh(\frac{Z_i-Z_0}{a_{z1}}))*(\frac{Y_i-Y_0}{a_y}+0.5+\left(0.5-\frac{Y_i-Y_0}{a_y}\right)*\tanh\left(\frac{X_i-X_0}{a_{x1}}\right)}, Z_i \le \frac{z_0+z_1}{2}, X_i \le \frac{X_0+X_1}{2}\right\} \quad (6-8)$$

$$\left\{\alpha = 10^{-(a_1+a_2*\tanh(\frac{Z_1-Z_i}{a_{z2}}))*(\frac{Y_i-Y_0}{a_y}+0.5+\left(0.5-\frac{Y_i-Y_0}{a_y}\right)*\tanh\left(\frac{X_i-X_0}{a_{x1}}\right)}, Z_i > \frac{z_0+z_1}{2}, X_i \le \frac{X_0+X_1}{2}\right\} \quad (6-9)$$

$$\left\{\alpha = 10^{-(a_1+a_2*\tanh(\frac{Z_i-Z_0}{a_{z1}}))*(\frac{Y_i-Y_0}{a_y}+0.5+\left(0.5-\frac{Y_i-Y_0}{a_y}\right)*\tanh\left(\frac{X_1-X_i}{a_{x2}}\right)}, Z_i \le \frac{z_0+z_1}{2}, X_i > \frac{X_0+X_1}{2}\right\} \quad (6-10)$$

$$\left\{\alpha = 10^{-(a_1+a_2*\tanh(\frac{Z_1-Z_i}{a_{z2}}))*(\frac{Y_i-Y_0}{a_y}+0.5+\left(0.5-\frac{Y_i-Y_0}{a_y}\right)*\tanh\left(\frac{X_1-X_i}{a_{x2}}\right)}, Z_i > \frac{z_0+z_1}{2}, X_i > \frac{X_0+X_1}{2}\right\} \quad (6-11)$$

Where: α stands for the permeability in the goaf area; a_1 and a_2 are the constants; X_i, Y_i and Z_i represent the coordinates of any position in the goaf area in the direction of the face length, face height and face retreat, respectively; X_0, Y_0 and Z_0 stand for the coordinates at the start of the goaf far away from the LW face; X_1 is the x coordinate at the goaf immediately behind the LW face; Z_1 stands for the z coordinate at the other side of the goaf; a_{x1}, a_{x2}, a_y, a_{z1} and a_{z2} represent the coefficients determining the permeability change in x, y and z direction, respectively.

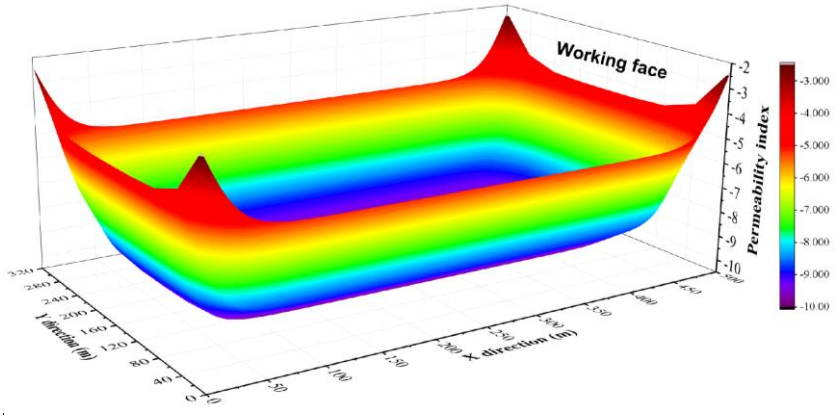

(a) 3D permeability distribution at Z=12m

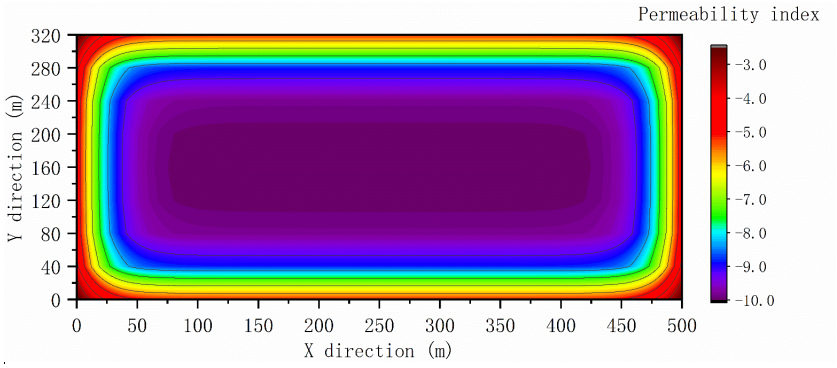

(b) plan view of the permeability distribution at Z=12m

Figure 6 4 Permeability distribution at Z=12m within the goaf area

The height of the LW model is 80 m, including 10 m of floor strata, 4 m average cutting height, and 66 m roof above the mined seam. The flow through the goaf area was handled using a User Defined Function (UDF) subroutines, in which flow through the porous goaf regions was simulated by adding a momentum sink to the momentum equations (Ren & Balusu 2005). Some subroutines were written to represent the goaf gas emissions and gas drainage scenarios, then combined with the main FLUENT program to carry out the simulations. The UDF is also used to define all the seals around the goaf areas.

The site data collected was used to define goaf gas emission and drainage. The drained gas from GD09 was 711 l/s, and the ventilated gas was 143 l/s, meaning that the total goaf gas emission rate is 854 l/s. Amid the monitoring period, inert gas containing 97% nitrogen (N_2) and 3% oxygen (O_2) was injected into the goaf area via CT34 with an injection rate of 2000 m^3/h.

6.3.3 Simulation results of the verified model

The tube bundle history data collected was used for model validation. There were minor differences in oxygen and nitrogen readings in TB11, TB19, and TB20. As a result, the average value of oxygen and nitrogen was calculated for model verification.

Convergence of the simulations was judged based on monitoring of the oxygen concentration on the MG and TG side of the goaf where convergence was acceptable when the results did not change by more than 0.1%.

The gas compositions at three locations were compared with the CFD simulation results listed in Table 6.4. It can be seen from Table 6.4 that the concentration of oxygen and nitrogen obtained by the CFD simulation was similar to the monitoring data at all three locations. Therefore, the model could predict gas distribution for the LW goaf and investigate the influence of different mining parameters on spontaneous combustion control and gas management in the goaf area.

The results of the calibrated-case simulations are presented in Figure 6.5 and Figure 6. 6, showing

the distribution of oxygen and methane (CH_4) in the LW goaf. The 3D figures show two slices along with the LW panel. The horizontal slice was midway through the seam, and the vertical slice was 50 m from the tailgate rib along the surface goaf holes line. The 2D figures in the plan view show the gas distribution at the working seam elevation.

Table 6.4 Comparison of gas composition at three locations

	Tube 11			Tube 19			Tube 20		
	O2	N2	Others	O2	N2	Others	O2	N2	Others
Numerical (%)	20.47	79.07	0.47	20.77	79.07	0.17	5.87	92.33	1.81
Actual (%)	20.38	79.24	0.39	20.72	79.12	0.16	5.79	92.64	1.57
Error (%)	0.09	-0.17	0.08	0.05	-0.06	-0.01	0.08	-0.31	0.24

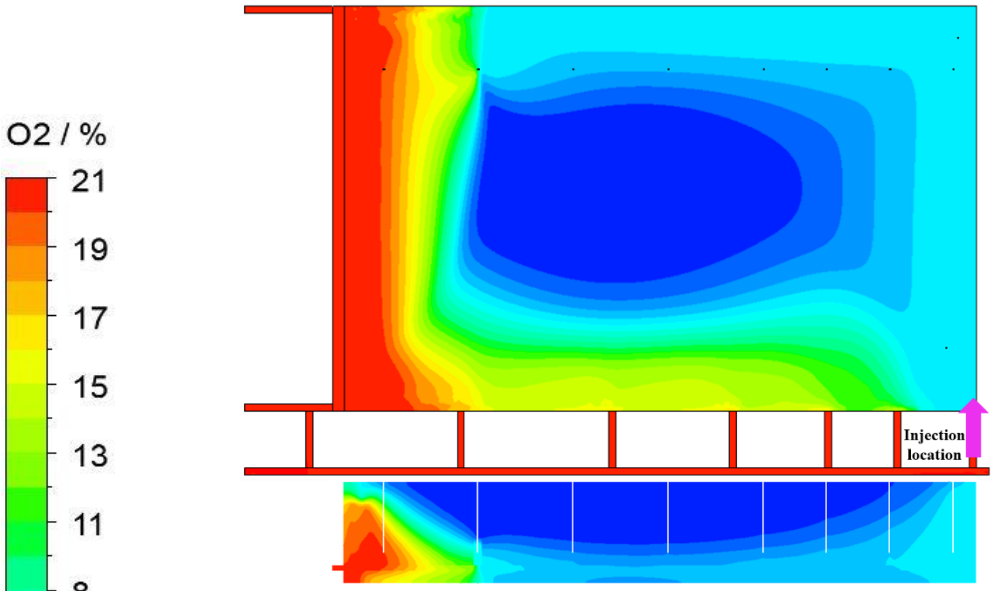

(a) Plan view

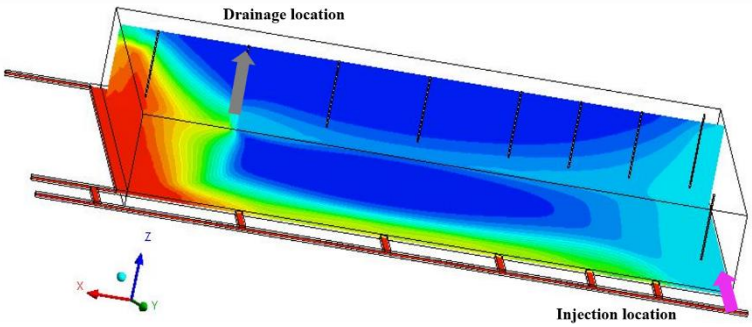

(b) 3D view with vertical sections superimposed on the base level

Figure 6.5 Oxygen distribution in the LW goaf-calibrated model results

Results showed that oxygen ingress into the goaf was high on the intake side of the goaf. This may be because more oxygen could flow into the goaf via cut-throughs under the high pressure

difference between the travel road on the MG side and the goaf area. Another reason for this may be attributed to a small portion of oxygen injected into the goaf via CT34. In contrast, the oxygen penetration into the goaf on the TG side was shorter as nitrogen injected could flow from the deep goaf towards the face under the pressure difference. The 3D figures showed the effect of gas buoyancy and the resultant air/gas layering in the goaf with higher oxygen concentration near the working seam level and methane gas displaced at the higher elevation parts of the caving.

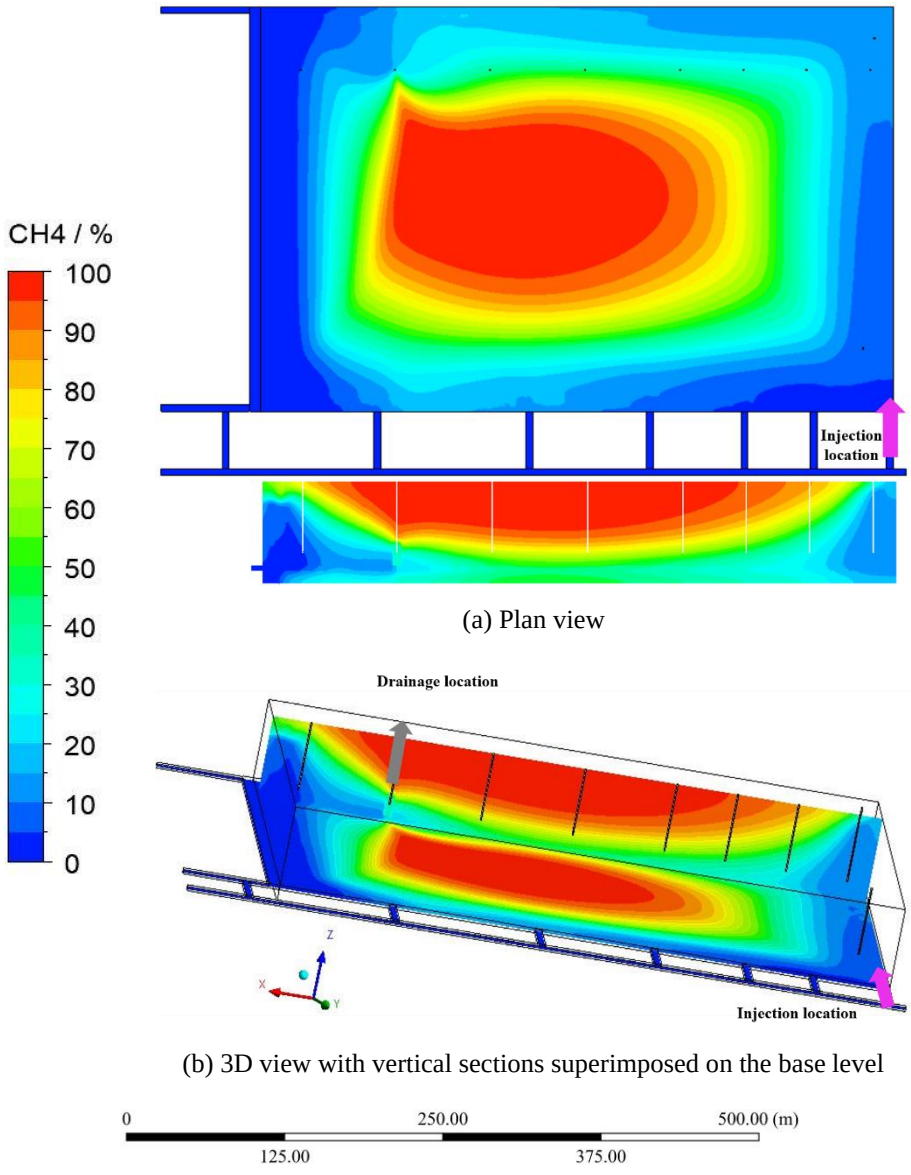

(a) Plan view

(b) 3D view with vertical sections superimposed on the base level

Figure 6.6 Methane distribution in the LW goaf-calibrated model results

The Reynolds number in the goaf area is as expected according to the literature (Ma et al. 2020a; Taraba & Michalec 2011; Yuan & Smith 2014; Zhu & Liu 2012) of laminar flow with a value of less than 200 in the centre of the goaf. On the periphery of the goaf area where the permeability was high, the cell Reynolds number was higher than 2300, which was considered a turbulent zone. In addition, the pressure at the travel road back (MG) and travel road (TG) was 57 Pa and -163 Pa, respectively. The pressure at the seam level slowly reduced from the deep goaf towards the LW

face, which was similar to the results obtained by Guo et al. (2015). The pressure at the bottom of the drainage hole was -559 Pa as a result of the significant suction effect of draining methane from the goaf area.

6.4 Results and Discussion

In order for better comparison and illustration in the parametric studies, a model without inert gas injection via CT34 and gas drainage via GD09 was developed as a secondary base model for comparison in the parametric studies, with oxygen distribution illustrated in Figure 6.7. In the secondary base model, the total methane emission rate in the goaf remained the same at 854 l/s, and the other parameter settings were kept unchanged to that of the verified model in section 6.3.3.

It can be seen that the oxygen concentration was higher at the periphery of the goaf, with the lowest oxygen concentration in the centre of the goaf area without gas drainage and nitrogen injection.

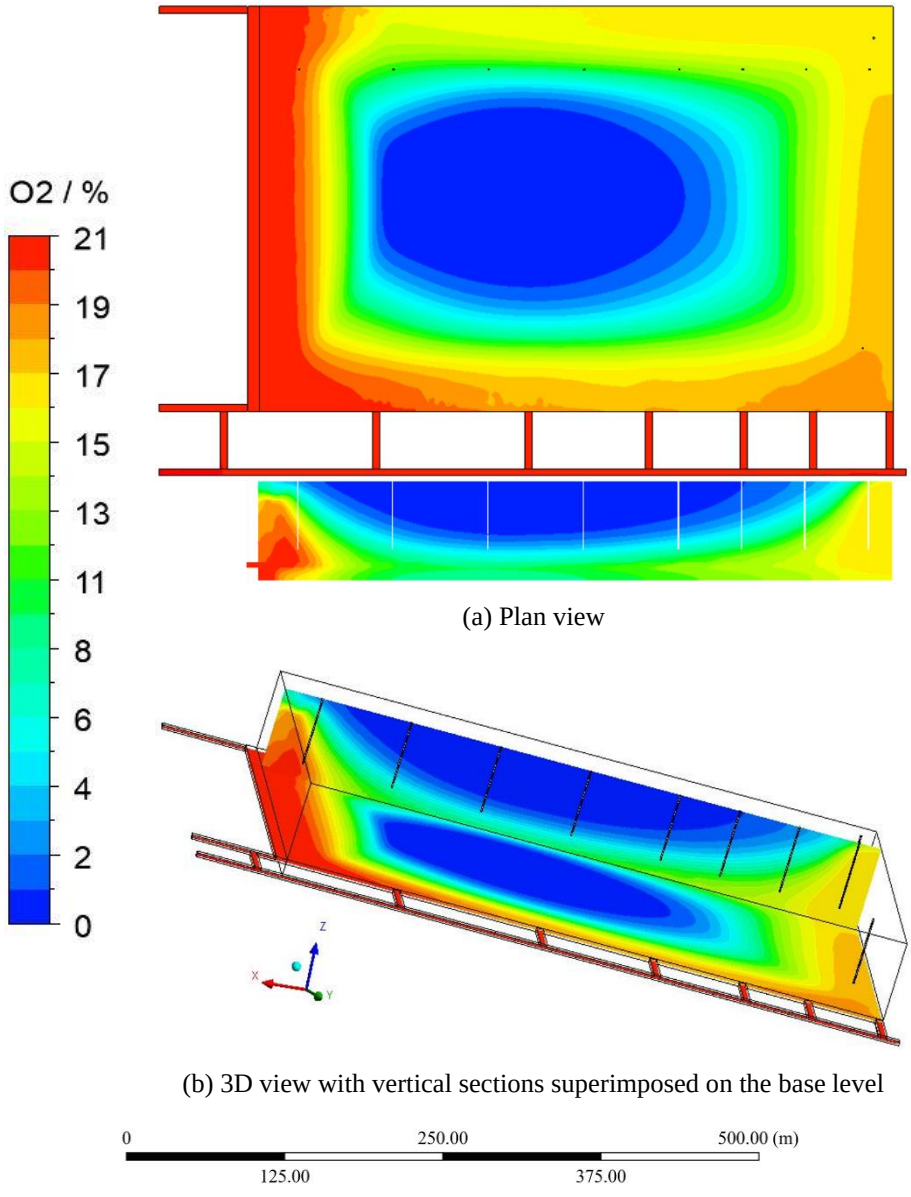

(a) Plan view

(b) 3D view with vertical sections superimposed on the base level

Figure 6.7 Oxygen concentration distribution in the goaf area

The ratio of the oxidation zone area (OZA) to the goaf area (GA) was introduced for the purpose of quantitatively studying the influence of ventilation patterns. The oxygen concentration in the oxidation zone varied among different scholars, as listed in Table 6.5. From the view of safety, oxygen concentration ranges from 5% to 18% in the oxidation zone in this study.

Table 6.5 Oxygen concentration in the oxidation zone defined by scholars

Scholars	Oxygen concentration in the oxidation zone
Liu et al. (2016a)	5% ~ 15%
Deng et al. (2018)	5% ~ 18%
Ma et al. (2019)	5% ~ 15%
Chen et al. (2020a)	5% ~ 15%
Liu et al. (2020b)	7.4% ~ 18%
Li et al. (2021b)	8% ~ 18%

6.4.1 Goaf gas emission rates

The effect of goaf gas emission rates under the same ventilation condition without gas drainage and nitrogen injection is shown in Figure 6.8.

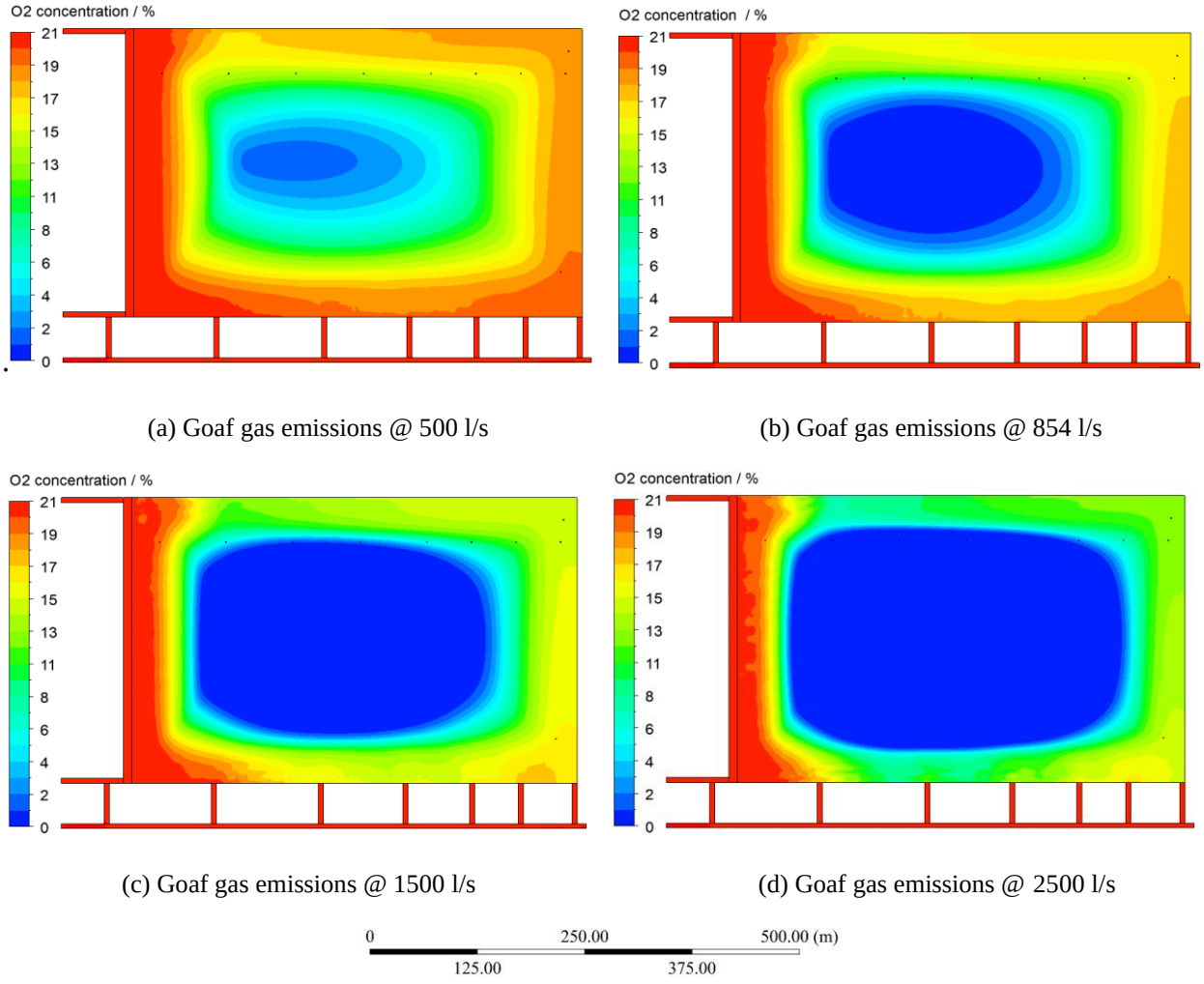

(a) Goaf gas emissions @ 500 l/s

(b) Goaf gas emissions @ 854 l/s

(c) Goaf gas emissions @ 1500 l/s

(d) Goaf gas emissions @ 2500 l/s

Figure 6.8 Effect of goaf gas emission rate on oxygen distribution in the LW goaf

It is noted that the goaf gas emission rate has a major impact on the oxygen distribution in the LW goaf. More specifically, with the increase in gas emission rate, the oxygen concentration on the MG and TG side reduced, and the oxygen peak value at the rear cut-throughs also dropped. In addition, as the gas emission rate rose from 500 l/s to 2500 l/s, the oxygen concentration in the deep goaf close to the starting-off line decreased from around 19% to 14%, while the low oxygen concentration area (<2%) mainly located at the centre of the goaf area rose dramatically. Quantitative analysis of simulation results indicated that the ratio of OZA to GA dropped from 58.41% to 35.79%, as the goaf gas emission rate increased from 500 l/s to 2500 l/s. This was because that methane with a high emission rate could prevent oxygen-bearing air from penetrating into the centre goaf area through various leakage pathways.

6.4.2 The tightness of goaf seals at the cut-throughs

Practically, the quality of seals built in the cut-throughs could significantly influence oxygen ingress characteristics in the goaf area. The air leakage into the goaf area via cut-throughs was evident due to the pressure difference between the maingate gateroad and the goaf area. Permeability was introduced to quantitatively describe the tightness of goaf seals built in the cut-throughs on the MG side. In comparison to the permeability of seals (normal permeability: 10^{-7} m^2) assigned in the verified base model, three more scenarios were proposed with permeability differences of one order of magnitude among scenarios, namely higher permeability (10^{-6} m^2), lower permeability (10^{-8} m^2), and much lower permeability (10^{-9} m^2). The simulation results were obtained under inert gas injection at CT34 and gas drainage via GD09, which corresponds to the calibrated model in section 6.3.3.

The oxygen concentration contours at the seam level are shown in Figure 6.9. It was apparent that the permeability of the seals played a significant role in oxygen distribution in the LW goaf. To be more specific, as the seals were constructed with higher standards and quality, the oxygen concentration in deep goaf reduced significantly. The air penetration into the goaf area via seals could be mitigated effectively, as shown in Figure 6.9 in which oxygen concentration in each cut-through on the MG side reduced considerably as the permeability of seals reduced. Mainly, oxygen spikes could be observed at the cut-throughs on the MG side. In addition, the oxygen concentration on the TG side could reduce to below 5% when the seals were sealed tightly, as shown in Figure 6.10. As a result, it was strongly recommended that the seals be constructed as tight and strong as possible to reduce the air leakage into the goaf area and improve goaf inertisation performance from the perspective of spontaneous combustion management.

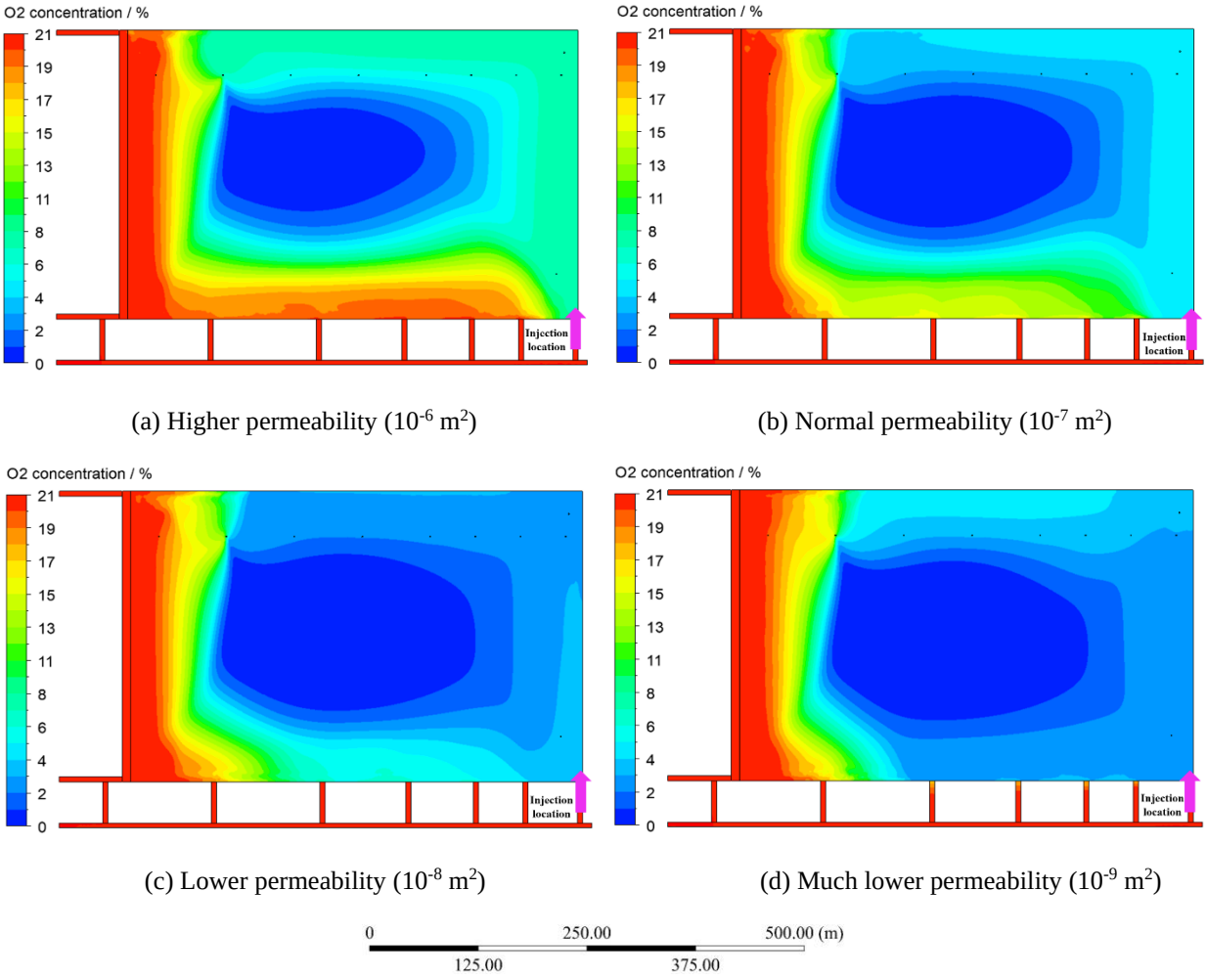

Figure 6.9 Effect of tightness of seals at cut-throughs on oxygen distribution at the seam level

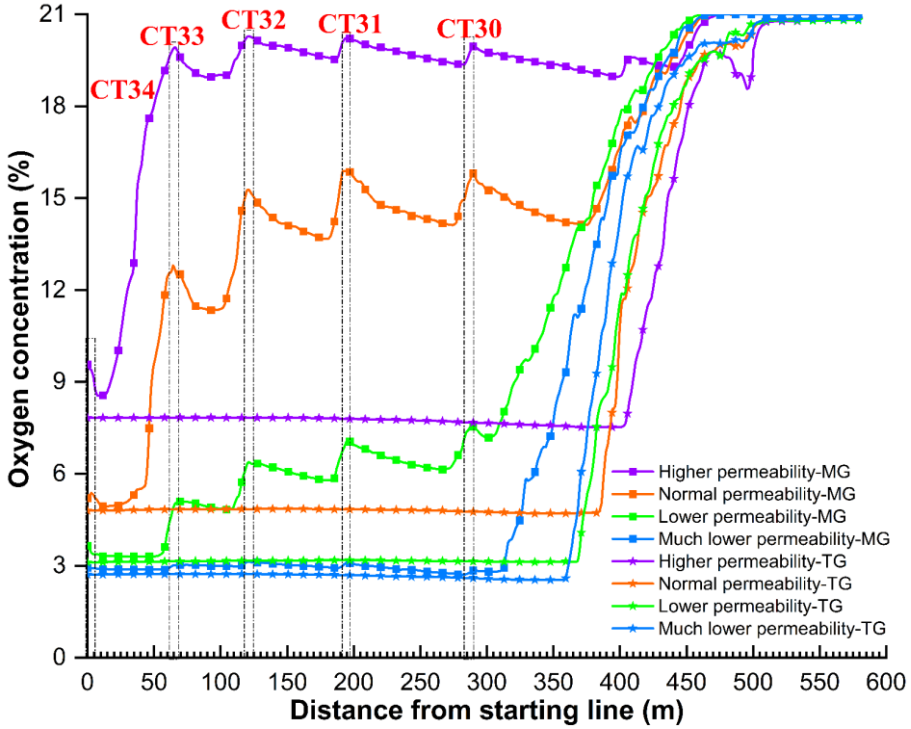

Figure 6.10 Oxygen concentration on the MG and TG side (2m from the rib)

6.4.3 Ventilation layouts

In practice, the ventilation layout is another significant factor influencing goaf gas flow patterns and is rarely considered in the previous CFD modelling research. In order to investigate the effect of different ventilation layouts on oxygen distribution in the goaf area, three more ventilation scenarios were put forward, as shown in Figure 6.11. The numerical simulations were performed with the inert gas (97% N_2 and 3% O_2) injected via CT34 at an injection flow rate of 2000 m^3/h and gas drainage via GD09 at a drainage rate of 711 l/s. The parameters were kept unchanged except for the airflow quantity in each gateroad.

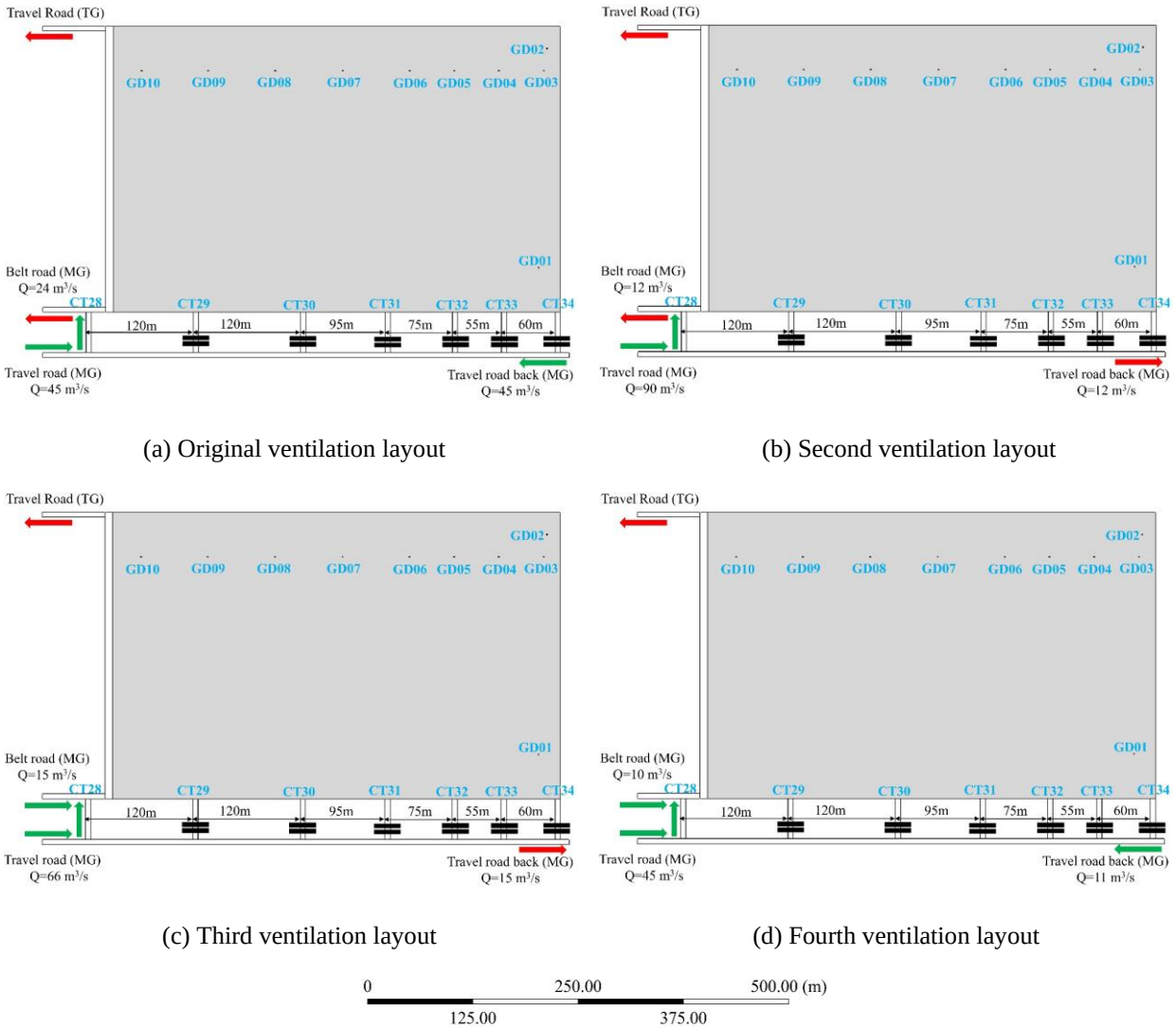

Figure 6.11 Layout of different ventilation scenarios

It was worth noting from Figure 6.12 and Figure 6.13 that different ventilation layouts had a major impact on the oxygen concentration distribution in the goaf area, especially on the MG and TG side. Oxygen concentration on the TG side was the smallest in the fourth ventilation layout with only 4% at around 100m behind the face, followed by the original (first) ventilation layout in which the oxygen concentration was below 5%. For the other two ventilation scenarios, the oxygen concentration on the TG side was all above 6%, showing a relatively poor goaf inertisation effect.

However, oxygen concentration on the MG side showed a different trend compared with that on the TG side. Oxygen concentration on the MG side was the smallest in the third ventilation layout, while it was the highest for the first ventilation layout.

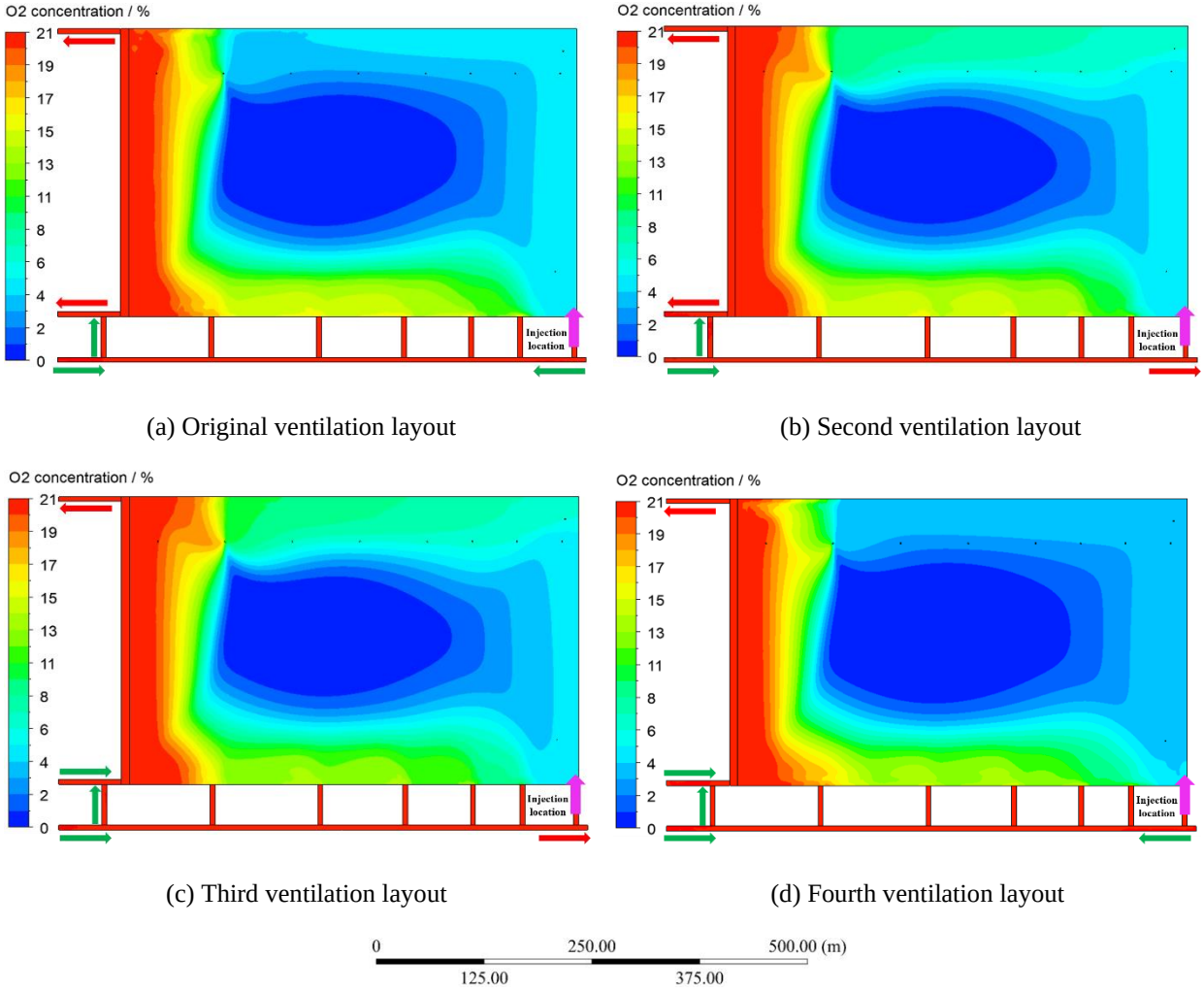

(a) Original ventilation layout

(b) Second ventilation layout

(c) Third ventilation layout

(d) Fourth ventilation layout

Figure 6.12 Effect of ventilation layouts on oxygen distribution

Table 6 6 Comparison of the ratio of OZA to GA among different ventilation layouts

	First ventilation	Second ventilation	Third ventilation	Fourth ventilation
Oxidation zone area (m^2)	43729	65831	63247	40614
Goaf area (m^2)	1600000	1600000	1600000	1600000
Ratio (%)	27.33	41.14	39.53	25.38

To further compare the effect of different ventilation layouts on oxygen distribution, particularly the area of the oxidation zone where oxygen concentration was in the range of 5%~18%, and the ratio of OZA to GA at the seam level was calculated, as listed in Table 6.6. This ratio analysis revealed that the fourth ventilation layout yielded the best performance in reducing oxygen content within the goaf area though it is only a minor improvement on the original layout.

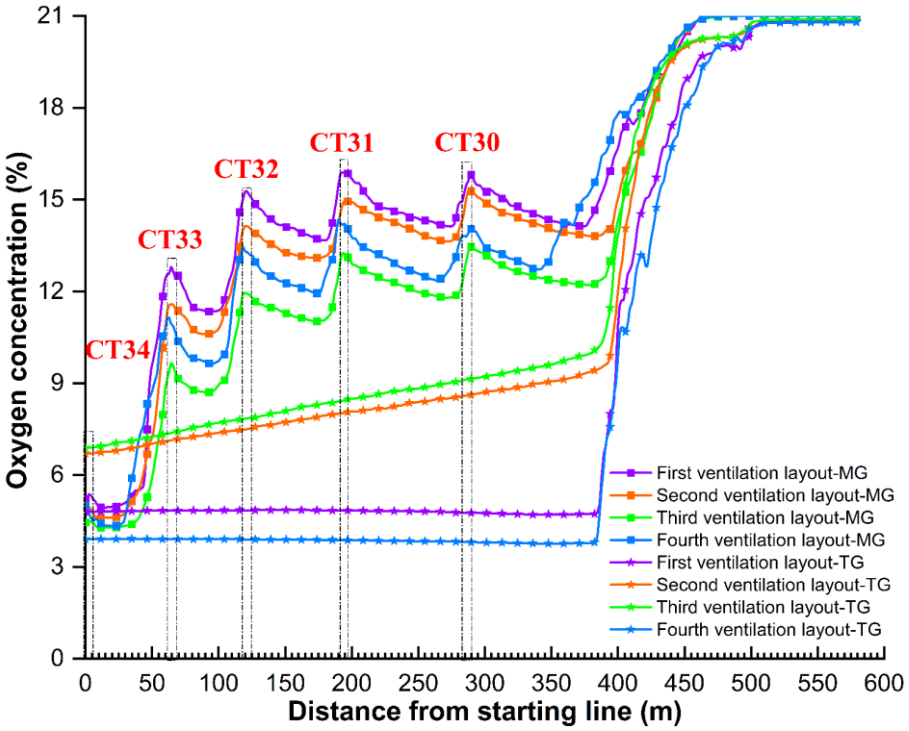

Figure 6.13 Oxygen concentration on the MG and TG side (2m from the rib)

6.4.4 Nitrogen injection locations

The effect of nitrogen injection locations on oxygen distribution under the original ventilation scenario was discussed. To inertise the goaf area, five kinds of injection strategies were proposed and studied: nitrogen injection via a single cut-through, injection via two cut-throughs, injection via a single surface borehole, injection via two surface boreholes, and injection via the combination of surface boreholes and cut-throughs. The total injection rate was kept constant for all scenarios for comparison purposes. The shallow borehole represents boreholes close to the LW face, while the deep borehole stands for those close to the starting-off line. Similarly, front cut-through refers to cut-through close to the LW face.

6.4.4.1 Nitrogen injection via single cut-through

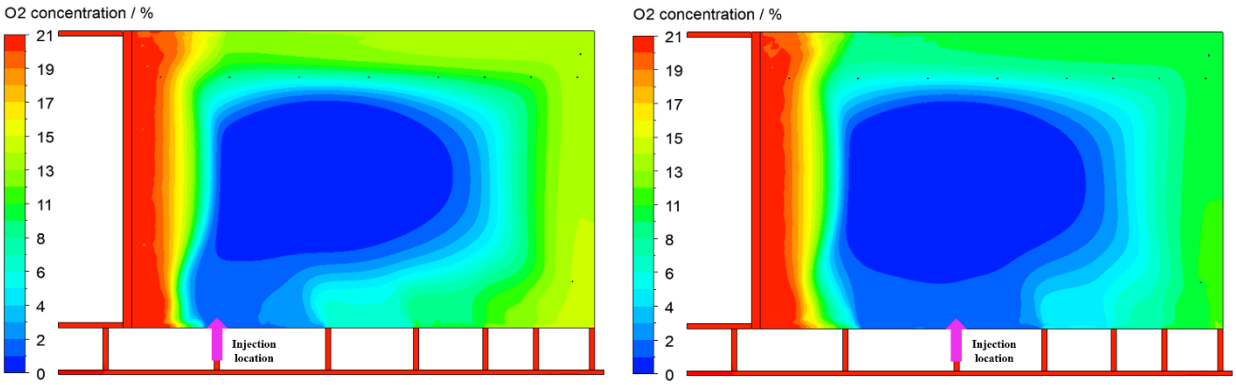

(a) Injection via CT29 @ 2000 m^3/h (b) Injection via CT30 @ 2000 m^3/h

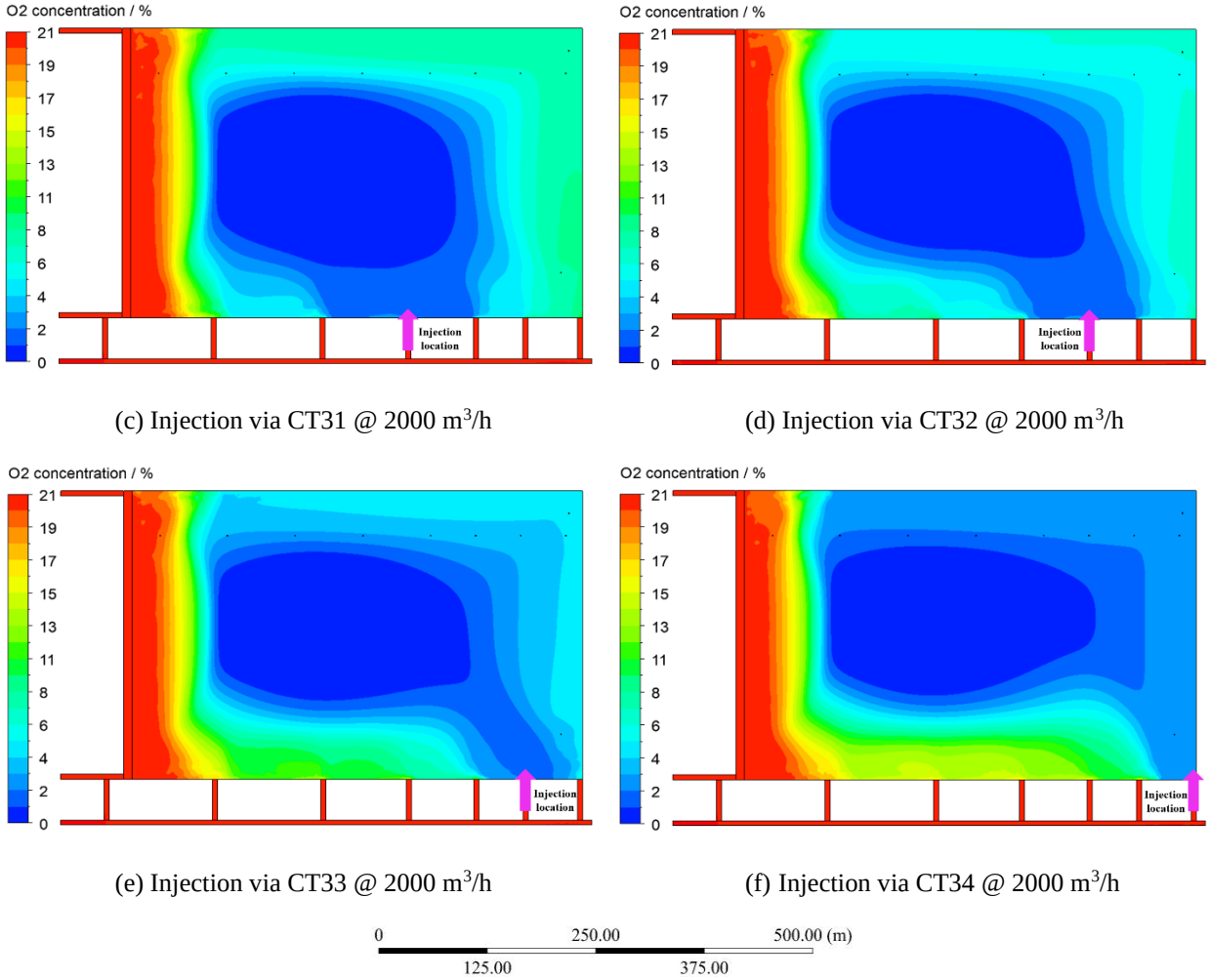

(c) Injection via CT31 @ 2000 m^3/h

(d) Injection via CT32 @ 2000 m^3/h

(e) Injection via CT33 @ 2000 m^3/h

(f) Injection via CT34 @ 2000 m^3/h

Figure 6.14 Effect of nitrogen injection via single cut-through on oxygen distribution

As can be seen from Figure 6.14(a) and (b), the oxygen concentration was higher in deep goaf when pure nitrogen was injected via a cut-through very close to the working face, reaching approximately 15% and 12%, respectively. When the injection point was moved from front cut-throughs to rear ones, a better inertisation effect can be obtained, with oxygen concentration in the deep goaf area reducing below 6% for scenarios(e) and (f). In addition, with injection moving from front cut-throughs to rear cut-throughs, the oxygen concentration on the TG side dropped significantly. On the contrary, when nitrogen was injected via the rear cut-through, the air leakage into goaf on the MG side was obvious, resulting in relatively higher oxygen concentration at each cut-through. Nitrogen injection via a single cut-through could not achieve a desirable goaf inertisation performance.

6.4.4.2 Nitrogen injection via double cut-throughs

It was noted from Figure 6.15 that the oxygen concentration on the TG side was the minimum (around 4%) when nitrogen was injected via CT33 and CT34, followed by the scenarios of nitrogen injection via CT32 and CT33, and CT32 and CT34 in which oxygen concentration was slightly dropped below 6%. However, for the other scenarios proposed, the oxygen concentration on the

TG side was higher than 7.5%, demonstrating an unsatisfactory inertisation effect.

Regarding oxygen concentration on the MG side, nitrogen injected via CT32 and CT33 and injection via CT33 and CT34 produced better results than other scenarios. When nitrogen injection was performed using two non-adjacent cut-throughs, a pronounced oxygen spike could be observed at the cut-throughs between the two injection locations. Thus it was strongly recommended that two neighbouring cut-throughs should be preferred rather than two non-adjacent ones.

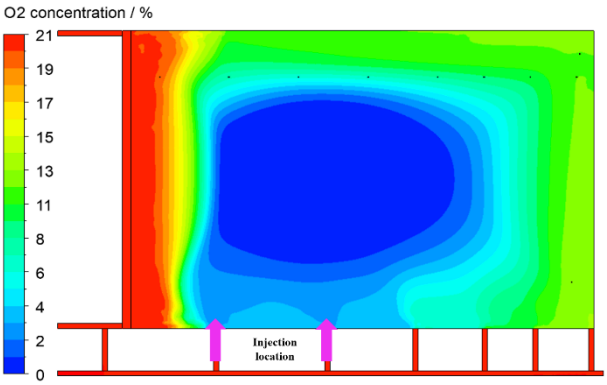

(a) Injection via CT29-CT30 @ 2000 m^3/h

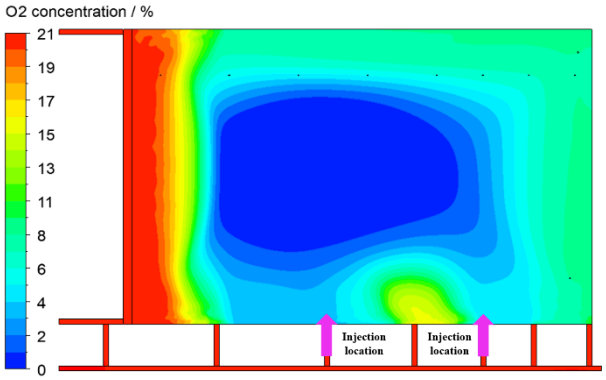

(b) Injection via CT30-CT32 @ 2000 m^3/h

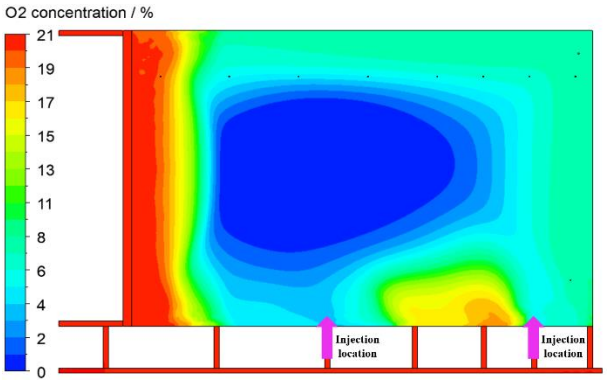

(c) Injection via CT30-CT33 @ 2000 m^3/h

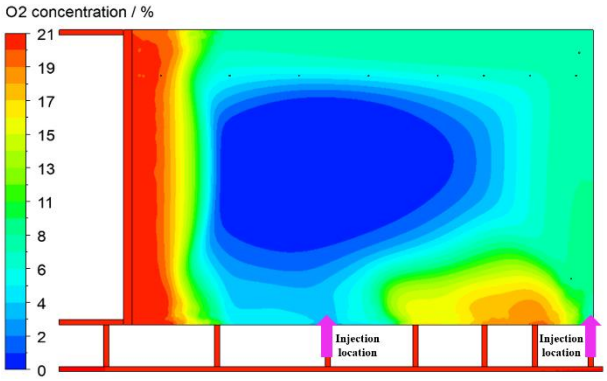

(b) Injection via CT30-CT34 @ 2000 m^3/h

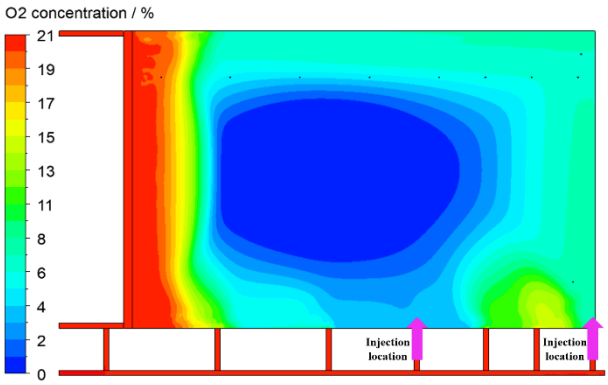

(e) Injection via CT31-CT34 @ 2000 m^3/h

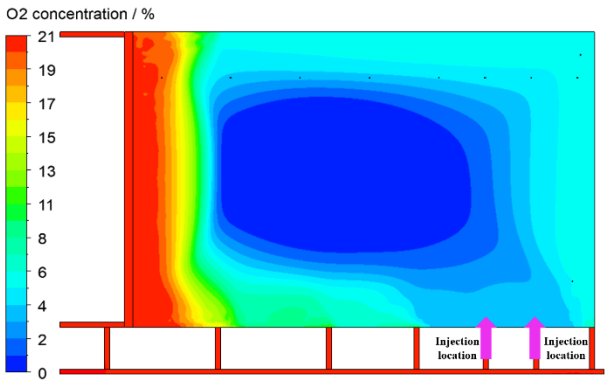

(f) Injection via CT32-CT33 @ 2000 m^3/h

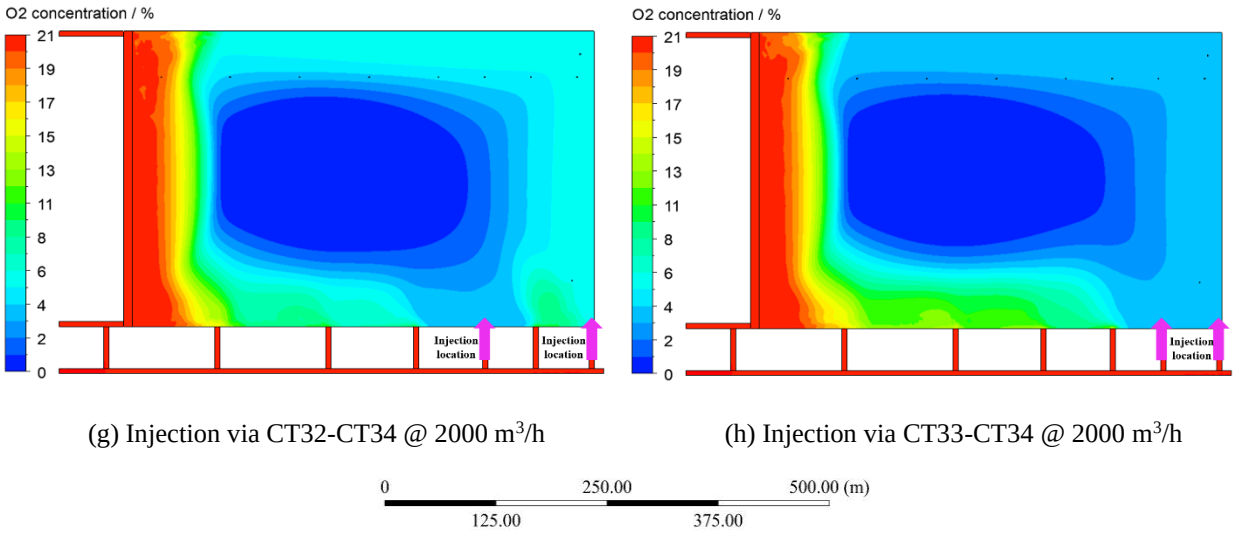

(g) Injection via CT32-CT34 @ 2000 m^3/h (h) Injection via CT33-CT34 @ 2000 m^3/h

Figure 6.15 Effect of nitrogen injection via double cut-throughs on oxygen distribution

6.4.4.3 Nitrogen injection via a single surface borehole

It can be seen from Figure 6.16 that pure nitrogen injection via a single surface borehole could reduce the oxygen concentration in the goaf area to a certain degree, demonstrating an inferior inertisation effect when compared with nitrogen injection via a single cut-through. Nitrogen injected via the surface borehole could only flow in a limited area due to the lower permeability within the goaf area.

In contrast to the four scenarios, it can be concluded that nitrogen injected via a deep borehole yielded a better effect in goaf inertisation than the shallow one, and nitrogen injected via a borehole close to the MG side produced better results than that close to the TG side. In consideration of oxygen concentration on the MG and TG side and in the deep goaf area, nitrogen injection via GD01 produced the best results among the four cases.

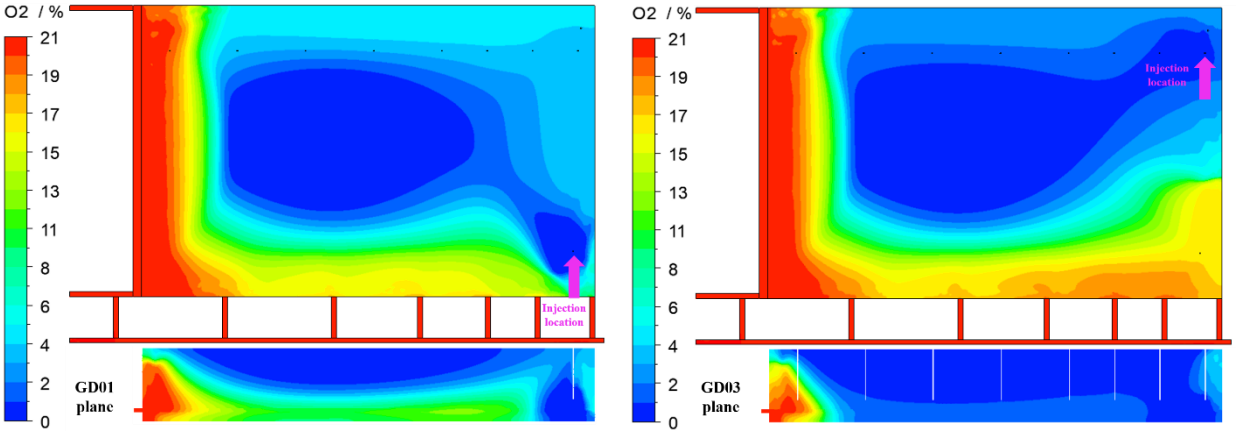

(a) Injection via GD01 @ 2000 m^3/h (b) Injection via GD03 @ 2000 m^3/h

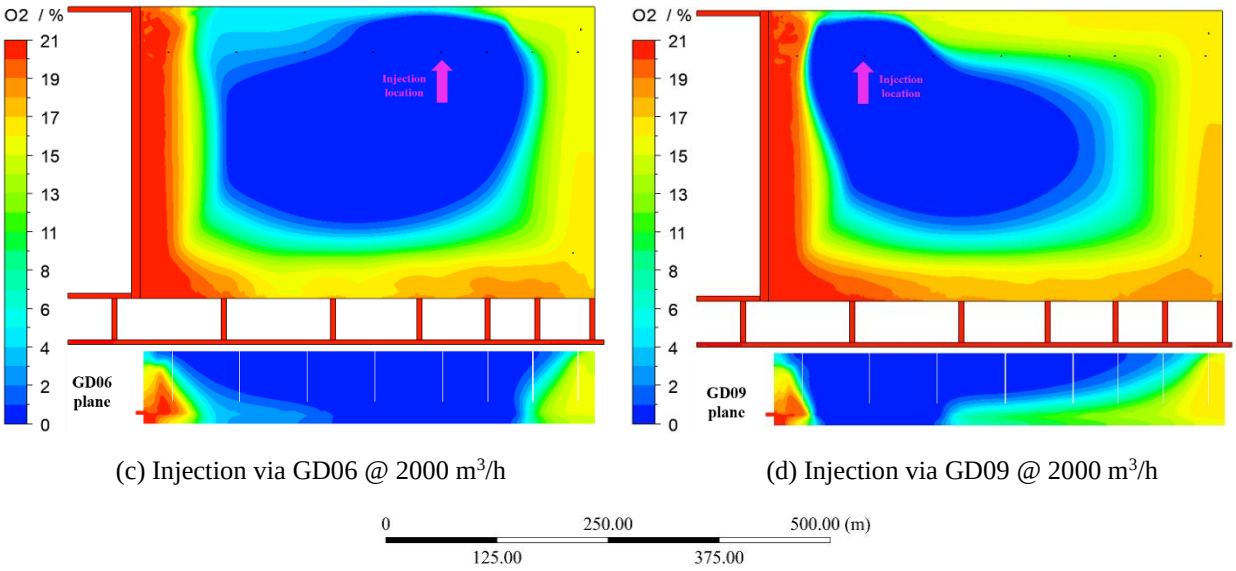

(c) Injection via GD06 @ 2000 m^3/h (d) Injection via GD09 @ 2000 m^3/h

Figure 6.16 Effect of nitrogen injection via a single surface borehole on oxygen distribution

6.4.4.4 Nitrogen injection via double surface boreholes

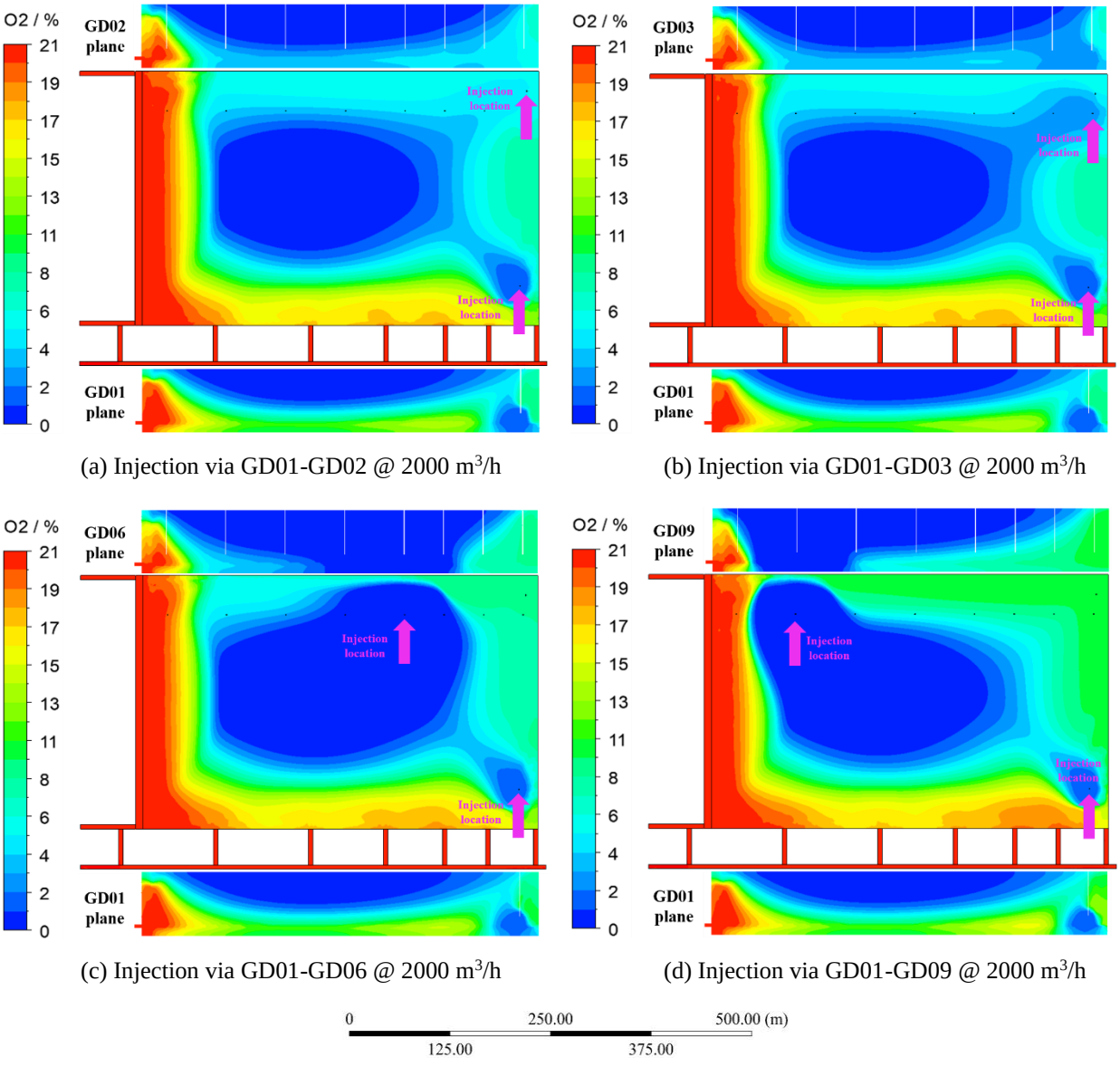

(a) Injection via GD01-GD02 @ 2000 m^3/h (b) Injection via GD01-GD03 @ 2000 m^3/h

(c) Injection via GD01-GD06 @ 2000 m^3/h (d) Injection via GD01-GD09 @ 2000 m^3/h

Figure 6.17 Effect of nitrogen injection via double surface boreholes on oxygen distribution

It was obvious in Figure 6.17 that nitrogen injection via two deep surface boreholes performed better in goaf inertisation than that via a deep hole and a shallow hole or a deep hole and a medium hole. When nitrogen was injected via two deep holes (scenario c and scenario d), oxygen concentration could reach as high as 12% on the MG side and exceed 5% on the TG side. Considering both oxygen concentration in the goaf area and operational cost saving, nitrogen injection via a single surface borehole GD01 yielded better performance than nitrogen injection via two surface boreholes.

6.4.4.5 Nitrogen combination injection via a single cut-through and surface borehole

From the above analysis, nitrogen injection via a rear cut-through or a deep surface borehole could produce better goaf inertisation. In order to further investigate the effect of nitrogen injection via the combination of surface borehole and cut-through, six different scenarios were studied, with results illustrated in Figure 6.18.

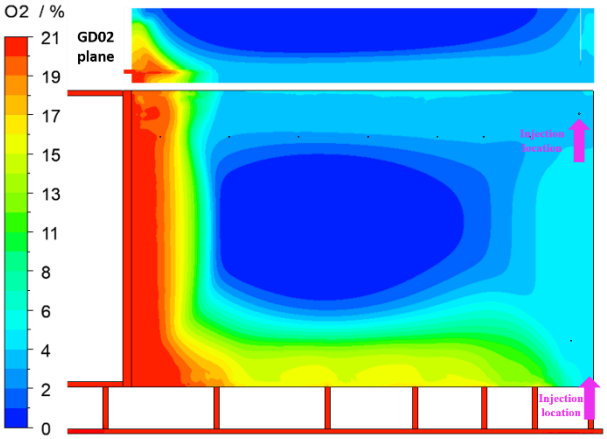

(a) Injection via GD02-CT34 @ 2000 m^3/h

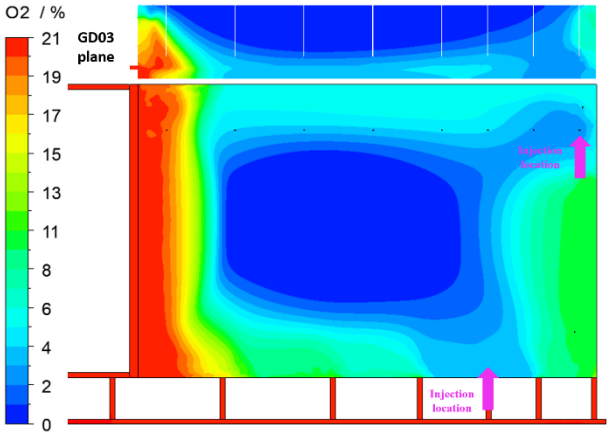

(b) Injection via GD03-CT32 @ 2000 m^3/h

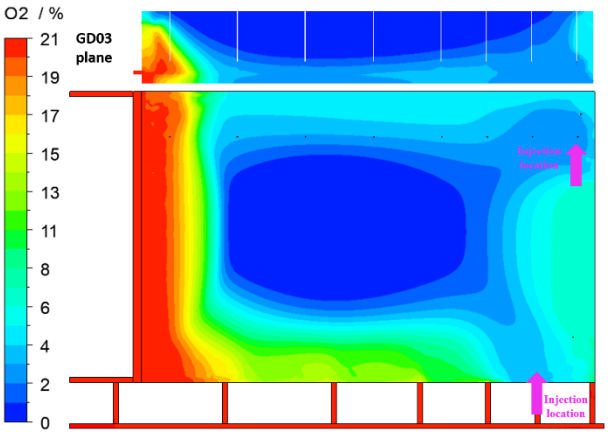

(c) Injection via GD03-CT33 @ 2000 m^3/h

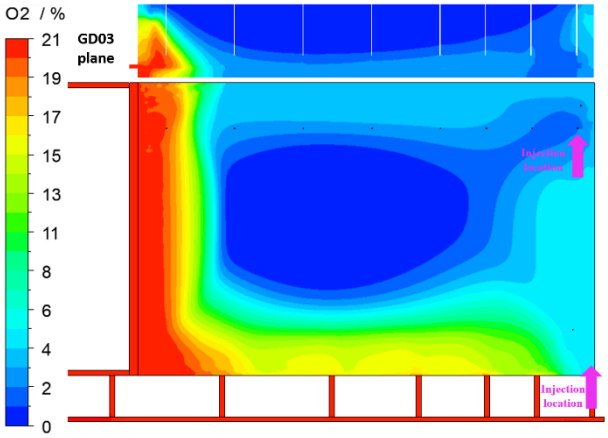

(d) Injection via GD03-CT34 @ 2000 m^3/h

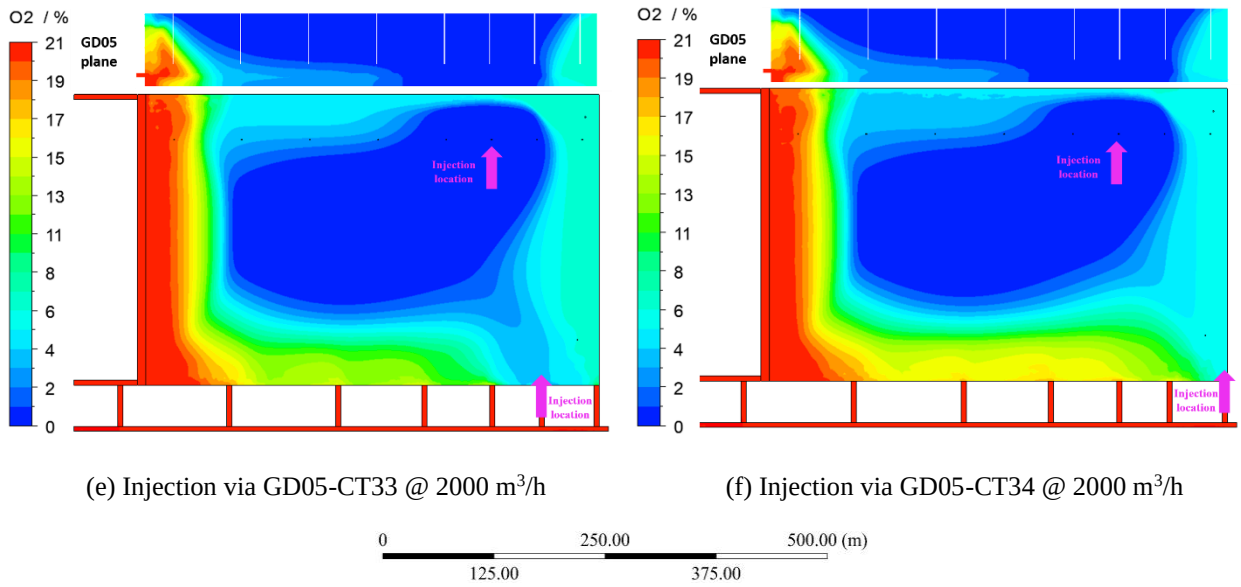

(e) Injection via GD05-CT33 @ 2000 m^3/h (f) Injection via GD05-CT34 @ 2000 m^3/h

Figure 6.18 Effect of nitrogen injection via both cut-through and surface borehole on oxygen distribution

The results showed a small higher-oxygen area in the vicinity of the starting-off line where oxygen concentration exceeded 6% when nitrogen was injected using CT32 or CT33. In terms of oxygen concentration on the MG side, it was generally higher with nitrogen injection via CT34 than that via CT32 or CT33, except in areas close to the starting-off line. To oxygen concentration on the TG side, it was lower than 5% when nitrogen was injected into the goaf via rear cut-through (CT34) and deep surface borehole (GD02 or GD03).

The analysis of oxygen distribution in the goaf area concludes that nitrogen injection via CT34 and GD03 performed the best among the six scenarios mentioned above.

Table 6.7 Comparison of typical injection scenarios

	CT33	**CT34**	**CT32-CT33**	**CT33-CT34**	**GD01**
Oxidation zone area (m^2)	29706	38151	51364	31301	41027
Goaf area (m^2)	160000	160000	160000	160000	160000
Ratio (%)	18.57	23.84	32.10	19.56	25.64
	GD03	**GD01-GD02**	**GD01-GD03**	**GD02-CT34**	**GD03-CT34**
Oxidation zone area (m^2)	49100	70237	64622	49433	48905
Goaf area (m^2)	160000	160000	160000	160000	160000
Ratio (%)	30.69	43.90	40.39	30.90	30.57

To further compare the different injection scenarios and determine the optimal injection strategies, the ratio of OZA to GA was calculated and listed in Table 6.7. The analysis of this ratio revealed that the ratio was the smallest under the scenario of nitrogen injection via CT33, producing better performance in goaf inertisation.

In summary, the simulation results demonstrated that injection via deep cut-through performed better than shallow cut-through, especially in reducing oxygen concentration on the tailgate side and oxygen in the deep goaf, which was a little different from the results obtained from Zhang et al.(2021) whose CFD model used a simple U-type ventilation system without a travel road on the MG side. In our model, the pressure difference between the travel road on the MG side and the goaf area was large so that air could leak into the goaf area via cut-throughs close to the starting-off line where the permeability was high. When nitrogen was injected into the goaf area via cut-through close to the face, oxygen concentration on the TG side and close to the starting-off line was high, yielding a bad goaf inertisation performance in comparison to the scenario where nitrogen was injected via cut-through close to the starting-off line. When considering nitrogen injection via two cut-throughs, the use of two contiguous cut-throughs could produce a better performance in goaf inertisation than that of two spaced cut-throughs in which oxygen could penetrate into goaf via interval cut-through due to the existence of strong pressure difference between gateroad on the MG side and goaf area. Therefore, it was recommended that two contiguous cut-throughs should be used for goaf inertisation rather than two spaced cut-throughs. In comparison to nitrogen injection via cut-throughs, nitrogen injection via surface boreholes has an inferior performance in goaf inertisation. This was different from the results obtained by Qiao et al. (2022b), which may be because of different permeability distributions in the goaf area. Compared to nitrogen injection via the combination of rear surface borehole and rear cut-through, nitrogen injection via two rear contiguous cut-throughs performed better in goaf inertisation, such as nitrogen injection via CT32 and CT33, and nitrogen injection via CT33 and CT34. Quantitative analysis of the oxidation zone area revealed that nitrogen injection via CT33 on the MG side performed better in minimizing oxygen ingress into the LW goaf and creating an inert atmosphere in the goaf area.

6.4.5 Inert gas type

Currently, three different inert gases are used in Australian coal mines: nitrogen (100%N_2), carbon dioxide (100%CO_2), and boiler gas (1%O_2, 14%CO_2, and 85%N_2) (Balusu et al. 2005b; Ren & Balusu 2009; Ren & Balusu 2010). To further investigate the optimal injection strategies, the influence of inert gas type on oxygen distribution within the goaf area was studied under the condition that different inert gas was injected into the goaf area via CT33 with a total injection rate of 2000 m^3/h.

As shown in Figure 6.19 and Figure 6.20, the injection with 100% carbon dioxide performed better in goaf inertisation than the injection with 100% nitrogen and boiler gas. Oxygen concentration is lower than 5% on the MG side about 70m behind the face, and lower than 5% on the TG side about

40m behind the face when 100% carbon dioxide was injected into the goaf. This is mainly because the starting-off line is at an elevation lower than the working face and the density of carbon dioxide is heavier than nitrogen and oxygen. As such, plenty of carbon dioxide diffuses at a lower position and surrounds the residual coal, thus yielding a better goaf inertisation effect. However, when carbon dioxide was injected into goaf via CT33 with a total injection rate of 2000 m^3/h, the oxygen concentration at the corner of the tailgate road was lower than 18.1%, which is below the statutory limit in Australia (19.5%). Thus, carbon dioxide should be injected into the goaf with a reasonable flow rate to avoid lower oxygen concentration at the tailgate corner.

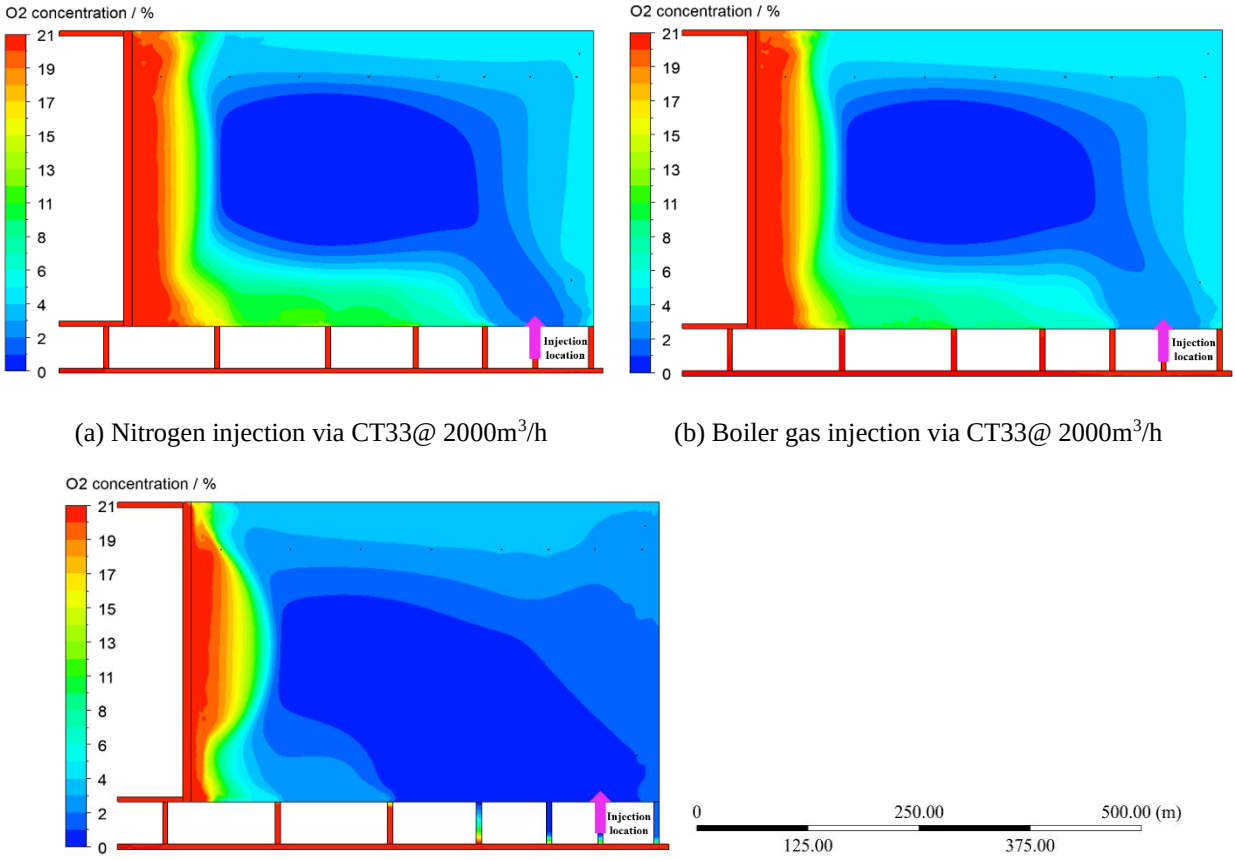

(a) Nitrogen injection via CT33@ 2000m^3/h

(b) Boiler gas injection via CT33@ 2000m^3/h

(c) Carbon dioxide injection via CT33@ 2000m^3/h

Figure 6.19 Effect of different inert gas on oxygen distribution

The simulation results showed that the area of the oxidation zone was the largest for nitrogen injection (29706 m^2), followed by boiler gas injection (28396 m^2), while it was the smallest for carbon dioxide injection (11902 m^2). Thus, carbon dioxide is a better option for goaf inertisation, which was the same as Liu et al. (2016a), who obtained that the suffocating zone area with carbon dioxide injection was approximately 1.25-2.4 times larger than nitrogen injection.

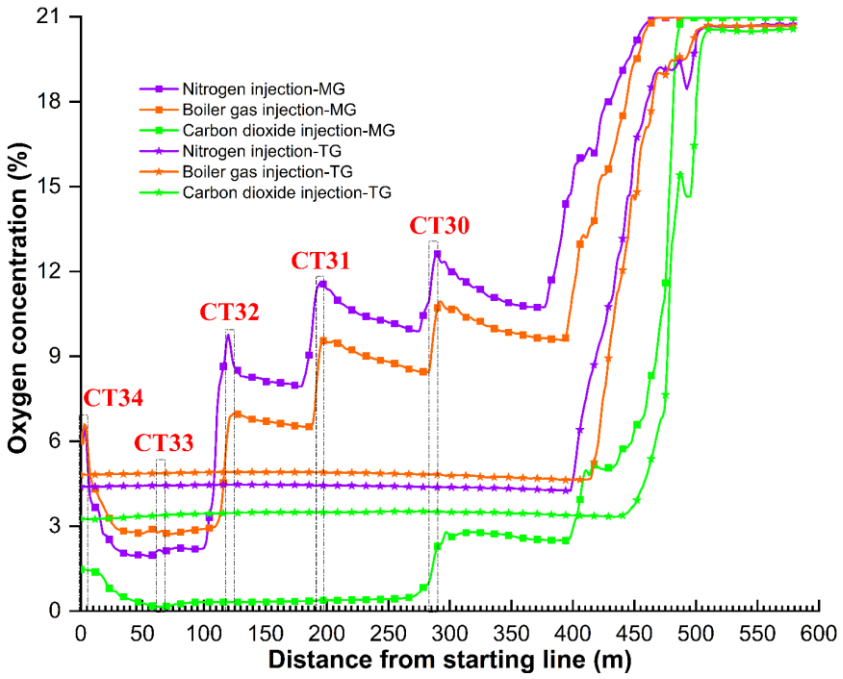

Figure 6.20 Oxygen concentration on the MG and TG side (2m from the rib)

6.4.6 Injection rate

It has been found that the carbon dioxide injection rate had a significant influence on oxygen distribution in the goaf area. With the injection rate gradually increased, the oxygen concentration on the MG and TG side was reduced accordingly, as depicted in Figure 6.21 and Figure 6.22.

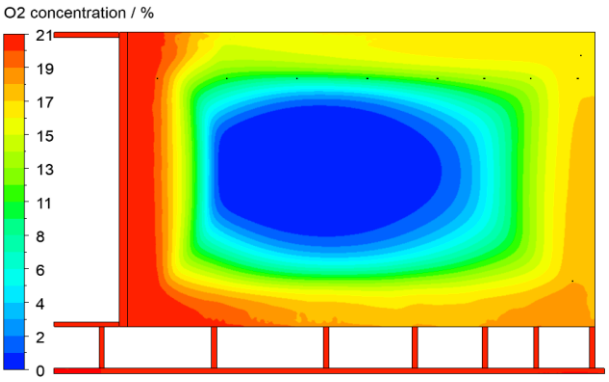

(a) Without injection

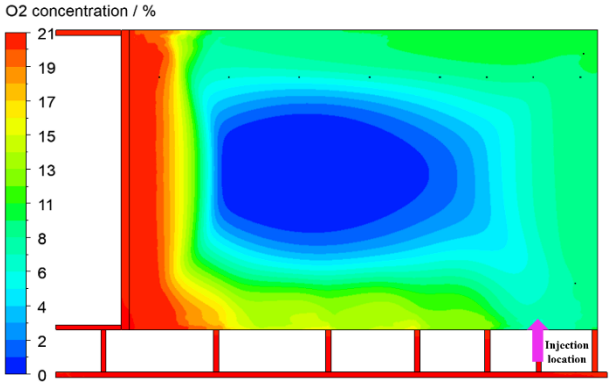

(b) Injection rate @ 500 m^3/h

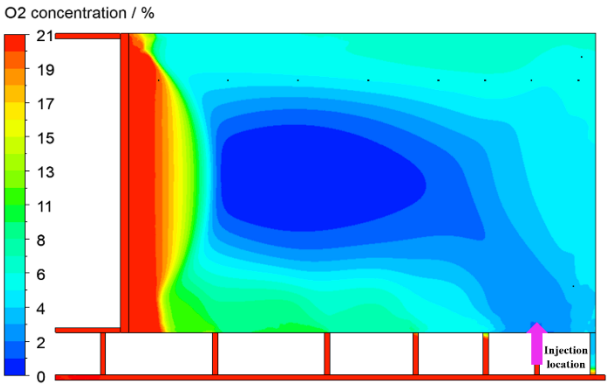

(c) Injection rate @ 1000 m^3/h

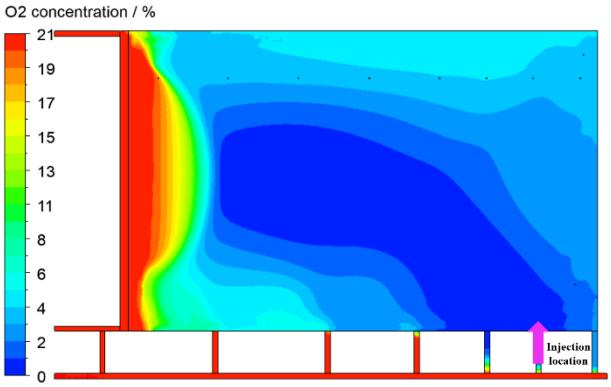

(d) Injection rate @ 1500 m^3/h

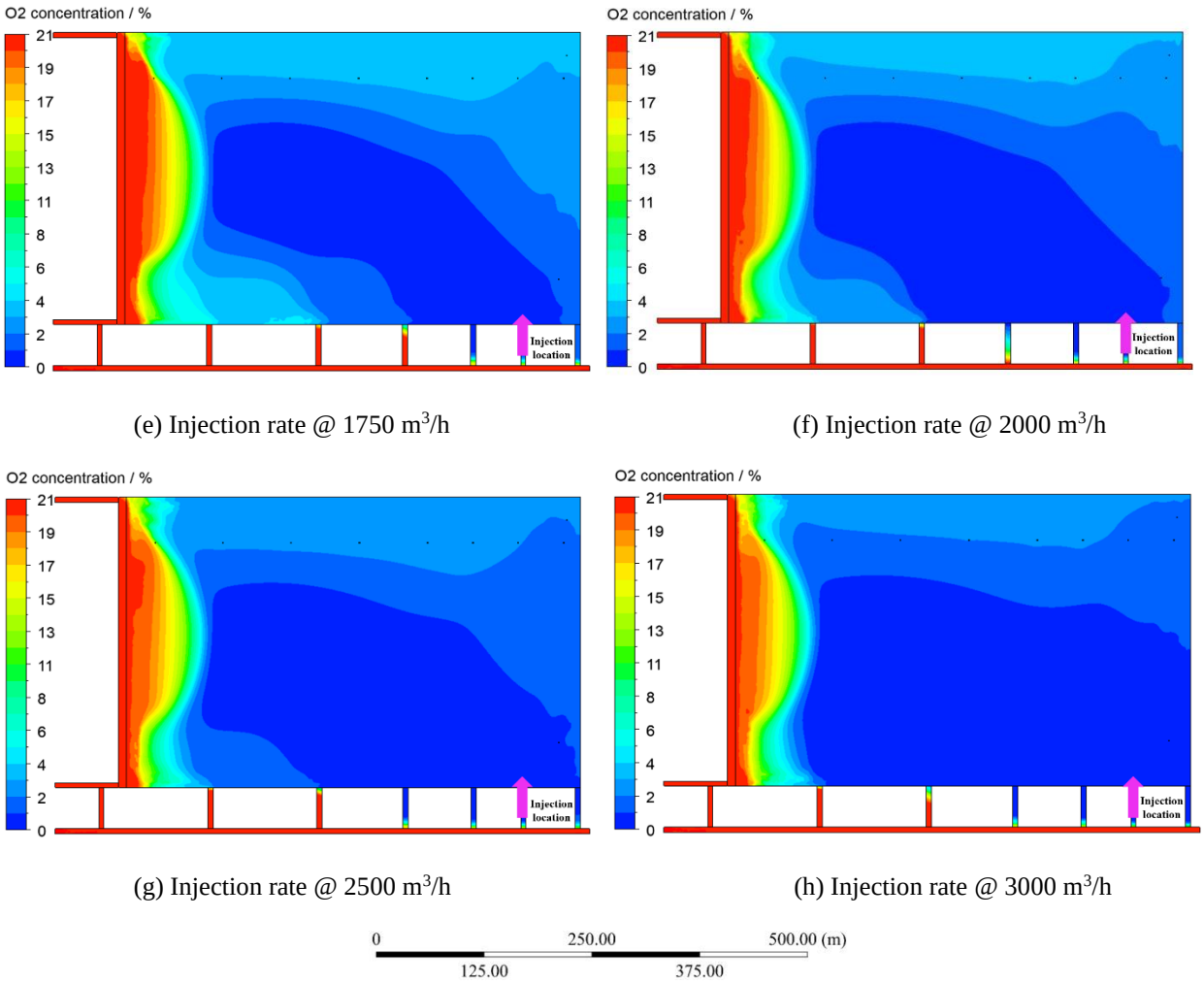

(e) Injection rate @ 1750 m^3/h (f) Injection rate @ 2000 m^3/h

(g) Injection rate @ 2500 m^3/h (h) Injection rate @ 3000 m^3/h

Figure 6.21 Effect of carbon dioxide injection rate on oxygen distribution

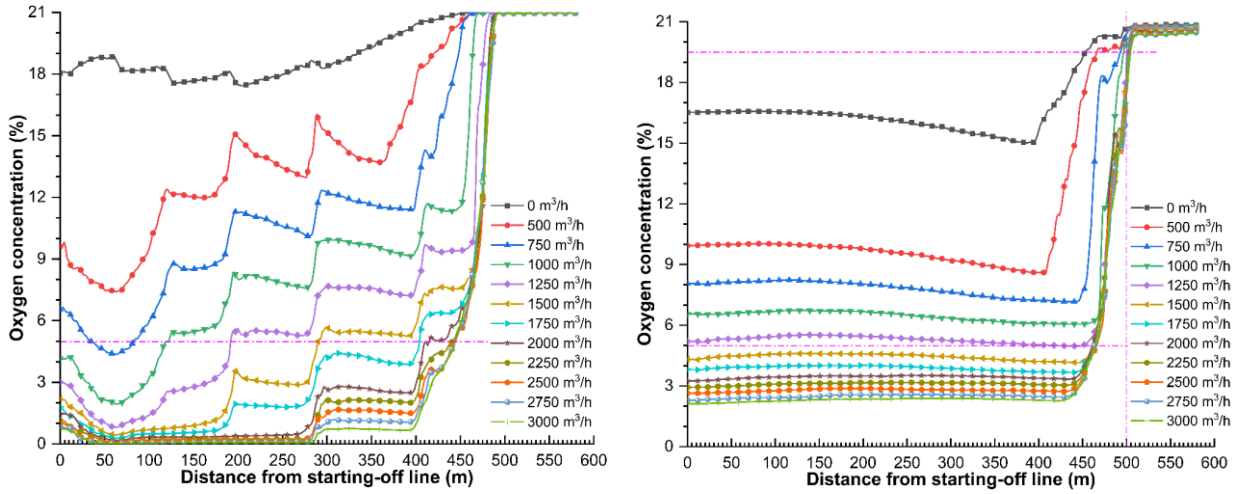

(a) On the MG side (b) On the TG side

Figure 6.22 Oxygen concentration on the MG and TG side (2m from the rib)

Figure 6.23 demonstrates this reduction in the oxidation zone overall and the ratio of OZA to GA as the carbon dioxide injection rate increases. However, when the injection rate increased above 1750 m^3/h, the ratio of OZA to GA remained relatively constant regardless of the continual

increase in injection rate, while the oxygen concentration on the MG and TG side was below 5% at a distance of 100 m and 40 m behind the face respectively. Although a good goaf inertisation performance could be achieved with an injection rate higher than 1750 m^3/h, oxygen concentration at the goaf stream of the tailgate end was lower than 19.5%, which could not meet the requirements stipulated by the government. This may be attributed to the low pressure at the tailgate end, resulting in carbon dioxide easily flowing to this localized area under the influence of the pressure difference between the injection location and the tailgate end. Therefore, particular attention should be paid to observing the oxygen concentration in this area when a higher injection rate of carbon dioxide is employed.

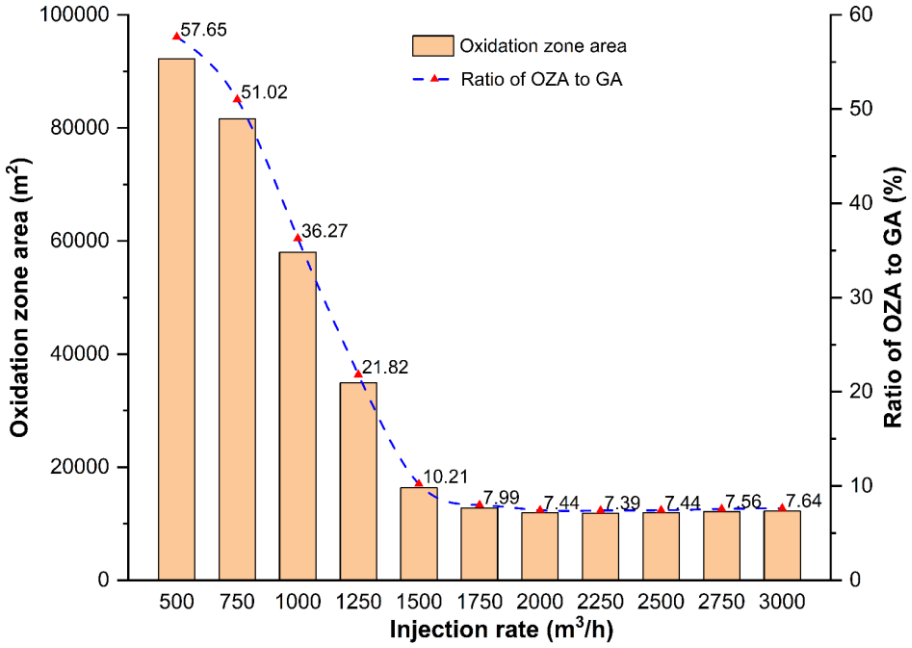

Figure 6.23 Spontaneous combustion area and ratio under different injection rates

In summary, ventilation layout and flowrate, goaf gas composition and emission rate, and seam orientation influenced the desired carbon dioxide injection rate for goaf inertisation. In terms of injection rate, several factors need to be considered, including the oxygen ingress distance on the MG side and TG side, oxygen levels at areas where miners could access, reduction rate in the oxidation zone area, availability of inert gas, state-of-art equipment for delivering the desired amount of inert gas, as well as operational cost.

The simulation results indicated that a carbon dioxide injection rate of 1750 m^3/h could achieve a good goaf inertisation performance, which was similar to results from Ren et al. (2009) who found that inert gas injection in the deep goaf could produce an effective goaf inertisation performance even at a low inert gas injection rate of 1800 m^3/h.

6.4.7 Abnormal gas emission control on the LW face

Ventilation control devices, particularly curtains and brattices, are also significant factors that

could influence the goaf gas flow dynamics in the goaf area and gas levels at the tailgate end.

Improved simulations were conducted to find the determining factors influencing methane exceedance mitigation performance at the tailgate end, and five scenarios were studied, as listed in Table 6.8. The layout of the brattices and curtains employed in the model is depicted in Figure 6.24. Curtain B and curtain C are kept in line with each other and parallel to the tailgate panel, while curtain A is perpendicular to the tailgate panel rib. Two brattices placed on the LW face mainly play a role in diverting the airflow toward the goaf fringe and are termed brattice A.

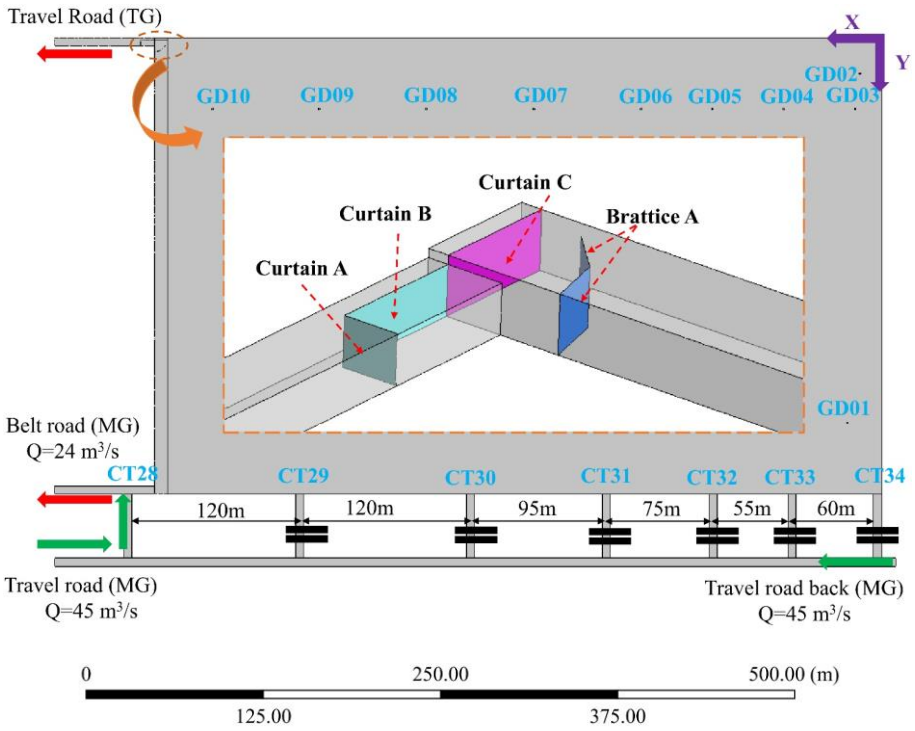

Figure 6.24 Layout of brattices and curtains

Table 6.8 Configuration scenarios of brattice and curtain

Scenario	Length of curtain B (m)	Width of curtain A (m)	Distance from brattice A to goaf side rib (m)	Distance from curtain C (B) to goaf side rib (m)	Length of curtain C (m)
1	6/10/14/18/22/ 26/30	4.0	10	1.5	9
2	14	2.0/2.5/3.0/3.5/4.0/4.1/	10	1.5	9
3	14	4.0	6/8/10/12/14/16/ 18/20	1.5	9
4	14	4.0	10	0.5/1.0/1.5/1.6	9
5	14	4.0	10	1.5	5/6/7/8/9/10/ 11

The simulations were performed under the same condition as the verified base model (inert gas injection via CT34 with an injection rate of 2000 m^3/h and gas drainage operated via GD09 with a rate of 711 l/s). As the focus was on the methane mitigation at the goaf stream in the tailgate end, only methane concentration along the LW face at the elevation of 2.0 m was plotted for comparison purposes.

6.4.7.1 The length of curtain B

It is apparent from Figure 6.25 that the use of brattices and curtains can significantly reduce methane concentration to a safe level at the goaf fringe, yielding desirable gas management performance. With the increase in the length of curtain B from 6 m to 14 m, peak methane concentration (PMC) at the goaf stream reduced from 0.59% to 0.56%. However, as the length extended from 14 m to 18 m, PMC increased to 0.64%. With the continued increase in the length to 30 m, PMC at the goaf fringe reduced marginally, lowering to 0.57%. PMC fluctuated between 0.55% and 0.65%, indicating the length of curtain B results in a minor effect on methane control at the tailgate end.

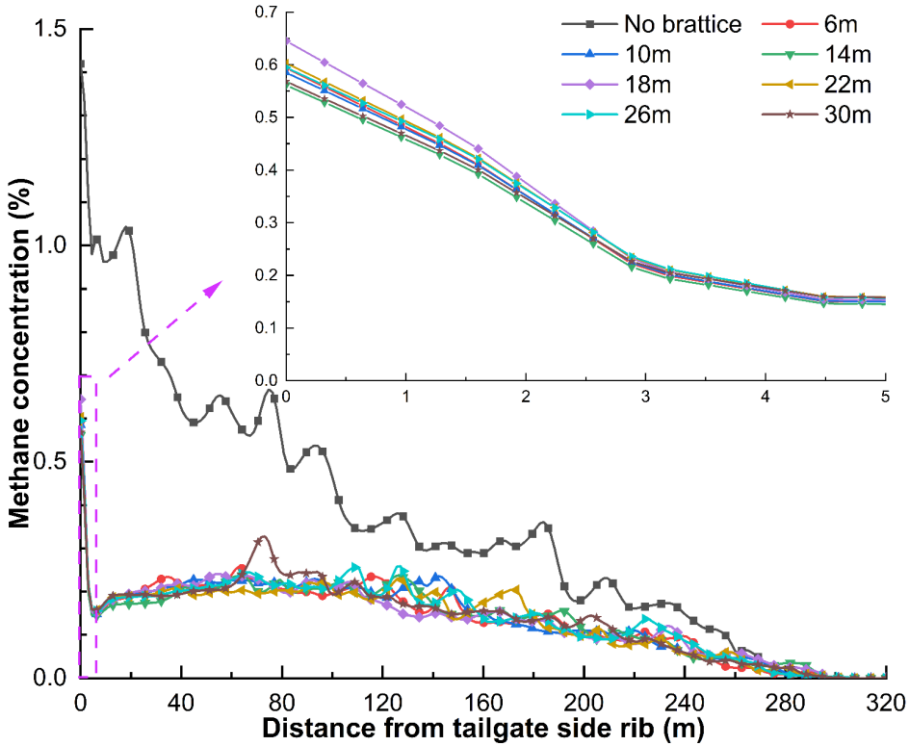

Figure 6.25 Effect of curtain B length on methane concentration at the tailgate end

6.4.7.2 The width of curtain A

A large difference in the PMC can be observed in Figure 6.26 with the change of the width of curtain A. As the width increased from 2.0 m to 4.0 m, generally, PMC showed a decreasing trend, reducing from around 1.22% to 0.56%. There was a marginal difference in methane concentration when the curtain width increased to 4.1 m. The simulation result revealed that a width of 4.0 m for

curtain A is optimal in mitigating high-level methane at the tailgate end.

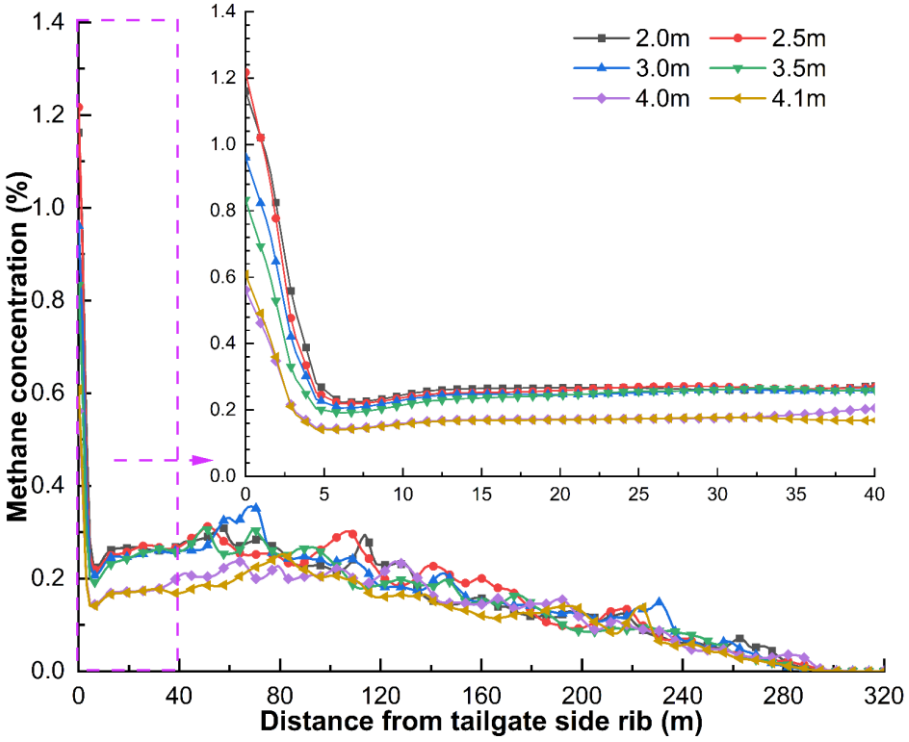

Figure 6.26 Effect of width of curtain A on methane concentration at the tailgate end

6.4.7.3 The distance from brattice A to the goaf side rib

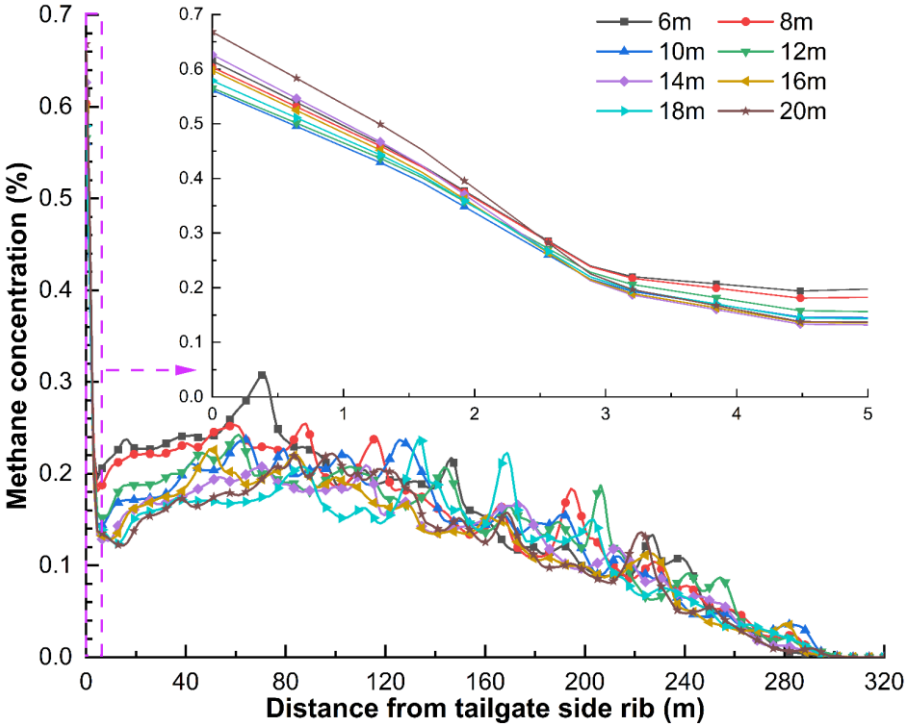

Figure 6.27 Effect of distance between brattice A and goaf side rib on methane concentration at tailgate end

Figure 6.27 shows that the distance between brattice A and goaf side rib played a trivial role in influencing methane levels at the tailgate end. With the increase in the distance, PMC varied between 0.56% and 0.67%. A distance of 10 m yielded the minimum peak methane level, thus it

is considered the optimal option.

6.4.7.4 The distance from the curtain C (B) to goaf side rib

The results showed that the distance from curtain C (B) to the goaf side rib dramatically influenced methane levels at the goaf fringe, as illustrated in Figure 6.28. As curtain C moved away from the goaf rib, PMC dropped obviously from 1.27% to 0.56%, reducing by 0.71%. There was no more significant change in methane concentration with the distance increasing from 1.5 m to 1.6 m, under which condition that curtain A would come into contact with the tailgate panel rib.

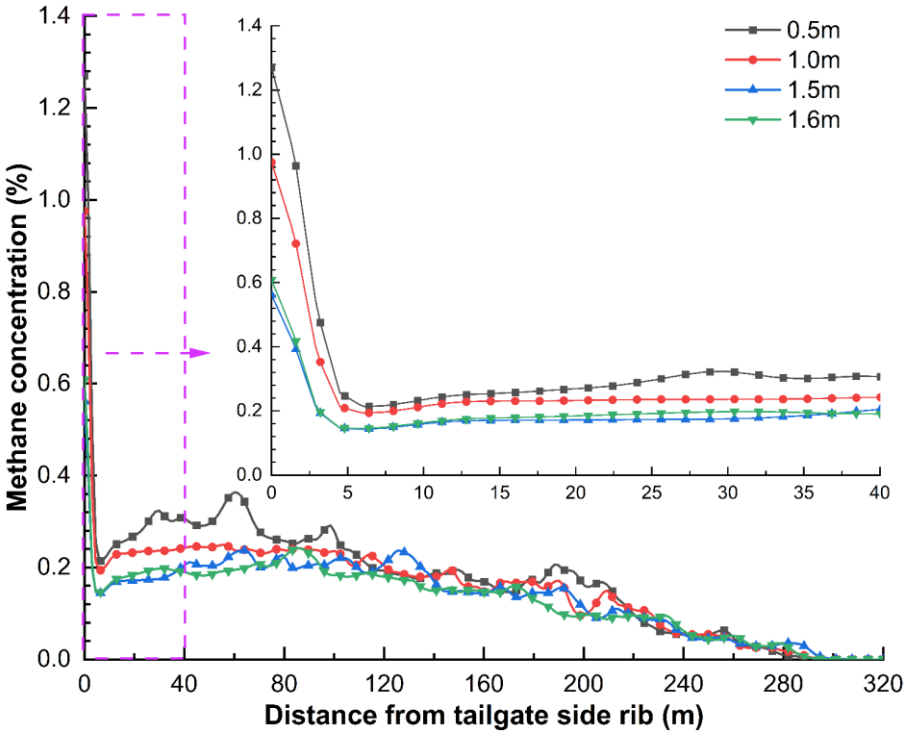

Figure 6.28 Effect of the distance from curtain C to goaf rib on methane concentration at the tailgate end

6.4.7.5 The length of curtain C

As shown in Figure 6.29, the analysis of simulation results revealed that the length of curtain C significantly influenced the methane management at the tailgate end. As the distance increased from 5 m to 9 m, PMC generally reduced from approximately 1.25% to 0.56%, dropping by 0.69%. Although the maximum methane level decreased to 0.49% while the length of the curtain C extended to 11 m (2m inside of the goaf area), oxygen ingress into the goaf area on the tailgate side was massive, increasing the risk of spontaneous combustion due to high oxygen levels.

In summary, it was noted that the use of curtains at the tailgate end assisted in reducing methane concentration at the intersection of the working face and tailgate end, which was consistent with results from Ren et al. (2018a) who did not conduct a thorough investigation into the influence of curtain and brattice configuration on methane mitigation at the tailgate end. The analysis of simulation results indicated that the width of curtain A, the distance between curtain C (B) and the

goaf side rib, and the length of curtain C significantly influence the methane concentration at the tailgate end. On the contrary, the length of curtain B and the distance from brattice A to the goaf side rib has a minor effect on mitigating abnormal methane emission at the goaf fringe.

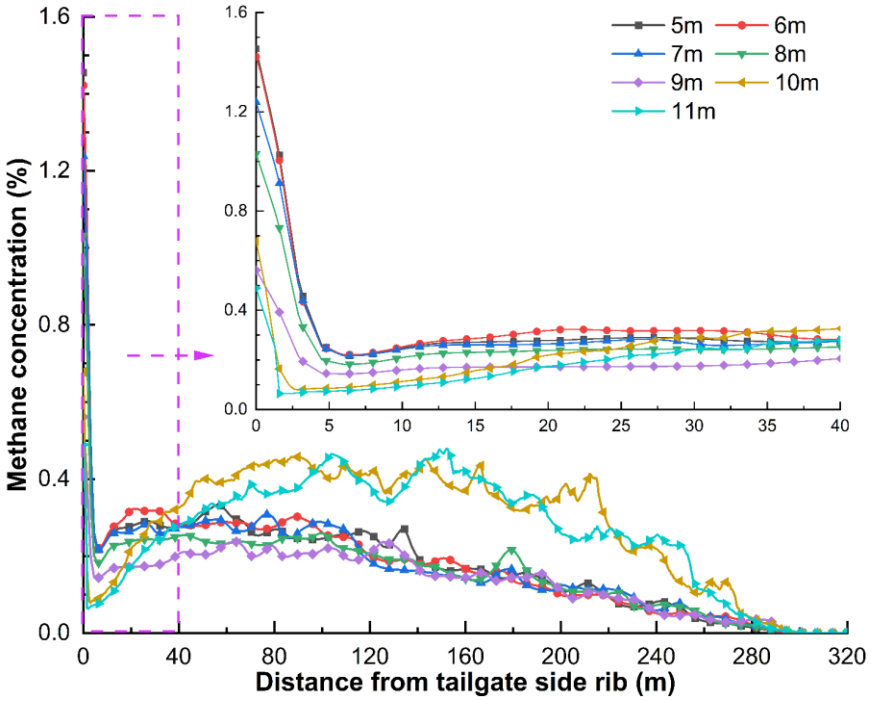

Figure 6.29 Effect of the length of curtain C on methane concentration at the tailgate end

6.5 Conclusions

Considering that the LW goaf is inaccessible and the gas distribution is complicated, improved CFD modelling was developed to better understand the gas flow dynamics and distribution patterns in the goaf area and investigate the impact of mining parameters on spontaneous combustion control in the goaf area and methane mitigation at the tailgate end. Numerical simulation results were compared with onsite monitoring data, and a good agreement was reached, which increased the confidence in studying scenarios outside of the base-model. The major conclusions can be summarised below:

(1) The ratio of oxidation zone area (OZA) and goaf area (GA) was introduced to qualitatively and quantitatively investigate the impact of mining parameters on oxygen distribution in the goaf area. The results indicated that (i) as the goaf gas emission rate increased from 500 l/s to 2500 l/s, the ratio of OZA to GA dropped from 58.41% to 35.79%, which meant that a high goaf gas emission rate could reduce the likelihood of spontaneous combustion to a certain degree; (ii) permeability was introduced to describe the tightness of seals built in the cut-throughs, and air leakage could be reduced when the permeability was lower than 10^{-9} m^2; (iii) the ratio of OZA to GA ranged between 25.38% and 41.14% for the proposed scenarios of different ventilation layouts, thus it shows the importance of evaluating the ventilation system prior to coal mining.

(2) Proactive goaf inertisation strategies were systematically optimized to effectively suppress spontaneous combustion in the goaf area. The results showed that (i) injection via cut-throughs on the MG side performed better than the surface borehole, and injection on the MG side via two contiguous cut-throughs produced better results than two spaced cut-throughs; (ii) from the perspective of the OZA, carbon dioxide injection through CT33 (11902 m^2) was superior to boiler gas (28396 m^2) and nitrogen (29706 m^2) injection for goaf gas being entirely composed of methane, yielding the desirable goaf inertisation performance; (iii) considering the reduction in the ratio of OZA to GA and oxygen levels at the tailgate end (higher than 19.5%), carbon dioxide injection rate of 1750 m^3/h was optimal for proactive goaf inertisation.

(3) The influence of the configuration of brattices and curtains at the LW face and the tailgate end on methane management at localized goaf fringe was numerically investigated. The results demonstrated that (i) the usage of curtains and brattices at the LW face and tailgate end could effectively reduce peak methane concentration (PMC) at the tailgate end when compared to the scenario without curtains and brattices; (ii) the width of the curtain perpendicular to the gateroad rib, the distance between the gateroad rib and the curtain parallel to the gateroad rib, and the length of the curtain at the tailgate end significantly impacted the methane mitigation performance at localized tailgate end; (iii) the length of the curtain at the return travel road and the distance from the face brattices and the goaf rib had a minor effect on mitigating abnormal methane emission at the goaf fringe.

The following limitations of the study are noted. The coal reaction with oxygen and the time-scale factor of inert gas injection were not considered in this study. Despite the above limitations, this work has demonstrated the benefits of improved CFD modelling methods approaching reality can have on spontaneous combustion control in the goaf area and methane management at localized tailgate end in the coal mining industry, particularly regarding coal mine health and safety. Although this study presents data related to a specific site and the related conditions, the results of the study demonstrate the significant improvements that can be made through detailed CFD studies of the ventilation system. As such, the outcome of this study would be to recommend that mine sites perform similar investigations for their specific site conditions in order to achieve optimal outcomes.

CHAPTER 7 VENTILATION ARRANGEMENT EVALUATION AND PROACTIVE GOAF INERTISATION FOR SPONTANEOUS HEATING AND GAS EXPLOSION MANAGEMENT DURING LONGWALL PANEL SEALING-OFF PROCESS

Summary

This chapter focuses on an investigation into face ventilation dynamics and methane dispersion characteristics during the longwall (LW) panel sealing-off process. When the LW face approaches the finish-off line, the LW face stops advancing and both the ventilation flow dynamics and goaf gas atmosphere change, which significantly increases the risk of spontaneous combustion and gas explosion in the active goaf area. To prevent these dynamics hazards, a detailed understanding of ventilation dynamics and the goaf gas atmosphere in the active goaf is crucial to improve the panel sealing-off process design and minimize the risk of spontaneous combustion and gas explosion. Based on site-specific geologic and mining conditions of an Australian underground coal mine in Queensland, two three-dimensional CFD models were developed and verified by field gas monitoring data collected from the Tube Bundle System. The LW sealing-off process was divided into six different stages and studied from face coming into the finish-off position to sealing-off with the following sequences: face coming into the finish-off line, face bolt up after production stop, pulling hydraulic supports from the TG to the LW chute road 1, from the LW chute road 1 to road 2, from LW chute road 2 to the MG, and all supports pulled off the face and the MG corner sealing-off. Extensive computational modelling was performed to better understand the behaviour of ventilation dynamics in the active goaf and evaluate the proposed ventilation arrangements at different stages of the LW sealing-off process. In addition, the final sealing-off strategy was optimized to improve the sealing performance, and appropriate gas sensor locations were identified to monitor gas atmosphere change. This computational modelling study can provide new insight into the ventilation dynamics and goaf atmosphere during the LW sealing-off process and help to evaluate the impact of the proposed ventilation arrangements on goaf atmosphere management. In addition, this study can also provide critical knowledge of appropriate positioning of gas monitoring locations to timely and reliably reflect the goaf atmosphere change during the panel sealing-off process, thus minimizing the risk of spontaneous heating and gas explosion to improve mine safety.

Citation

This paper has been submitted to **FUEL** and is currently under review.

Abstract

When a longwall (LW) face approaches the finish-off line, one month is normally required to relocate the LW equipment and seal the LW panel, during which time ventilation dynamics and goaf gas atmosphere change and the risk of spontaneous combustion and gas explosion considerably increases. To minimise the occurrence of these hazards, an improved insight into ventilation behaviour and gas flow dynamics within the LW panel is essential to develop fit-for-purpose proactive goaf inertisation strategies during the panel sealing-off process. Based on the mining conditions of an Australian underground coal mine, three-dimensional computational models were developed and calibrated with onsite gas monitoring data, allowing for evaluating ventilation arrangements and understanding oxygen and methane dispersion patterns in the LW workings during the panel sealing-off process involving six stages with confidence. The simulation results indicate that nitrogen should be injected via cut-through 12 on the travel road at a flowrate of 0.75 m^3/s and the rear of the travel road should be tightly sealed at the final sealing-off stage, resulting in oxygen levels lowering than 5% in the LW workings and producing desired panel sealing-off performance. In addition, six gas sensors should be employed and positioned at the appropriate locations at the final sealing-off stage to reliably monitor goaf atmosphere change. This study sheds improved insights into evaluating ventilation arrangements and understanding ventilation dynamics during the panel sealing-off process, and provides critical knowledge of effective proactive goaf inertisation strategies, thus mitigating spontaneous heating and gas explosion risks with much-improved mine safety.

Keywords

Panel sealing-off process; CFD modelling; Ventilation arrangement evaluation; Proactive goaf inertisation; Gas explosion management; Spontaneous heating control.

7.1 Introduction

When the longwall (LW) face is approaching its finish-off line, the coal mining process generally slows down and then stops to allow the LW equipment to be relocated to a newly prepared installation face following standard procedures, which usually takes approximately 1~2 months (Kang et al. 2016). During this period, the air is highly likely to penetrate into the active goaf via various leakage pathways and react with remnant coal, resulting in self-heating and spontaneous combustion if the stopping period exceeds the incubation period (Beamish & Theiler 2019; Shi et al. 2019; Taraba & Michalec 2011; Zhang et al. 2019a); whilst the caved strata can provide a favourable condition for heating build-up in some regions in the mined-out area, potentially causing spontaneous hating to escalate to open fire (Liu et al. 2021). If the explosive gas mixture is formed in the vicinity of the heating sites, a gas explosion can be initiated by heating released

by spontaneous combustion or fire (Li et al. 2021b; Xia et al. 2016). Therefore, production slowdown and even stoppage are conducive to the development of spontaneous heating and potential gas explosion (Cliff 2015), which can be proven by several incidents occurring in underground coal mines. Fire and explosion took place close to the tailgate (TG) roadway in a New South Wales (NSW) coal mine on 5 January 2011, and a subsequent investigation report by NSW Trade and Investment revealed that the LW face was stopped for maintenance at the time of the incident, and serious consideration should be taken into spontaneous combustion as the culprit of the explosion (Tim & Jennie 2012). Serious accidents involving two forceful pressure waves also occurred on 6 May 2020 in a Queensland underground coal mine, and a subsequent official report revealed that production delays and stoppage happened prior to the incidents and further contributed to the risk of spontaneous combustion which was considered as a primary reason for the severe accidents (Terry Martin SC & Clough 2021).

To address problems associated with spontaneous heating and gas explosion in the LW panel experiencing production stoppage and elevated gas levels, many researchers have performed theoretical analyses and numerical simulations. Computational modelling was performed by Tutak and Brodny (2017a) to evaluate the effectiveness of isolation-sealing agents and their configurations in goaf sealing under simple U-type ventilation, and it was found that goaf sealing from both maingate (MG) and tailgate (TG) outperformed that of TG solely in reducing methane levels at the outlet of the TG. Ren et al. (2018c) theoretically analyzed the characteristics of spontaneous combustion during the withdrawal period of the working face employing a U-type ventilation system, and the field application of foamed gel for sealing air leakage pathways and controlling spontaneous heating was discussed. Liu et al. (2019d) numerically investigated the dynamic evolution of spontaneous heating in the goaf amid the stoppage of the working face utilising U-type ventilation, and simulation results indicated that a reduction in crushed coal thickness and ventilation flowrate or an increase in face advancing rate assisted in reducing the risk of spontaneous heating and safely withdrawing LW equipment from the current face. Extensive numerical simulations were conducted by Shi et al. (2021) to study the evolution of methane, oxygen and temperature during and after sealing the fire zone in the U-type ventilated LW face by means of installing walls at both MG and TG gateroads, and the results from the simulation helped to minimise the risk of the gas explosion. Wang et al. (2021a) numerically studied the onset and development of methane explosion in the LW face with simple U-type ventilation amid the fire zone sealing process, and revealed that inert gas should be injected into the fire zone at the return air side to improve explosion prevention performance. Zuo and Li (2021) numerically simulated CO, O_2, and temperature distribution in the enclosed goaf with U-type

ventilated LW face and pointed out that gas drainage and nitrogen injection assisted in mitigating gas explosion risk and improving mining safety.

From the literature review, it is noted that previous studies mainly focus on the evolution of typical gases and temperature in the simple U-type ventilated LW face during the mining stoppage period or gateroad sealing process, while there is limited research on ventilation behaviour in the LW panel, where many inter-connecting gateroads have been excavated ahead of the LW face approaching the finish-off line, in the process of the panel sealing-off, during which time the ventilation patterns in the panel change at different stages of sealing-off process and gas flow dynamics vary accordingly. The lack of this knowledge has a significant impact on managing the goaf gas atmosphere and developing sound plans to seal off both the goaf area and LW face to minimize the risk of spontaneous heating and gas explosion that are likely to occur with stopped LW face. To bridge this knowledge gap, three-dimensional (3D) computational fluid dynamics (CFD) models are developed based on the mining information collected from an underground coal mine situated in Queensland, and then calibrated with field gas data from the daily monitoring system, which allows the base model to be used for parametric studies with high confidence. A variety of ventilation control devices (e.g., ventilation doors, regulators seals and barricades) are considered, and cut-throughs and inter-connecting gateroad ahead of the LW face serving for removing LW equipment and modifying ventilation are built in the CFD model. The panel sealing-off process consists of six stages, during which the panel ventilation systems change stage by stage, the performance of ventilation controls is evaluated, and the monitoring locations of gas sensors are identified accordingly. At the final sealing-off stage, the proactive inertisation strategies are optimized to reduce the oxygen concentration in the LW panel to a safe level at which spontaneous combustion and gas explosion can be effectively prevented and managed. This computational modelling study allows for improved insight into the ventilation dynamics and goaf gas atmosphere variation during the panel sealing-off process, and provides much-needed knowledge of appropriately positioning gas monitoring sensors to reliably reflect the goaf atmosphere change and developing effective proactive inertisation plans to significantly reduce oxygen levels in the LW panel, thus minimizing the risk of spontaneous combustion and gas explosion and improving coal mining safety.

7.2 CFD Modelling

7.2.1 Geologic and mining conditions

An underground coal mine operating punch LWs in Queensland, Australia, was chosen in this modelling study. The finish-off line of the LW face is just outbye of the cut-through (CT) 11 on the maingate (MG) side with a chainage of approximately 1880 m from the starting-off line. The

LW layout approaching the finish-off line is depicted in Figure 7.1. The panel width and cutting height are 320 and 4 m, respectively. The roadway width and height are 5.6 and 3.4 m, respectively. The length of cut-throughs at the MG and TG of the active LW goaf is 42.2 and 46.5 m, respectively. In addition, the TG is 2 m lower than the MG, and the starting-off line is 43 m lower than the LW face. The goaf gas is composed of 100% CH_4 with a gas emission rate of 0.59 m^3/s. Pure nitrogen was pumped through CT19 and CT26A at the MG of the active goaf with a flow rate of 0.19 and 0.38 m^3/s, respectively, as shown in Figure 7.1 marked in purple circles.

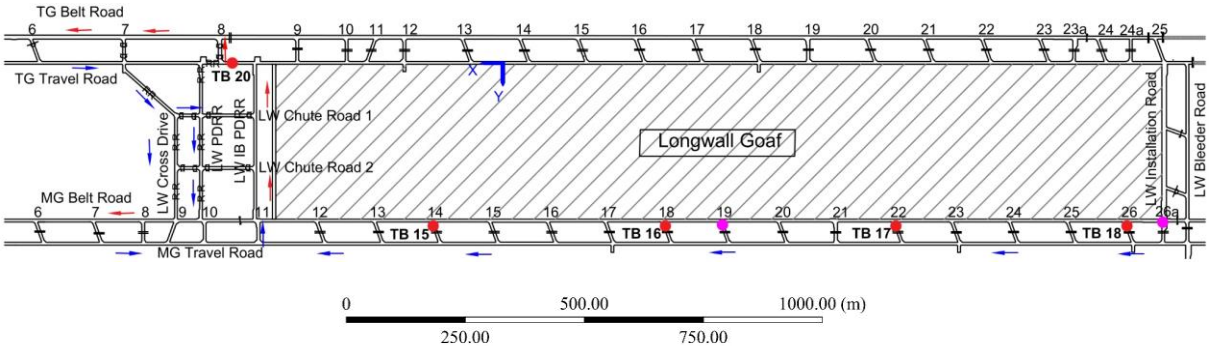

(a) Before approaching the finish-off line

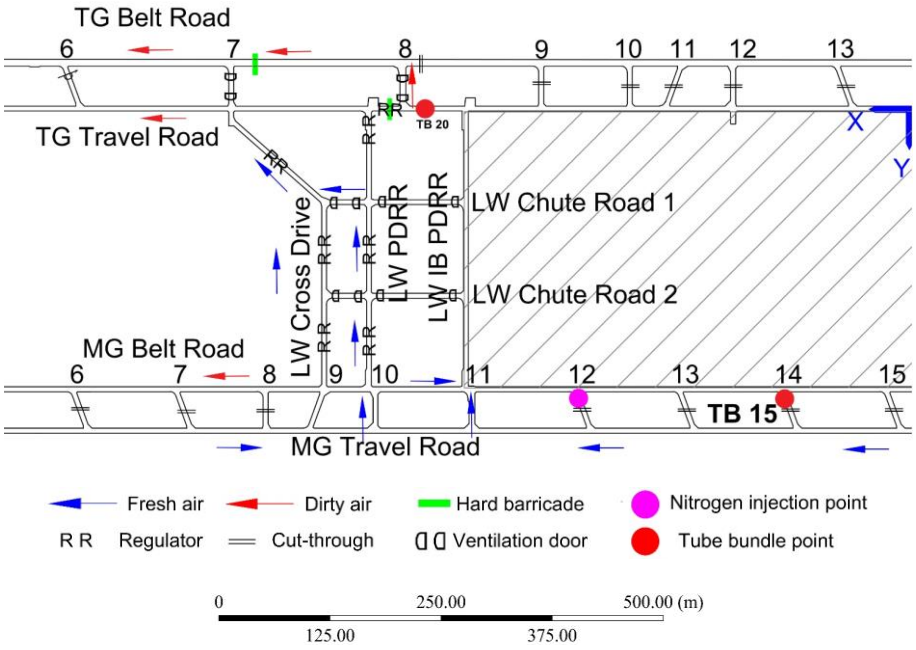

(b) At the finish-off line

Figure 7.1 LW layout

7.2.2 Model construction

Based on the ventilation layout shown in Figure 7.1, two different 3D computational models were constructed in DesignModeler to denote two different positions of the LW face. The origin of the models was both set at the TG of the active goaf over a distance of 500 m from the LW face. The

total height of CFD models reached 80 m to cover coal seam, floor and roof strata. The dimensions of the models are detailed in Table 7.1.

Table 7.1 Dimensions of the models

Parameter	Dimension (m)	Parameter	Dimension (m)	Parameter	Dimension (m)
Face length	320	Face height	4.0	Goaf depth	1880/500
Gateroad width	5.6	Gateroad height	3.4	Cut-through length	42.2 (MG)/46.5 (TG)
Floor strata	10.0	Coal seam	4.0	Roof strata	66.0

The models were meshed in Ansys Meshing using the hexahedron meshing method for all gateroads and goaf areas to significantly improve simulation speed and accuracy (Ren et al. 2005; Ren et al. 2012). A mesh independence study was carried out to eliminate the influence of mesh size on simulation results (Qiao et al. 2022a; Qiao et al. 2022b). The coal seam sizes in the 1880-meter goaf were 1.5, 2 and 2.5 m for fine, medium and coarse mesh models, respectively, with total cells of 1592756, 1120932 and 904356. As illustrated in Figure 7.2, minimal differences in velocity along the belt road (MG) and travel road (TG) were observed, hence the model with medium coal seam size was utilized in the following modelling studies. The orthogonal quality and skewness were 1 and 0 for the 1880-m model, indicating that the quality of the models was excellent as guided by ANSYS Meshing User's Guide (ANSYS 2018b). The total elements for the 500-meter panel model were 1138537 when using the same meshing method and size as the medium-meshed 1880-meter panel. As depicted in Figure 7.3, the meshed models were further refined in Fluent in certain areas above and under the mined-out coal seam with the aid of the region adaption function.

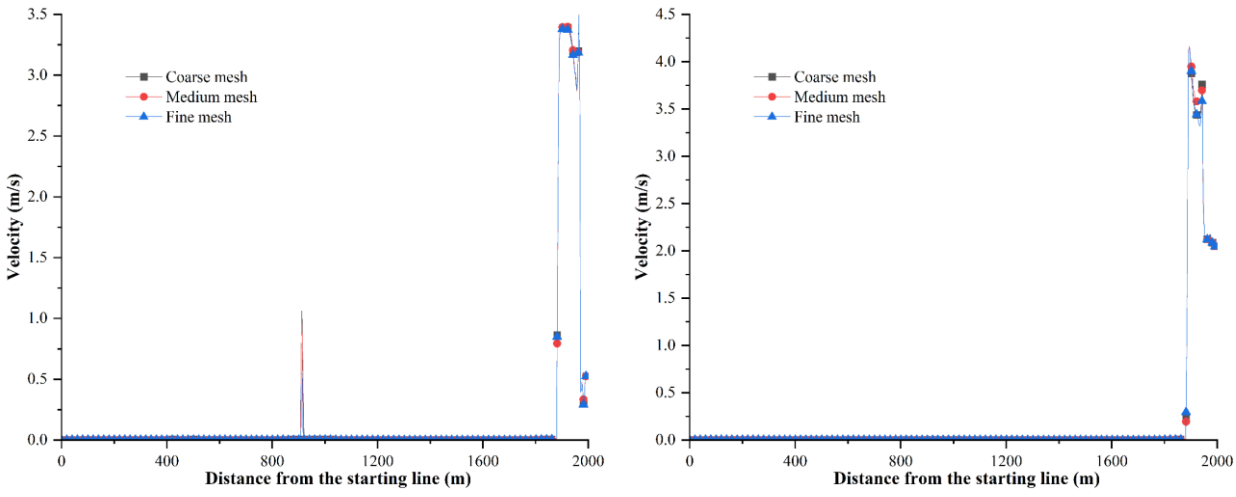

(a) Velocity along the MG belt road (b) Velocity along the TG travel road

Figure 7.2 Mesh independence study results

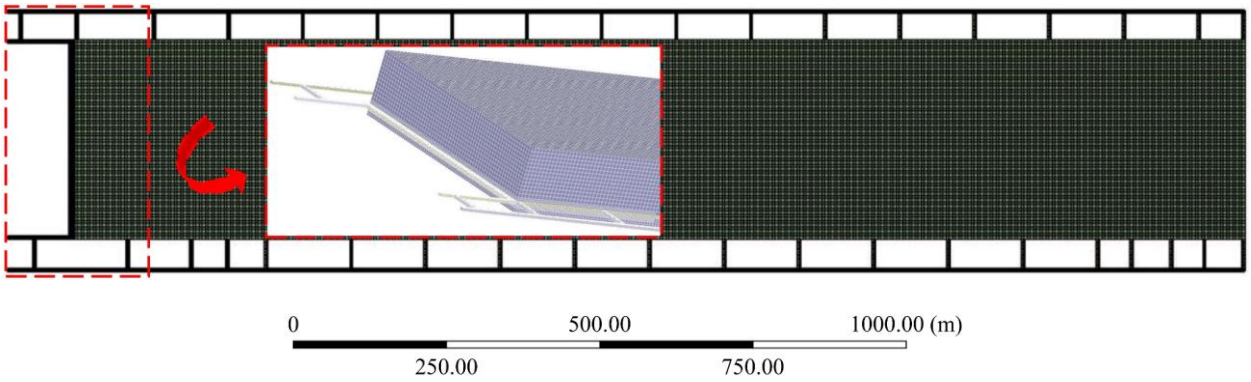

(a) 1880-meter goaf model

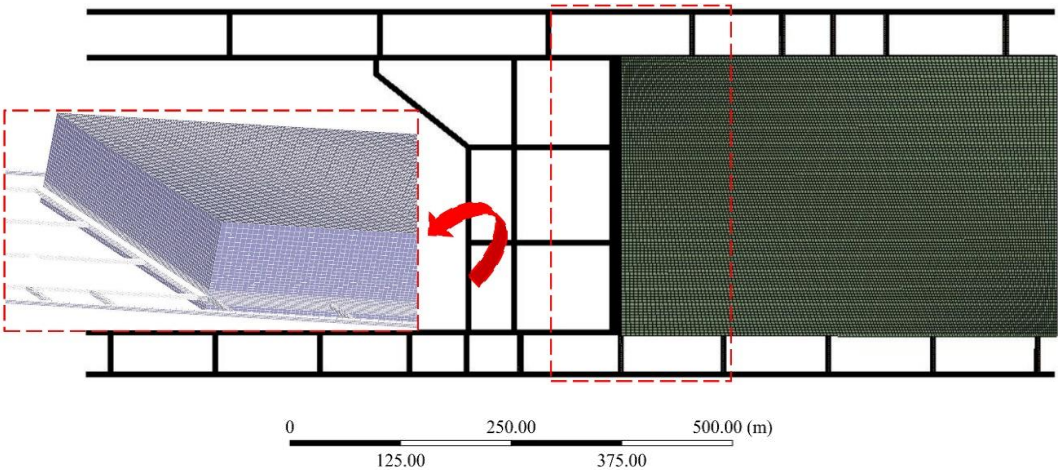

(b) 500-meter goaf model

Figure 7.3 Meshed model for numerical simulations

7.2.3 Boundary conditions

The standard k-epsilon turbulence model was adopted for the purpose of predicting gas flow within the fluid domain (Mishra et al. 2016; Ren & Balusu 2005; Tanguturi & Balusu 2015; Tutak & Brodny 2017b). The coal ribs, roof walls and floor walls were regarded as no-slip standard walls. In addition, CFD modelling was established with a view to reflecting laminar flow within the active goaf and turbulent flow within the working face and roadways (Ma et al. 2020a; Taraba & Michalec 2011; Yuan & Smith 2014; Zhu & Liu 2012) by activating the corresponding settings in Fluent. Considering the difference in the coal seam orientation between the CFD models and the real-world condition, the gravity option was activated in Fluent and decomposed accordingly to present the influence of the buoyancy effect on gas flow dynamics in the LW panel and make CFD modelling closer to reality. To study gas flow characteristics within the mined-out goaf, species transport was activated with a mixture material of methane-air being selected in Fluent. Velocity inlet was defined for the MG travel road, MG back travel road, MG belt road and TG travel road with the value of 2.31, 1.52, -0.53 and 2.05 m/s, respectively, while Outflow was defined for the TG belt road (Li et al. 2021a; Liu et al. 2020b; Zhang et al. 2020; Zhuo et al. 2021). The seam gas

composition and emission rate, nitrogen injection location and flow rate, and the tightness of seals erected in CTs at the MG and TG of the active goaf were written in user-defined functions (UDFs) and interpreted in Fluent. Taking various ventilation control devices into account in CFD modelling, different permeabilities were assigned to different ventilation control devices and written in UDF mainly following their functions.

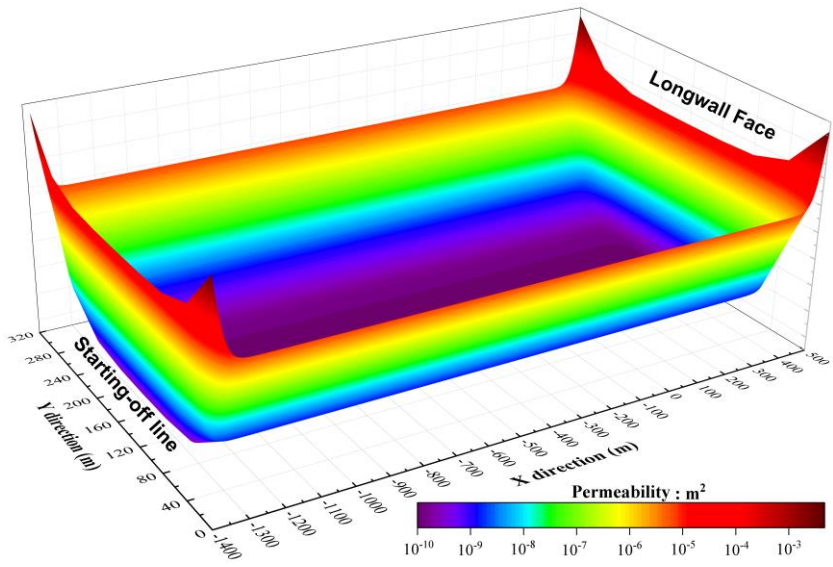

(a) 1880-meter goaf model

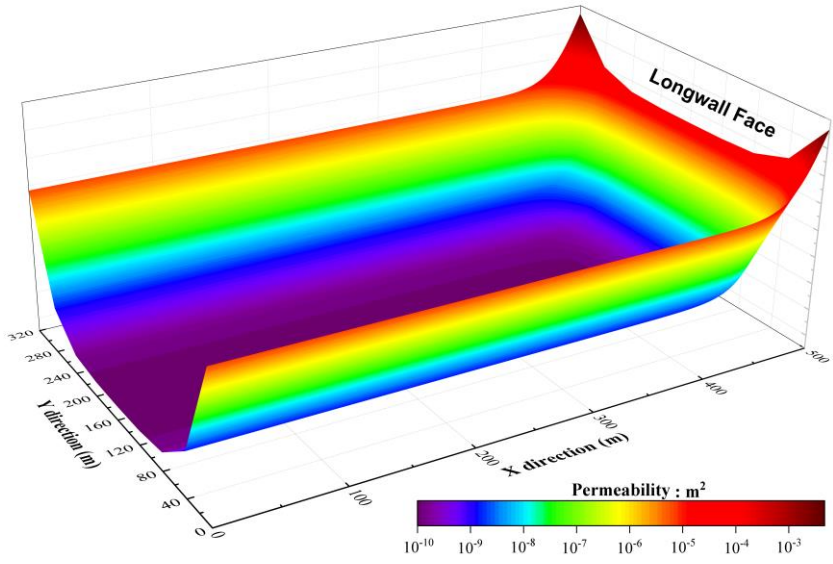

(b) 500-meter goaf model

Figure 7.4 Permeability distribution in the goaf

Research conducted by Guo et al. (2012) revealed that the spatial distribution of permeability within the active goaf was approximate to an O-ring shape, which has been widely applied by many scholars to investigate spontaneous combustion in the goaf area (Chen et al. 2020a; Liu et al. 2022; Yang et al. 2018). Specifically, the permeability value was small in the goaf centre due

to the consolidation of overlying strata, while it was high at the periphery of the goaf. On the basis of the geologic report provided by the mine site, the permeability value was estimated, with the value ranging between 10^{-2} and 10^{-10} m^2. Figure 7.4 illustrates the permeability distribution in the active goaf. The permeability distribution was written in a UDF file and interpreted in Fluent.

7.2.4 Model validation

The tube bundle system has been widely used in Australian underground coal mines to monitor four typical gases in a continuous manner (Liang et al. 2019). As shown in Figure 7.1, five tube bundle points marked in red circles were set by the mine site to monitor the goaf gas atmosphere. The oxygen concentration at each tube bundle location in the LW panel was collected and compared with results obtained from CFD simulations where the simulation results tallied well with the gas monitoring data, as illustrated in Figure 7.5. The variation of oxygen concentration between numerical simulation and monitoring data was smaller than 3%, meaning that the computational models can be used to investigate the other scenarios with sufficient confidence.

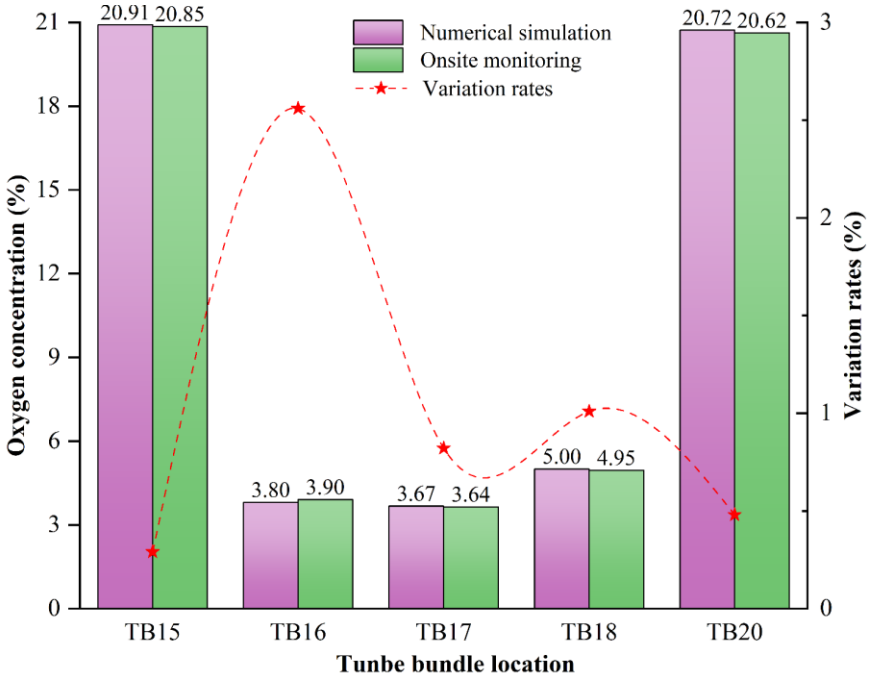

Figure 7.5 Model validation and calibration

7.2.5 Base model results

Figure 7.6 presents oxygen distribution at 2 m above the coal seam floor. Air ingress was observed to be noticeable at the MG of the active goaf, particularly at about 500 m behind the LW face, as evidenced by oxygen concentration registered at TB15 (Figure 7.5). An explanation for this observation was that a considerable amount of air was able to penetrate into the active goaf through CTs where substantial pressure differences existed between the travel road and the inner goaf (Qiao et al. 2022a). Evidently, an oxygen spike was also observed at each cut-through at the MG

of the active LW goaf. By contrast, air leakage was weak at the TG of the goaf, and oxygen levels at about 100 m behind the LW face lower than 5%.

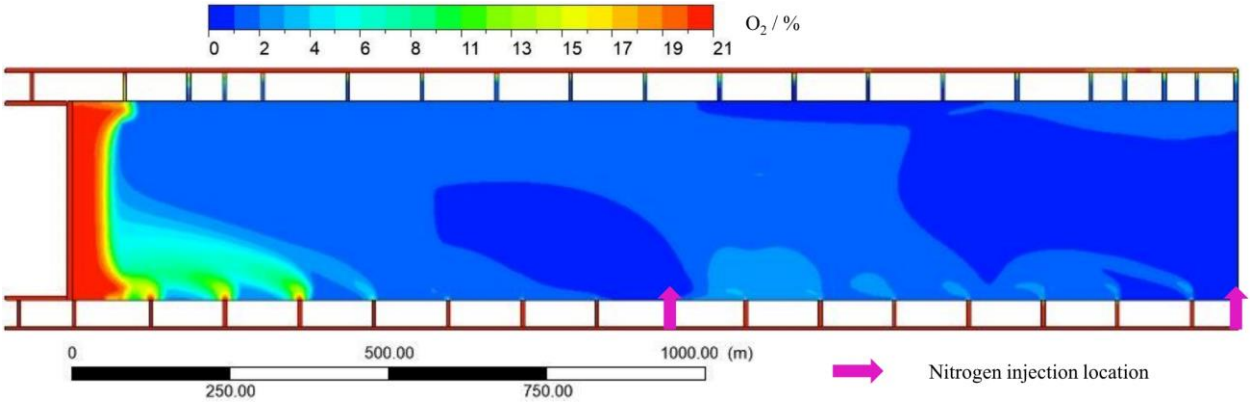

Figure 7.6 Oxygen distribution in the LW panel

A gas explosion is likely to occur when an explosive methane-air mixture is formed and ignited. The nose limit of oxygen for the explosive gas mixture is 12.24%. Spontaneous heating of coal can potentially occur when the oxygen concentration lies in the range of 5~18 % (Deng et al. 2018). To effectively manage and prevent spontaneous heating and gas explosions in the active goaf, the oxygen concentration within the mined-out goaf should be lower than 5%.

7.3 Results and Discussion

7.3.1 LW sealing at different stages

When the LW face approaches the finish-off line, the panel sealing-off process starts and mainly includes six different stages. At different stages of the LW panel sealing-off process, the ventilation schemes change where the ventilation rates proposed by the mine site are detailed in Table 7.2. The positive value of airflow rate denotes fresh intake air is provided, whereas a negative value of airflow rate represents dirty return air flows through this gateroad.

Table 7.2 Ventilation flow rates at different stages of the LW sealing process

Stage	Airflow rate (m^3/s)				
	Travel road (MG)	Back travel road (MG)	Belt road (MG)	Travel road (TG)	Belt road (TG)
1	44	29	-10	39	-102
2	44	29	-10	-63 (in total)	
3	50	20	9	-79 (in total)	
4	46	8	10	-64 (in total)	
5	50	10	6	-66 (in total)	
6	41	6	8	-55 (in total)	

Considering the oxygen concentration is lower than 5% at 500 m behind the LW face and saving computational time, the modelling of ventilation behaviour and gas flow dynamics at each stage is based on the 500-meter goaf model, and the permeability distribution is the same as the 1880-meter goaf model, as shown in Figure 7.4(b).

7.3.1.1 Stage 1-LW face coming into the finish-off position

The ventilation plan is illustrated in Figure 7.7 when the LW face comes into the finish-off position. At this stage, nitrogen is only pumped through CT13 at the MG of the LW panel at a flow rate of 0.5 m^3/s. Both LW chute road 1 and road 2 are closed. With reference to Figure 7.7, the regulators at LW cross drive and LW PDRR gateroad take effect to regulate airflow. In this study, oxygen and methane concentration stands for mole fraction rather than mass fraction.

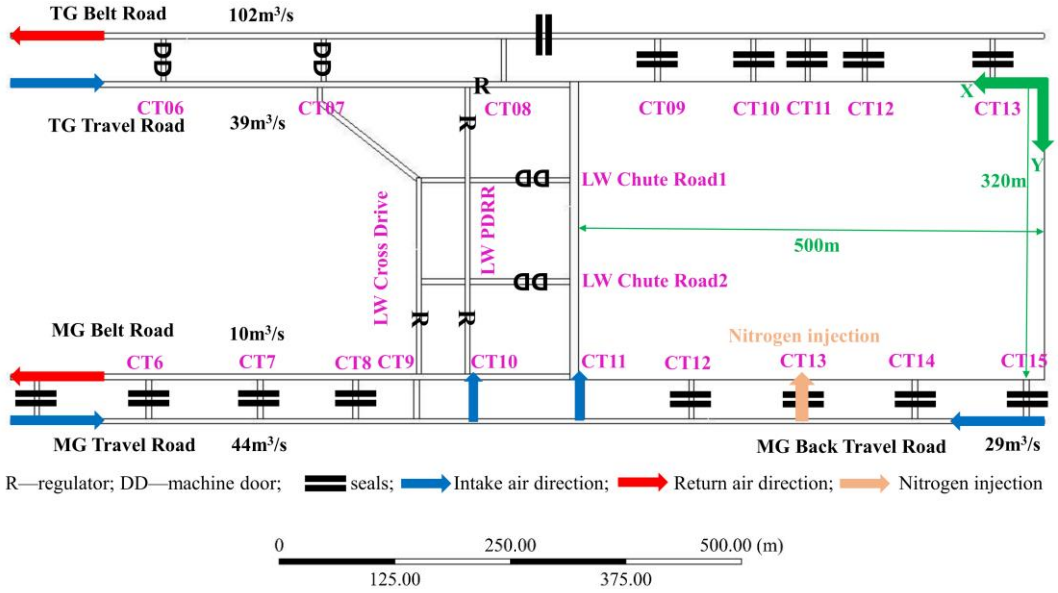

Figure 7.7 LW Panel ventilation layout

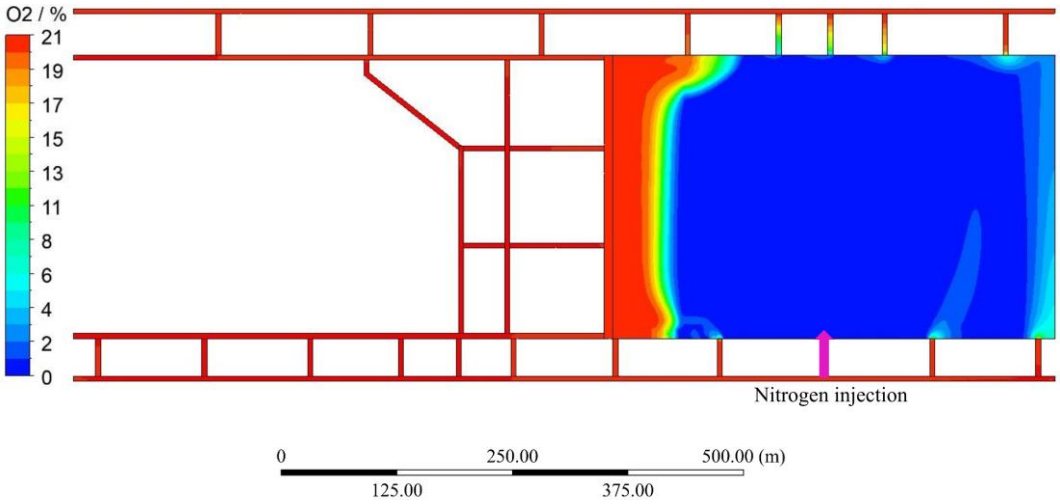

Figure 7.8 Oxygen concentration at 2 m above the coal seam floor at stage 1

Oxygen distribution at 2 m above the coal seam floor is presented in Figure 7.8. It was noted that air ingress at both sides of the LW goaf was alleviated, except at some cut-throughs where an oxygen spike could be observed. The reason for this is that oxygen-containing air is able to leak into the mined-out area through insufficiently tight seals situated in the cut-throughs as a result of significant pressure differences existing between the MG travel road and the inner active goaf. Thus, it is recommended that seals erected within the cut-throughs at the MG of the LW goaf be constructed as tight as possible. At this stage, at least two gas monitors should be used. One gas sensor should be placed at the goaf fringe to monitor localized methane levels in a real-time manner. Another gas sensor should be positioned outbye of the seal built between CT8 and CT9 of the MG belt road, which can assist in judging the potential air leakage from the seal.

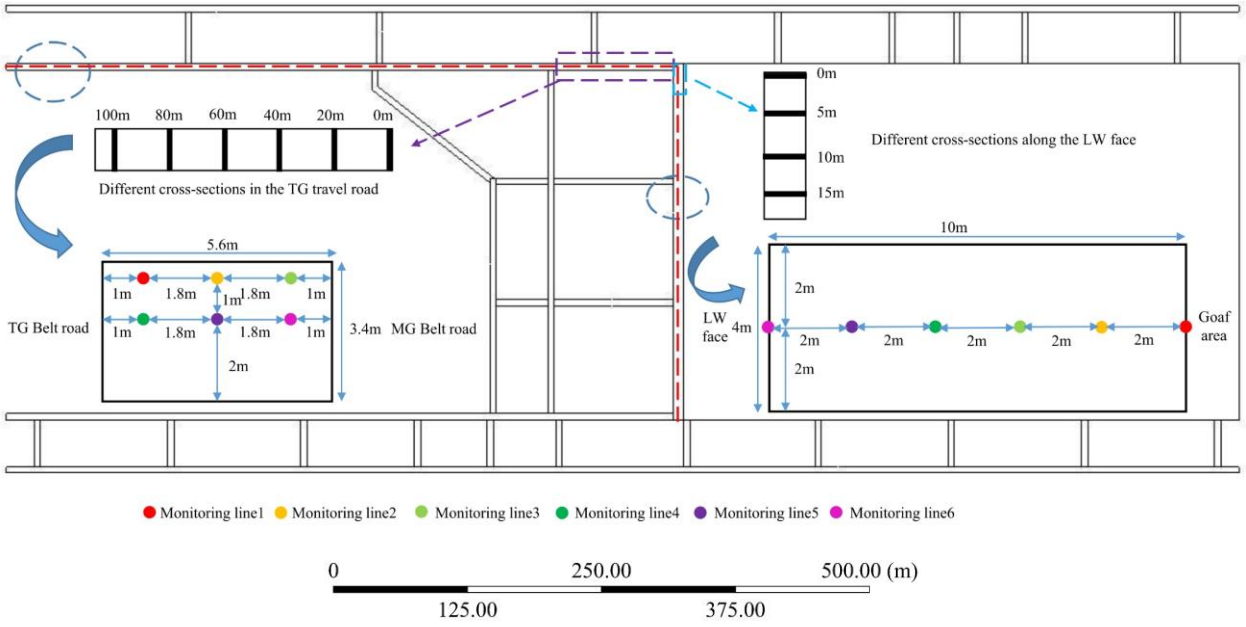

Figure 7.9 Locations of different monitoring points at TG travel road and along with the LW face

As shown in Figure 7.9, different monitoring lines were applied to better obtain methane concentration variation along the TG travel road and the LW face. The monitoring line along the TG travel road starts from the LW face close to the goaf. The dimension of the cross section is 5.6m in width and 3.4 m in height in the TG travel road, while it is 10 m in width and 4.0 m in height in the LW face.

The methane concentration at different monitoring lines in the TG travel road is depicted in Figure 7.10(a). Regarding the peak methane concentration on the LW face, it was highest at monitoring line 3, followed by monitoring line 2 and monitoring line 1. In the TG travel road, methane concentration reduced below 0.3%. In addition, Methane distribution along with the TG travel road is shown in Figure 7.10(b), in which 0 m face denotes the interface between the LW face and TG travel road. It was apparent that the high concentration of methane mainly existed at the left

side of the gateroad (close to the TG belt road), and the methane concentration gradually reduced as the distance outbye of the LW face increased.

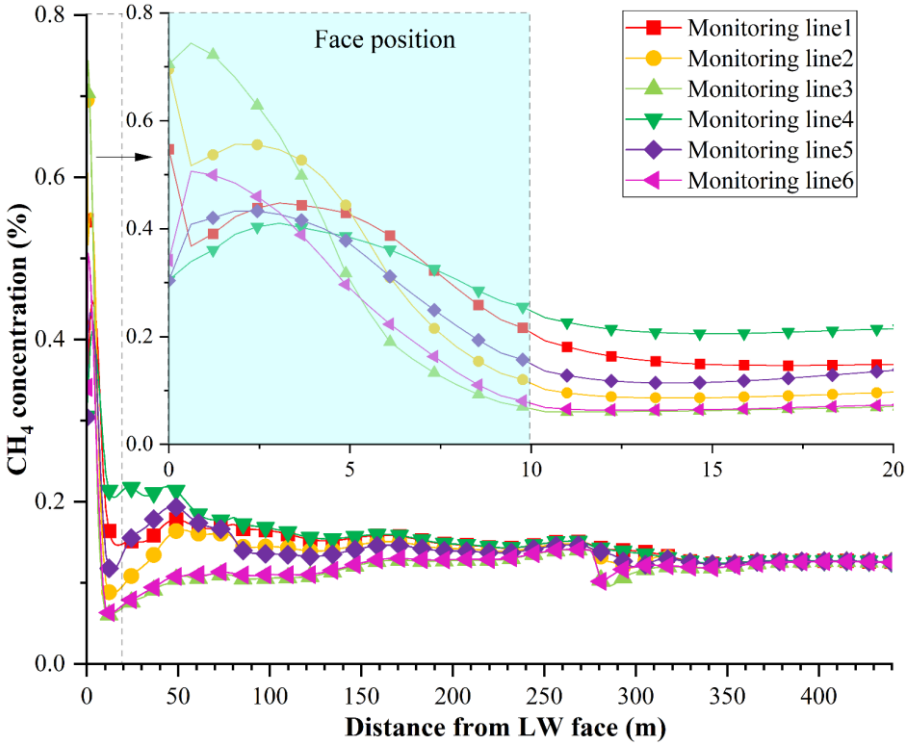

(a) Methane concentration at different monitoring lines

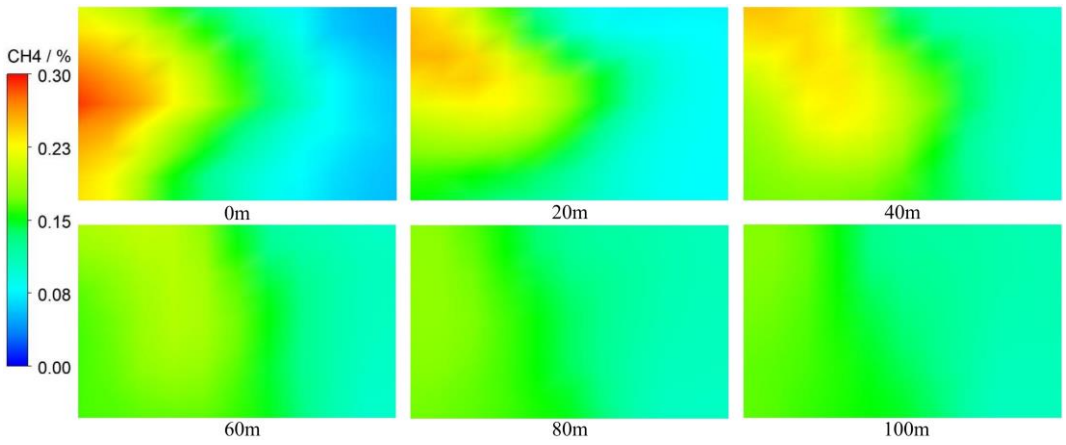

(b) Methane distribution at different cross sections

Figure 7.10 Methane distribution along the TG travel road outbye of the LW face at stage 1

Methane concentration along the LW face is shown in Figure 7.11(a). Methane concentration generally reduced as the monitoring line moved away from the goaf side towards the coal side. In addition, methane concentration dropped gradually from the TG to the MG of the LW face. In particular, methane concentration at monitoring line 1 and line 2 first rose and then dropped, with peak methane concentration reaching about 0.5%. In addition, methane distribution patterns along the LW face are illustrated in Figure 7.11(b) in which the 0 m face represents the LW face cross-section that was in line with the left rib of the TG travel road. It was observed that methane mainly

concentrated at the upper corner of different cross-sections, and the maximum methane concentration dropped quickly as the distance from the TG side increased.

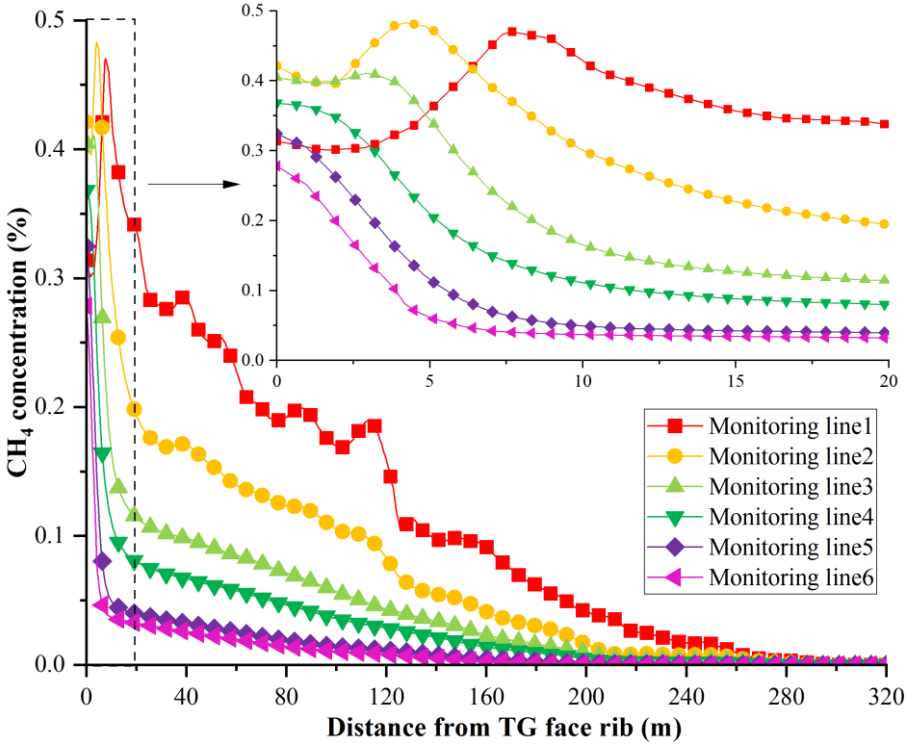

(a) Methane concentration at different monitoring lines

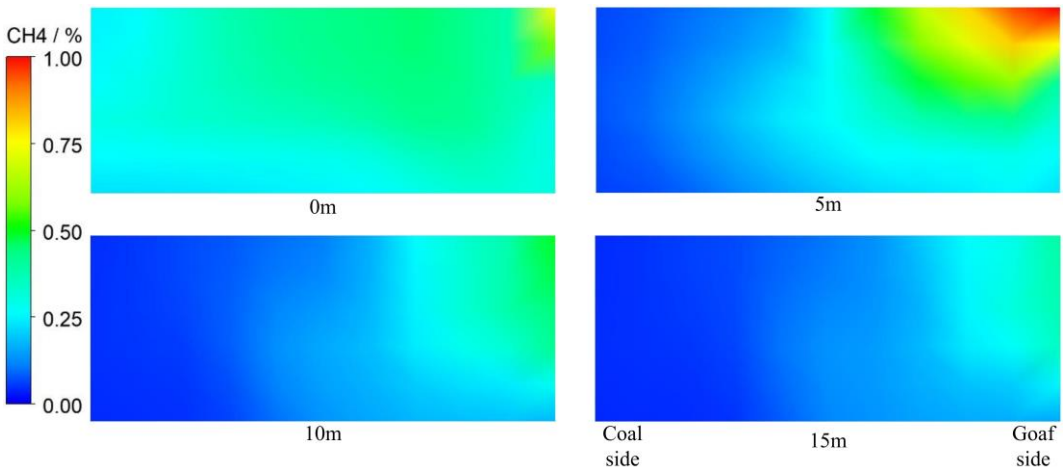

(b) Methane distribution at different cross sections

Figure 7.11 Methane distribution along the LW face at stage 1

7.3.1.2 Stage 2-LW face bolt up after production stop

The ventilation pattern changes at the second stage with the LW face coming into the PDRR position. The ventilation direction at the TG travel road is reversed from intake to return. The machine door installed at CT7 on the TG side is opened, and the regulator installed at the immediate outbye of CT8 in TG travel road is open. The machine door at CT8 on the TG side is closed, but the sliders are left open. In addition, one hard barricade is installed at the immediate

outbye of CT8 in the TG travel road, and another hard barricade is positioned at the immediate inbye of CT7 in the TG belt road. The nitrogen injection location is moved from CT13 to CT12 at the MG of the goaf with a flow rate of 0.5 m^3/s.

Figure 7.12 illustrates oxygen concentration in the LW panel. It was observed that oxygen concentration along the TG travel road was below 5% at 200 m behind the LW face, while oxygen levels along the MG belt road were below 5% at 50 m behind the LW face except at the rear cut-throughs where apparent oxygen spikes were noticed, which could be attributed to the pressure difference between the inner goaf area and MG travel road.

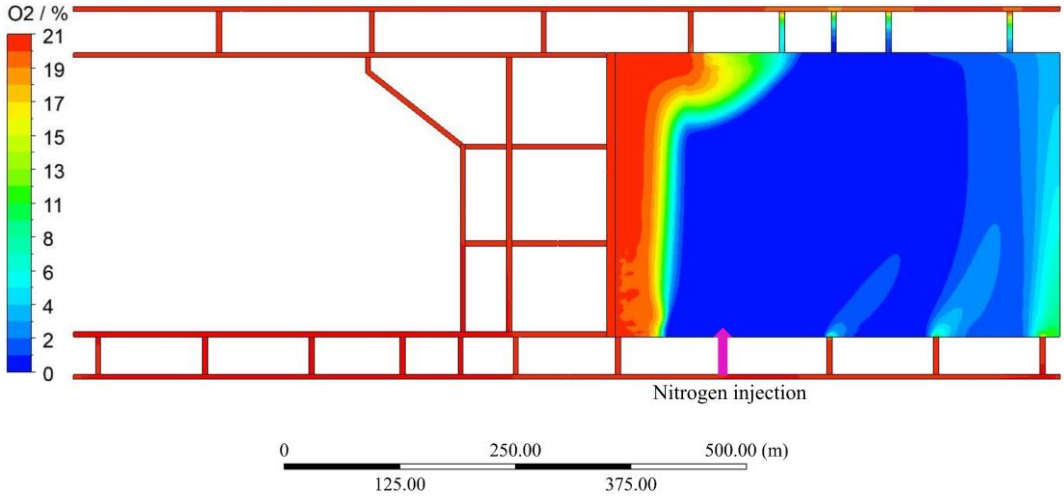

Figure 7.12 Oxygen concentration at 2 m from the coal seam floor at stage 2

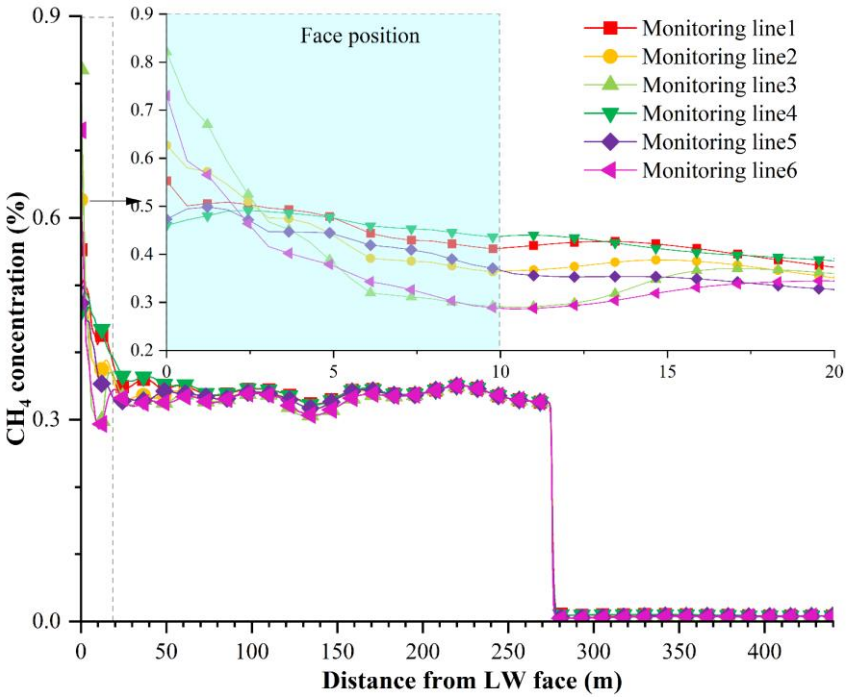

(a) Methane concentration at different monitoring lines

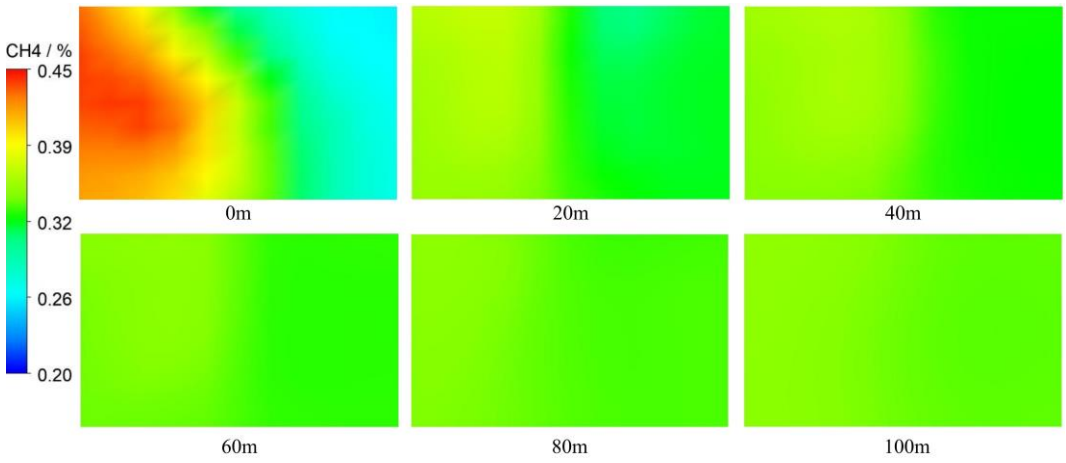

(b) Methane distribution at different cross sections

Figure 7.13 Methane distribution at the TG travel road outbye of LW face at Stage 2

The methane concentration at different monitoring lines in the TG travel road is demonstrated in Figure 7.13(a). It was noted that on the LW face, the peak methane concentration at monitoring line 3 was the highest (0.82%), followed by monitoring line 6 (0.73%) and monitoring line 2 (0.63%). In the TG travel road, methane concentration reduced below 0.5%. Methane distribution along with the TG travel road is shown in Figure 7.13(b). It was apparent that the high-concentration methane mainly existed at the left side of the gateroad (close to TG belt road), and the methane concentration gradually reduced as the distance outbye of LW face increased. To monitor the gas atmosphere in the LW face, at least two methane sensors should be used and placed at the locations which are the same as those at stage 1.

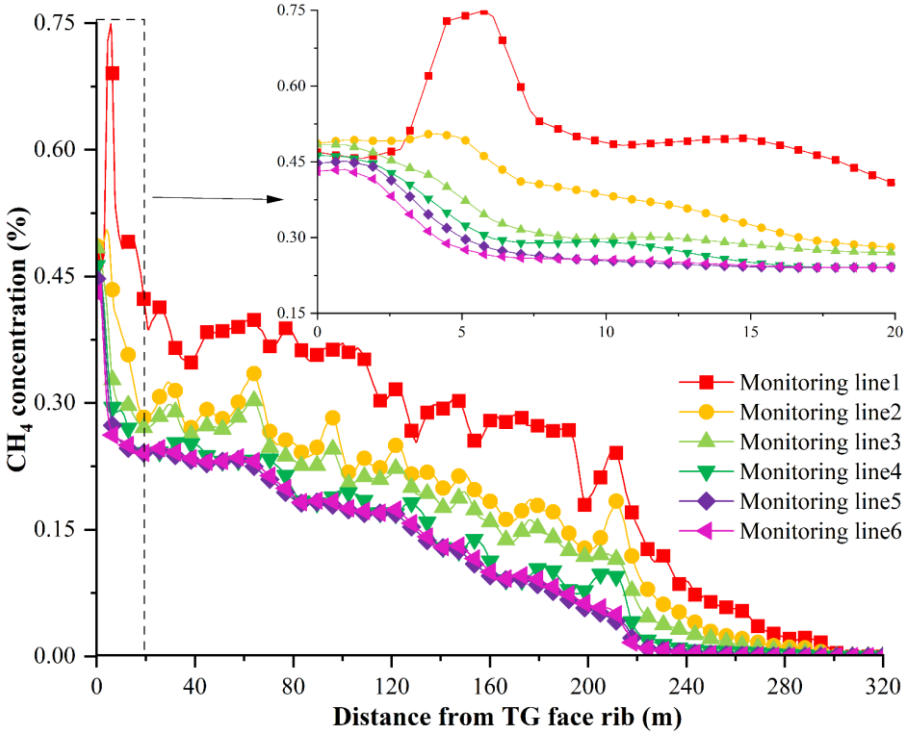

(a) Methane concentration at different monitoring lines

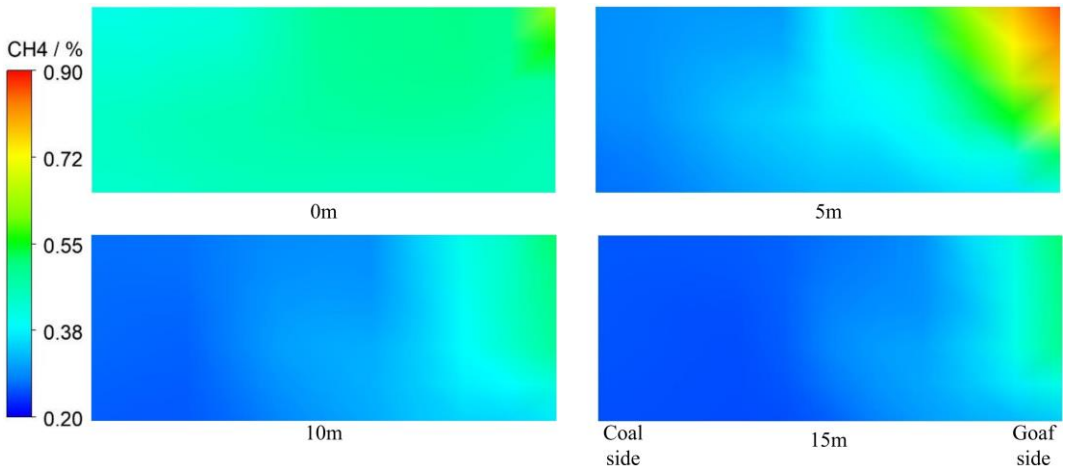

(b) Methane distribution at different cross sections

Figure 7.14 Methane distribution along the LW face at Stage 2

Methane concentration along the LW face is shown in Figure 7.14(a). Methane concentration generally reduced as the monitoring line moved away from the goaf side towards the coal side. In addition, methane concentration dropped gradually from the TG travel road side to the MG belt road side. In particular, methane concentration at monitoring line 1 firstly increased and then decreased, with peak methane concentration reaching about 0.75%. Figure 7.14(b) depicts methane distribution patterns along the LW face. Evidently, methane was mainly layered at the upper corner of different cross-sections, and the maximum methane concentration dropped quickly as the distance increased from the TG side.

7.3.1.3 Stage 3-Pulling hydraulic supports from the TG to the LW chute road 1

At this stage, the seal termed seal 11 is built in the MG belt road between CT4 and CT5 once the belt structure is removed to this point. The PDRR gateroad is regulated at the tailgate end to push the maximum ventilation down the face. The machine door installed in CT4 at the MG of the active goaf is opened to reverse the airflow direction within the MG belt road, with the airflow rate being regulated through hatches at seal 11. In addition, the regulator doors at the TG end of outbye PDRR gateroad are opened to allow the MG gateroads to change to dual intakes. In addition to two hard barricades used at stage 2, two more hard barricades are utilized. One hard barricade is installed in the LW PDRR gateroad between the TG travel road and LW chute road 1, and the other one is positioned in the gateroad that connects the TG travel road and LW cross drive.

As illustrated in Figure 7.15, the oxygen volume fraction at the TG of the active goaf was below 5% at 200 m behind the LW face, whilst oxygen levels at the MG of the goaf were below 5% at about 50 m behind the LW face except at the rear CTs where noticeable oxygen spikes were observed, which was similar to the oxygen distribution at stage 2.

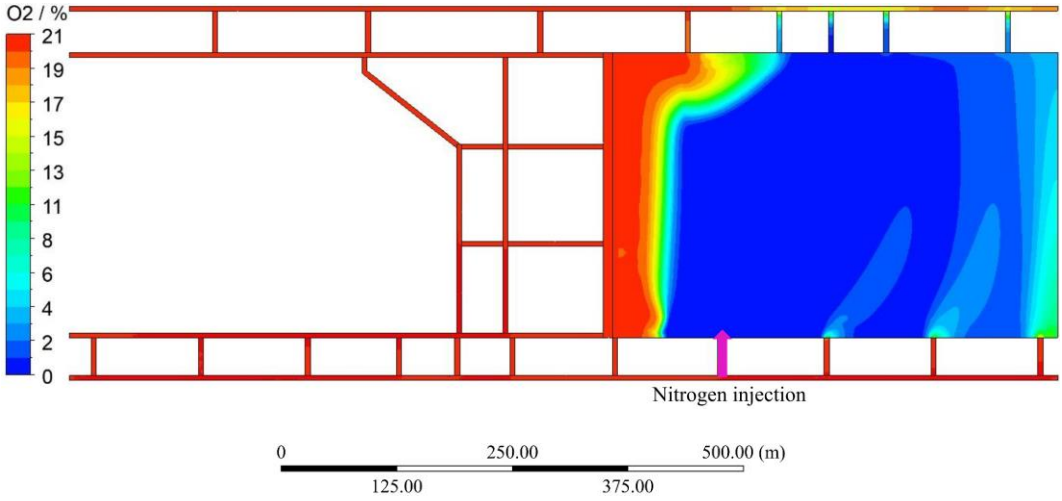

Figure 7.15 Oxygen concentration at 2 m above the coal seam floor at stage 3

Figure 7.16(a) demonstrates methane concentration at different monitoring lines in the TG travel road at Stage 3. The results indicated that on the LW face, the peak methane concentration of monitoring line 3 was the highest (0.71%), followed by monitoring line 2 (0.68%) and monitoring line 6 (0.60%). At the outbye of the TG travel road, methane concentration reduced below 0.3%. The methane distribution along the TG travel road is illustrated in Figure 7.16(b). As the distance outbye of the LW face increased, methane concentration dropped gradually. The highest methane concentration was mainly distributed on the left rib side of the TG travel road (close to the TG belt road).

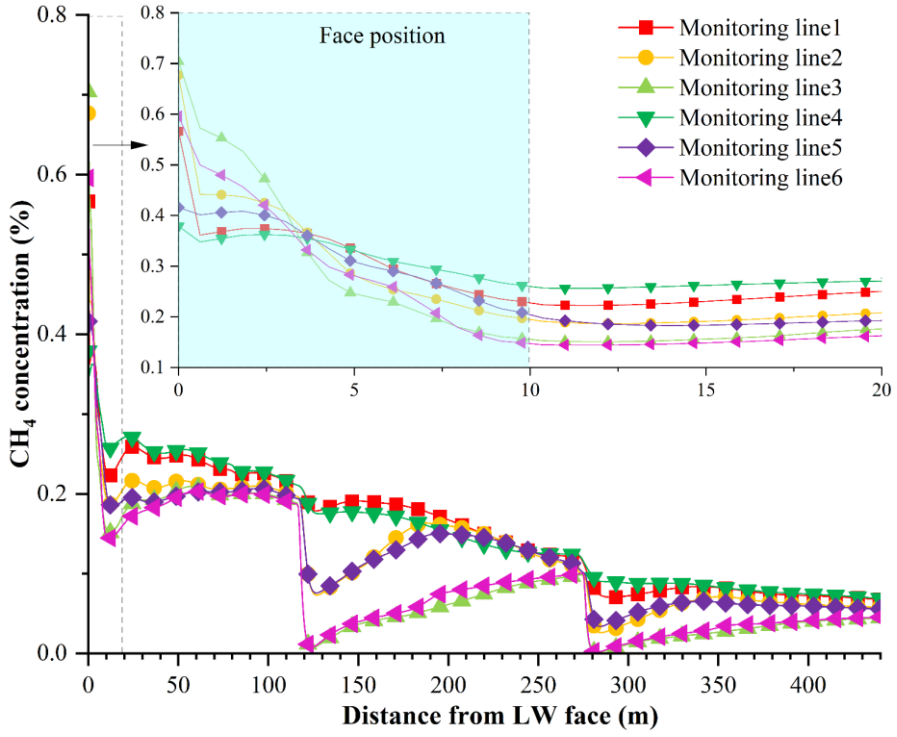

(a) Methane concentration at different monitoring lines

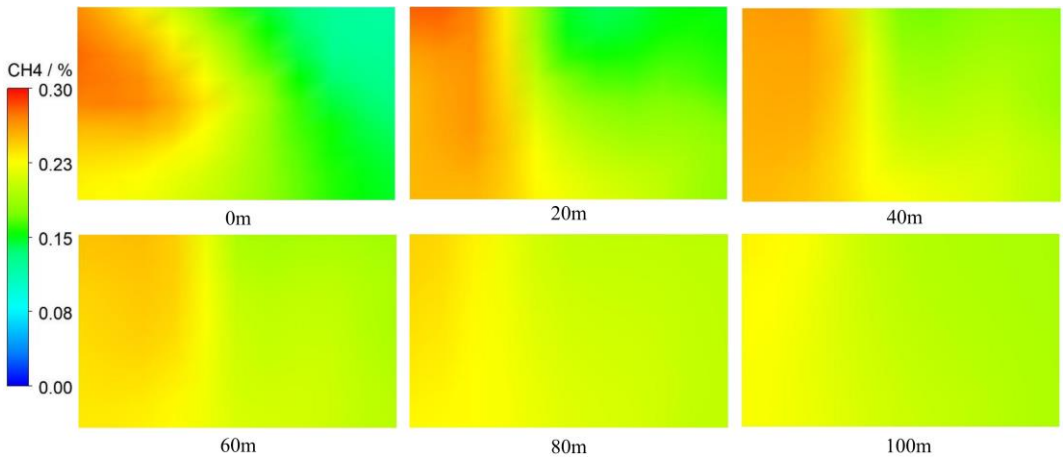

(b) Methane distribution at different cross sections

Figure 7.16 Methane distribution in the TG travel road outbye of LW face at Stage 3

Methane concentration along the LW face at Stage 3 is presented in Figure 7.17(a). The highest methane concentration was observed at monitoring line 1, with its value registering approximately 0.65%. As the distance moved from the TG side to the MG side, methane concentration was generally reduced. As depicted in Figure 7.17(b), methane mainly accumulated at the upper corner of the LW face. As a result, a monitoring point should be positioned in this area, particularly at an approximate distance of 5 m away from the rib.

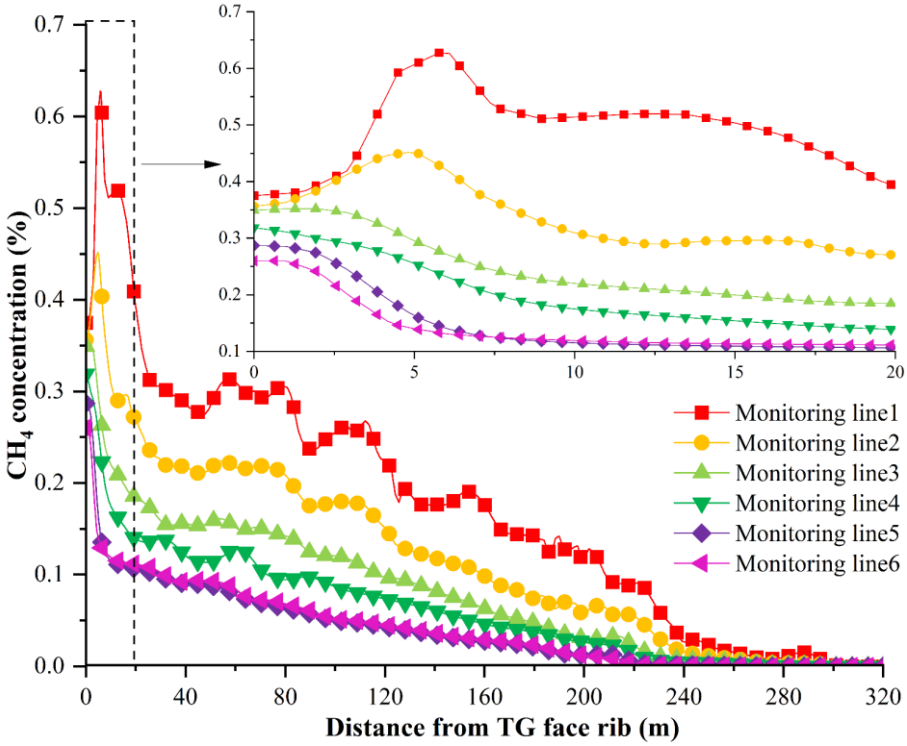

(a) Methane concentration at different monitoring lines

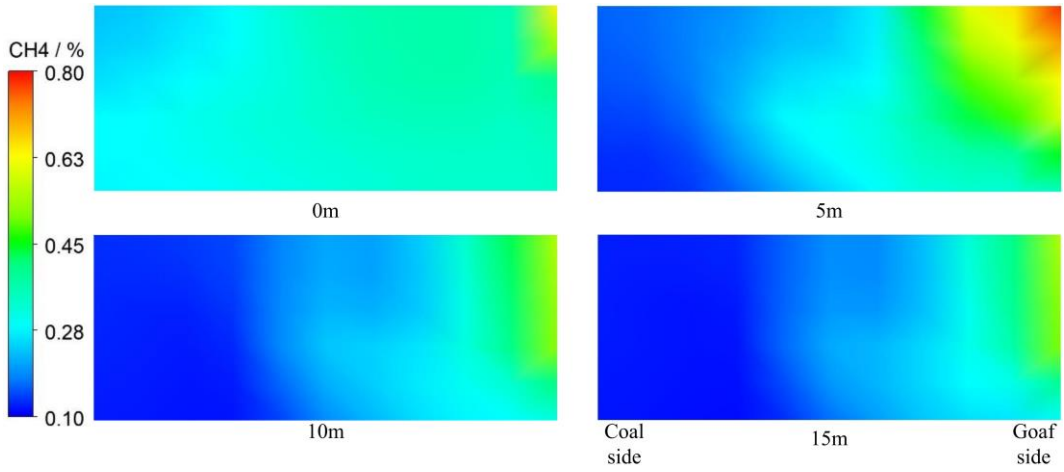

(b) Methane distribution at different cross sections

Figure 7.17 Methane distribution along the LW face at Stage 3

7.3.1.4 Stage 4-Pulling hydraulic supports from the LW chute road 1 to road 2

At this stage, two hard barricades that are installed in the LW PDRR gateroad between the TG travel road and LW chute road 1 and positioned in the gateroad connecting the TG travel road and LW cross drive are removed, but the other two barricades are kept when compared to barricade specifications at stage 3. To regulate the airflow, two more barricades are installed in the LW cross drive and the LW PDRR road, both of which are located between LW chute road 1 and chute road 2. The machine door at the LW chute road 1 is opened once the shields are past this chute road. In addition, the LW face is regulated via the mid-face regulators in the outbye of the PDRR gateroad, which allows the face air to exit via the chute road 1. The regulator that is installed in the gateroad connecting the LW cross drive and the TG travel road is opened.

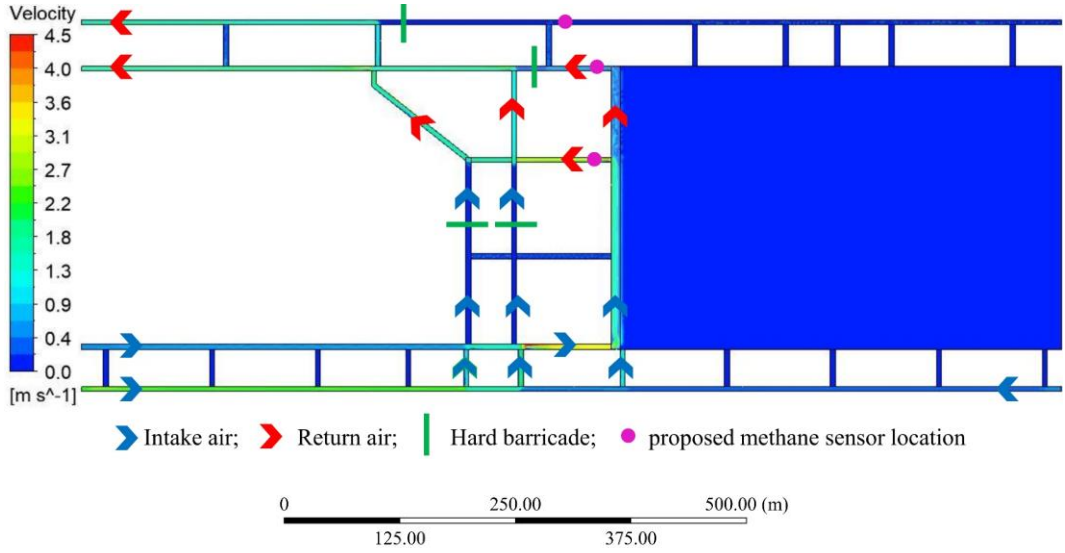

Figure 7.18 Velocity distribution at the seam level (2m from seam floor) at Stage 4

Compared with oxygen distribution in the panel at stage 3, there was no apparent difference at stage 4. However, the ventilation patterns in the LW panel changed a lot, as shown in Figure 7.18.

The majority of return airflow would flow through the LW chute road1 and then back to the TG travel road and TG belt road. Due to the utilization of hard barricades in the LW cross drive and the LW PDRR gateroad, the air flowing from MG travel road through these two gateroads was limited. Besides two methane sensors used at the former stages, one more methane sensor should be placed in the LW chute road 1 to monitor the methane concentration of the general body atmosphere in a real-time manner, as relatively high-concentration methane could accumulate on the partial LW face between the chute road 1 and TG travel road due to low velocity in this region.

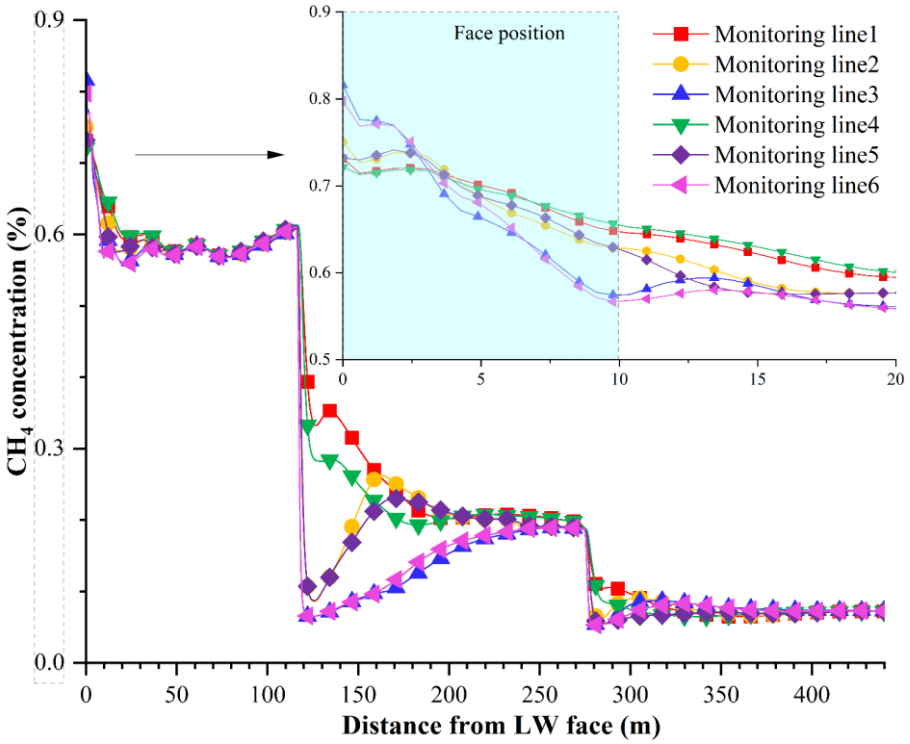

(a) Methane concentration at different monitoring lines

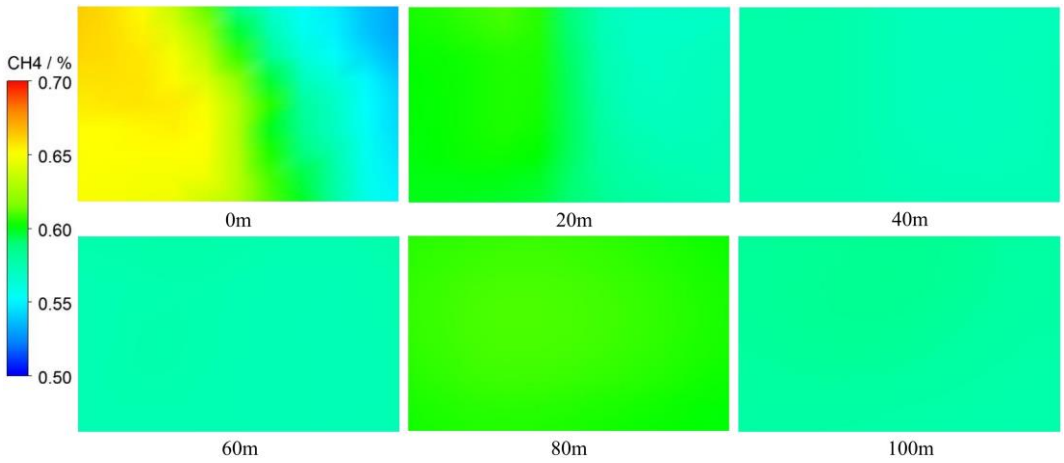

(b) Methane distribution at different cross sections

Figure 7.19 Methane distribution in the TG travel road outbye of LW face at Stage 4

Figure 7.19(a) presents methane concentration at different monitoring lines in the TG travel road at Stage 4. The results indicated that on the LW face, the peak methane concentration of monitoring line 3 was the highest (0.82%), followed by that of monitoring line 6 (0.80%) and monitoring line 2 (0.75%). A significant reduction in methane concentration was observed at an approximate distance of 110 m from the LW face, dropping below 0.4%. As illustrated in Figure 7.19(b), methane concentration along the TG travel road dropped gradually as the distance outbye of the TG travel road increased.

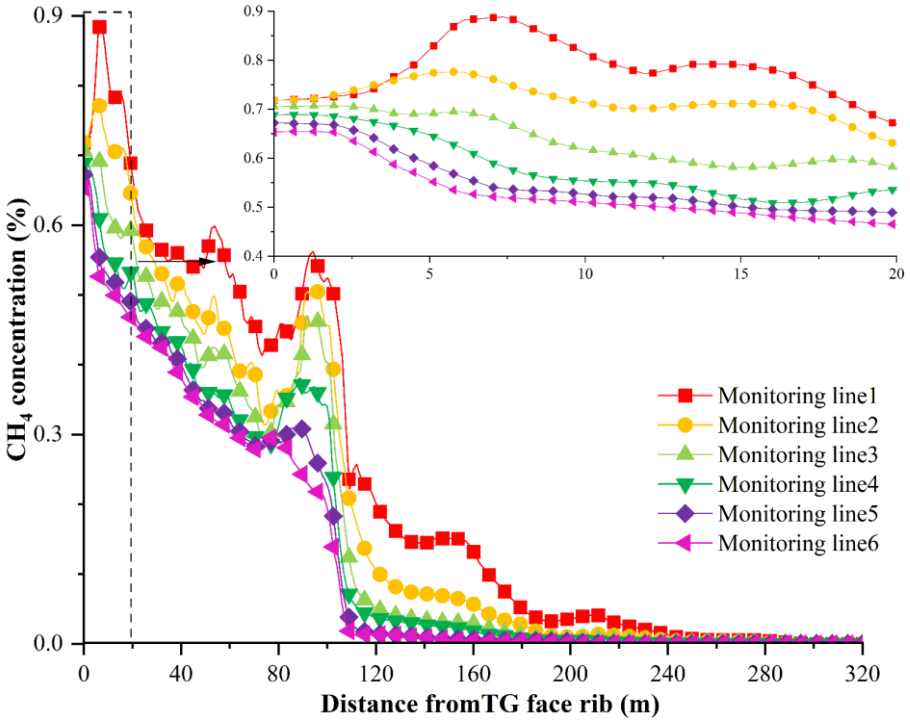

(a) Methane concentration at different monitoring lines

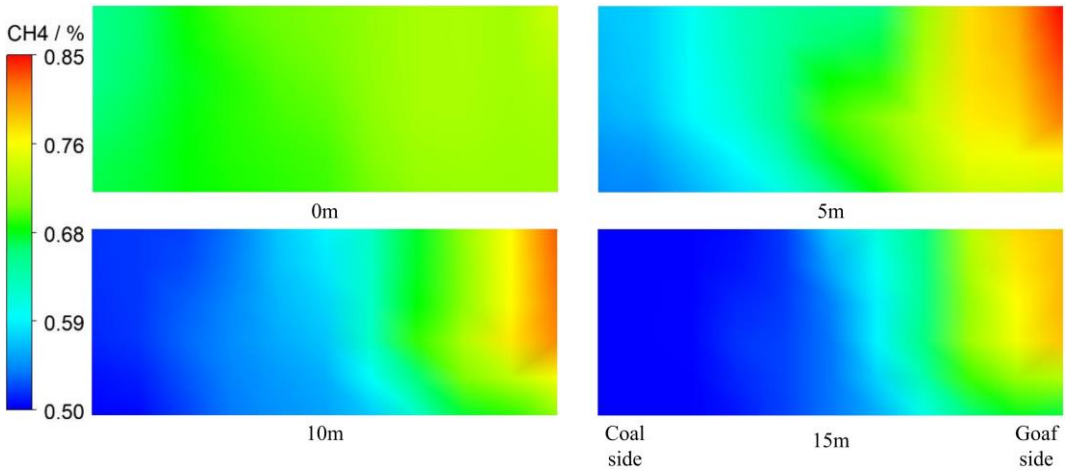

(b) Methane distribution at different cross sections

Figure 7.20 Methane distribution along the LW face at Stage 4

It was evident from Figure 7.20(a) that the peak methane volume fraction could reach 0.9% at monitoring line 1, so it is essential to continuously monitor methane levels at the goaf stream. A

high methane concentration could also be observed at the face area between the TG travel road and the LW chute road 1. Methane concentration dropped below 0.3% when the distance away from the TG travel road rib was higher than 100 m. In addition, high-concentration methane could be observed at the upper corner of the LW face, so particular attention should be paid to monitoring gas levels in this localized area, as depicted in Figure 7.20(b).

7.3.1.5 Stage 5-Pulling hydraulic supports from the LW chute road 2 to the MG

Once the shields are past LW chute road 2, the machine door in this chute road is opened, and the machine door in LW chute road 1 is closed. The mid-face regulator is also closed. In addition, all four hard barricades used at stage 4 are removed, but two hard barricades are used in other locations at this stage. One is installed in the LW cross drive, and the other one is positioned in the LW PDRR gateroad, both of which are located between MG belt road and the LW chute road 2.

Similarly, there was no significant difference in oxygen distribution patterns in the LW panel at stage 5 when compared to stage 4. However, the velocity distribution in the LW panel changed a lot, as illustrated in Figure 7.21. It was evident that the LW air partially flowed through the LW chute road 2 and returned back to TG gateroads via the LW cross drive and LW PDRR gateroad; another part of LW air would flow towards the TG end and back to the TG gateroads. Besides three methane sensors used at stage 4, one more sensor should be used and installed in the LW chute road 2 to monitor the gas levels of the general body, which could provide an early warning of abnormal gas emissions in the process of removing shields back to MG gateroad.

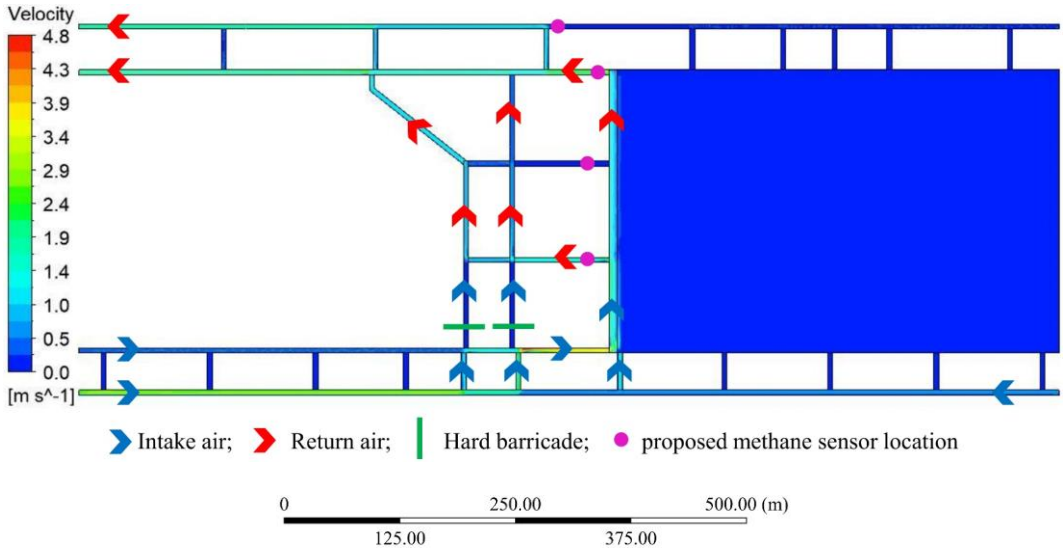

Figure 7.21 Velocity distribution at the seam level (2m from seam floor) at Stage5

Methane concentration along the TG travel road is shown in Figure 7.22(a). The simulation results indicated that the peak methane concentration was approximately 0.67% at monitoring line 3, while it was only 0.59% and 0.55% for monitoring line 6 and monitoring line 2, respectively. The methane concentration dropped below 0.35% at the outbye of the TG travel road. It could be

observed from Figure 7.22(b) that methane was mainly distributed at the left rib (close to the TG belt road). As the distance outbye of the TG travel road increased, methane concentration generally reduced.

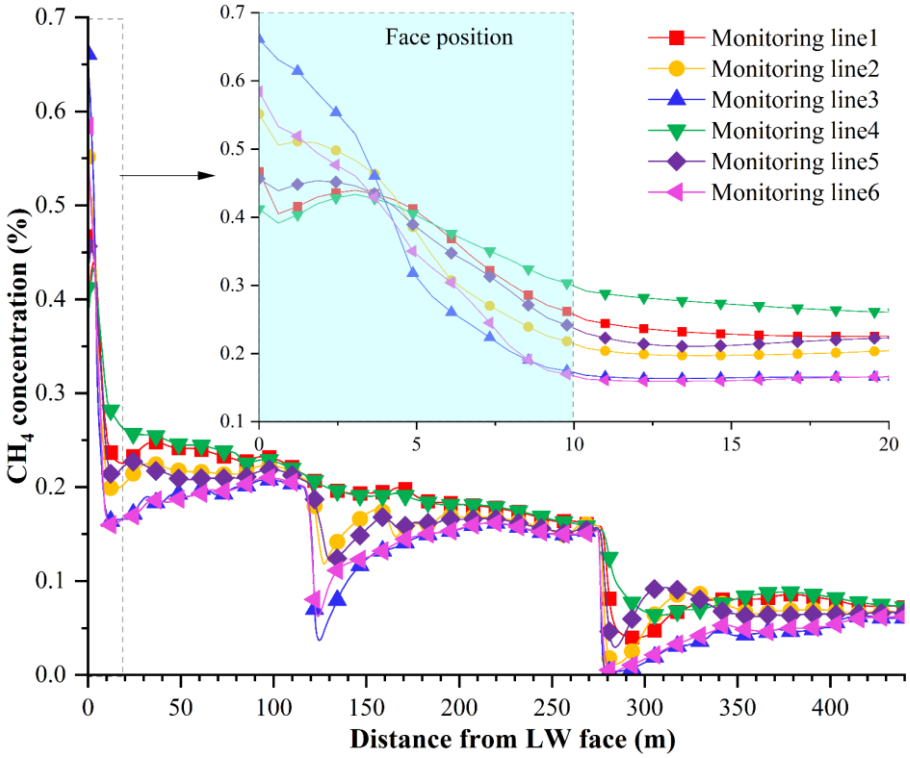

(a) Methane concentration at different monitoring lines

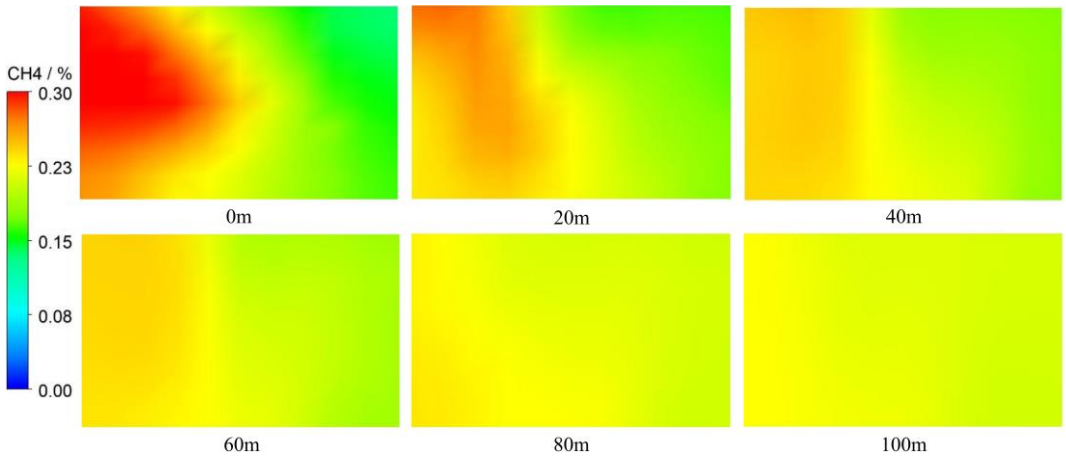

(b) Methane distribution at different cross sections

Figure 7.22 Methane distribution in the TG travel road outbye of LW face at Stage 5

Methane concentration along the LW face is shown in Figure 7.23(a). At monitoring line 1 and monitoring line 2, methane concentration first increased to a peak value and then gradually dropped. While for the other four monitoring lines, methane levels showed a downward trend in general. The peak methane concentration was approximately 0.57%. Methane distribution along the LW face showed that a high methane concentration was observed at the upper corner of the

face cross-section (close to the goaf side). As the distance increased from the TG side, methane concentration gradually reduced, as illustrated in Figure 7.23(b).

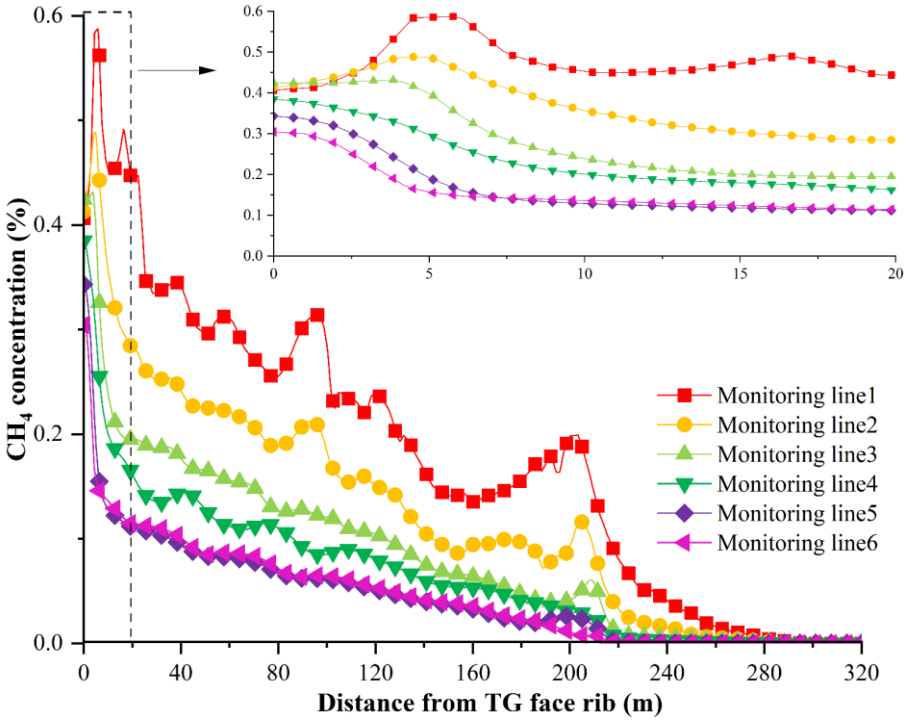

(a) Methane concentration at different monitoring lines

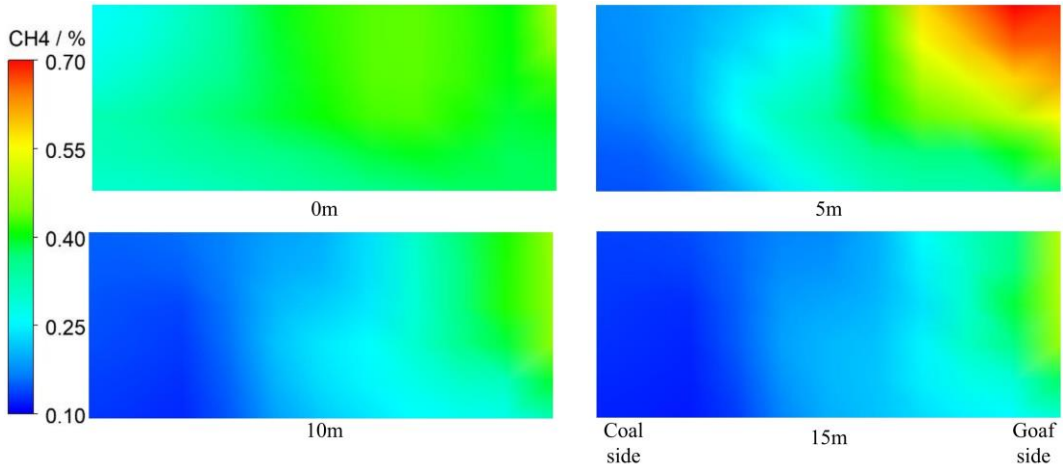

(b) Methane distribution at different cross sections

Figure 7.23 Methane distribution along the LW face at Stage 5

7.3.1.6 Stage 6-Pulling all supports off the face and sealing off the MG corner

At this stage, the machine doors in the LW chute road 2 are closed once all shields have been removed from the LW face. A substantial stopping and tight seal are built in MG belt road inbye of CT10 and at CT11 on the MG side, respectively. The TG regulators that are installed in the TG travel road at the immediate outbye of CT8 are closed. In addition, the nitrogen injection through CT12 at the MG of the goaf is stopped, and the pumping location is moved from CT12 to CT11 once the seal construction at CT11 is completed. The pipeline is run from CT10 on the MG side

to the LW chute road 1 and road 2 through doors for the purpose of nitrogen injection. The nitrogen injection flow rates at CT11 (MG), the LW chute road1 and road2 are 0.25, 0.125 and 0.125 m^3/s, respectively.

Figure 7.24 demonstrates oxygen concentration in the LW panel. It was noted that nitrogen injection through CT11(MG), LW chute road 1 and road 2 yielded an inferior result in sealing the LW panel. Air leakage was noticeable at the rear cut-throughs at the MG of the goaf. The oxidation zone area in the deep goaf was enlarged compared to stage 5 as the majority of nitrogen pumped would directly flow towards the return side, leading to low oxygen levels at the goaf stream. However, the oxygen volume fraction at the TG corner still exceeded 5%. Spontaneous heating could potentially occur at the deep goaf and the TG corner where oxygen levels were higher than 5%, demonstrating an unsatisfactory LW sealing performance. Therefore, this nitrogen pumping plan was required to be optimized to achieve a better LW sealing purpose.

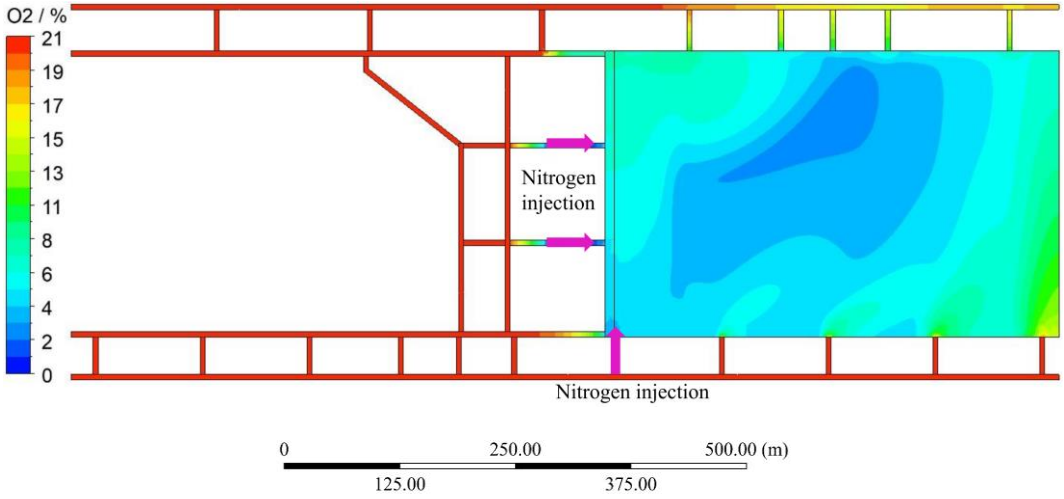

Figure 7.24 Oxygen concentration at 2 m above the coal seam floor at stage 6

7.3.2 Optimization of the panel sealing strategies at stage 6

7.3.2.1 Different injection locations

It has been seen that if nitrogen injection was performed at the TG of the LW goaf at a close distance from the face, then nitrogen would directly flow towards the return and would not effectively deplete oxygen levels and thus resulting in unsatisfactory LW sealing. Thus, nitrogen should be considered to be pumped via cut-throughs at the MG of the LW goaf, in this case at a total rate of 0.5 m^3/s. Two plans were proposed and studied, with results depicted in Figure 7.25.

It was evident from Figure 7.25(a) that high-level oxygen mainly existed in the deep goaf with nitrogen pumped through CT11 at the MG of LW goaf, and high-concentration oxygen was sourced from air leakage from insufficiently-erected seals in the cut-throughs. In addition, oxygen levels at the TG corner were less than 5%. When nitrogen was pumped through CT12 at the MG of the LW goaf, oxygen levels in most of the goaf area were below 5% except at areas in the

vicinity of the cut-throughs at the MG of the goaf. The oxidation zone area for nitrogen injection through CT11(MG)-LW chute road1-road2, solo CT11(MG) and solo CT12(MG) was 76412, 31812 and 3313 m^2, respectively. Nitrogen injection through CT12 at the MG of the goaf performed better than the proposed plans, however there was still a small coal oxidation zone area in the active goaf. Consequently, LW sealing strategies needed to be optimized further.

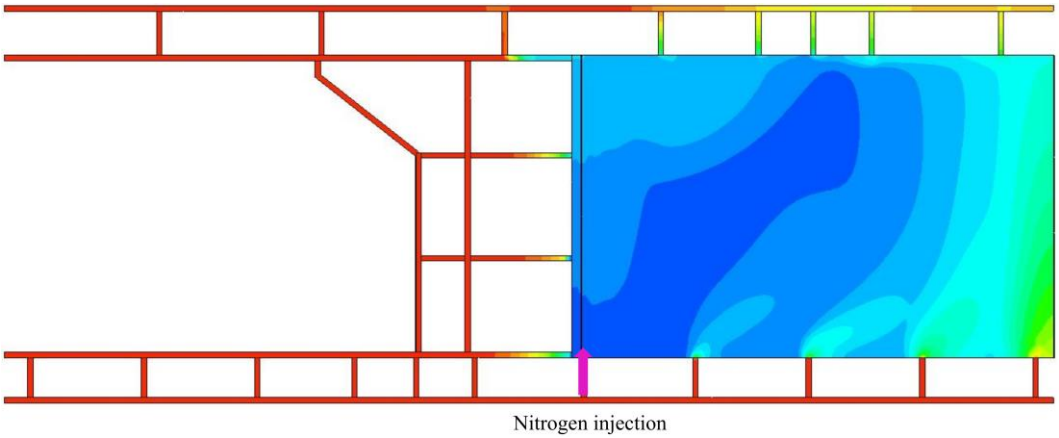

(a) Nitrogen injection through CT11-MG @ 0.5 m^3/s

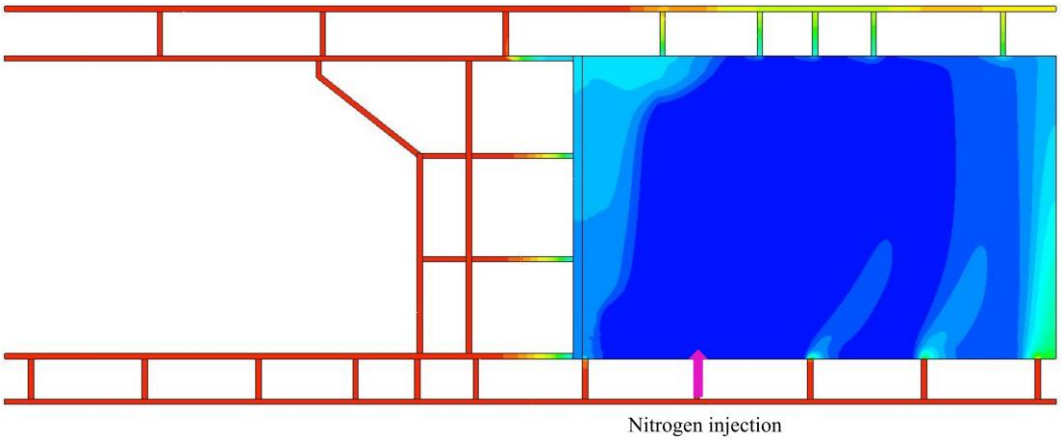

(b) Nitrogen injection through CT12-MG @ 0.5 m^3/s

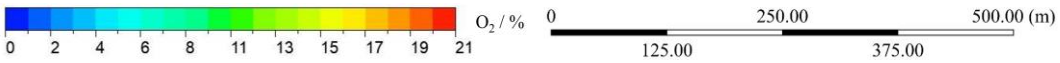

Figure 7.25 Oxygen distribution in the LW panel with different injection locations

7.3.2.2 Sealing-off partial MG travel road

Considering noticeable air leakage via cut-throughs at the MG of the LW panel and continuous fresh air flowing from the back of the MG travel road towards the LW face, a strategy was proposed and simulated with the rear part of the MG travel road being sealed off to reduce the pressure differential between the inner LW goaf and the MG travel road, with results presented in Figure 7.26. It was obvious that an improved LW sealing-off performance was achieved, as oxygen levels in the deep goaf were below 5%. However, there was still a small area close to the TG corner where oxygen levels exceeded 5%, which was potentially conducive to spontaneous heating.

Therefore, LW sealing plans required modification to deplete oxygen levels at the localized TG corner.

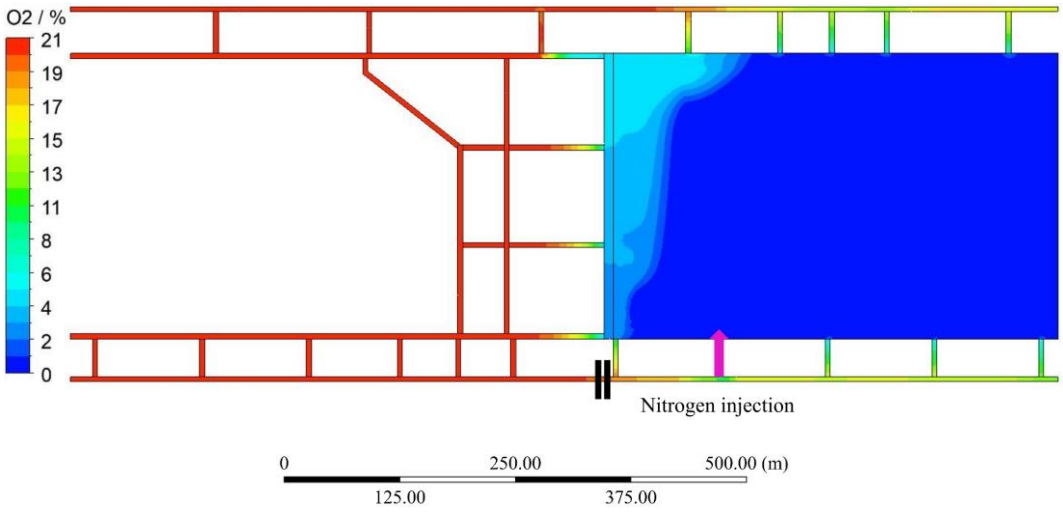

Figure 7.26 Oxygen distribution in the LW panel with nitrogen pumped through CT12-MG and MG travel road being sealed-off

7.3.2.3 Nitrogen injection rates

The influence of nitrogen pumping rates on oxygen distribution in the LW panel was further evaluated with nitrogen being pumped through CT12 at the MG of the travel road. Two different scenarios of sealing-off or keeping the MG travel road were studied, with results illustrated in Figure 7.27 and Figure 7.28, respectively. It was evident in Figure 7.27 that when nitrogen was pumped through CT12 at a flow rate of 0.75 m^3/s and the rear part of the MG travel road was sealed-off, oxygen levels within the active goaf and on the LW face both decreased below 5%, which significantly reduced the probability of spontaneous heating and gas explosion and effectively achieved the desired LW sealing performance.

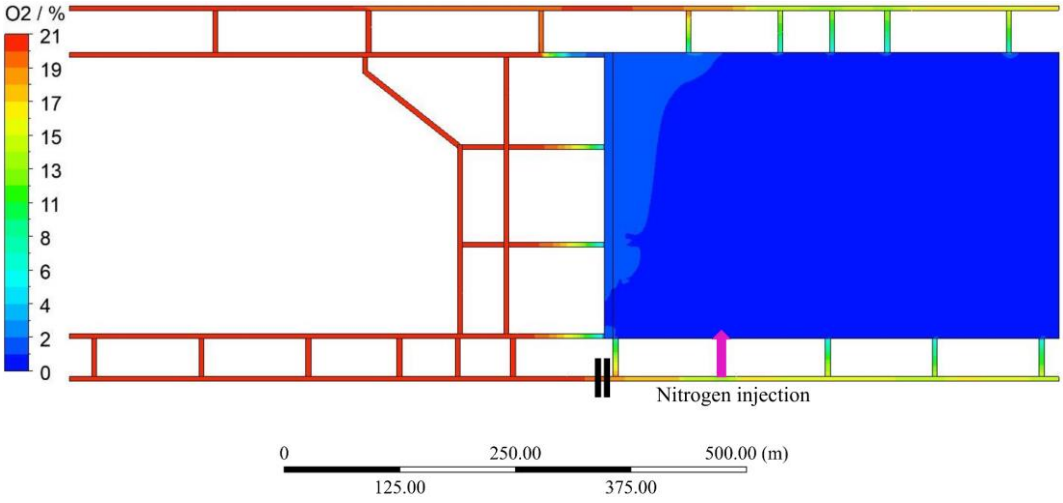

Figure 7.27 Oxygen distribution in the LW panel with nitrogen pumped through CT12-MG at a rate of 0.75 m^3/s and MG travel road being sealed-off

For scenarios where the MG travel road served as an intake gateroad, it was shown from Figure 7.28 that as the flow rates rose, oxygen levels in the vicinity of the rear cut-throughs at the MG of the active goaf decreased, and oxygen concentration remained below 5% along with the TG of the active goaf. When the flow rate reached 1.75 m^3/s, the oxygen volume fraction on the LW face and within the active goaf was less than 5%, under which condition the risk of spontaneous combustion and gas explosion in the active goaf area was minimized and a satisfactory panel seal-off result was achieved.

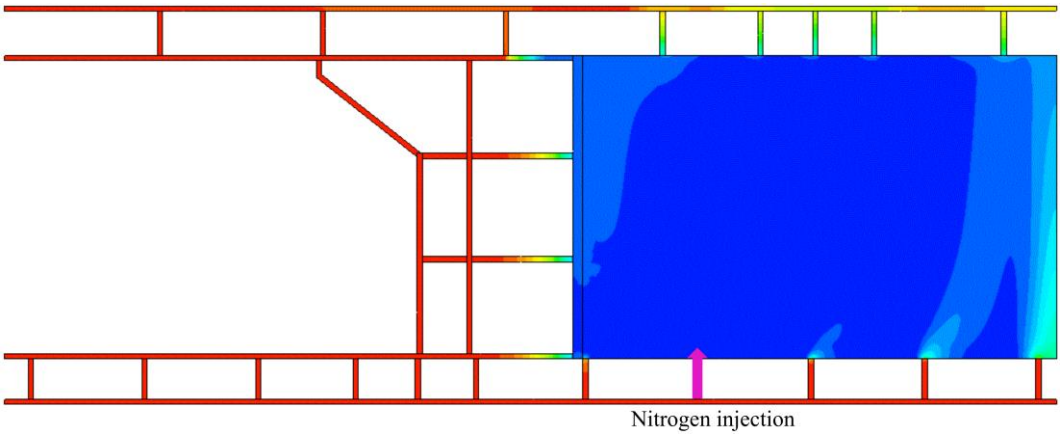

(a) Nitrogen injection through CT12-MG @ 0.75 m^3/s

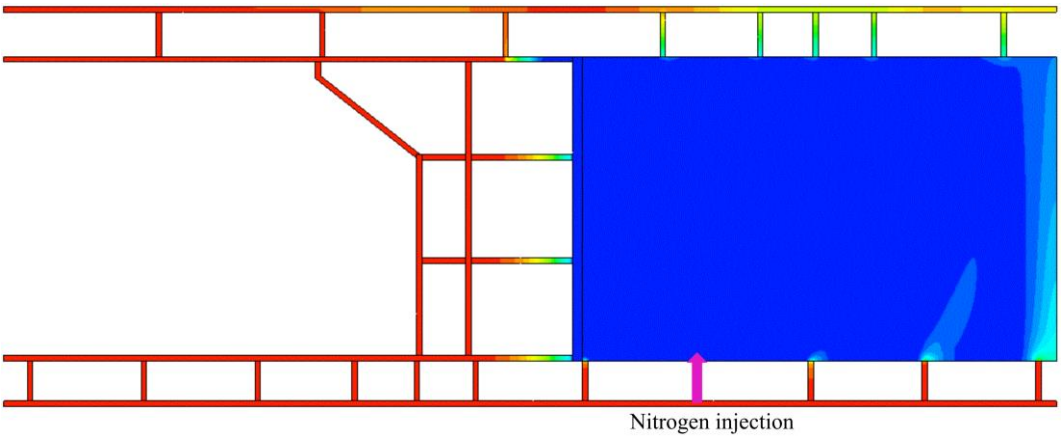

(b) Nitrogen injection through CT12-MG @ 1.0 m^3/s

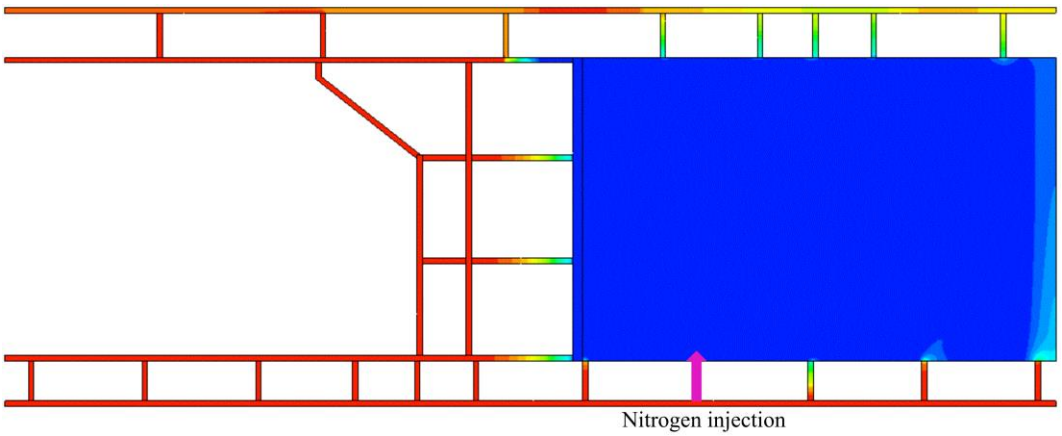

(c) Nitrogen injection through CT12-MG @ 1.25 m^3/s

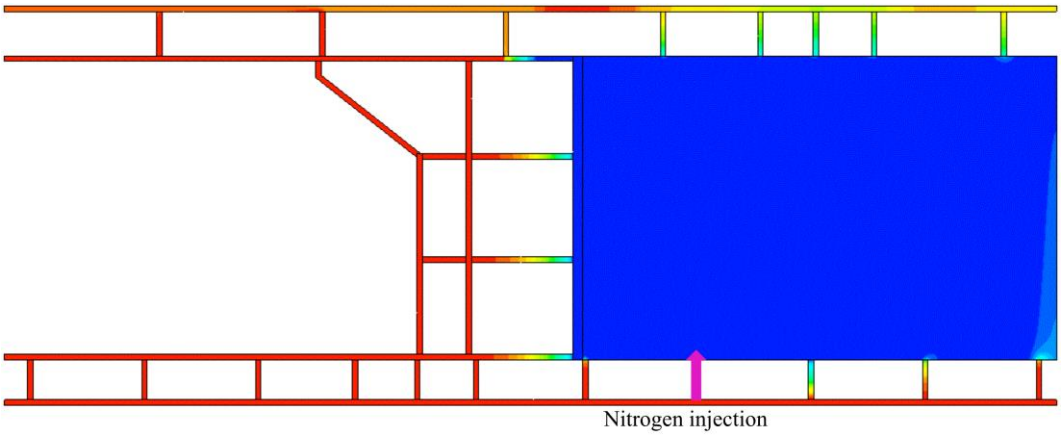

(d) Nitrogen injection through CT12-MG @ 1.5 m^3/s

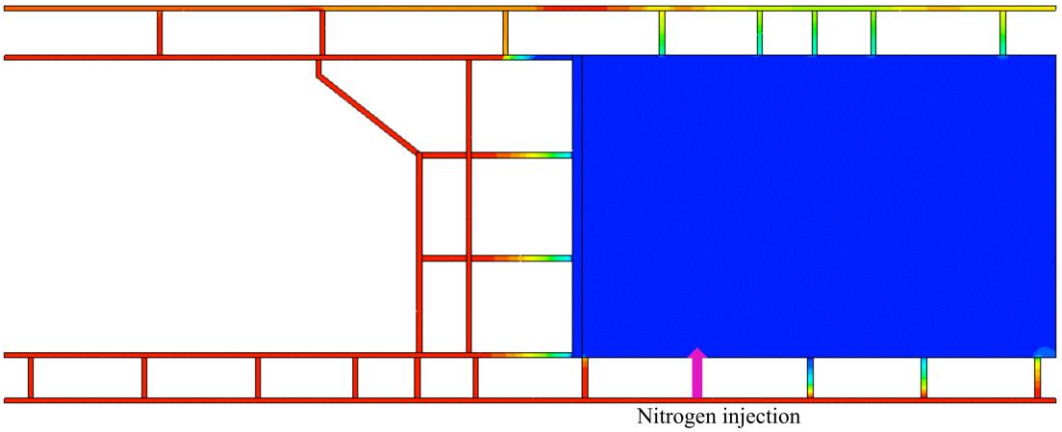

(e) Nitrogen injection through CT12-MG @ 1.75 m^3/s

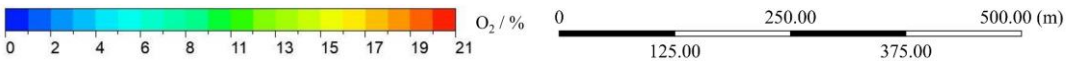

Figure 7.28 Oxygen distribution in the LW panel with different nitrogen pumping rates and keeping the MG travel road

To summarise, two different plans were feasible to achieve the desirable LW sealing-off performance. The first option was to seal off the rear part of the MG travel road and simultaneously pump nitrogen through CT12 at the MG of the active goaf with a flow rate of 0.75 m^3/s, while the second choice was to keep the rear part of the MG travel road as an intake gateroad and simultaneously pumped nitrogen through CT12 at the MG of the goaf with a flow rate of 1.75 m^3/s. From the perspective of economics and practicability, the first option is superior to the second choice in rendering the atmosphere in the LW panel inert, as the first option requires low nitrogen injection rates and is easier to set up.

For the first choice, methane distribution in the LW panel is given in Figure 7.29. It was evident that methane emitted from the active goaf could flow onto the LW face, with methane levels exceeding 2% on the LW face. Thus, four sensors should be employed and installed at the MG belt road inbye of CT10, LW chute road 1 and road 2, and TG travel road inbye of CT8 to monitor

methane concentration in real time. In addition, two more sensors should be located in the TG belt road inbye of CT8 and MG travel road outbye of CT11 to monitor methane levels.

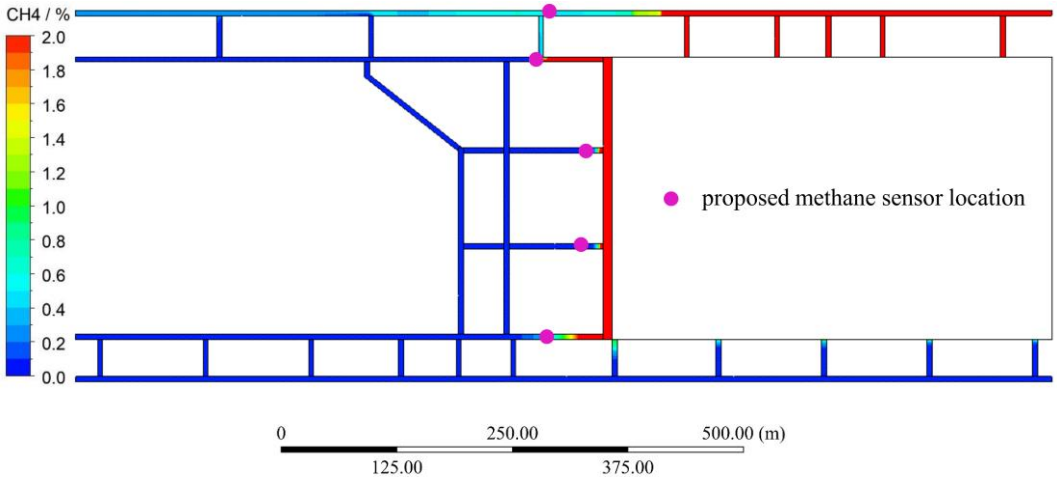

Figure 7.29 Methane concentration at 2 m above the coal seam floor and proposed sensor locations

7.4 Conclusions

Previous studies and field observation indicated that the risk of spontaneous heating and gas explosion significantly increased when the LW face advanced slowly or even stopped. When the LW face approaches the finish-off line, the LW equipment is required to relocate to the new installation face, and the ventilation dynamics and goaf gas atmosphere change, posing significant challenges to spontaneous heating and gas explosion management. To prevent these dynamics hazards potentially from arising during the panel sealing-off process, a detailed understanding of ventilation and goaf gas behaviour in the LW goaf is essential to identify appropriate gas monitoring locations and improve the panel sealing-off process design. On the basis of the geologic and mining conditions of an Australian underground coal mine in Queensland, two three-dimensional CFD models were developed, and boundary conditions were defined in Fluent. To calibrate the computational model, field gas monitoring data was collected from the Tube Bundle system where simulation results correlated well with monitoring data, indicating the model was able to simulate other scenarios with high confidence. Extensive simulations were performed to better understand the behaviour of ventilation dynamics in the LW panel at different stages of the LW sealing-off process, and major conclusions are listed below:

(1) The LW sealing-off process was divided into six different stages and studied from face coming into the finish-off position to sealing-off with the following sequences: face coming into the finish-off line, face bolt up after production stop, pulling hydraulic supports from the TG to the LW chute road 1, from the LW chute road 1 to road 2, from LW chute road 2 to the MG, and all supports pulled off the face and the MG corner sealing-off.

(2) At different stages of the LW sealing-off process, ventilation flow dynamics and goaf gas atmosphere in the LW goaf were obtained, and the ventilation arrangements were evaluated. Results showed that: (i) at the first five stages, oxygen concentration along the TG travel road was below 5% at 200 m behind the LW face, while oxygen levels along the MG belt road were below 5% at 50 m behind the LW face except at the rear cut-throughs where oxygen spikes were noticed, which indicated that the ventilation arrangements were acceptable for the face recovery; (ii) At the sixth stage of the LW sealing-off process, the proposed ventilation arrangement was unsatisfactory in considerably reducing the likelihood of spontaneous combustion and gas explosion due to a relatively-high-oxygen goaf environment conducive to coal oxidation and self-heating in the active goaf.

(3) The final sealing-off operation at the sixth stage was optimized from the perspective of practicability and operational cost, and the effective gas sensor positions were identified. The results indicated that: (i) when nitrogen was pumped through CT12 at a flow rate of 0.75 m^3/s and the rear part of the MG travel road was sealed off, oxygen levels within the active goaf and on the LW face both decreased below 5%, producing the desired LW sealing-off performance; (ii) To effectively and timely monitor goaf atmosphere and evaluate the panel sealing-off performance, at least six gas sensors should be employed and located at the MG belt road inbye of CT10, LW chute road 1 and road 2, TG travel road inbye of CT8, TG belt road inbye of CT8 and MG travel road outbye of CT11, respectively.

This computational modelling study allows for enhanced insight into ventilation dynamics and goaf gas atmosphere variation and the evaluation of the ventilation arrangement at each stage of the LW sealing-off process. In addition, this study also provides much-needed knowledge of developing effective proactive inertisation plans and appropriately positioning the gas monitoring sensors to reliably reflect the goaf atmosphere change during the panel sealing-off process, thus minimizing the risk of spontaneous heating and gas explosion with much-improved mine safety.

CHAPTER 8 DISPERSION AND MIGRATION CHARACTERISTICS OF RESPIRABLE DUST IN DEVELOPMENT PANELS

Summary

This chapter considers the current gaps in the literature related to the understanding of airflow migration and dust dispersion characteristics within a continuous-miner-driven heading under an auxiliary exhausting ventilation system, as is commonly used in the Australian coal mine industry. Based on site-specific conditions of a development heading in an underground coal mine in New South Wales, a three-dimensional CFD model incorporating a continuous miner, shuttle car and exhausting ventilation tube was built and validated with field dust measuring data, where a good agreement was attained. The airflow migration patterns and temporal-spatial dust dispersion characteristics were investigated for three cutting scenarios, namely cutting the middle, floor, and roof positions at the heading face. The dust was produced at four different locations corresponding to site observations and allowing for the complete dust dispersion dynamics to be understood compared to many existing studies which generally focus on dust released from the face. Based on the validated model, a study was conducted on the effectiveness of common dust mitigation strategies, including variation in airflow rates through the exhausting ventilation tube, the distance between tube inlet and heading face as well as on-board ventilation. The results from extensive simulations can assist in improving the knowledge of airflow migration patterns and dust dispersion characteristics in a continuous-miner-driven development heading under the exhausting ventilation system and provide some guidance on dust mitigation and operator protection strategies, thus improving the health and safety of miners and creating a cleaner underground working environment during the tunnelling process.

Citation

This paper has been submitted to **Tunnelling Underground and Space Technology** and is currently under review.

Abstract

Underground miners in Australia are facing increasing threats from dust-related diseases. To address these issues, improved knowledge of airflow patterns and respirable dust dispersion characteristics within a continuous-miner-driven heading under an exhausting ventilation system is required. Based on site-specific conditions of a development heading in New South Wales, a three-dimensional Computational Fluid Dynamics (CFD) model was constructed and validated with onsite dust monitoring data, where a good agreement was achieved. Three scenarios of coal cutting at the middle, floor and roof positions were considered and simulated, with dust generated at four different sources. The simulation results indicated that left-hand-side (LHS) operators should be equipped with fit-for-purpose personal protective equipment and stay behind the ventilation duct inlet during coal cutting process, while miners standing at the right-hand-side (RHS) of the continuous miner for roof and rib bolting and machine operating should stay immediately behind the roof and rib bolting rig where dust concentration was relatively low. In addition, an increase in airflow rate through the exhausting ventilation duct or a reduction in the distance from the duct inlet to the heading face assisted in reducing dust levels within the heading, particularly at the LHS of the continuous miners. Finally, compared to the scenario of the current ventilation scheme, an on-board exhausting ventilation system could improve dust removal performance, with dust concentration at the breathing level reducing by approximately 43.6%. This modelling study can advance the understanding of dust diffusion characteristics from different sources in the heading face and provide guidance on dust mitigation, thus improving the health and safety of miners and creating a cleaner underground working environment.

Keywords

Airflow migration patterns; Dust dispersion characteristics; Multi-source respirable dust; Exhausting ventilation system; CFD modelling; Dust mitigation strategies

8.1 Introduction

As considerable coal resources are exploited annually, a substantial amount of coal and silica dust is generated by mining-related activities, including cutting, drilling, crushing, loading and transporting, which has re-emerged as a serious health threat to the mine workers. Longwall faces and development panels are two major dust-producing areas in underground coal mines. Prolonged exposure to the underground working environment where high levels of respirable and inhalable dust exist can pose significant threats to the health of coal mine workers, potentially causing them to develop irreversible, life-threatening respiratory diseases, such as coal workers' pneumoconiosis (CWP), silicosis, mixed dust pneumoconiosis, chronic obstructive pulmonary diseases, occupational asthma, bronchitis symptoms, and even progressive massive fibrosis (PMF) which is

regarded as the most severe form of CWP (Baur et al. 2019; Joy et al. 2012; McBean et al. 2018; Ren et al. 2018b; Wang et al. 2020; Wang & Ren 2013). As a result of improvements implemented to adhere to legislative requirements such as technological advances in dust management and control, better personal protective equipment (PPE) available for coal workers, and routine medical surveillance and screening, it had been approximately 30 years since a case of miners diagnosed with CWP had been formally reported in Australia (Coal Workers' Pneumoconiosis Select Committee 2017; Zosky et al. 2016). However, in May 2015 this changed when the first CWP case re-emerged in Queensland ((Parliament of Australia 2016; Queensland Audit Office 2019). In the following approximate 5-year period, a total of 207 miners employed in a mining or mining-related industry in Queensland were identified as victims of mine dust lung diseases by 31 March 2021, among which 50, 46 and 27 workers were diagnosed with CWP, silicosis and mixed pneumoconiosis, respectively (Queensland Government 2021). It is noted from Figure 8.1 that CWP cases identified annually remained at 6~7 in the recent 5 years in Queensland except in 2017 when 14 employees working in the mining industry contracted CWP. In NSW, it was reported that 8 male workers employed in the mining industry were diagnosed with either CWP or silicosis from December 2016 to May 2020, while another two cases of interstitial lung disease and pneumoconiosis were under investigation at the time of reporting (NSW Government 2021).

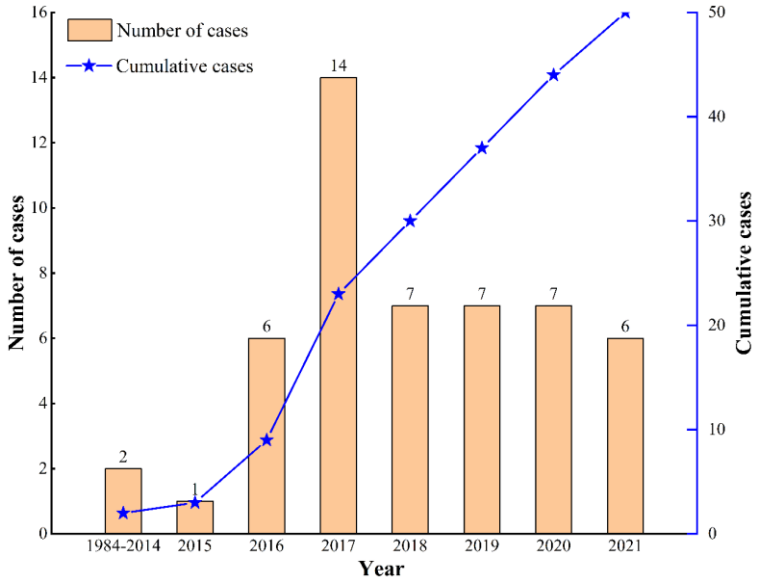

Figure 8.1 Case of CWP in Queensland since 1984 (Queensland Government 2021)

In order to improve the health and safety of coal workers and create a cleaner underground working environment, strict regulations on dust exposure are enforced by the different states in Australia. The new workplace exposure standards for respirable coal dust (1.5 mg/m^3) and respirable crystalline silica (0.05 mg/m^3) took effect in NSW on 1 February 2021 and 1 July 2020, respectively (NSW Government 2020). From 1 September 2020, the statutory occupational

exposure limits for respirable coal and crystalline silica dust are 1.5 and 0.05 mg/m^3, respectively, for Queensland (Queensland Government 2020). According to an annual report released by Coal Services (2020), the average exposure for respirable dust, respirable quartz, and inhalable dust was all below the statutory workplace exposure standard of 2.5 mg/m^3, 0.1 mg/m^3, and 10 mg/m^3 respectively. However, in spite of the tremendous effort put into controlling dust concentration below the legislative standard, there are still a significant number of occurrences where airborne dust sampled in the required workplace exceeded the workplace exposure standard (Coal Services 2020), as depicted in Figure 8.2. It is noted that the exceedances of dust exposure limits generally showed a downward trend in recent years, but the exceedance rates for respirable quartz were still as high as 1.9% in 2020. Respirable coal dust and quartz (diameter smaller than 5 microns) are more harmful than inhalable dust (diameter smaller than 100 microns) as they are invisible and can be retained in the deepest regions of the lungs (Australian Institute of Occupational Hygienists 2014). As a result, improved knowledge of dust dispersion and migration characteristics in the primary dust-generating activities of a coal mine is important for identifying the reasons for the dust exceedances continuing to be recorded and improving mitigation and control practices.

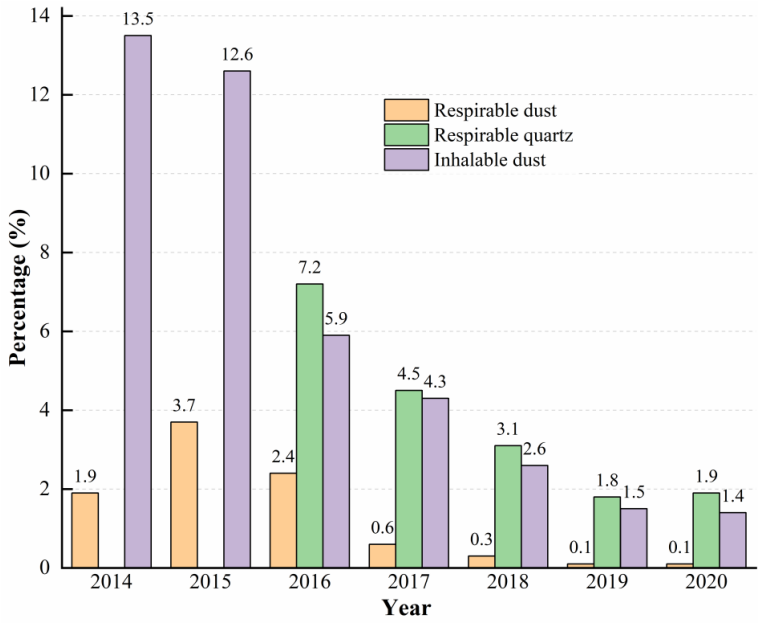

Figure 8.2 The percentage of sampling dust exceeding the statutory exposure standard (Coal Services 2020)

Tunnelling machines employed in excavating underground tunnels or heading faces are mainly classified into two types: roadheaders and continuous miners (CM). The cutting process and gateroad dimensions differ significantly for these two tunnelling methods; accordingly, airflow patterns and dust migration characteristics within the heading vary considerably. Parra et al. (2006) numerically analyzed the impact of ventilation schemes on airflow fields and methane distribution in the gallery, which provided guidance on ventilation design. CFD modelling was performed by Wang et al. (2015) to evaluate the impacts of dust injection rates, forcing air velocity from the

duct, and different ventilation schemes on dust distribution in the laneway, where an Euler model was utilized to simulate dust trajectory. An attempt was made by Li et al. (2016) to investigate dust, oxygen and temperature distribution patterns in an underground development with a large cross-section area, and it was concluded that an air velocity of 0.15 m/s was adequate to manage dust levels and supply necessary oxygen. Geng et al. (2017) numerically investigated the dust behaviour in a simplified roadway under different ventilation systems, and the simulation results indicated that dust of different sizes presented different dispersion characteristics. An effort was made by Wang et al. (2017b) to understand the distribution characteristics of spray droplets in the heading, and the optimum spray pressure of 2.4 MPa was determined for effective dust mitigation. Although these studies have made a good contribution to the understanding of ventilation and dust dispersion dynamics in underground development panels, none of them included the relevant mining machines or materials handling equipment; this limits the accuracy of these studies when considering them against the very strict regulator requirements that need to be met through the understanding of dust dispersion and mitigation mechanisms that these studies aim to assist.

In order to obtain more realistic results, many scholars incorporated a complicated roadheader model into their heading models for dust-related problems. Toraño et al. (2011) studied the airflow streamlines and dust dispersion patterns under two different ventilation systems (the forcing ventilation tube was hung from the roof, and simultaneously the exhausting tube was hung from the roof or placed on the floor) and validated the models using onsite measured data. Using the CFD-DEM coupling method, Cheng et al. (2016b) investigated the relationship between dust diffusion distance and time and the trajectories of dust with different sizes in a heading with single forcing ventilation, which guided the design of dust prevention strategies. Shi et al. (2017) numerically optimized the air duct location in the heading under different ventilation schemes (e.g., single forcing ventilation, forcing and exhausting ventilation with the exhausting ventilation tube positioned at the middle of the heading or the opposite side of the forcing tube), where the dust control efficiency could reach approximately 75.88%. Focusing on the heading face ventilated by one forcing and one exhausting tube, Wang et al. (2017a), Yu et al. (2017a), Liu et al. (2019b), and Hua et al. (2020a) studied the airflow patterns and dispersion characteristics in the heading face where an air-curtain generator was mounted on the forcing duct, and the optimal working parameters were determined for best dedusting performance. Attention was paid by Hu et al. (2019) to improving the knowledge of dust sources at the location of the roadheader driver in a heading using a single forcing ventilation method, and it was suggested that countermeasures should be taken to mitigate dust that migrated from the back of the driver. Guo et al. (2020b) studied the temporal-spatial distribution characteristics of dust in a roadheader-tunnelled heading under single forcing ventilation, and the optimal duct airflow rate was obtained by evaluating dust mitigation

performance. Cai et al. (2021) numerically investigated airflow and dust migration patterns in a heading face with hybrid ventilation (a combination of forcing and exhausting ventilation), and the optimal airflow rate in the exhausting duct and the location of the forcing duct were determined. Dust diffusion characteristics in the forcing-ventilation heading were analyzed by Lu et al. (2022a) under the conditions of nine different cutting positions of roadheader, and the impact of cutting sequences was also evaluated. A modularized airflow diverging system was proposed by Yang et al. (2022a) to effectively control high-concentration dust in a heading with hybrid ventilation, and the optimal working conditions were numerically obtained and validated with experiments.

There are also many scholars who have focused on CFD simulations in the heading faces driven by CM. Hargreaves and Lowndes (2007) conducted numerical simulations to study the impact of the scrubber fan and cutting cycles on airflow patterns in a heading, but the simulation of dust was not considered in their study. A computational model incorporating two ventilation ducts and a CM (JOY 12CM27) was built by Wang et al. (2019) to understand the dispersion characteristics of respirable dust at two different cutting sections within the heading under a forcing ventilation system, and dust removal efficiency was improved by relocating the ventilation duct and utilizing throat venturi and directional sprays. Focusing on dust issues in the CM (12CM-15-10D)-driven heading face under single forcing ventilation, Guo et al. (2020a) optimized the parameters of the spray nozzle installed on the CM to achieve the best dust mitigation performance. A similar study was conducted by Nie et al. (2022c) to optimize the type and layout of spray nozzles on the CM, and the dedusting performance was evaluated in the heading face. However, the ventilation patterns applied in these studies were either forcing or hybrid ventilation (including forcing and exhausting), and only the cutting process was taken into consideration for dust sources.

From the above literature review, there is limited research on dust-airflow migration characteristics in a CM-driven heading under single exhausting ventilation widely used in underground development headings in Australia. Furthermore, existing studies have primarily focused on dust generated at the cutting face, ignoring other important dust sources during the removal and transport of coal from the face into the shuttle car (SC). This study aims to bridge this gap through the development of a validated simulation model based on a site-specific heading layout, and a three-dimensional (3D) CFD model incorporating a CM, SC and exhausting ventilation duct, with boundary conditions defined accordingly to match onsite monitoring data. This is achieved through extensive parametric studies conducted to improve the understanding of dust-airflow migration characteristics in the heading face ventilated by an exhausting auxiliary fan under the conditions of three different cutting positions (including cutting the floor, middle, and roof sections of the heading face). The simulation results will cast light on respirable dust diffusion and

migration characteristics in a CM-driven tunnelling face with an exhausting auxiliary ventilation system and provide guidance on reducing dust concentration in the heading face, particularly at the critical locations around CM drivers and other mine workers.

8.2 Field Investigation

8.2.1 Site-specific conditions

A field study was undertaken in an Australian underground coal mine where the development panels are driven by 12CM30-type CM, and coal is transported outbye of the heading face by a 2011SS-type SC. The layout of the development panels is illustrated in Figure 8.3. The major tunnelling machines are located in the belt road, including CM, SC, Auxiliary exhausting fan and associated ventilation tube, with the specific area marked in an orange rectangle. The fresh air sourced from the travel road passes through cut-through 15 and then diverts in the belt. The width and height of the gateroad are 5.2 and 2.9 m, respectively. The distance between the fan duct and the heading face is 5 m.

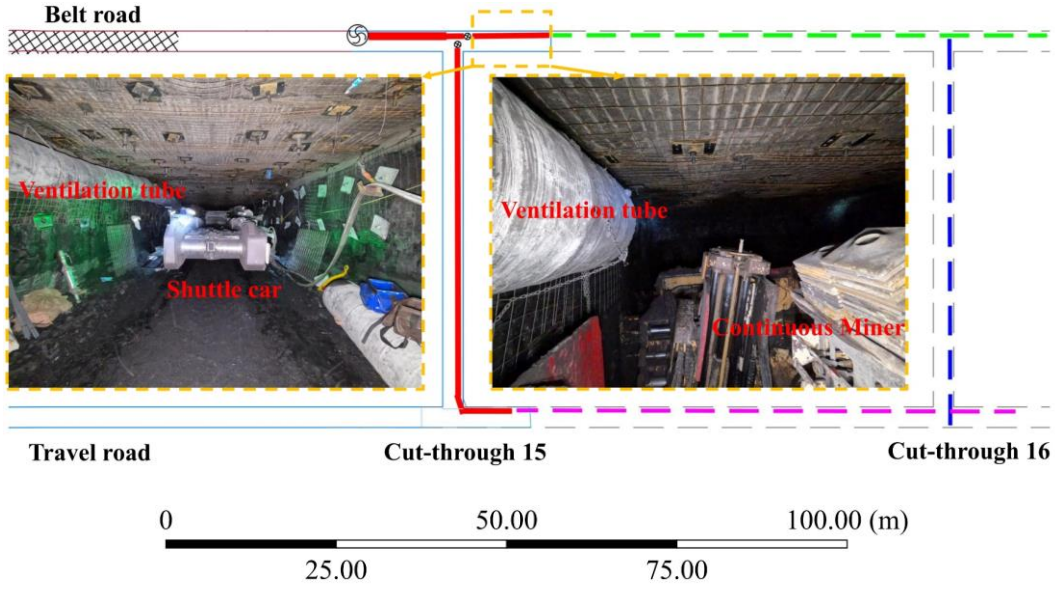

Figure 8.3 The layout of the development panels

8.2.2 Dust monitoring

Dust monitoring at the heading face was carried out in the operational development panels. Two types of real-time dust monitors were used, including the AM520i dust monitor and the PDM3700 dust monitor. AM520i dust monitor is capable of monitoring dust concentration in a real-time manner with 1 s interval and working in a variety of volatile environments. The PDM3700 is a Tapered Element Oscillating Microbalance (TEOM) gravimetric device providing continuous measurement and display of respirable dust exposures giving it significant advantages over other real-time dust monitors based on light scattering techniques, where it can monitor dust concentration in an interval of 1 min. In the process of dust monitoring, six AM520i dust monitors

and four PDM3700 dust monitors were put in the vicinity of CM. To be specific, one AM520i dust monitor was placed at the front left-hand-side (LHS) of CM (No.1) and front right-hand-side (RHS) of CM (No.4), while one AM520i and one PDM3700 dust monitor were positions at the middle LHS (No.2), middle RHS (No.5), rear LHS (No.3) and rear RHS of CM (No.6), as illustrated in Figure 8.4. During the period of dust monitoring, two PDM dust monitors experienced failures due to the warning of temperature out-range. The 1-min average dust monitoring results are listed in Table 8.1.

Table 8.1 1-min average dust monitoring results

Monitoring location	Front RHS	Middle RHS	Rear RHS	Front LHS	Middle LHS	Rear LHS
Dust concentration (mg/m^3)	1.410	9.400	1.267	49.226	13.306	1.001

It is notable that the field studies indicated that the dust concentration based on 1-minute average values at the front LHS, Middle LHS and Middle RHS of CM significantly exceeded the statutory limits of 1.5 mg/m^3 for respirable coal dust in Australia. Of course, these limits are based on full shift averages, though it is still important to consider short-term exposure of mine workers to hazardous dust.

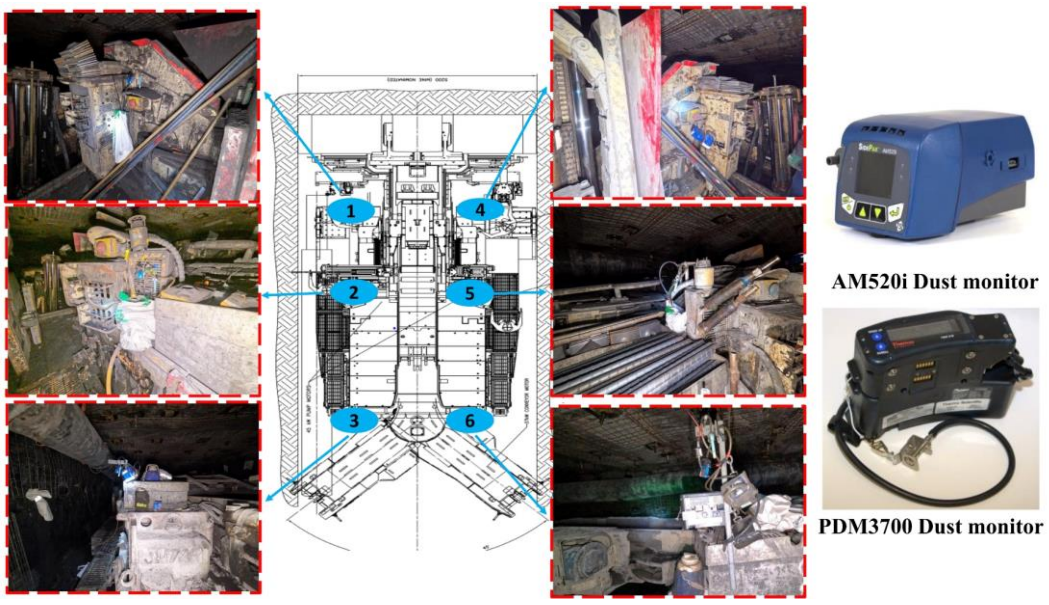

Figure 8.4 Underground dust monitoring

8.3 CFD Modelling

8.3.1 Mathematical model

The movement of airflow and dust within the heading face complies with conservation equations of mass and momentum and gas-solid two-phase flow theory. Given that the volume fraction of respirable dust particles within the CM-tunnelled development headings is less than 10%, the

Euler-Lagrange approach is more appropriate than Euler-Euler for an investigation into the motion of dust (Ren et al. 2018b; Zhang et al. 2022). Regarding the Euler-Lagrange approach, dust particles are regarded as a discrete phase, while airflow is treated as a continuous phase. The realizable k-ε turbulence model was applied to reflect the airflow characteristics within the heading face.

The mass and momentum conservation equations can be obtained by using equations 6-1, 6-2 and 6-3, while the transport of flow can be calculated by using the following equations:(ANSYS 2022a):

$$\frac{\partial}{\partial t}(\rho k)+\frac{\partial}{\partial x_i}(\rho k\vec{u})=\frac{\partial}{\partial x_i}\left[\left(\mu+\frac{\mu_t}{\sigma_k}\right)\frac{\partial k}{\partial x_i}\right]+G_k+G_b-\rho\varepsilon-Y_M+S_k \quad (8-1)$$

$$\frac{\partial}{\partial t}(\rho\varepsilon)+\frac{\partial}{\partial x_i}(\rho\varepsilon\vec{u})=\frac{\partial}{\partial x_i}\left[\left(\mu+\frac{\mu_t}{\sigma_\varepsilon}\right)\frac{\partial \varepsilon}{\partial x_i}\right]+\rho C_1 S\varepsilon-\rho C_2\frac{\varepsilon^2}{k+\sqrt{v\varepsilon}}+C_{1\varepsilon}\frac{\varepsilon}{k}C_{3\varepsilon}G_b+S_\varepsilon \quad (8-2)$$

Where k is the turbulent kinetic energy; ε stands for the dissipation rate corresponding to the turbulent kinetic energy; x_i represents the direction component; μ_t denotes the turbulent viscosity; G_k and G_b represent the generation of turbulence kinetic energy due to the mean velocity gradients and buoyancy, respectively; Y_M is the contribution of the fluctuating dilatation in compressible turbulence to the overall dissipation rate; S_k and S_ε represent user-defined source terms; C_2 and $C_{1\varepsilon}$ are constants with a value of 1.9 and 1.44, respectively; σ_k and σ_ε denote the turbulent Prandtl numbers for k and ε with a constant value of 1.0 and 1.2, respectively.

Regarding the motion of dust particles within the heading, the trajectory of particles can be predicted using the following equations (ANSYS 2022a):

(1) Particle force balance

$$m_p\frac{d\overrightarrow{u_p}}{dt}=m_p\frac{\vec{u}-\overrightarrow{u_p}}{\tau_r}+m_p\frac{\vec{g}(\rho_p-\rho)}{\rho_p}+\vec{F} \quad (8-3)$$

Where: m_p denotes the particle mass; $\vec{u}$ and $\overrightarrow{u_p}$ represent the velocity of fluid and particle, respectively; ρ_p and ρ are the density of particle and fluid, respectively; $\vec{F}$ stands for the additional force. Particularly, $m_p\frac{\vec{u}-\overrightarrow{u_p}}{\tau_r}$ denotes the drag force, and τ_r represents the particle relaxation time calculated by equation (7):

$$\tau_r=\frac{\rho_p d_p^2}{18\mu}\frac{24}{C_d Re} \quad (8-4)$$

Where: μ denotes the fluid molecular viscosity; d_p represents the particle diameter; Re stands for the relative Reynolds number.

(2) Stochastic tracking

$$u = \vec{u} + u' \tag{8-5}$$

Where: u stands for the instantaneous value of the fluctuating gas flow velocity, $\vec{u}$ denotes the mean fluid phase velocity; u' represents fluctuating velocities with the fluctuating components;

The trajectories of dust particles within the development heading are predicted using the mean fluid phase velocity under the condition of turbulent flow, while the dispersion of dust particles resulting from turbulence can be predicted using the instantaneous value of the fluctuating gas flow velocity.

(3) Discrete random walk model

$$u' = \zeta\sqrt{\overline{u'^2}} = \zeta\sqrt{\overline{uv'^2}} = \zeta\sqrt{\overline{u'^2}} = \sqrt{\frac{2k}{3}} \tag{8-6}$$

Where: ζ denotes a normally distributed random number; u, v and w are the velocity component in x, y and z direction, respectively; k is the turbulent kinetic energy.

8.3.2 Computational model

8.3.2.1 Model construction

The T-junction layout of the development heading is shown in Figure 8.5. The fresh air marked with a blue arrow is provided via a cut-through connecting with the travel road and the belt road, while the dirty air marked with a red arrow is returned to the belt road. Exhausting auxiliary ventilation is applied to significantly reduce dust levels at the development heading. The green arrows denote the X and Y direction centred on the origin of the model. Z-direction starts from the floor of the development heading.

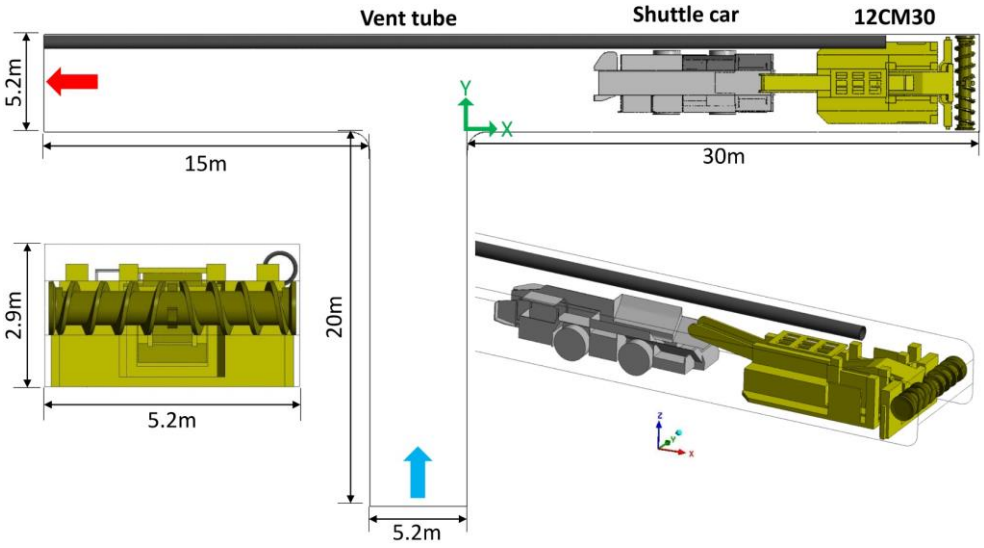

Figure 8.5 Layout of development heading

Based on the information collected during the field study, a 3D computational model that incorporates CM and SC was built using DesignModeler and Autodesk Inventor, after which the model was imported into Fluent Meshing to mesh the numerical model. Compared to the tetrahedral meshing method, it has previously been found that polyhedral and hexahedral meshing methods provide a significant reduction in computing expense, however hexahedral meshing can cause convergence issues with the discrete phase model in ANSYS Fluent (Roberts et al. 2022). As a result, the polyhedral meshing method was applied in this study, as shown in Figure 8.6. It was observed from the field study that dust was mainly distributed around the CM under an exhausting auxiliary ventilation system. Given the tiny size of respirable dust particles compared to the heading domain, the area in the vicinity of CM was divided into three different zones and refined with progressively smaller mesh sizes. Specifically, the area extending 10.5 m from the heading face was equally divided into three different parts with an element size of 0.035, 0.05 and 0.075 m, respectively.

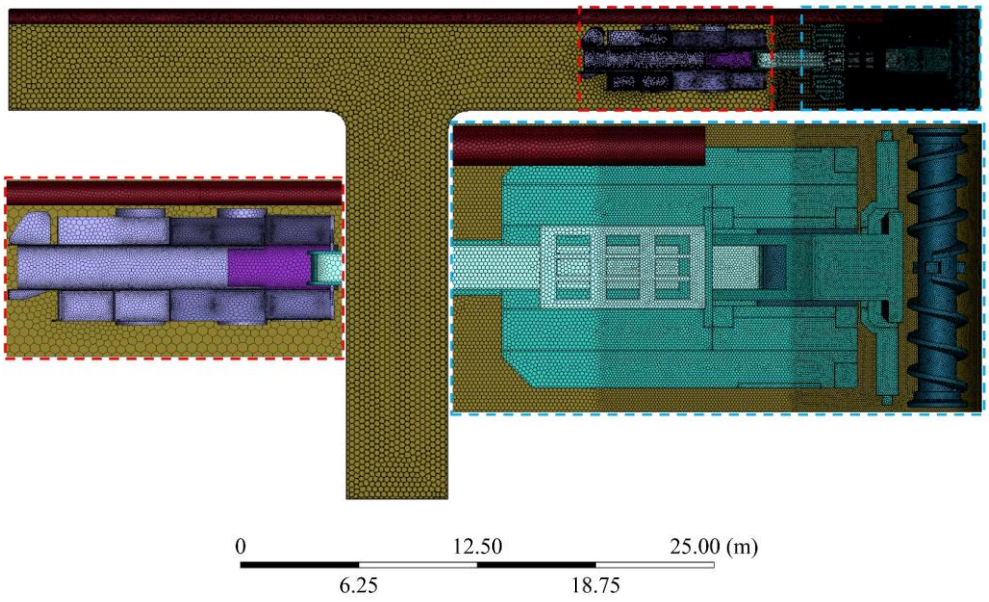

Figure 8.6 Meshed model

In order to avoid the influence of mesh size on simulation results, a mesh independence study was conducted, as detailed in Table 8.2. At the height of 2.6 m, three monitoring lines were set in the model, and the simulation results are shown in Figure 8.7. It is evident that only a marginal difference in velocity distribution between the medium-mesh and fine-mesh model occurs. Therefore, the medium-mesh model was utilized for all further simulations. According to the mesh quality standard released by ANSYS (2022b), the quality of the mesh is classified into unacceptable, bad, acceptable, good, very good and excellent levels, with orthogonal quality ranging from 0~0.001, 0.001~0.14, 0.14~0.20, 0.20~0.69, 0.70~0.95, 0.95~1.00. As shown in Figure 8.8, the minimum orthogonal quality of the medium-meshed model was higher than 0.20,

and approximately 79.5% of total elements are categorized as excellent. As a result, the medium-meshed model was capable of simulating airflow-dust migrations within the development heading with high accuracy.

Table 8.2 Parameters for the mesh independence study

	Cell size (m)			Total elements
	Zone1	Zone2	Zone3	
Coarse mesh	0.060	0.075	0.090	952947
Medium mesh	0.035	0.050	0.075	2391101
Fine mesh	0.030	0.045	0.060	3493936

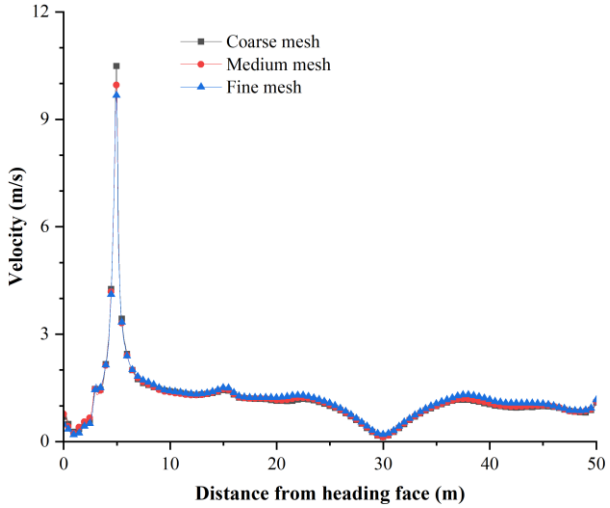

(a) 0.8 m from the left rib (close to tube)

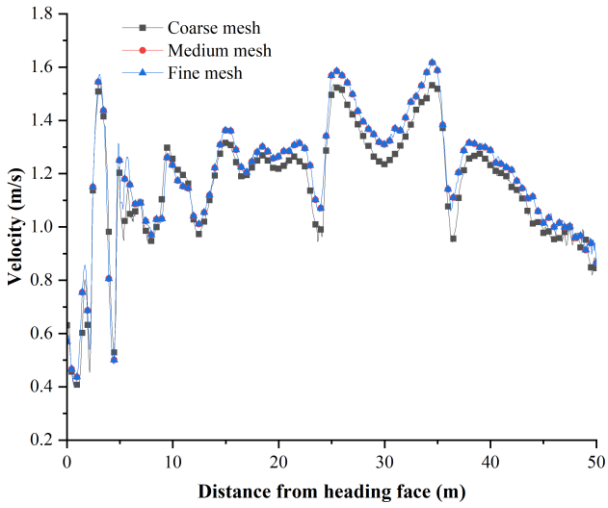

(b) 2.6 m from the left rib (middle position)

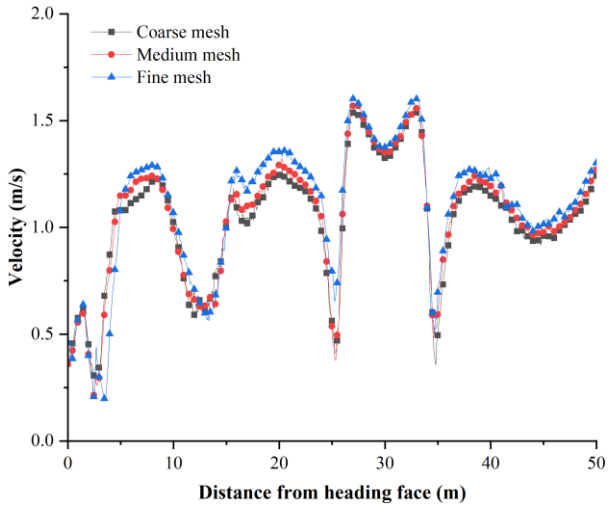

(c) 4.4 m from the left rib (opposite tube)

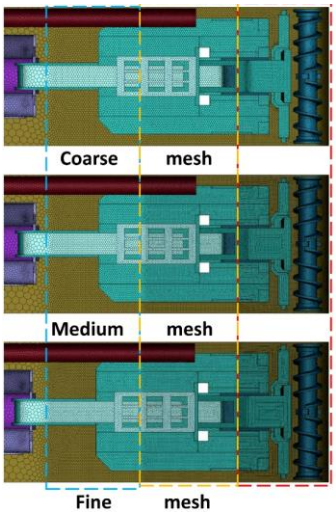

(d) Different meshed models

Figure 8.7 Mesh independence study results

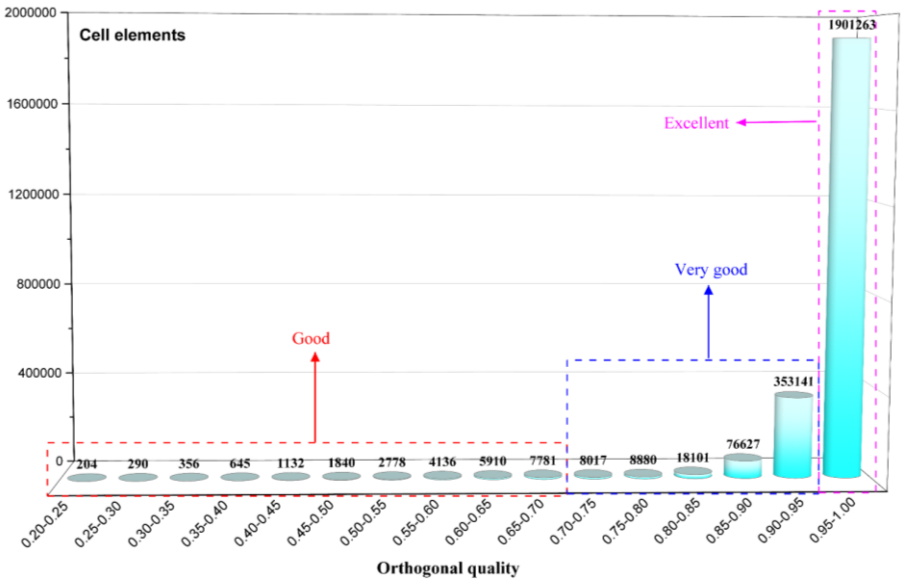

Figure 8.8 Orthogonal quality of medium-meshed model

8.3.2.2 Boundary conditions

Based on the site-specific conditions, boundary conditions were defined and set in Fluent, as listed in Table 8.3. The diameter of dust follows the Rosin-Rammler distribution characteristics, and the minimum, mean, and maximum diameters of dust were 1, 7 and 30 μm, respectively. The dust was produced at four different locations, including the heading face due to coal cutting, the shovel and conveyor belt of CM due to coal transporting, and SC as a result of coal loading, with dust flowrates of 0.0003, 1.5×10^{-5}, 1.0×10^{-5} and 5×10^{-6} kg/s, respectively; these values were determined such that the dust concentration measured on site could be matched. Two-way turbulence coupling was activated to investigate the dust-airflow migration patterns.

Table 8.3 boundary conditions

Name	Type	Value	Name	Type	Value
Solver	Pressure-based	/	Gravity	Z-direction	-9.81 (m/s^2)
Viscous model	Realizable k-ε	/	Inert particle	Coal-hv	1400 (kg/m^3)
Panel inlet	Velocity-inlet	1.6 (m/s)	Panel outlet	Pressure-outlet	/
Fan-duct inlet	Mass-flow-outlet	14.7 (kg/s)	Cutting drum	Rotational wall	4.40 (rad/s)
Conveyor belt	Translational wall	2.44 (m/s)	Solution scheme	Coupled	/

8.3.2.3 Model validation

To calibrate the CFD modelling results, 1-min-average dust concentration was calculated and compared with CFD modelling results, with results shown in Figure 8.9. It is apparent that the error rate between monitoring data and simulation results is lower than 5%. Based on the accuracy of this prediction, it was concluded that the model should be sufficient to simulate other scenarios

with sufficient confidence and high accuracy. The accurate prediction of dust concentration around the entire CM draws light on the importance of including all dust sources in a model such as this. Preliminary studies conducted by the authors focused on the dust released from the cutting face, as is common in literature (particularly with forced flow ventilation systems). However, it was quickly identified this does not correlate well with onsite data. This is an important recommendation for future studies modelling this style of ventilation and dust control in mine headings.

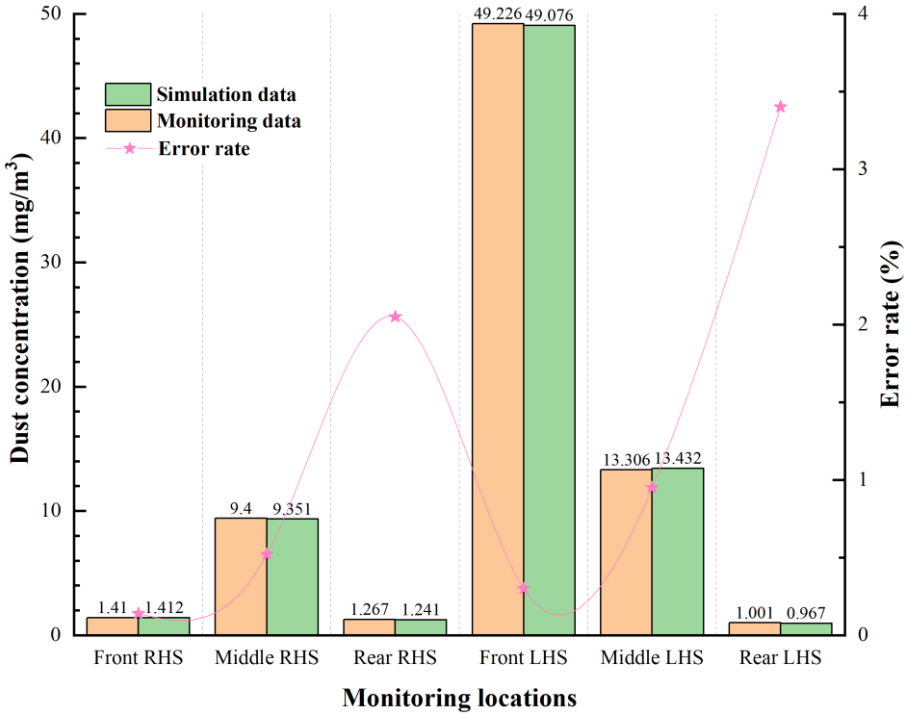

Figure 8.9 CFD model calibration results

8.4 Results and Discussion

8.4.1 Coal cutting at the middle position-base model results

8.4.1.1 Airflow migration patterns

The airflow migration patterns within the development heading are depicted in Figure 8.10. The fresh air sourcing from the travel road uniformly flows to the cut-through and enters into the belt road where the CM and SC are located. The airflow from the cut-through diverges in the belt road, with one stream of air migrating towards the heading face and another stream of air flowing outbye of the heading.

The air flowing towards the heading face is in a turbulent state. Due to the existence of SC and CM and the reduction in the cross-section area, the average air velocity generally increases as air migrates to the heading face. When air approaches the CM, the airflow diverts, as illustrated in Figure 8.10(a). As the CM's drivers stand on the platform of the CM during working and the distance of their breathing zone from the floor is approximately 2.1 m, the breathing level of 2.1

m is determined in this study. Considering the ventilation flow patterns, some streams of air migrate to the LHS of CM and are sucked into the exhausting fan duct due to the negative pressure in the vicinity of the duct outlet. While streams of air flowing to the RHS of CM are shown to be sucked into the fan duct across the top of the miner, or continue towards the heading face with a relatively small velocity and then either circulate around the drum or across the face to the exhausting duct. In the vertical view of the CM centre in Figure 8.10(b), several vortexes marked in black circles can be observed. This occurs due to air migrating along the conveyor belt to either short circuit to the ventilation duct through the gap between the top cover and beam, or create a recirculating pattern around the drum. This air that circulates around the drum can be considered to be dust-laden and is a good predictor for the flow of dust around the miner close to the cutting face.

Regarding the air flowing outbye of the heading face, it is also in a turbulent state at a distance of 20 m from the cut-through, with an average velocity of approximately 0.7 m/s.

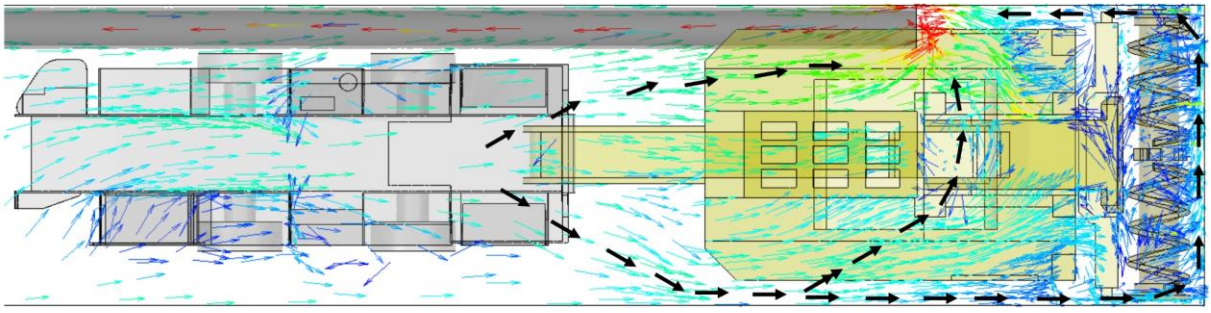

(a) Velocity vector at Z=2.1 m

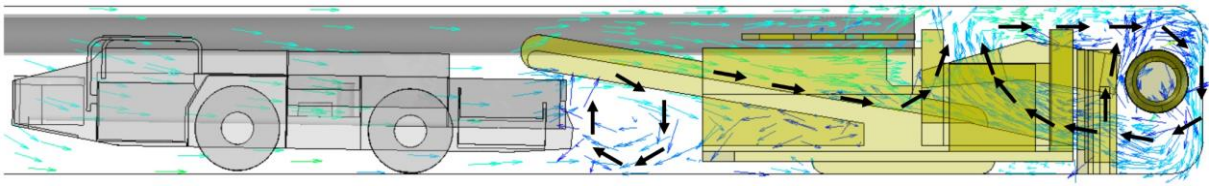

(b) Velocity vector at Y=2.6 m

Figure 8.10 Velocity migration patterns with coal cutting at the middle position

8.4.1.2 Dust dispersion characteristics

The temporospatial diffusion characteristics of respirable dust in the heading face with coal cutting at the middle position are illustrated in Figure 8.11. The maximum dust concentration is set at 100 mg/m^3 in the legend to provide a better illustration of the concentration range. The dust is generated from four locations, including the cutting face, shovel, conveyor belt, and part of SC. Dust produced from the coal-cutting process tends to drift down initially as a result of the entrainment

effect of air coming off the drum and the downward gravity force, and then can be seen to be drawn across the face towards the ventilation duct or recirculate around the cutting drum. At t=5 s, high-concentration dust is mainly distributed in the vicinity of the cutting drum. At t=10 s, high-level dust has migrated to the inlet of the ventilation duct, and it is apparent that dust originating from the shovel and conveyor belt is sucked into the duct, with a dust concentration of approximately 30 mg/m^3. A stream of dust sourcing from SC can be observed to migrate towards the heading face. At t=15 s, the area within a distance of approximately 4 m from the heading face becomes contaminated with high-concentration dust, particularly at the LHS of the CM. More dust from the shovel and conveyor belt will also disperse between the gap in the beam and the top cover of the CM and then be sucked into the ventilation duct, as demonstrated by high-concentration dust in this area. When t=60 s, there is almost no evident difference in the distribution of high-concentration dust within the heading in comparison to the scenario of t=20 s, at which time high-level dust is mainly distributed in the area at approximately 5 m from the heading face. The simulation results indicate that operators standing at the LHS of CM for roof and rib bolting and duct advancement can be easily exposed to a high level of dust during coal cutting. Therefore, it is recommended that LHS operators should be equipped with high-quality personal protective equipment and stay behind the inlet of the ventilation duct during coal cutting. For miners standing at the RHS of CM for roof and rib bolting and machine operating, it is suggested that they should stay immediately behind the roof and rib bolting rig, where dust concentration is relatively low.

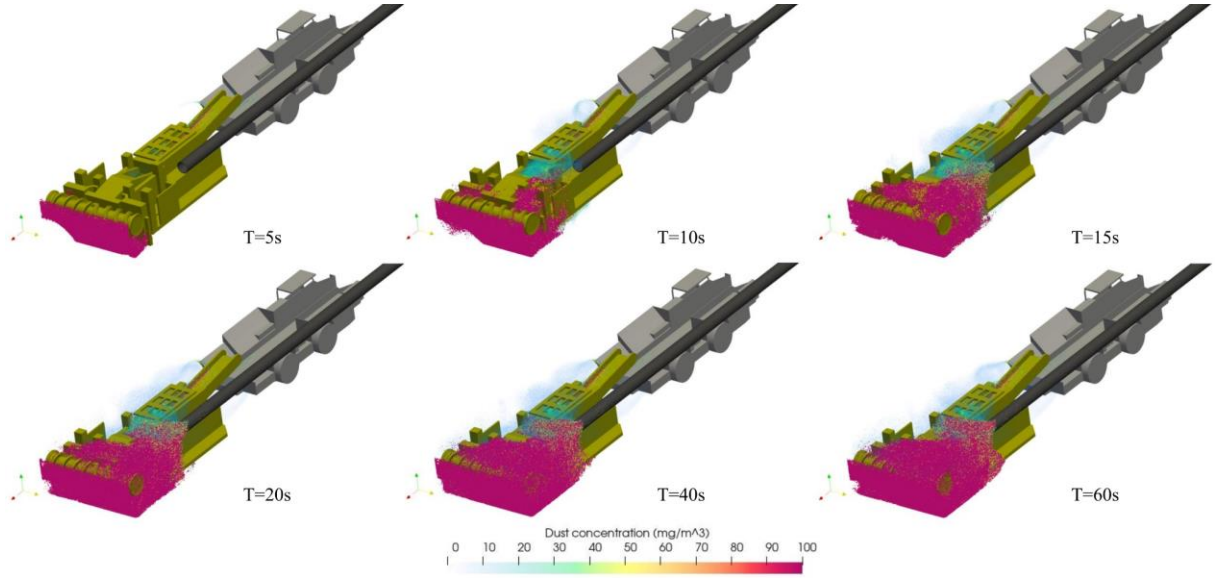

Figure 8.11 Dust dispersion characteristics with coal cutting at the middle position

8.4.2 Coal cutting at the floor position

8.4.2.1 Airflow migration patterns

The airflow patterns within the development heading with coal cutting at the floor position are illustrated in Figure 8.12. Similar to the scenario of coal cutting at the middle position, airflow

from the cut-through diverges into the belt road, where air migrates towards the heading face or flows outbye of the heading face in a turbulent state. Air flowing inbye along the heading can be seen to increase its average velocity as a result of the reduction in effective cross-section area. As the air reaches the rear of the CM, it diverts due to the blockage of the conveyor belt on the CM. At the LHS of the CM, the air is drawn into the duct directly. Regarding the airflow at the RHS of the CM, the major streams of air gradually change direction a portion is sucked directly into the fan duct across the top of the CM. While the rest continues to migrate a long distance towards the heading face before dispersing across the face, at which point it is sucked into the duct, as illustrated in Figure 8.12(a). In the mid-plane of the CM shown in Figure 8.12(b), there is the greatest change in airflow patterns as a result of the cutting position where it is evident that recirculating patterns can be observed above the cutting drum and around the cutting drum in contrast to the single recirculation zone generated when cutting mid-face. Air can be seen to travel down the conveyor opposing the direction of material flow before rising above the CM and contributing to the largest recirculating zone that flows around the boom of the CM and is likely to contribute significantly to the transport of dust around the front end of the CM.

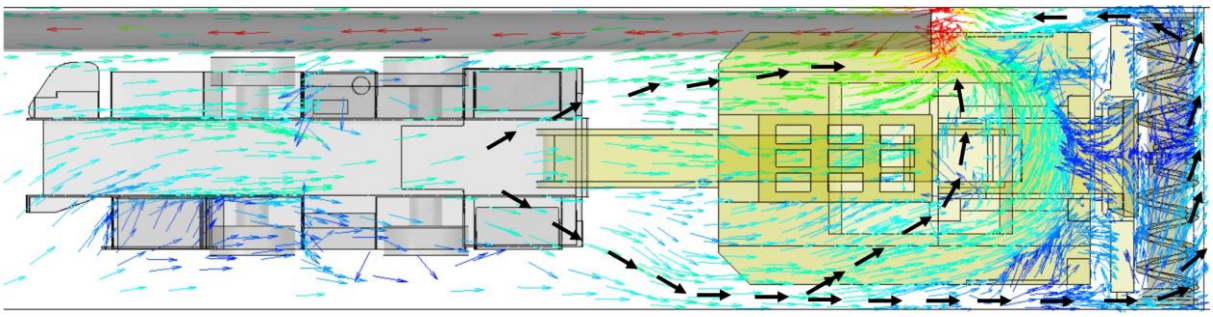

(a) Velocity vector at Z=2.1 m

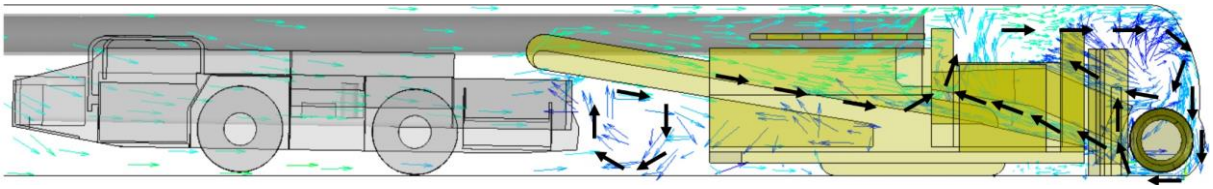

(b) Velocity vector at Y=2.6 m

Figure 8.12 Velocity migration patterns with coal cutting at the floor position

8.4.2.2 Dust dispersion characteristics

The temporospatial diffusion characteristics of respirable dust in the development heading with coal cutting at the floor position are illustrated in Figure 8.13. As with the scenario of coal cutting in the middle position, dust is generated at the four locations with the same flow rates and dust

particle distribution. At t=5 s, dust from the cutting face is forced towards the floor by the cutting action before getting caught in the airflow generated by the cutting drum and ventilation flow which cause it to start dispersing into the air. Dust produced at the shovel and conveyor belt migrates toward the gap between the top cover and the beam of the CM due to the ventilation flow. By t=10 s, it is evident that dust lifted from the shovel and conveyor belt becomes entrained in the airflow and sucked into the ventilation duct with a mass concentration of approximately 30 mg/m^3. At t=15 s, a significant portion of dust from the coal cutting can be observed being sucked into the duct, and the LHS of the CM between the roof and rib bolt rig becomes contaminated with high-concentration dust. In addition, a stream of dust flow from the SC with a mass concentration of about 15 mg/m^3 migrates towards the heading face before changing direction due to the sucking effect of the exhausting fan duct. With the increase in time from 20 s to 60 s, there is not a significant difference in dust distribution characteristics, though it can be observed that the concentration of dust travelling along the floor is slightly reduced compared to cutting mid-face. For operators standing at the front of the LHS of the CM, exposure to a high level of respirable dust will likely occur and increase the risk of contracting a respiratory disease, thus it is strongly recommended that they should stand well behind the ventilation duct inlet at all times when coal is being cut and loaded.

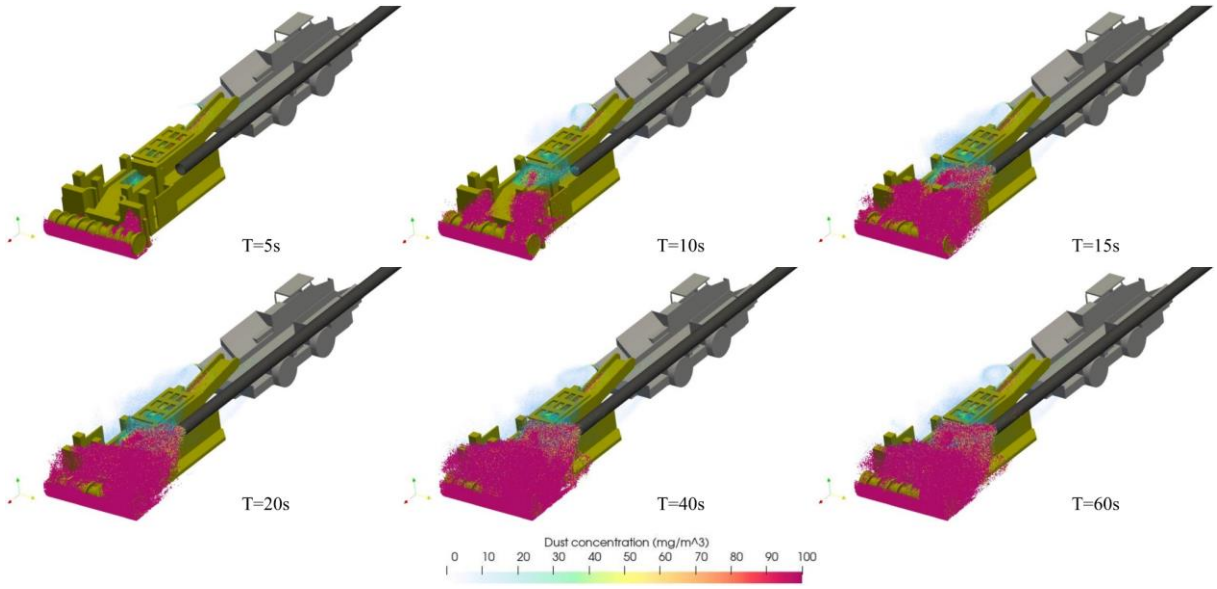

Figure 8.13 Dust dispersion characteristics with coal cutting at the floor position

8.4.3 Coal cutting at the roof position

8.4.3.1 Airflow migration patterns

The airflow patterns within the development heading with coal cutting at the roof position are illustrated in Figure 8.14. It is apparent that airflow migration patterns in the belt road show a similar trend to the scenario of coal cutting at the middle and floor position. There is no change in

the flow dynamics outbye of the CM. As air approaches the rear of the CM, it is divided into two different streams, where the flow travelling on the LHS of the CM is sucked almost directly into the ventilation duct, while the flow on the RHS will travel continue onto the heading face. Due to the obstacle created by the cutting drum and overall miner in this position, the air is more turbulent around the roof and recirculation of flow occurs around the below the drum in a counter-current fashion, as illustrated in Figure 8.14(a) and 8.14(b). At the mid-plane of the CM centre in Figure 8.14(b), the airflow patterns are similar along the conveyor creating a sealing effect that will aid in holding dust closer to the face and ensure it is drawn into the ventilation duct.

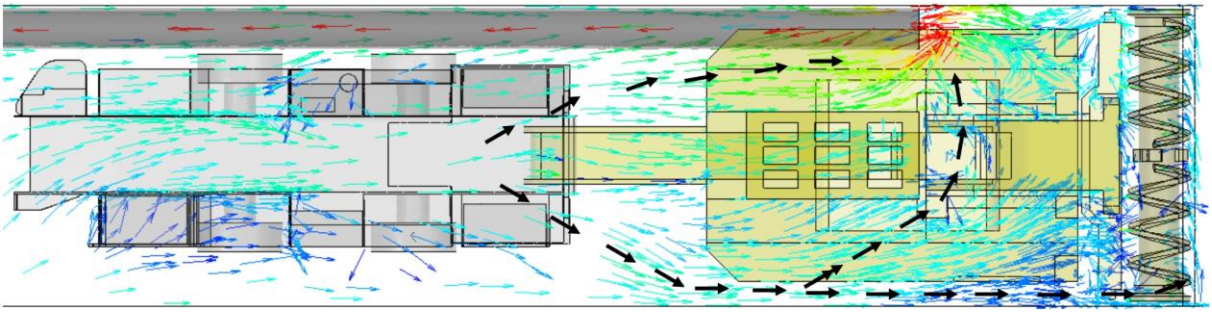

(a) Velocity vector at Z=2.1 m

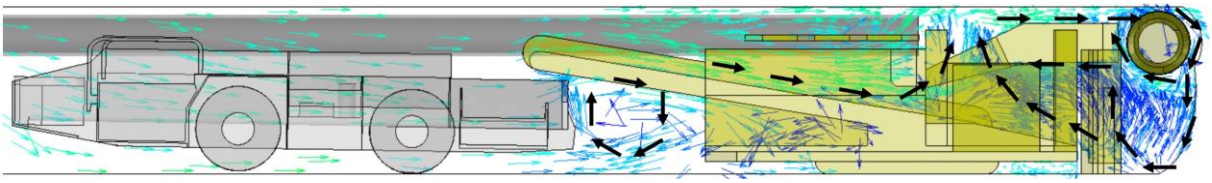

(b) Velocity vector at Y=2.6 m

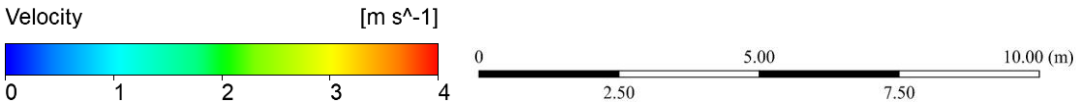

Figure 8.14 Velocity migration patterns with coal cutting at the roof position

8.4.3.2 Dust dispersion characteristics

The temporospatial diffusion characteristics of respirable dust in the development heading with coal cutting at the floor position are illustrated in Figure 8.15. At t=5 s, dust generated by coal cutting will become caught in one of the two recirculating zones around or below the cutting drum before being drawn towards the ventilation duct. At t=10 s, relatively high-concentration dust from the shovel and conveyor belt passes through the gap between the top cover and beam of the CM and is sucked into the duct. In addition, a great amount of dust from coal cutting is exhausted via the ventilation duct, and the area on the LHS of the CM between the roof and rib rig becomes contaminated with high dust concentrations. At t=15 s, dust from the SC can be seen migrating along the RHS of the CM before being sucked into the duct with an average dust concentration of 15 mg/m^3. With the increase in time from 20 s to 60 s, there is no considerable difference in dust

migration and distribution characteristics within the heading face, and high-concentration dust only migrated to the location of the ventilation duct without dispersing further outbye of the heading.

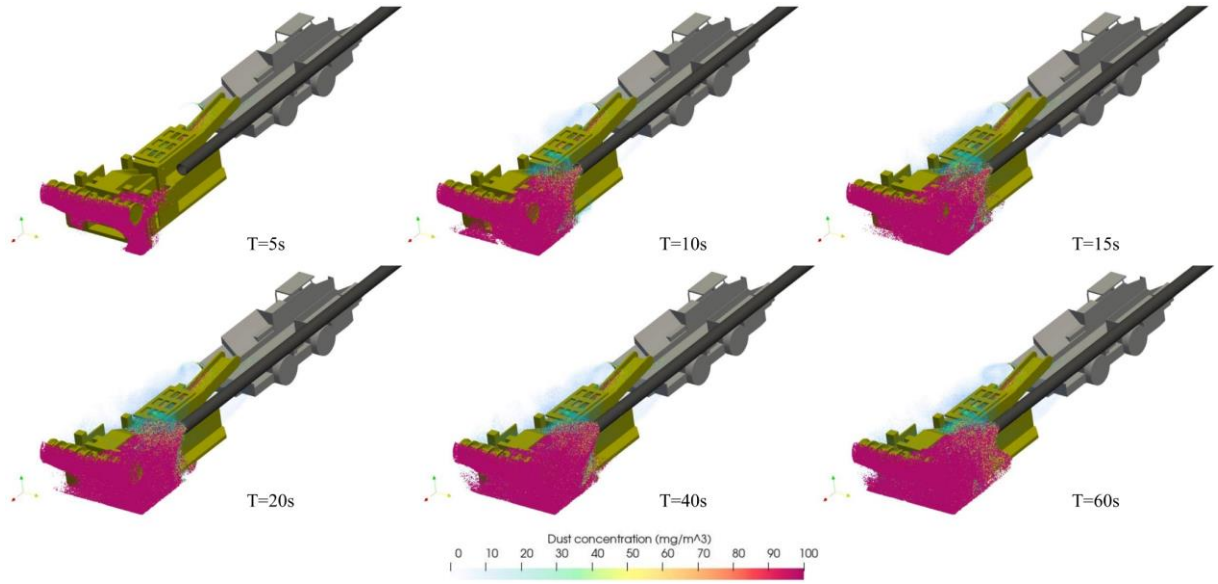

Figure 8.15 Dust dispersion characteristics with coal cutting at the roof position

8.5 Dust Mitigation Strategies

8.5.1 Airflow rates through the ventilation duct

In order to investigate the influence of airflow rates through the exhausting ventilation duct, six different scenarios are simulated, with dust concentration at the breathing level (Z=2.1 m) depicted in Figure 8.16. For better visualization, dust concentration in the area inbye of the shuttle car is present, and the maximum dust concentration is set at 50 mg/m^3. The dust concentration higher than 50 mg/m^3 is shown in the beige colour in Figure 8.16. With the increase in airflow rates through the exhausting ventilation duct from 6 m^3/s to 12 m^3/s, dust concentration at the walkway platform of the CM behind the duct inlet significantly reduces, particularly at the LHS of the CM. However, there remains a small area where dust concentration is higher than 7.5 mg/m^3 at the LHS of the CM with a ventilation rate of 12 m^3/s. With the airflow rate continuing to rise from 12 to 16 m^3/s, this high-concentration dust area gradually disappears, under which condition the operator standing at the LHS of the CM is free from exposure to high-concentration dust when standing behind the ventilation duct. It is clearly evident that an increase in airflow rate assists in reducing dust levels in the heading, but the dust mitigation effect does not change significantly once the airflow rate reaches 12 m^3/s, and thus it could be considered an optimal exhaust rate for this mining configuration.

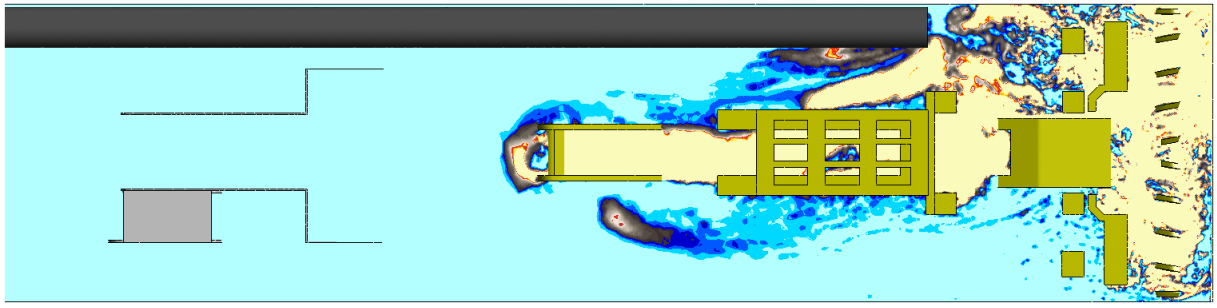

(a) 6 m^3/s

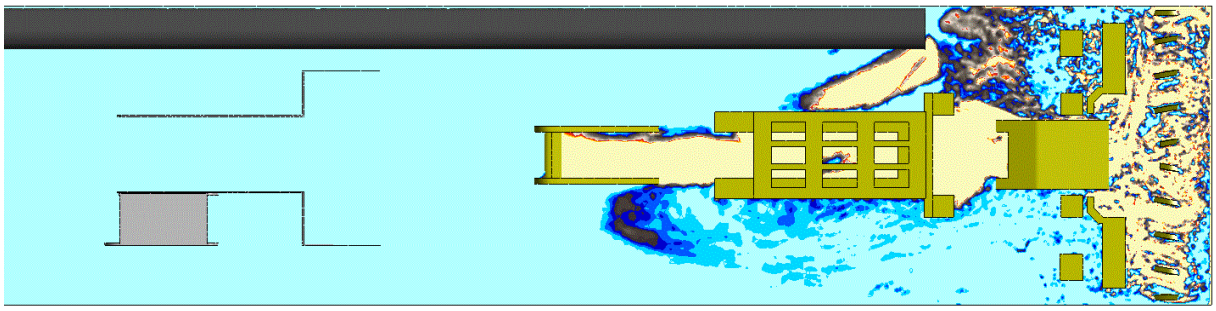

(b) 8 m^3/s

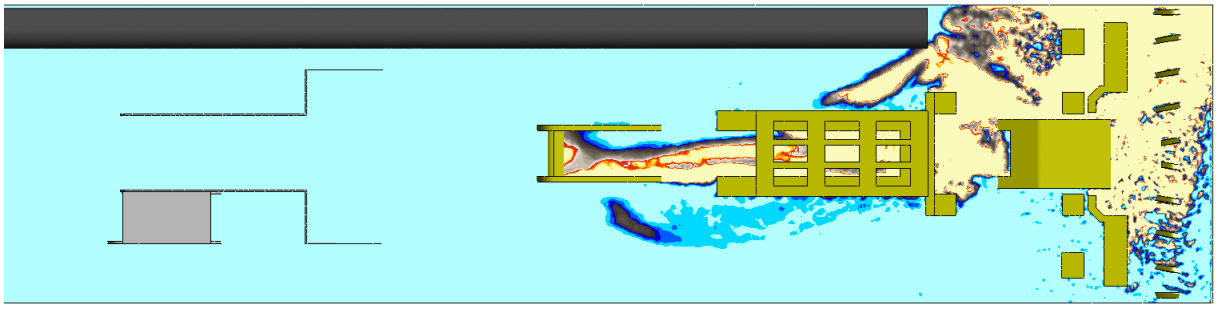

(c) 10 m^3/s

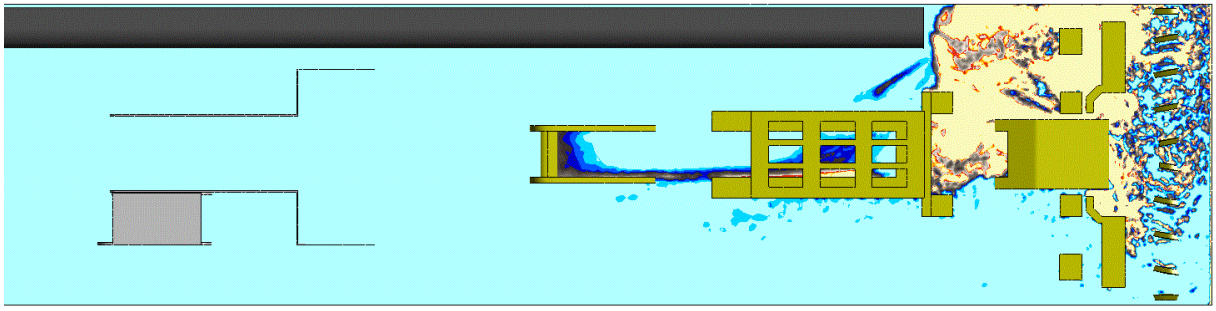

(d) 12 m^3/s

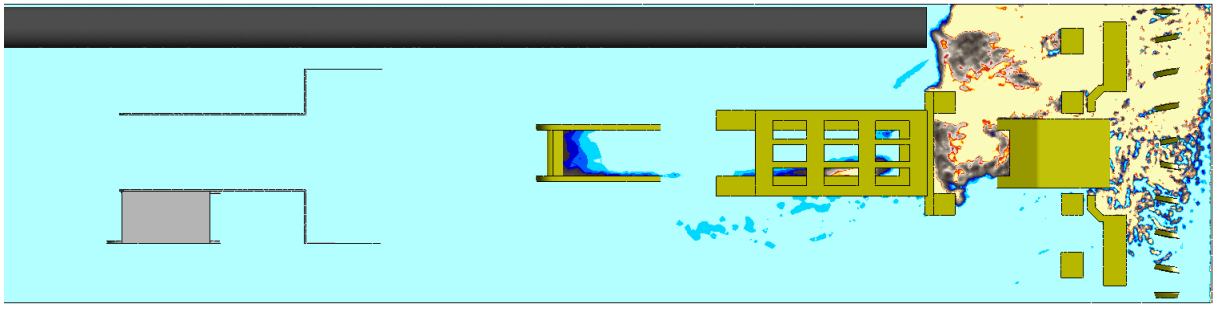

(e) 14 m^3/s

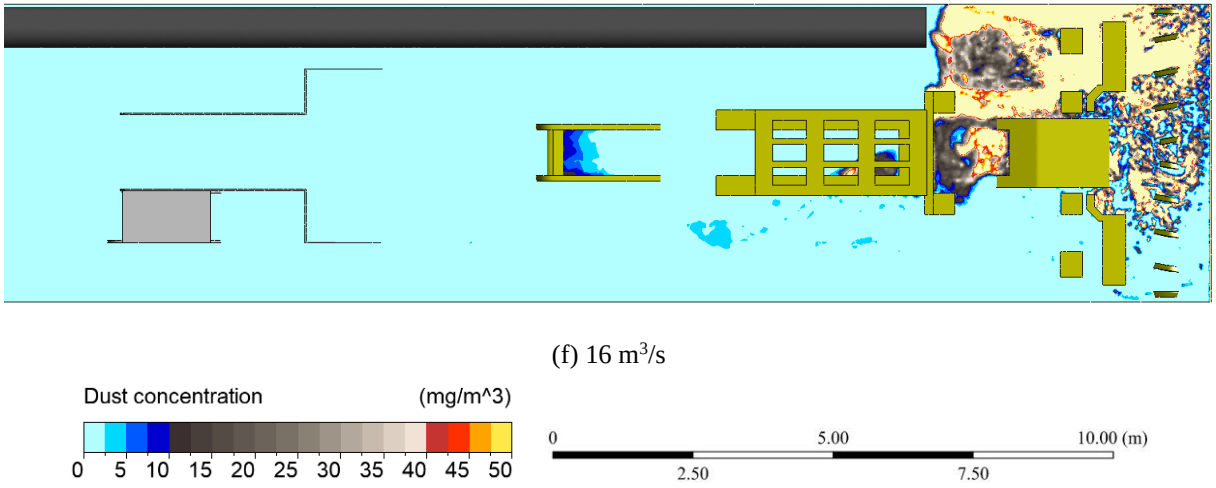

(f) 16 m^3/s

Figure 8.16 Dust concentration at the breathing level under different airflow rates through the ventilation duct

8.5.2 Distance from the ventilation duct inlet to the heading face

In order to evaluate dust mitigation performance under different distances from the ventilation duct inlet to the heading face, four scenarios are proposed and simulated with a ventilation rate of 12 m^3/s, with simulation results of dust concentration at the breathing level shown in Figure 8.17. It is evident that the distance between the ventilation duct inlet and the heading face has a considerable impact on the dust removal effect. As the distance between the duct inlet and the heading face reduces from 7.0 m to 1.5 m, the area with high-concentration dust reduces dramatically, particularly at the walkway platform of the LHS of the CM behind the roof bolt rig. The areas where dust mass concentration exceeds 1.5 mg/m^3 at the breathing level for the duct distance of 1.5, 3, 5 and 7 m are 13.802, 16.672,19.249 and 26.809 m^2, respectively. Quantitative analysis of high-concentration dust area reveals that a dust reduction rate of approximately 50% can be reached with the distance from the ventilation duct inlet to the heading face reducing from 7 to 1.5 m. Therefore, it is suggested that the exhausting ventilation tube should be extended regularly during the tunnelling process, and the distance between the ventilation duct inlet and the heading face should be set as close as possible without intervening with the normal tunnelling process.

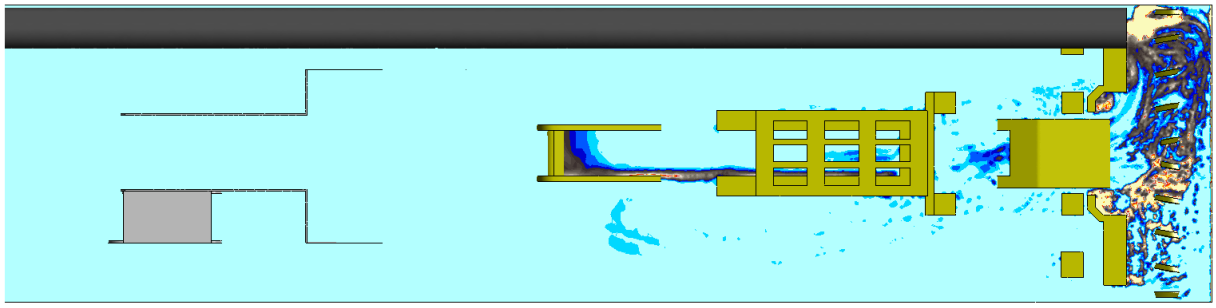

(a) 1.5 m

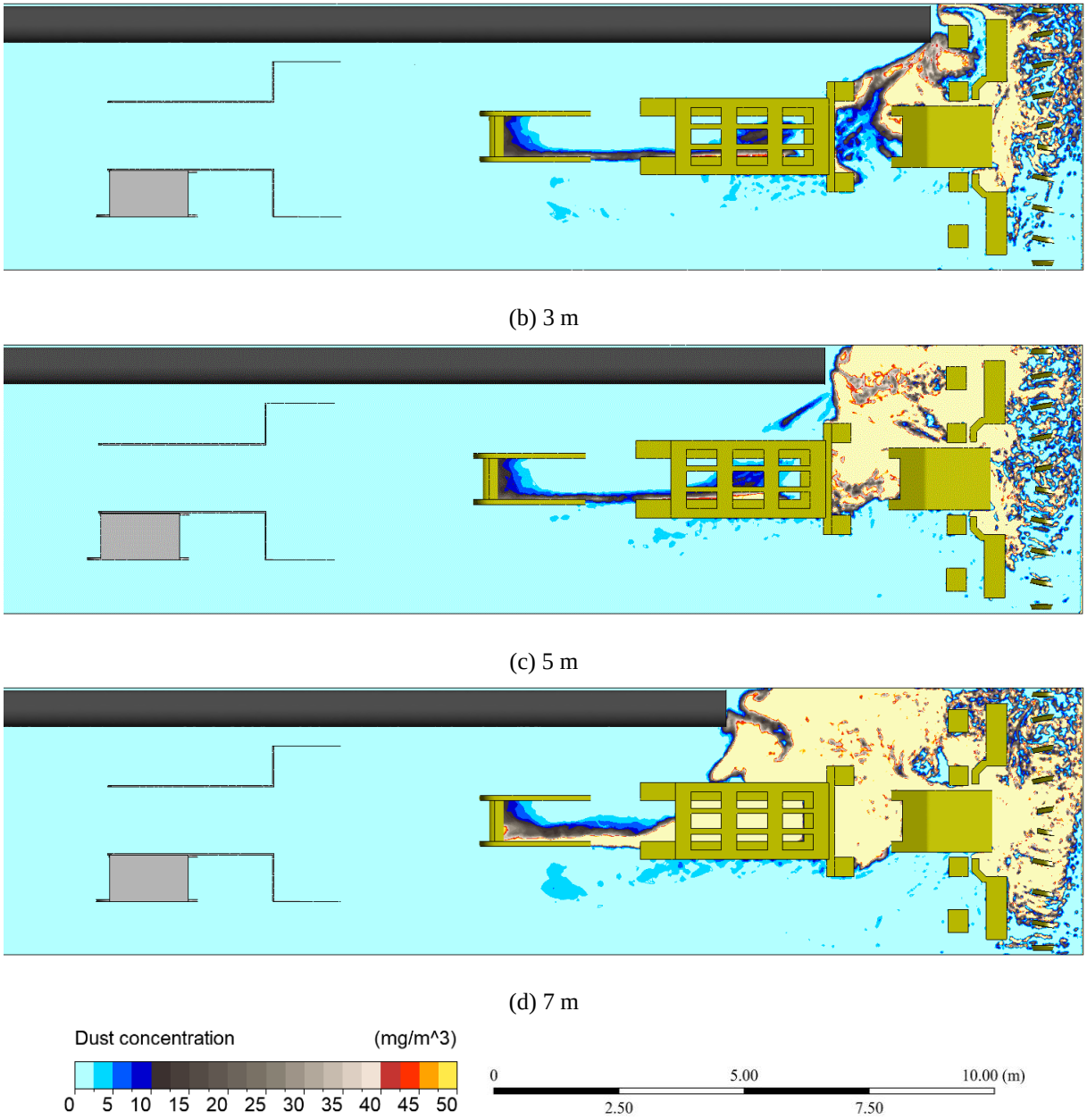

Figure 8.17 Dust concentration at the breathing level under different distances from the ventilation duct inlet to the heading face

8.5.3 On-board ventilation

The on-board ventilation system is proposed and simulated with a ventilation flow rate of 12 m^3/s, and the dust concentration at the breathing level is shown in Figure 8.18. In comparison to the current ventilation scheme shown in Figure 8.16(d), the area of dust concentration exceeding 1.5 mg/m^3 under the on-board ventilation decreases from 19.249 to 10.848 m^2, dropping by approximately 43.6%. It is notable that the vast majority of dust is contained in front of the CM baffle except for a small area at the RHS of the CM, where high-concentration dust can be observed. Overall, on-board ventilation assists in reducing dust concentration during the coal-cutting process and can be recommended as an effective strategy where the mine layout allows it.

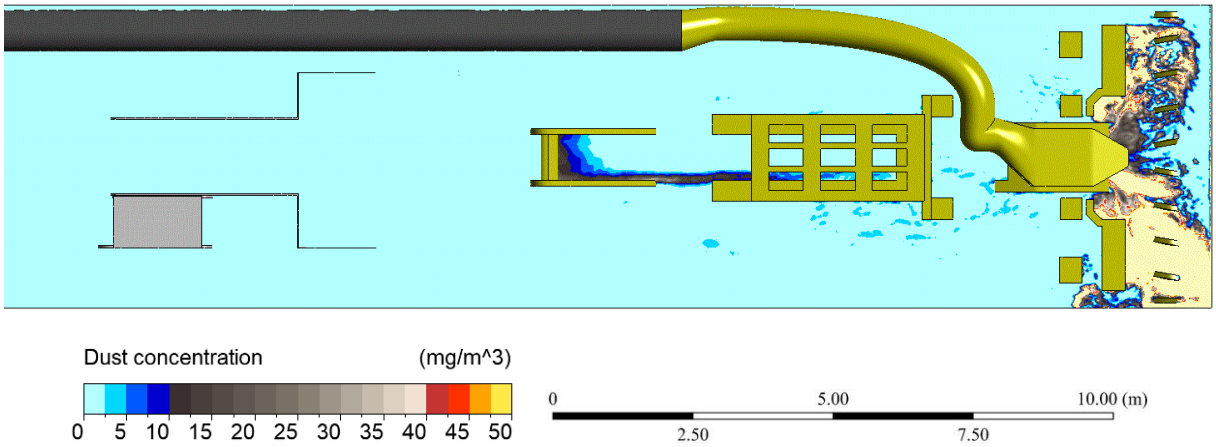

Figure 8.18 Dust concentration at the breathing level with on-board ventilation

8.6 Conclusions

This paper considered the current gaps in the literature related to the understanding of dust dispersion characteristics within a development heading under an auxiliary exhausting ventilation system as is commonly used in the Australian coal mine industry. The modelling methodology has shown the importance of proper identification of dust sources in the validation of the model against real-world data collected on site in combination with an accurate and representative 3D model of the site including all relevant equipment. By injecting dust into the domain from a range of locations corresponding to site observations, the model was able to predict dust concentrations throughout the domain with a high level of accuracy. This is an important recommendation for future studies of a similar nature, although it does rely on a comprehensive analysis of on-site dust release and concentration measurements. From the validated model, it was possible to interrogate the airflow migration patterns and dust dispersion characteristics in more comprehensive detail, including the effects of cutting position at the face which is not well documented in current literature. As expected, the effects of cutting position mainly contribute to the ventilation flow close to the face, where the development of vortices occurs as a by-product of the rotating drum. When cutting mid-face, the drum develops a single large vortex centred on the drum that drives dust down to the floor before being drawn into the ventilation duct through space around the CM; similar dynamics occur when cutting the roof though a greater amount of dust is able to be drawn directly into the ventilation duct due to its relative proximity. In comparison, cutting the floor has slightly different flow dynamics where a vortex is formed above the drum which draws clean air in from outbye and helps contain dust against the floor close to the face before it disperses over the machine and into the ventilation duct. It is suggested that this insight may provide some opportunities for further study where the cutting procedure used onsite could potentially be optimized to reduce time spent with the cutting drum in locations exacerbating dust generation.

The consideration of typical mitigation strategies used by sites has also provided some important insight into the optimal procedures mines sites can adopt with exhaust ventilation systems to reduce worker dust exposure. Maximizing airflow rate shows a clear and measurable reduction in dust dispersion over the CM into the typical working zones, however there are diminishing returns and it is recommended for the layout studied here that a ventilation rate of 12 m^3/s should be utilized, though this will be site-specific, and a similar study should be conducted using the same methodology demonstrated here for each specific mine site. In contrast, the proximity of the duct inlet to the cutting face can be recommended to be maintained as close as practicable, for the heading layout, to minimize mine worker dust exposure. Similarly, on-board ventilation assists in confining high-concentration dust from dispersing in the heading and hence can contribute significantly to reducing dust concentration at the breathing level. In all cases utilizing exhausting ventilation, the simulation results indicate that left-hand-side (LHS) operators should be equipped with high-quality personal protective equipment and stay behind the ventilation duct inlet during the coal-cutting process, while miners standing at the right-hands-side (RHS) of the continuous miner for roof and rib bolting and machine operating should stay immediately behind the roof and rib bolting rig where dust concentration was relatively low. There are, however, further opportunities for studies on dust mitigation techniques related to ventilation setup, additional control methods, or optimization of equipment configuration and operating parameters that can be considered in the future.

Overall, it is expected that this study can assist in improving the knowledge of airflow migration patterns and dust dispersion characteristics in a continuous-miner-driven development heading under the exhausting ventilation system and provide some guidance on dust mitigation and operator protection strategies, thus improving the health and safety of miners and creating a cleaner underground working environment during the tunnelling process.

CHAPTER 9 CONCLUSIONS AND RECOMMENDATIONS

9.1 Conclusions

Due to the increase in production outputs and extraction depth of cover, underground coal mining is facing increasing threats from principal mining hazards, including but not limited to spontaneous combustion and heating in the LW goaf areas, abnormal gas emissions at localised tailgate end area, gas exceedance during LW panel sealing-off processes and airborne respirable dust. To control and mitigate these engineering problems, advanced Computational Fluid Dynamics (CFD) modelling can be used to simulate various scenarios portraying these hazards that may occur in underground LW workings and provide much-needed knowledge and fundamental science that can be used to develop robust and effective control and mitigation strategies against these hazards. Throughout different case studies presented in this thesis, the capability and application of advanced CFD modelling for managing and controlling principal mining hazards have been demonstrated. The major conclusions reached are summarised as follows:

9.1.1 Spontaneous combustion in LW goaf areas

(1) Case study one

Based on the site-specific conditions of an underground coal mine in New South Wales, Australia, a three-dimensional (3D) CFD model incorporating floor and roof strata, mined-out seam, LW face and associated gateroads was built. The goaf gas is comprised of approximately 80% carbon dioxide (CO_2) and 20% methane (CH_4), with a total gas emission rate of 2000 l/s. Real-time gas monitoring data collected from the Tube Bundle System was used to calibrate the simulation model, where a good agreement between the monitoring data and simulation results was reached. Then extensive parametric studies were conducted to improve the understanding of goaf gas flow dynamics and optimize proactive goaf inertisation strategies. The analysis of simulation results indicates that:

- Due to the fact that the elevation of the tailgate (TG) is higher than that of the maingate (MG) side and the elevation of the starting-off line is higher than the working face, nitrogen injection via one cut-through (CT) or two cut-throughs on the MG side demonstrates undesirable strategies for spontaneous combustion control, as the oxygen concentration is high on the TG side of the deep goaf. On the contrary, nitrogen injection should be injected into the goaf area from the TG side or both MG and TG sides at the appropriate distance from the LW face;
- To avoid high oxygen levels on the TG side of the deep goaf, injection locations on the TG side should be set at approximately 550 m behind the LW face when nitrogen is injected

via one location;

- Nitrogen injection via surface boreholes (drilled close to the TG of the LW panel) previously used from gas drainage performs better than cut-throughs on the TG side;
- Quantitative analysis of the oxidation zone area reveals that it is largest for carbon dioxide injection (68005 m^2), followed by boiler gas (45606 m^2), while it is the smallest for nitrogen (35375 m^2), which means that nitrogen is superior to boiler gas and carbon dioxide in containing spontaneous combustion;
- The qualitative and quantitative analysis of simulation results shows that the desirable goaf inertisation strategy is to inject nitrogen into the goaf area via cut-through at 250 m on the MG side and surface borehole at 100 m and 700 m on the TG side with a total injection rate higher than 1750 l/s. Oxygen ingress into the goaf area on both sides is reduced significantly with an oxidation zone area of 35375 m^2, which is approximately one-third of the oxidation zone area of the scenario without any inert gas injection (106666 m^2);
- Both geological conditions (e.g., seam orientation, goaf gas composition and emission) and mining parameters (e.g., face layout and ventilation rate, advance rate) have impacts on goaf gas flow dynamics and distribution patterns, which need to be taken into consideration in determining goaf inertisation strategies.

(2) Case study two

Based on the CFD model built in case study one, the impact of coal seam orientations, dictated by the elevation of the MG and the TG and the height of the LW face and the starting-up line, on goaf gas flow dynamics and proactive goaf inertisation for spontaneous combustion control was investigated. The other geological and mining parameters were kept the same except for coal seam orientations. The main findings are summarised as follows:

- Nine scenarios of different coal seam orientations were studied. For the base model without inert gas injection, air ingress at both sides of the active LW goaf is evident, and the area ratio of oxidation zone to active LW goaf ranges between 25.2% and 28.7%;
- For cases where the MG is higher than the TG and at the same time the starting-up line is lower than or at the same elevation as the LW face, it is better to inject nitrogen at the MG of the active LW goaf, otherwise nitrogen injection is required at the TG of the goaf;
- If the LW face is lower than the starting-up line, the nitrogen injection point at the TG of the active goaf should be located at least 500~600 m behind the LW face to prevent oxygen accumulation at the TG of the deeper goaf. Conversely, if the working face is higher than

or at the same elevation as the starting-up line, the nitrogen injection point at the TG of the goaf should be set about 100~200 m behind the LW face with an appropriate injection rate to avoid low oxygen volume fraction at the goaf stream;

- Regardless of the coal seam orientations, nitrogen is superior to carbon dioxide in reducing the oxidation zone area and containing spontaneous heating under the condition that seam gas is primarily comprised of 80% carbon dioxide and 20% methane with a total gas emission rate of 2 m^3/s;
- A total nitrogen flow rate of 1.5 m^3/s is required to contain spontaneous heating, with the area ratio of oxidation zone to active goaf of approximately 10%, which is approximately 15% less than scenarios without inert gas injection.

(3) Case study three

To enhance the knowledge of the gas flow dynamics and gas distribution in the active goaf with different seam gas composition and develop the corresponding proactive goaf inertisation strategies, extensive CFD simulations were performed using the model built in case study one. Five different scenarios were studied, and goaf gas was composed of 100% carbon dioxide, 80% carbon dioxide and 20% methane, 50% carbon dioxide and 50% methane, 20% carbon dioxide and 80% methane, and 100% methane, which were denoted as scenario (a), (b), (c), (d) and (e), respectively. Except for the difference in goaf gas composition, the other parameters were kept the same as the modelling in case study one. The major findings are summarised below:

- Air ingress on both sides of the goaf is evident for scenarios (a), (b), (d) and (e), with oxygen concentration higher than 10% in the deep goaf, while oxygen penetration on both sides of the goaf is limited at 550 m behind the face for scenario (c), with oxygen concentration dropping below 5%;
- Oxygen is primarily distributed at the middle and upper regions of the goaf for scenarios (a), (b) and (c), whereas it is mainly layered at the bottom of the goaf area for scenarios (d) and (e), which is attributed to the buoyancy effect and density difference among goaf gases;
- The oxidation ratio (the ratio of the oxidation zone area to the goaf area) shows a decreasing trend as the methane composition rises from 0% to 50%, conversely, the oxidation ratio increases with the continued increase in methane composition from 50% to 100%;
- Nitrogen produces a better goaf inertisation result than carbon dioxide for scenarios (a), (b) and (c) where the carbon dioxide composition is higher than its methane counterpart, while carbon dioxide is superior to nitrogen in rendering the goaf atmosphere inert for scenarios

(d) and (e) where methane composition exceeds carbon dioxide composition;

- Under the condition of a total injection rate of 0.5 m^3/s, nitrogen injection at the TG of the goaf performs better in managing spontaneous heating than MG injection for scenarios (a) and (b) where the goaf gas is composed of 100% carbon dioxide and 80% carbon dioxide, whereas an acceptable goaf inertisation result can be produced by pumping inert gas at both sides of the goaf area for scenarios (c), (d) and (e);
- The optimal inert gas injection rates for scenarios (a), (b), (c), (d) and (e) are 1.5, 1.75, 0.75, 0.5 and 1.0 m^3/s, and the oxidation zone area reduces by 55.76%, 67.21%, 58.04%, 78.17% and 81.82% for the five scenarios, respectively.

(4) Case study four

Based on the site-specific conditions of an underground coal mine in Queensland, Australia, improved CFD modelling was developed to better understand the gas flow dynamics and distribution patterns in the goaf area and investigate the impact of mining parameters on spontaneous combustion control in the goaf area. Numerical simulation results were validated with onsite monitoring data collected from the Tube Bundle System, and a good agreement was reached, which increased the confidence in studying scenarios outside of the base model. The ratio of the oxidation zone area (OZA) to the goaf area (GA) was introduced to qualitatively and quantitatively investigate the impact of mining parameters on oxygen distribution in the active goaf area. The major findings can be summarised below:

- As the goaf gas emission rate increases from 500 l/s to 2500 l/s, the ratio of OZA to GA drops from 58.41% to 35.79%, which means that a high goaf gas emission rate can reduce the likelihood of spontaneous combustion to a certain degree;
- Permeability is introduced to describe the tightness of seals built in the cut-throughs, and air leakage can be reduced when the permeability is lower than 10^{-9} m^2;
- The ratio of OZA to GA ranges between 25.38% and 41.14% for the proposed scenarios of different ventilation layouts, thus it shows the importance of evaluating the ventilation system prior to coal mining;
- Injection via cut-throughs on the MG side performs better than the surface borehole, and injection on the MG side via two contiguous cut-throughs produces better results than two spaced cut-throughs;
- From the perspective of the OZA, carbon dioxide injection through CT33 (11902 m^2) is superior to boiler gas (28396 m^2) and nitrogen (29706 m^2) injection for goaf gas being

entirely composed of methane, yielding the desirable goaf inertisation performance;

- Considering the reduction in the ratio of OZA to GA and oxygen levels at the tailgate end (higher than 19.5%), a carbon dioxide injection rate of 1750 m^3/h is optimal for proactive goaf inertisation.

To summarise, it is noted that geological parameters (e.g., coal seam orientations and seam gas composition) and mining factors (e.g., different ventilation patterns of LW panels and tightness of seals built in the cut-through) play a significant role in goaf gas flow dynamics patterns and oxygen distribution in the goaf area, which further influence the oxidation zone area under the condition of different proactive goaf inertisation strategies. These factors need to be considered when formulating proactive goaf inertisation plans. The above study results will improve current goaf inertisation practices in Australia to effectively contain spontaneous heating in large LW goaf areas with high production rates, high ventilation rates, as well as high gas emission rates, and improve coal mining safety.

9.1.2 Gas-related issues in the LW panel

(1) Methane exceedance at the tailgate end

Ventilation control devices, particularly curtains and brattices, are significant factors that could influence the goaf gas flow dynamics in the goaf area and gas levels at the tailgate end. On the basis of the CFD model developed in Chapter 6, improved simulations were conducted to find the determining factors influencing methane exceedance mitigation performance at the tailgate end, particularly the configuration of brattices and curtains at the LW face and the tailgate end. Three curtains and two brattices were applied. Specifically, two curtains are separately placed in the working face and return gateroad, and they are kept in line with each other and parallel to the tailgate panel. One curtain is positioned in the return gateroad and perpendicular to the tailgate panel rib. Two brattices placed on the LW face mainly play a role in diverting the airflow toward the goaf fringe. The major findings are summarised as follows:

- The usage of curtains and brattices at the LW face and tailgate end can effectively reduce peak methane concentration (PMC) at the tailgate end when compared to the scenario without curtains and brattices;
- The width of the curtain perpendicular to the gateroad rib, the distance between the gateroad rib and the curtain parallel to the gateroad rib, and the length of the curtain at the tailgate end significantly impact the methane mitigation performance at the localized tailgate end;
- The length of the curtain at the return travel road and the distance from the face brattices

and the goaf rib have a minor effect on mitigating abnormal methane emission at the goaf fringe.

(2) Gas flow dynamics in the LW panel during the panel sealing-off process

Previous studies and field observation indicated that the risk of spontaneous heating and gas explosion significantly increased when the LW face advanced slowly or even stopped. When the LW face approaches the finish-off line, the LW equipment is required to relocate to the new installation face, and the ventilation dynamics and goaf gas atmosphere change during the face recovery period, which poses significant challenges to spontaneous heating and gas explosion management. To prevent these dynamics hazards during a six-stage LW panel sealing-off process, a detailed understanding of ventilation dynamics and goaf gas atmosphere in the LW goaf is essential to identify appropriate gas monitoring locations and improve the panel sealing-off process design. On the basis of the geologic and mining conditions of an Australian underground coal mine in Queensland, two three-dimensional CFD models were developed, and boundary conditions were defined in Fluent. To calibrate the computational model, field gas monitoring data was collected from the Tube Bundle System where simulation results correlated well with monitoring data, indicating the model was able to simulate other scenarios with high confidence. Extensive simulations were performed to better understand the behaviour of ventilation dynamics in the LW panel at different stages of the LW sealing-off process, and major conclusions are listed below:

- The LW sealing-off process is divided into six different stages and studies from the face coming into the finish-off position to sealing-off with the following sequences: face coming into the finish-off line, face bolt up after production stop, pulling hydraulic supports from the TG to the LW chute road 1, from the LW chute road 1 to road 2, from LW chute road 2 to the MG, and all supports pulled off the face and the MG corner sealing-off;
- At the first five stages, oxygen concentration along the TG travel road is below 5% at 200 m behind the LW face, while oxygen levels along the MG belt road are below 5% at 50 m behind the LW face except at the rear cut-throughs where oxygen spikes are noticed, which indicates that the ventilation arrangements are acceptable for the face recovery;
- At the sixth stage of the LW sealing-off process, the proposed ventilation arrangement is unsatisfactory in considerably reducing the likelihood of spontaneous combustion and gas explosion due to a relatively-high-oxygen goaf environment conducive to coal oxidation and self-heating in the active goaf;

- When nitrogen is pumped through CT12 at a flow rate of 0.75 m^3/s and the rear part of the MG travel road is sealed off, oxygen levels within the active goaf and on the LW face both decrease below 5%, producing the desired LW sealing-off performance;
- To achieve effective and timely monitoring of the goaf atmosphere and evaluate the sealing performance, at least six gas sensors should be employed and located at the belt road and the travel road on the MG side (immediately outbye of the LW face), two LW chute roads, and the belt road and travel road on the TG side (immediately outbye of the LW face), respectively.

9.1.3 Respirable dust in the development heading

To address dust-related issues in the development heading, improved knowledge of airflow migration patterns and respirable dust dispersion characteristics within a continuous-miner-driven heading under an exhausting ventilation system is required. Based on site-specific conditions of a development heading in New South Wales, a three-dimensional Computational Fluid Dynamics (CFD) model was constructed and validated with onsite dust monitoring data, where a good agreement was achieved. Three scenarios of coal cutting at the middle, floor and roof positions were considered and simulated. The major conclusions are summarised below:

- By injecting dust into the domain from a range of locations corresponding to site observations, the model is able to predict dust concentrations throughout the domain with a high level of accuracy. This is an important recommendation for future studies of a similar nature, although it does rely on a comprehensive analysis of on-site dust release and concentration measurements;
- As expected, the effects of cutting position mainly contribute to the ventilation flow close to the face, where the development of vortices occurs as a by-product of the rotating drum;
- When cutting mid-face, the drum develops a single large vortex centred on the drum that drives dust down to the floor before being drawn into the ventilation duct through space around the CM; similar dynamics occur when cutting the roof though a greater amount of dust is able to be drawn directly into the ventilation duct due to its relative proximity;
- Cutting the floor has slightly different flow dynamics where a vortex is formed above the drum which draws clean air in from outbye and helps contain dust against the floor close to the face before it disperses over the machine and into the ventilation duct;
- Maximizing airflow rate shows a clear and measurable reduction in dust dispersion over the CM into the typical working zones, however there are diminishing returns and it is recommended for the layout studied here that a ventilation rate of 12 m^3/s should be

utilized, though this will be site-specific, and a similar study should be conducted using the same methodology demonstrated here for each specific mine site;

- The proximity of the duct inlet to the cutting face can be recommended to be maintained as close as practicable, for the heading layout, to minimize mine worker dust exposure. Quantitative analysis of high-concentration dust (exceeding 1.5 mg/m^3) area reveals that a dust reduction rate of approximately 50% can be reached with the distance from the ventilation duct inlet to the heading face reducing from 7 to 1.5 m;
- In comparison to the current ventilation scheme, the area of dust concentration exceeding 1.5 mg/m^3 under the onboard ventilation decreases from 19.2 to 10.8 m^2, dropping by approximately 43.6%;
- In all cases, the simulation results indicate that left-hand-side (LHS) operators should equip themselves with high-quality personal protective equipment and stay behind the ventilation duct inlet during coal-cutting processes, while miners standing at the right-hands-side (RHS) of the continuous miner for roof and rib bolting and machine operating should stay immediately behind the roof and rib bolting rig where dust concentration was relatively low.

9.2 Recommendations for Future Work

Future work should be performed in the following areas:

- Coal reaction with oxygen in the active goaf should be studied further, both experimentally and numerically. The distribution of oxygen and temperature field in the goaf area assists in the prediction of spontaneous heating and developing countermeasures to manage and control spontaneous combustion;
- Major LW equipment (such as hydraulic supports, shearer, armoured face conveyor, and bridge stage loader) should be incorporated into the model to better understand the gas accumulation mechanism near the tailgate ends of typical high gas events and the impacts of various controls/practices on a range of gas events and common failure mechanisms of these measures, thus identifying best controls/practices;
- As a significant factor, time should be considered and transient simulation should be performed, particularly in terms of goaf inertisation and LW sealing-off, which can provide some guidance on normal operations;
- Airflow migration characteristics and dust dispersion patterns during break-away and holing-through processes should be further investigated. In particular, the performance of

different measures for avoiding air circulation between two headings during the holing-through process can be evaluated, thus guiding practical operations under these difficult conditions;

- In addition to the change in ventilation rates through the exhausting tube, the distance between the tube inlet and heading face as well as on-board ventilation schemes, the effectiveness of other dust mitigation strategies should be evaluated further, such as water sprays, venturi, air movers, and scrubber units;
- Dust-gas coupling simulations in the continuous-miner-driven heading should be conducted to investigate the air-gas-dust behaviour during the tunnelling process and evaluate the effectiveness of control measures for reducing gas concentration in the heading, particularly venturi and curtain/brattices while simultaneously understanding the effects on dust flow;
- Airflow migration characteristics and dust dispersion patterns on the LW face should be investigated further, and corresponding dust control measures can be numerically evaluated for better performance.

REFERENCES

Aminossadati, SM & Hooman, K 2008, 'Numerical simulation of ventilation air flow in underground mine workings', in *Proceeding of 12th US/North American Mine Ventilation Symposium*, pp. 253-9.

ANSYS, I 2018a, *ANSYS Fluent Theory Guide*, Canonsburg, PA 15317.

ANSYS, I 2018b, *ANSYS Meshing User's Guide*, Canonsburg, PA 15317.

ANSYS, I 2022a, *ANSYS Fluent Theory Guide-2022R1*, Canonsburg, PA 15317.

ANSYS, I 2022b, *ANSYS Meshing User's Guide-2022R1*, Canonsburg, PA 15317.

Arısoy, A 2010, 'Coal mine safety and preventing self-combustion of coal', in *Conference: Inerma, At Istanbul, Turkey*.

Australasian Mine Safety Journal 2019, *Preliminary report released on Peabody Energy Metropolitan Colliery mine gas incident*, Australasian Mine Safety Journal <http://ebook.aprs.com.au/australasian-mine-safety-journal/preliminary-report-released-on-peabody-energy-metropolitan-colliery-mine-gas-incident>.

Australian Institute of Occupational Hygienists 2014, 'Dusts not otherwise specified (dust nos) and occupational health issues—Position paper'.

Bai, Z, Wang, C, Deng, J, Kang, F & Shu, C-M 2020, 'Experimental investigation on using ionic liquid to control spontaneous combustion of lignite', *Process Safety and Environmental Protection*, vol. 142, pp. 138-49.

Balusu, R, Belle, B & Tanguturi, K 2019, 'Development of goaf gas drainage and inertisation strategies in 1.0-km-and 3.0-km-long panels', *Mining, Metallurgy & Exploration*, vol. 36, no. 6, pp. 1127-36.

Balusu, R, Ren, T & Humphries, P 2005a, *Proactive Inertisation Strategies and Technology Development, ACARP Project C12020*, CSIRO Exploration & Mining, Kenmore, Queensland, Australia.

Balusu, R, Ren, T & Humphries, P 2005b, *Proactive inertisation strategies and technology development, ACARP Project C12020*, CSIRO Exploration & Mining, Kenmore, Queensland, Australia.

Baur, X, Sanyal, S & Abraham, JL 2019, 'Mixed-dust pneumoconiosis: Review of diagnostic and classification problems with presentation of a work-related case', *Science of the Total Environment*, vol. 652, pp. 413-21.

Beamish, B 2005, 'Comparison of the R70 self-heating rate of New Zealand and Australian coals to suggate rank parameter', *International Journal of Coal Geology*, vol. 64, no. 1-2, pp. 139-44.

Beamish, B & Arisoy, A 2008, 'Effect of intrinsic coal properties on self-heating rates', in *Proceedings of the 12th US/North American Mine Ventilation Symposium*, pp. 149-53.

Beamish, B & Beamish, R 2010, 'Benchmarking moist coal adiabatic oven testing', paper presented to Proceedings of the 2010 Coal Operators' Conference.

Beamish, B & Beamish, R 2011, 'Experience with using a moist coal adiabatic oven testing method for spontaneous combustion assessment', in *Proceedings of the 2011 Coal Operators' Conference*.

Beamish, B, Edwards, D & Theiler, J 2018, 'Implementation of interactive spontaneous combustion hazard assessment and management at Meandu mine', paper presented to Proceedings of the 18th Coal Operators' Conference.

Beamish, BB, Barakat, MA & George, JDS 2001, 'Spontaneous-combustion propensity of New Zealand coals under adiabatic conditions', *International Journal of Coal Geology*, vol. 45, no. 2-3, pp. 217-24.

Beamish, BB, Barakat, MA & St George, JD 2000, 'Adiabatic testing procedures for determining the self-heating propensity of coal and sample ageing effects', *Thermochimica Acta*, vol. 362, no. 1-2, pp. 79-87.

Beamish, BB & Blazak, DG 2005, 'Relationship between ash content and R_{70} self-heating rate of Callide coal', *International Journal of Coal Geology*, vol. 64, no. 1-2, pp. 126-32.

Beamish, BB & Theiler, J 2019, 'Coal spontaneous combustion: Examples of the self-heating incubation process', *International Journal of Coal Geology*, vol. 215.

Bob, G 2004, *Southland heating and mine fire-Part 1*, Australia's Mining Monthly, viewed September 13 2021, <https://www.miningmonthly.com/markets/international-coal-news/1284859/southland-heating>.

British Petroleum 2020, *Statistical review of world energy 2020*.

Brodny, J & Tutak, M 2016, 'Determination of the zone endangered by methane explosion in goaf with caving of longwalls ventilated on "Y" system', *Management Systems in Production Engineering*.

Brodny, J & Tutak, M 2018, 'Determination of the Zone with a Particularly High Risk of Endogenous Fires in the Goaves of a Longwall with Caving', *Journal of Applied Fluid Mechanics*, vol. 11, no. 3, pp. 545-53.

Brune, JF, Grubb, JW, Bogin, GE, Marts, JA, Gilmore, RC & Saki, SA 2016, 'Lessons learned from research about methane explosive gas zones in coal mine gobs', *International Journal of Mining and Mineral Engineering*, vol. 7, no. 2, pp. 155-69.

Brune, JF, Grubb, JW, Bogin jr, GE, Zipf jr, RK, Marts, J, Gilmore, RC, Ion, SL & Saki, SA 2015, 'A critical look at longwall bleeder ventilation', paper presented to 15th North American Mine Ventilation Symposium.

Brune, JF & Saki, SA 2017, 'Prevention of gob ignitions and explosions in longwall mining using dynamic seals', *International Journal of Mining Science and Technology*, vol. 27, no. 6, pp. 999-1003.

Cai, J, Yang, S, Hu, X, Song, W, Xu, Q, Zhou, B & Song, Y 2019, 'Forecast of coal spontaneous combustion based on the variations of functional groups and microcrystalline structure during low-temperature oxidation', *Fuel*, vol. 253, pp. 339-48.

Cai, X, Nie, W, Yin, S, Liu, Q, Hua, Y, Guo, L, Cheng, L & Ma, Q 2021, 'An assessment of the dust suppression performance of a hybrid ventilation system during the tunnel excavation process: Numerical simulation', *Process Safety and Environmental Protection*, vol. 152, pp. 304-17.

Cao, C, Zhao, J & Ding, H 2018a, 'Dust removal of large cross-section tunnels: following ventilation and its adjustment strategy', *Journal of the Brazilian Society of Mechanical Sciences and Engineering*, vol. 40, no. 10.

Cao, C, Zhao, J & Ding, H 2018b, 'Ventilation system arrangement in large cross-section tunnels: A CFD simulation based on direct initial concentration assessment', *International Journal of Environmental Health Research*, pp. 1-11.

Chang, P, Chen, Y, Xu, G, Huang, J, Ghosh, A & Liu, WV 2019, 'Numerical study of coal dust behaviours and experimental investigation on coal dust suppression efficiency of surfactant solution by using wind tunnel tests', *Energy Sources, Part A: Recovery, Utilization, and Environmental Effects*, pp. 1-16.

Chen, L, Yang, J & Ding, P 2020a, 'Dynamic evolution of negative pressure impact of cross-cut on oxygen concentration field in coal mine Goaf', *Heat and Mass Transfer*, pp. 1-13.

Chen, W, Liu, Y, Huang, X & Rong, Y 2012, 'Respiratory diseases among dust exposed workers', *Respiratory Diseases*, p. 131.

Chen, X, Bi, R, Huang, J, Shan, W, Xiao, J & Wang, D 2020b, 'Experimental study on early prediction index gas for spontaneous combustion', *Energy Sources, Part A: Recovery, Utilization, and Environmental Effects*, pp. 1-15.

Cheng, J, Li, S, Zhang, F, Zhao, C, Yang, S & Ghosh, A 2016a, 'CFD modelling of ventilation optimization for improving mine safety in longwall working faces', *Journal of Loss Prevention in the Process Industries*, vol. 40, pp. 285-97.

Cheng, J, Ma, Y, Lu, W, Liu, G & Cai, F 2022, 'Using inverting CO critical value to predict coal spontaneous combustion severity in mine gobs with considering air leakages–A case study', *Process Safety and Environmental Protection*, vol. 167, pp. 45-55.

Cheng, W, Yu, H, Zhou, G & Nie, W 2016b, 'The diffusion and pollution mechanisms of airborne dusts in fully-mechanized excavation face at mesoscopic scale based on CFD-DEM', *Process Safety and Environmental Protection*, vol. 104, pp. 240-53.

Chu, T, Li, P & Chen, Y 2018, 'Risk assessment of gas control and spontaneous combustion of coal under gas drainage of an upper tunnel', *International Journal of Mining Science and Technology*, vol. 29, no. 3, pp. 491-8.

Claassen, C 2011, 'Goaf inertisation and sealing utilising methane from in-seam gas drainage system', paper presented to Proceedings of the 2011 Coal Operators' Conference.

Cliff, D 2015, *Spontaneous combustion in Australian coal mines*, published by Simtars, Redbank, Queensland, Australia.

Cliff, D, Brady, D & Watkinson, M 2014, 'Developments in the management of spontaneous combustion in Australian underground coal mines', paper presented to 14th Coal Operators' Conference.

Coal Services 2010, *Annual report 2009-2010*, Coal Services, New South Wales.

Coal Services 2017, *2017 NSW coal airborne dust results*, Coal Services, NSW.

Coal Services 2020, *Coal Services annual report 2019-2020*, Coal Services.

Coal Workers' Pneumoconiosis Select Committee 2017, *Inquiry into the re-identification of Coal Workers' Pneumoconiosis in Queensland*.

Davis, J & Byrne, J 1924, 'An adiabatic method for studying spontaneous heating of coal', *Journal of the American Ceramic Society*, vol. 7, no. 11, pp. 809-16.

Deng, J, Lei, C, Xiao, Y, Cao, K, Ma, L, Wang, W & Laiwang, B 2018, 'Determination and prediction on "three zones" of coal spontaneous combustion in a gob of fully mechanized caving face', *Fuel*, vol. 211, pp. 458-70.

Deng, J, Zhao, J, Zhang, Y, Huang, A, Liu, X, Zhai, X & Wang, C 2016, 'Thermal analysis of spontaneous combustion behavior of partially oxidized coal', *Process Safety and Environmental Protection*, vol. 104, pp. 218-24.

Esterhuizen, G & Karacan, C 2007, 'A methodology for determining gob permeability distributions and its application to reservoir modeling of coal mine longwalls'.

Fishwick, D & Barber, C 2012, 'Pneumoconiosis', *Medicine*, vol. 40, no. 6, pp. 310-3.

Flowers, T & Stewart, J 2011, *Investigation report-Fire and explosion on Longwall No 1 tailgate at the Blakefield South Mine*, NSW Trade & Investment, NSW Trade & Investment.

Gao, K, Qi, Z, Jia, J, Li, S, Liu, Z & Liu, Z 2020, 'Investigation of coupled control of gas accumulation and spontaneous combustion in the goaf of coal mine', *AIP Advances*, vol. 10, no. 4, p. 045314.

Geng, F, Gui, C, Teng, H, Tang, J, Niu, H, Zhou, F, Liu, C, Hu, S & Li, S 2020, 'Dispersion characteristics of dust pollutant in a typical coal roadway under an auxiliary ventilation system', *Journal of Cleaner Production*, vol. 275.

Geng, F, Luo, G, Wang, Y, Peng, Z, Hu, S, Zhang, T & Chai, H 2018, 'Dust dispersion in a coal roadway driven by a hybrid ventilation system: A numerical study', *Process Safety and Environmental Protection*, vol. 113, pp. 388-400.

Geng, F, Luo, G, Zhou, F, Zhao, P, Ma, L, Chai, H & Zhang, T 2017, 'Numerical investigation of dust dispersion in a coal roadway with hybrid ventilation system', *Powder Technology*, vol. 313, pp. 260-71.

Gilmore, R, Brune, J, Lolon, S, Juganda, A, Saki, S, Bogin Jr, G, Zipf Jr, R & Grubb, J 2016, 'Explosive gas zone formation in underground coal longwall bleeder ventilated gobs with an adjacent panel using CFD modeling', in *Proceeding of SME Annual Conference and Exhibit, Phoenix*.

Gilmore, R, Marts, J, Brune, J, Bogin Jr, G, Grubb, J & Saki, S 2014, 'CFD modeling explosion hazards-bleeder vs. progressively sealed gobs', in *10th International Mine Ventilation Congress*, pp. 47-53.

Gilmore, R, Marts, J, Brune, J, Saki, S, Bogin Jr, G & Grubb, J 2015, 'Impact of regulator settings on the formation of explosive gas zones in bleeder ventilated longwall gobs', in *SME Annual Meeting, Denver*, pp. 15-086.

Gluyas, A 2019, *Peabody starts North Goonyella re-entry following fire*, Australian Mining, viewed September 13 2021, <https://www.australianmining.com.au/news/peabody-starts-north-goonyella-re-entry-following-fire/>.

Gong, X, Jia, C, Sun, K, Cui, J, Lei, K, Xue, Y & Xue, H 2019, 'Distribution Law and Prediction Model of Dust Concentration under Airflow Adjustment in Fully Mechanized Heading Face', *Mathematical Problems in Engineering*, vol. 2019, pp. 1-17.

Graber, JM, Harris, G, Almberg, KS, Rose, CS, Petsonk, EL & Cohen, RA 2017, 'Increasing severity of pneumoconiosis among younger former US coal miners working exclusively under modern dust-control regulations', *Journal of Occupational Environmental Medicine*, vol. 59, no. 6, pp. e105-e11.

Graham, J 1920, 'The normal production of carbon monoxide in coal-mines', *Transaction Institution of Mining Engineers*, vol. 60, pp. 1920-21.

Gui, X, Xue, H, Zhan, X, Hu, Z & Song, X 2022, 'Measurement and Numerical Simulation of Coal Spontaneous Combustion in Goaf under Y-type Ventilation Mode', *ACS Omega*.

Guo, C, Nie, W, Xu, C, Peng, H, Zhang, C, Li, S, Yue, N, Liu, Z, Yang, S, Ma, Q & Li, M 2020a, 'A study of the spray atomization and suppression of tunnel dust pollution based on a CFD-based simulation', *Journal of Cleaner Production*, vol. 276.

Guo, H, Todhunter, C, Qu, Q & Qin, Z 2015, 'Longwall horizontal gas drainage through goaf pressure control', *International Journal of Coal Geology*, vol. 150, pp. 276-86.

Guo, H, Yuan, L, Shen, B, Qu, Q & Xue, J 2012, 'Mining-induced strata stress changes, fractures and gas flow dynamics in multi-seam longwall mining', *International Journal of Rock Mechanics and Mining Sciences*, vol. 54, pp. 129-39.

Guo, L, Nie, W, Yin, S, Liu, Q, Hua, Y, Cheng, L, Cai, X, Xiu, Z & Du, T 2020b, 'The dust diffusion modeling and determination of optimal airflow rate for removing the dust generated during mine tunneling', *Building and Environment*, vol. 178.

Ham, B 2005, 'A review of spontaneous combustion incidents', paper presented to Proceedings of the 2005 Coal Operators' Conference.

Hargreaves, D & Lowndes, I 2007, 'The computational modeling of the ventilation flows within a rapid development drivage', *Tunnelling and Underground Space Technology*, vol. 22, no. 2, pp. 150-60.

Heerden, J & Sullivan, P 1993, 'The application of CFD for evaluation of dust suppression and auxiliary ventilating systems used with continuous miners', in *Proceeding of The 6th US Mine Ventilation Symposium*, pp. 293-7.

Hou, Z, Yang, S, Shao, H, Zhou, B, Cai, J & Miao, J 2022, 'Identification of zones with coal spontaneous combustion hazards in the three goafs surrounding an isolated Island working face: A case study on Qianyingzi Coal Mine', *Combustion Science and Technology*, pp. 1-23.

Hu, S, Feng, G, Ren, X, Xu, G, Chang, P, Wang, Z, Zhang, Y, Li, Z & Gao, Q 2016, 'Numerical study of gas–solid two-phase flow in a coal roadway after blasting', *Advanced Powder Technology*, vol. 27, no. 4, pp. 1607-17.

Hu, S, Gao, Y, Feng, G, Huang, Y, Shao, H, Liao, Q & Hu, F 2021, 'Characteristics of dust distributions and dust control measures around road-header drivers in mining excavation roadways', *Particuology*, vol. 58, pp. 268-75.

Hu, S, Liao, Q, Feng, G, Huang, Y, Shao, H, Fan, Y & Ye, Y 2019, 'Numerical study of gas-solid two-phase flow around road-header drivers in a fully mechanized excavation face', *Powder Technology*, vol. 344, pp. 959-69.

Hu, S, Liao, Q, Feng, G, Huang, Y, Shao, H, Gao, Y & Hu, F 2020, 'Influences of ventilation velocity on dust dispersion in coal roadways', *Powder Technology*, vol. 360, pp. 683-94.

Hu, S, Wang, Z & Feng, G 2015, 'Temporal and Spatial Distribution of Respirable Dust After Blasting of Coal Roadway Driving Faces: A Case Study', *Minerals*, vol. 5, no. 4, pp. 679-92.

Hua, Y, Nie, W, Cai, P, Liu, Y, Peng, H & Liu, Q 2018a, 'Pattern characterization concerning spatial and temporal evolution of dust pollution associated with two typical ventilation methods at fully mechanized excavation faces in rock tunnels', *Powder Technology*, vol. 334, pp. 117-31.

Hua, Y, Nie, W, Liu, Q, Peng, H, Wei, W & Cai, P 2020a, 'The development and application of a novel multi-radial-vortex-based ventilation system for dust removal in a fully mechanized tunnelling face', *Tunnelling and Underground Space Technology*, vol. 98.

Hua, Y, Nie, W, Liu, Q, Yin, S & Peng, H 2020b, 'Effect of wind curtain on dust extraction in rock tunnel working face: CFD and field measurement analysis', *Energy*, vol. 197.

Hua, Y, Nie, W, Wei, W, Liu, Q, Liu, Y & Peng, H 2018b, 'Research on multi-radial swirling flow for optimal control of dust dispersion and pollution at a fully mechanized tunnelling face', *Tunnelling and Underground Space Technology*, vol. 79, pp. 293-303.

Huang, Z, Ma, Z, Song, S, Yang, R, Gao, Y & Zhang, Y 2018, 'Study on the influence of periodic weighting on the spontaneous combustion "three-zone" in a gob', *Journal of Loss Prevention in the Process Industries*, vol. 55, pp. 480-91.

MaE Department of Natural Resources 2019, *Methane management in underground coal mines-Best practice and recommendations*, by Inspectorate, M.

International Energy Agency 2020, *Coal 2020-Analysis and forecast to 2025*, International Energy Agency,.

Jiang, W, Xu, X, Wen, Z & Wei, L 2021, 'Applying the similarity theory to model dust dispersion during coal-mine tunneling', *Process Safety and Environmental Protection*, vol. 148, pp. 415-27.

Joy, GJ, Colinet, JF & Landen, DD 2012, 'Coal workers' pneumoconiosis prevalence disparity between Australia and the United States', *Mining Engineering*.

Juganda, A, Strebinger, C, Brune, JF & Bogin, GE 2020, 'Discrete modeling of a longwall coal mine gob for CFD simulation', *International Journal of Mining Science and Technology*, vol. 30, no. 4, pp. 463-9.

Kang, H, Lv, H, Zhang, X, Gao, F, Wu, Z & Wang, Z 2016, 'Evaluation of the ground response of a pre-driven longwall recovery room supported by concrete cribs', *Rock Mechanics and Rock Engineering*, vol. 49, pp. 1025-40.

Karacan, C 2008, ‘A new method to calculate permeability of gob for air leakage calculations and for improvements in methane control’, *National Institute of Occupational Safety and Health (NIOSH), Office of Mine Safety and Health Research, Pittsburgh*.

Karacan, C, Ren, T & Balusu, R 2008, ‘Advances in grid-based numerical modeling techniques for improving gas management in coal mines’, paper presented to 12th US/North American Mine Ventilation Symposium.

Krawczyk, J 2020, ‘A preliminary study on selected methods of modeling the effect of shearer operation on methane propagation and ventilation at longwalls’, *International Journal of Mining Science and Technology*, vol. 30, no. 5, pp. 675-82.

Kurnia, JC, Sasmito, AP, Hassani, FP & Mujumdar, AS 2015, ‘Introduction and evaluation of a novel hybrid brattice for improved dust control in underground mining faces: A computational study’, *International Journal of Mining Science and Technology*, vol. 25, no. 4, pp. 537-43.

Levi, T, Beamish, B, Brown, R, J., T & Pope, J 2015, ‘Early detection of spontaneous combustion using laboratory gas evolution tests’, in *Proceedings of the 24th International Mining Congress of Turkey*.

Li, L, Qin, B, Liu, J, Leong, Y-K, Li, W, Zeng, J, Ma, D & Zhuo, H 2021a, ‘Influence of airflow movement on methane migration in coal mine goafs with spontaneous coal combustion’, *Process Safety and Environmental Protection*, vol. 156, pp. 405-16.

Li, M, Aminossadati, SM & Wu, C 2016, ‘Numerical simulation of air ventilation in super-large underground developments’, *Tunnelling and Underground Space Technology*, vol. 52, pp. 38-43.

Li, S, Zhou, G, Wang, Y, Jing, B & Qu, Y 2019, ‘Synthesis and characteristics of fire extinguishing gel with high water absorption for coal mines’, *Process Safety and Environmental Protection*, vol. 125, pp. 207-18.

Li, T, Wu, B, Lei, B & Huang, Q 2020a, ‘Study on air leakage and gas distribution in goaf of Y-type ventilation system’, *Energy Sources, Part A: Recovery, Utilization, and Environmental Effects*, pp. 1-14.

Li, X, Wang, C, Chen, Y, Tang, J & Li, Y 2018, ‘Design of gas drainage modes based on gas emission rate in a gob: a simulation study’, *Arabian Journal of Geosciences*, vol. 11, no. 16, pp. 1-12.

Li, Y, Su, H, Ji, H & Cheng, W 2020b, ‘Numerical simulation to determine the gas explosion risk in longwall goaf areas: A case study of Xutuan Colliery’, *International Journal of Mining Science and Technology*, vol. 30, no. 6, pp. 875-82.

Li, Z 2008, 'CFD simulation of spontaneous coal combustion in irregular patterns of goaf with multiple points of leaking air', *Journal of China University of Mining and Technology*, vol. 18, no. 4, pp. 504-15.

Li, Z, Lu, Z, Qiang, W & Zhang, A 2007, 'Numerical simulation study of goaf methane drainage and spontaneous combustion coupling', *Journal of China University of Mining and Technology*, vol. 17, no. 4, pp. 503-7.

Li, Z, Xu, Y, Liu, H, Zhai, X, Zhao, S & Yu, Z 2021b, 'Numerical analysis on the potential danger zone of compound hazard in gob under mining condition', *Process Safety and Environmental Protection*, vol. 147, pp. 1125-34.

Liang, Y, Zhang, J, Wang, L, Luo, H & Ren, T 2019, 'Forecasting spontaneous combustion of coal in underground coal mines by index gases: A review', *Journal of Loss Prevention in the Process Industries*, vol. 57, pp. 208-22.

Liu, A 2019, 'Abnormal Gas Emission and Explosion in Underground Coal Mines-A Computational Modelling Study', Doctor of Philosophy thesis, University of Wollongong.

Liu, H, Wang, F, Ren, T, Qiao, M & Yan, J 2021, 'Influence of methane on the prediction index gases of coal spontaneous combustion: A case study in Xishan coalfield, China', *Fuel*, vol. 289.

Liu, H, Wu, X, Mao, S, Li, M & Yue, J 2017, 'A time varying ventilation and dust control strategy based on the temporospatial characteristics of dust dispersion', *Minerals*, vol. 7, no. 4.

Liu, J, Gao, J, Yang, M, Wang, D & Wang, L 2019a, 'Numerical simulation of parameters optimization for goaf gas boreholes', *Advances in Civil Engineering*, vol. 2019.

Liu, M, Shi, G, Guo, Z, Wang, Y & Ma, L 2016a, '3-D simulation of gases transport under condition of inert gas injection into goaf', *Heat and Mass Transfer*, vol. 52, no. 12, pp. 2723-34.

Liu, Q, Lin, B, Zhou, Y, Li, Y & Ting, L 2022, 'Experimental verification of permeability and inertial resistance coefficient model in the goaf', *Energy Sources, Part A: Recovery, Utilization, and Environmental Effects*, pp. 1-20.

Liu, Q, Nie, W, Hua, Y, Peng, H, Liu, C & Wei, C 2019b, 'Research on tunnel ventilation systems: Dust diffusion and pollution behaviour by air curtains based on CFD technology and field measurement', *Building and Environment*, vol. 147, pp. 444-60.

Liu, Q, Nie, W, Hua, Y, Peng, H & Liu, Z 2018, 'The effects of the installation position of a multi-radial swirling air-curtain generator on dust diffusion and pollution rules in a fully-mechanized excavation face: A case study', *Powder Technology*, vol. 329, pp. 371-85.

Liu, R, Li, Y, Wang, P, Shu, W & Gou, S 2019c, 'Influence of the ratio of the blowing and sucking flow on the wall-rotating circulating airflow in fully mechanized excavation face', in *Proceedings of the 11th International Mine Ventilation Congress*, pp. 49-57.

Liu, S, Wu, Y, Zhou, C, Wu, J & Zhang, Y 2020a, 'Study on the CO Formation Mechanism during Coal Ambient Temperature Oxidation', *Energies*, vol. 13, no. 10, p. 2587.

Liu, W & Qin, Y 2017a, 'Multi-physics coupling model of coal spontaneous combustion in longwall gob area based on moving coordinates', *Fuel*, vol. 188, pp. 553-66.

Liu, W & Qin, Y 2017b, 'A quantitative approach to evaluate risks of spontaneous combustion in longwall gobs based on CO emissions at upper corner', *Fuel*, vol. 210, pp. 359-70.

Liu, W, Qin, Y, Shi, C & Guo, D 2019d, 'Dynamic evolution of spontaneous combustion of coal in longwall gobs during mining-stopped period', *Process Safety and Environmental Protection*, vol. 132, pp. 11-21.

Liu, Y, Shao, S, Wang, X, Chang, L, Cui, G & Zhou, F 2016b, 'Gas flow analysis for the impact of gob gas ventholes on coalbed methane drainage from a longwall gob', *Journal of Natural Gas Science and Engineering*, vol. 36, pp. 1312-25.

Liu, Y, Wen, H, Guo, J, Jin, Y, Wei, G & Yang, Z 2020b, 'Coal spontaneous combustion and N2 suppression in triple goafs: A numerical simulation and experimental study', *Fuel*, vol. 271.

Liu, Z, Nie, W, Peng, H, Yang, S, Chen, D & Liu, Q 2019e, 'The effects of the spraying pressure and nozzle orifice diameter on the atomizing rules and dust suppression performances of an external spraying system in a fully-mechanized excavation face', *Powder Technology*, vol. 350, pp. 62-80.

Loane, E, Bulloch, R, Carthew, J, Maesall, R & Rowlands, D 1975, *Kianga No. 1 underground mine accident: report of the Warden's inquiry*, Queensland.

Lolon, SA, Brune, JF, Bogin, GE & Juganda, A 2020, 'Study of methane outgassing and mitigation in longwall coal mines', *Mining, Metallurgy & Exploration*, vol. 37, no. 5, pp. 1437-49.

Lolon, SA, Brune, JF, Bogin Jr, GE, Grubb, JW, Saki, SA & Juganda, A 2017, 'Computational fluid dynamics simulation on the longwall gob breathing', *International Journal of Mining Science and Technology*, vol. 27, no. 2, pp. 185-9.

Lu, X, Shen, C, Xing, Y, Zhang, H, Wang, C, Shi, G-y & Wang, M 2022a, 'The spatial diffusion rule and pollution region of disorganized dust in the excavation roadway at different roadheader cutting positions', *Powder Technology*, vol. 396, pp. 167-80.

Lu, X, Wang, C, Shen, C, Wang, M & Xing, Y 2022b, 'Verisimilar research on the dust movement in the underground tunneling at the roadheader cutterhead dynamic rotation', *Energy*, vol. 238.

Lu, Y, Gu, W, Wang, G, Li, H, Shi, S, Niu, H & Ye, Q 2020a, 'Numerical assessment of the influences of the coal spontaneous combustion on gas drainage methods optimization and Its application', *Combustion Science and Technology*, pp. 1-17.

Lu, Y, Liu, Y, Shi, S, Wang, GG, Li, H & Wang, T 2020b, 'Micro-particles stabilized aqueous foam for coal spontaneous combustion control and its flow characteristics', *Process Safety and Environmental Protection*, vol. 139, pp. 262-72.

Ma, D, Qin, B, Li, L, Gao, A & Gao, Y 2019, 'Study on the methane explosion regions induced by spontaneous combustion of coal in longwall gobs using a scaled-down experiment set-up', *Fuel*, vol. 254.

Ma, L, Guo, R, Wu, M, Wang, W, Ren, L & Wei, G 2020a, 'Determination on the hazard zone of spontaneous coal combustion in the adjacent gob of different mining stages', *Process Safety and Environmental Protection*, vol. 142, pp. 370-9.

Ma, L, Zou, L, Ren, L-F, Chung, Y-H, Zhang, P-Y & Shu, C-M 2020b, 'Prediction indices and limiting parameters of coal spontaneous combustion in the Huainan mining area in China', *Fuel*, vol. 264.

Marts, JA, Gilmore, RC, Brune, JF, Bogin jr, GE, Grubb, JW & Saki, SA 2014a, 'Dynamic gob response and reservoir properties for active longwall coal mines', *Mining Engineering*, vol. 66, no. 12, pp. 59-66.

Marts, JA, Gilmore, RC, Brune, JF, E, BG, Grubb, JW & Saki, SA 2014b, 'Accumulations of explosive gases in longwall gobs and mitigation through nitrogen injection and face ventilation method', in *AIMS 2014–6th International Symposium" High Performance Mining*.

Marts, JA, Gilmore, RC, Brune, JF, Saki, SA, E, BG & Grubb, JW 2015, 'Optimizing nitrogen injection for progressively sealed panels', in *SME 2015 Annual Meeting*, pp. 15-093.

McBean, R, Newbigin, K, Dickinson, S & Edwards, R 2018, 'Radiological appearance of coal mine dust lung diseases in Australian workers', *Journal of Medical Imaging Radiation Oncology*, vol. 62, no. 6, pp. 794-7.

Mishra, DP, Kumar, P & Panigrahi, DC 2016, 'Dispersion of methane in tailgate of a retreating longwall mine: a computational fluid dynamics study', *Environmental Earth Sciences*, vol. 75, no. 6, p. 475.

Mishra, DP, Panigrahi, DC & Kumar, P 2018, 'Computational investigation on effects of geo-mining parameters on layering and dispersion of methane in underground coal mines-A case study of Moonidih Colliery', *Journal of Natural Gas Science and Engineering*, vol. 53, pp. 110-24.

Mishra, DP, Sahu, A & Panigrahi, DC 2019, 'Design of auxiliary ventilation system for effective dust dispersion in underground coal mine development heading—A computational simulation approach', in *Proceedings of the 11th International Mine Ventilation Congress*, pp. 146-58.

Morla, R, Balusu, R, Tanguturi, K & Khanal, M 2013, 'Prediction and control of spontaneous combustion in thick coal seams', paper presented to Proceedings of the 2013 Coal Operators' Conference.

MfRa Energy 2002, *Coal Mine Health and Safety Act 2002 No 129*, by New South Wales, Parliamentary Counsel's Office.

NEWS 2020, *Moranbah mine explosion leaves five people in serious condition*, <https://www.abc.net.au/news/2020-05-06/moranbah-mine-explosion-five-people-injured/12220924>.

Nie, W, Cai, X, Peng, H, Ma, Q, Liu, Q, Hua, Y, Guo, L, Cheng, L, Sun, N & Bao, Q 2022a, 'Distribution characteristics of an airflow–dust mixture and quantitative analysis of the dust absorption effect during tunnel sub-regional coal cutting', *Process Safety and Environmental Protection*, vol. 164, pp. 319-34.

Nie, W, Cheng, L, Yin, S, Liu, Q, Hua, Y, Guo, L, Cai, X, Ma, Q & Guo, C 2022b, 'Effects of press-in airflow rate and the distance between the pressure duct and the side wall on ventilation dust suppression performance in an excavating tunnel', *Environmental Science and Pollution Research*, vol. 29, no. 13, pp. 19404-19.

Nie, W, Guo, C, Zhang, S, Peng, H, Xu, C, Ma, Q, Yuan, M, Zhou, W, Guo, L & Cheng, L 2022c, 'Optimization of spraying dust reduction technology of continuous miner machine and the dust environment in a tunnel, based on computational fluid dynamics (CFD) technology', *Powder Technology*, vol. 398.

Nie, W, Hua, Y, Zhou, W, Liu, Q, Cai, X & Cheng, L 2022d, 'Design and application of a dust suppression technology of the forcing air curtain in fully mechanized rock tunnelling faces', *Environmental Science and Pollution Research*, vol. 29, no. 23, pp. 34943-54.

Niu, W, Jiang, Z & Tian, D 2011, 'Numerical simulation of the factors influencing dust in drilling tunnels: Its application', *Mining Science and Technology (China)*, vol. 21, no. 1, pp. 11-5.

MSOB NSW Department of Industry and Innovation 2011a, *MDG 1006-Spontaneous combustion management guideline*, by NSW Department of Industry and Investment.

MSOB NSW Department of Industry and Innovation 2011b, *MDG 1006 -Technical reference for spontaneous combustion management guideline*, by NSW Department of Industry and Investment.

NSW Government 2020, *Standards for respirable dust*, viewed May 22 2022, <https://www.resourcesregulator.nsw.gov.au/safety/health-and-safety-management/dust-diseases>.

NSW Government 2021, *Dust diseases*, viewed 11 April 2021, <https://www.resourcesregulator.nsw.gov.au/safety-and-health/topics/dust-diseases>.

2016, *Preparing a principal hazard management plan*, by NSW Resources Regulator, NSW Resources Regulator.

NSW Resources Regulator 2019, *Causal investigation report - Workers evacuated after gas levels rise*.

NSW South Wales 2021, *Work Health and Safety (Mines and Petroleum Sites) Regulation 2014*, NSW legislation, NSW.

Onifade, M & Genc, B 2020, 'A review of research on spontaneous combustion of coal', *International Journal of Mining Science and Technology*, vol. 30, no. 3, pp. 303-11.

Parliament of Australia 2016, *Fifth interim report-Black Lung: "It has buggered my life"*.

Parra, M, Villafruela, J, Castro, F & Mendez, C 2006, 'Numerical and experimental analysis of different ventilation systems in deep mines', *Building and Environment*, vol. 41, no. 2, pp. 87-93.

Penrose, B 2020, '" Re-Emergence" of silicosis and coal workers pneumoconiosis in Australia', *Labour History: A Journal of Labour and Social History*, vol. 119, no. 1, pp. 65-92.

Qi, Y, Wang, W, Qi, Q, Ning, Z & Yao, Y 2021, 'Distribution of spontaneous combustion three zones and optimization of nitrogen injection location in the goaf of a fully mechanized top coal caving face', *PLoS One*, vol. 16, no. 9, p. e0256911.

Qian, M & Xu, J 1998, 'Study on the "O-shape" circle distribution characteristics of mining induced fractures in the overlaying strata', *Journal of China Coal Society*, vol. 23, no. 5, pp. 466-9.

Qiao, M, Ren, T, Roberts, J, Liu, H, Yang, X, Tan, L & Wu, J 2022a, 'Improved computational fluid dynamics modelling of coal spontaneous combustion control and gas management', *Fuel*, vol. 324, p. 124456.

Qiao, M, Ren, T, Roberts, J, Yang, X, Li, Z & Wu, J 2022b, 'New insight into proactive goaf inertisation for spontaneous combustion management and control', *Process Safety and Environmental Protection*, vol. 161, pp. 739-57.

Qin, B, Li, L, Ma, D, Lu, Y, Zhong, X & Jia, Y 2016a, 'Control technology for the avoidance of the simultaneous occurrence of a methane explosion and spontaneous coal combustion in a coal mine: A case study', *Process Safety and Environmental Protection*, vol. 103, pp. 203-11.

Qin, B, Lu, Y, Li, Y & Wang, D 2014, 'Aqueous three-phase foam supported by fly ash for coal spontaneous combustion prevention and control', *Advanced Powder Technology*, vol. 25, no. 5, pp. 1527-33.

Qin, B, Wang, H, Yang, J & Liu, L 2016b, 'Large-area goaf fires: a numerical method for locating high-temperature zones and assessing the effect of liquid nitrogen fire control', *Environmental Earth Sciences*, vol. 75, no. 21, pp. 1-14.

Qin, J, Qu, Q & Guo, H 2017, 'CFD simulations for longwall gas drainage design optimisation', *International Journal of Mining Science and Technology*, vol. 27, no. 5, pp. 777-82.

Qin, Z, Guo, H & Qu, Q 2019, 'Investigation of effect of barometric pressure on gas emission in longwall mining by monitoring and CFD modelling', *International Journal of Coal Geology*, vol. 205, pp. 32-42.

Qin, Z, Yuan, L, Guo, H & Qu, Q 2015, 'Investigation of longwall goaf gas flows and borehole drainage performance by CFD simulation', *International Journal of Coal Geology*, vol. 150, pp. 51-63.

Qu, Q, Guo, H & Loney, M 2016, 'Analysis of longwall goaf gas drainage trials with surface directional boreholes', *International Journal of Coal Geology*, vol. 156, pp. 59-73.

Qu, Q, Xu, J, Wu, R, Qin, W & Hu, G 2015, 'Three-zone characterisation of coupled strata and gas behaviour in multi-seam mining', *International Journal of Rock Mechanics and Mining Sciences*, vol. 78, pp. 91-8.

Queensland Audit Office 2019, *Addressing mine dust lung disease*, Queensland.

Queensland Government 1972, *Box Flat Colliery mining accident inquiry report*.

Queensland Government 2017, *Coal Mining Safety and Health Regulation 2017*, Queensland Government, Queensland, https://www.legislation.qld.gov.au/view/html/inforce/2021-01-01/sl-2017-0165.

Queensland Government 2020, *Dust monitoring data - coal mines*, viewed May 22 2022, <https://www.business.qld.gov.au/industries/mining-energy-water/resources/safety-health/mining/hazards/dust/monitoring-data-coal-mines>.

Queensland Government 2021, *Mine dust lung diseases*, Business Queensland, viewed 11 April 2021, <https://www.business.qld.gov.au/industries/mining-energy-water/resources/safety-health/mining/accidents-incidents-reports/mine-dust-lung-diseases>.

Queensland Mines Inspectorate 2019, *Queensland Mines Inspectorate preliminary observations: North Goonyella high potential incident*.

Ray, S & Singh, R 2007, 'Recent developments and practices to control fire in undergound coal mines', *Fire Technology*, vol. 43, no. 4, pp. 285-300.

Ren, T 2019, *Mine fires and spontaneous heating: Part 2*.

Ren, T & Balusu, R 2005, 'CFD modelling of goaf gas migration to improve the control of spontaneous combustion in longwalls', paper presented to Proceedings of the 2005 Coal Operators' Conference.

Ren, T & Balusu, R 2009, 'Proactive goaf inertisation for controlling longwall goaf heatings', *Procedia Earth and Planetary Science,* vol. 1, no. 1, pp. 309-15.

Ren, T & Balusu, R 2010, 'The use of CFD modelling as a tool for solving mining health and safety problems', paper presented to 10th Underground Coal Operators' Conference.

Ren, T, Balusu, R & Claassen, C 2011, 'Computational fluid dynamics modelling of gas flow dynamics in large longwall goaf areas', paper presented to 35th APCOM Symposium.

Ren, T, Balusu, R & Humphries, P 2005, 'Development of innovative goaf inertisation practices to improve coal mine safety', paper presented to Proceedings of the 2005 Coal Operators' Conference.

Ren, T, Edwards, J & Clarke, D 1999, 'Adiabatic oxidation study on the propensity of pulverised coals to spontaneous combustion', *Fuel,* vol. 78, no. 14, pp. 1611-20.

Ren, T & Wang, Z 2019, 'CFD modelling of ventilation, dust and gas flow dispersion patterns on a longwall face', in *Proceedings of the 11th International Mine Ventilation Congress,* pp. 198-208.

Ren, T, Wang, Z, Liang, Y & Zhang, J 2018a, 'Numerical investigation of CO2 fringe behaviour on a longwall face and its control', *International Journal of Coal Geology*, vol. 186, pp. 80-96.

Ren, T, Wang, Z, Nemcik, J, Aziz, N & Wu, J 2012, 'Investigation of spontaneous heating zones and proactive inertisation of longwall goaf in Fenguangshan Mine', paper presented to 12th Coal Operators' Conference.

Ren, T, Wang, Z & Zhang, J 2018b, 'Improved dust management at a longwall top coal caving (LTCC) face – A CFD modelling approach', *Advanced Powder Technology*, vol. 29, no. 10, pp. 2368-79.

Ren, W, Guo, Q & Yang, H 2018c, 'Analyses and prevention of coal spontaneous combustion risk in gobs of coal mine during withdrawal period', *Geomatics, Natural Hazards and Risk*.

Roberts, J, Wypych, P, Hastie, D & Liao, R 2022, 'Analysis and validation of a CFD-DPM method for simulating dust suppression sprays', *Particulate Science and Technology*, vol. 40, no. 4, pp. 415-26.

Said, KO, Onifade, M, Genc, B, Lawal, AI, Abdulsalam, J, Githiria, JM & Bada, S 2021, 'On the dependence of predictive models on experimental dataset: a spontaneous combustion studies scenario', *International journal of mining, reclamation and environment,* pp. 1-17.

Saki, SA, Brune, JF & Khan, MU 2020, 'Optimization of gob ventilation boreholes design in longwall mining', *International Journal of Mining Science and Technology*, vol. 30, no. 6, pp. 811-7.

Saki, SA, Marts, JA, Gilmore, RC, Brune, JF, Bogin, GE & Grubb, JW 2015, 'CFD study of face ventilation effect on tailgate methane concentration and explosive mixture of gob in underground longwall coal mining', in *Society for Mining, Metallurgy and Exploration 2015 Annual Meeting*, pp. 15-001.

Salisbury, O, Linde, G & Beamish, B 2022, 'Some operational perspectives on spontaneous combustion management of a longwall goaf', paper presented to 2022 Resource Operators Conference, University of Wollongong.

Şensöğüt, C 2011, 'Spontaneous combustion related fire ratios', *Pamukkale Üniversitesi Mühendislik Bilimleri Dergisi*, vol. 5, no. 1.

Shen, R, Jiao, Z, Parker, T, Sun, Y & Wang, Q 2020, 'Recent application of Computational Fluid Dynamics (CFD) in process safety and loss prevention: A review', *Journal of Loss Prevention in the Process Industries*, vol. 67, p. 104252.

Shi, G, Ding, P, Guo, Z & Wang, Y 2019, 'Modeling temperature distribution upon liquid-nitrogen injection into a self heating coal mine goaf', *Process Safety and Environmental Protection*, vol. 126, pp. 278-86.

Shi, G, Liu, M, Guo, Z, Hu, F & Wang, D 2017, 'Unsteady simulation for optimal arrangement of dedusting airduct in coal mine heading face', *Journal of Loss Prevention in the Process Industries*, vol. 46, pp. 45-53.

Shi, G, Liu, M, Wang, Y, Wang, W & Wang, D 2015, 'Computational fluid dynamics simulation of oxygen seepage in coal mine goaf with gas drainage', *Mathematical Problems in Engineering*, vol. 2015.

Shi, G, Wang, G, Ding, P & Wang, Y 2021, 'Model and simulation analysis of fire development and gas flowing influenced by fire zone sealing in coal mine', *Process Safety and Environmental Protection*, vol. 149, pp. 631-42.

Shi, Q, Qin, B, Hao, Y & Li, H 2022, 'Experimental investigation of the flow and extinguishment characteristics of gel-stabilized foam used to control coal fire', *Energy*, p. 123484.

Si, G & Belle, B 2019, 'Performance analysis of vertical goaf gas drainage holes using gas indicators in Australian coal mines', *International Journal of Coal Geology*, vol. 216, p. 103301.

Si, J, Cheng, G & Zhu, J 2019, 'Optimisation of multisource injection of carbon dioxide into goafs based on orthogonal test and fuzzy comprehensive theory', *Heliyon*, vol. 5, no. 5, p. e01607.

Smith, EB 2017, ‘Black lung in the 21st century: Disease, law, and policy’, *West Virginia Law Review,* vol. 120, p. 797.

Song, S, Zhou, G, Duan, J, Meng, Q, Sun, B & Wang, Y 2021a, ‘CFD simulation of multi-phase and multi-component diffusion of air-dust-gas in a fully mechanized mining face’, *Environmental Science and Pollution Research,* vol. 28, no. 14, pp. 18260-75.

Song, S, Zhou, G, Duan, J, Zhang, L, Gao, D & Sun, B 2021b, ‘Numerical simulation investigation on optimal dust-exhausting airflow volume in fully mechanized caving face of high-gas coal mine’, *Process Safety and Environmental Protection,* vol. 146, pp. 853-66.

Song, Z & Kuenzer, C 2014, ‘Coal fires in China over the last decade: a comprehensive review’, *International Journal of Coal Geology,* vol. 133, pp. 72-99.

Srinivasa, R, Baafi, E, Aziz, N & Singh, R 1993, ‘Three dimensional modeling of air velocities and dust control techniques in a longwall face’, in *Proceeding of The 6th US Mine Ventilation Symposium,* pp. 287-92.

Stewart, G & Hsin, WW 2012, *Analysis of Blakefield South Mine (BSM) explosion,* Brisbane Australia.

Stewart Gillies, HWW 2013, ‘Australian longwall panel ventilation practices’, paper presented to 13th Coal Operators' Conference.

Szurgacz, D, Tutak, M, Brodny, J, Sobik, L & Zhironkina, O 2020, ‘The method of combating coal spontaneous combustion hazard in goafs—a case study’, *Energies,* vol. 13, no. 17, p. 4538.

Tang, M, Jiang, B, Zhang, R, Yin, Z & Dai, G 2016, ‘Numerical analysis on the influence of gas extraction on air leakage in the gob’, *Journal of Natural Gas Science and Engineering,* vol. 33, pp. 278-86.

Tanguturi, K & Balusu, R 2014, ‘CFD modeling of methane gas distribution and control strategies in a gassy coal mine’, *The Journal of Computational Multiphase Flows,* vol. 6, no. 1, pp. 65-77.

Tanguturi, K & Balusu, R 2015, ‘Fundamental understanding of goaf gas displacement in longwall goaf’, *Journal of Mining and Environment,* vol. 6, no. 2, pp. 191-203.

Tanguturi, K, Balusu, R & Belle, B 2020, ‘Gas control in TG motor region in longwall gassy mines’, *Podzemni radovi,* no. 37, pp. 1-18.

Tanguturi, K, Balusu, R, Morla, R & Khanal, M 2013, ‘Effect of buoyancy on methane gas distribution and gas control strategies at tailgate region in a gassy coal mine’, in *9th International Conference on CFD in the minerals and process Industries, Melbourne,* pp. 1-6.

Taraba, B & Michalec, Z 2011, 'Effect of longwall face advance rate on spontaneous heating process in the gob area–CFD modelling', *Fuel*, vol. 90, no. 8, pp. 2790-7.

Terry Martin SC & Clough, A 2021, *Queensland coal mining board of inquiry-PartII*, Queensland Coal Mining Board, State of Queensland.

Thiruvengadam, M, Zheng, Y, Lan, H & Tien, JC 2016, 'A diesel particulate matter dispersion study inside a single dead end entry using dynamic mesh model', *International Journal of Mining and Mineral Engineering*, vol. 7, no. 3.

Tim, F & Jennie, S 2012, *Investigation report-Fire and explosion on longwall No.1 Tailgate at the Blakefield South Mine*, NSW Trade & Investment.

Timko, RJ & Derick, R 2006, 'Methods to determine the status of mine atmospheres-an overview'.

Toraño, J, Torno, S, Menendez, M & Gent, M 2011, 'Auxiliary ventilation in mining roadways driven with roadheaders: Validated CFD modelling of dust behaviour', *Tunnelling and Underground Space Technology*, vol. 26, no. 1, pp. 201-10.

Tutak, M & Brodny, J 2017a, 'Analysis of Influence of Goaf Sealing from Tailgate on the Methane Concentration at the Outlet from the Longwall', in *IOP Conference Series: Earth and Environmental Science*, vol. 95, p. 042025.

Tutak, M & Brodny, J 2017b, 'Determination of particular endogenous fires hazard zones in goaf with caving of longwall', in *IOP Conference Series: Earth and Environmental Science*, vol. 95, p. 042026.

Tutak, M & Brodny, J 2018, 'Analysis of the impact of auxiliary ventilation equipment on the distribution and concentration of methane in the tailgate', *Energies*, vol. 11, no. 11, p. 3076.

Tutak, M & Brodny, J 2019, 'The impact of the strength of roof rocks on the extent of the zone with a high risk of spontaneous coal combustion for fully powered longwalls ventilated with the y-type system—A case study', *Applied Sciences*, vol. 9, no. 24, p. 5315.

Tutak, M, Brodny, J, Szurgacz, D, Sobik, L & Zhironkin, S 2020, 'The impact of the ventilation system on the methane release hazard and spontaneous combustion of coal in the area of exploitation—a case study', *Energies*, vol. 13, no. 18, p. 4891.

Wala, A, Jacob, J, Brown, J & Huang, G 2003, 'New approaches to mine-face ventilation', *Mining Engineering*, vol. 55, no. 3, pp. 25-30.

Wang, C, Yang, S & Li, X 2018a, 'Simulation of the hazard arising from the coupling of gas explosions and spontaneously combustible coal due to the gas drainage of a gob', *Process Safety and Environmental Protection*, vol. 118, pp. 296-306.

Wang, G, Shi, G, Wang, Y & Shen, H 2021a, 'Numerical study on the evolution of methane explosion regions in the process of coal mine fire zone sealing', *Fuel*, vol. 289, p. 119744.

Wang, H, Cheng, W, Sun, B & Ma, Y 2017a, 'Effects of radial air flow quantity and location of an air curtain generator on dust pollution control at fully mechanized working face', *Advanced Powder Technology*, vol. 28, no. 7, pp. 1780-91.

Wang, H, Cheng, W, Sun, B, Yu, H & Jin, H 2018b, 'The impacts of the axial-to-radial airflow quantity ratio and suction distance on air curtain dust control in a fully mechanized coal face', *Environmental Science Pollution Research*, vol. 25, no. 8, pp. 7808-22.

Wang, H, Nie, W, Cheng, W, Liu, Q & Jin, H 2018c, 'Effects of air volume ratio parameters on air curtain dust suppression in a rock tunnel's fully-mechanized working face', *Advanced Powder Technology*, vol. 29, no. 2, pp. 230-44.

Wang, H, Sa, Z, Cheng, W, Zhang, R & Yang, S 2021b, 'Effects of forced-air volume and suction region on the migration and dust suppression of air curtain during fully mechanized tunneling process', *Process Safety and Environmental Protection*, vol. 145, pp. 222-35.

Wang, H, Wang, C & Wang, D 2017b, 'The influence of forced ventilation airflow on water spray for dust suppression on heading face in underground coal mine', *Powder Technology*, vol. 320, pp. 498-510.

Wang, X, Jiang, Z & Liu, Y 2006, 'Numerical simulation of distribution regularities of dust concentration during the ventilation process of coal drift driving with exhaust ventilation', *Journal of Safety Science and Technology*, vol. 2, no. 5.

Wang, X, Luo, Y & Vieira, B 2018d, 'Experimental technique and modeling for evaluating heat of rewetting effect on coals' propensity of spontaneous combustion based on adiabatic oxidation method', *International Journal of Coal Geology*, vol. 187, pp. 1-10.

Wang, Y, Chen, H, Long, R & Yang, M 2020, 'Health economic loss measurement and risk assessment of new cases of coal worker's pneumoconiosis in China', *Safety Science*, vol. 122, p. 104529.

Wang, Y, Luo, G, Geng, F, Li, Y & Li, Y 2015, 'Numerical study on dust movement and dust distribution for hybrid ventilation system in a laneway of coal mine', *Journal of Loss Prevention in the Process Industries*, vol. 36, pp. 146-57.

Wang, Y, Wu, J, Xue, S, Wang, J & Zhang, Y 2017c, 'Experimental study on the molecular hydrogen release mechanism during low-temperature oxidation of coal', *Energy & Fuels*, vol. 31, no. 5, pp. 5498-506.

Wang, Z, Li, S, Ren, T, Wu, J, Lin, H & Shuang, H 2019, 'Respirable dust pollution characteristics within an underground heading face driven with continuous miner – A CFD modelling approach', *Journal of Cleaner Production*, vol. 217, pp. 267-83.

Wang, Z & Ren, T 2013, 'Investigation of airflow and respirable dust flow behaviour above an underground bin', *Powder Technology*, vol. 250, pp. 103-14.

Wang, Z, Ren, T & Cheng, Y 2017d, 'Numerical investigations of methane flow characteristics on a longwall face Part II: Parametric studies', *Journal of Natural Gas Science and Engineering*, vol. 43, pp. 254-67.

Wang, Z, Ren, T & Cheng, Y 2017e, 'Numerical investigations of methane flow characteristics on a longwall face Part I: Methane emission and base model results', *Journal of Natural Gas Science and Engineering*, vol. 43, pp. 242-53.

Wang, Z, Ren, T, Ma, L & Zhang, J 2018e, 'Investigations of ventilation airflow characteristics on a longwall face—A computational approach', *Energies*, vol. 11, no. 6.

Whittles, D, Lowndes, I, Kingman, S, Yates, C & Jobling, S 2006, 'Influence of geotechnical factors on gas flow experienced in a UK longwall coal mine panel', *International Journal of Rock Mechanics and Mining Sciences*, vol. 43, no. 3, pp. 369-87.

Windridge, F, Parkin, R, Neilson, P, Roxborough, F & Ellicott, C 1994, *Moura No.2 underground mine accident: report of the Warden's inquiry*, Queensland.

Xia, T, Zhou, F, Gao, F, Kang, J, Liu, J & Wang, J 2015, 'Simulation of coal self-heating processes in underground methane-rich coal seams', *International Journal of Coal Geology*, vol. 141-142, pp. 1-12.

Xia, T, Zhou, F, Liu, J, Kang, J & Gao, F 2014, 'A fully coupled hydro-thermo-mechanical model for the spontaneous combustion of underground coal seams', *Fuel*, vol. 125, pp. 106-15.

Xia, T, Zhou, F, Wang, X, Kang, J & Pan, Z 2017, 'Safety evaluation of combustion-prone longwall mining gobs induced by gas extraction: A simulation study', *Process Safety and Environmental Protection*, vol. 109, pp. 677-87.

Xia, T, Zhou, F, Wang, X, Zhang, Y, Li, Y, Kang, J & Liu, J 2016, 'Controlling factors of symbiotic disaster between coal gas and spontaneous combustion in longwall mining gobs', *Fuel*, vol. 182, pp. 886-96.

Xu, G, Chang, P, Mullins, B, Zhou, F & Hu, S 2018, 'Numerical study of diesel particulate matter distribution in an underground mine isolated zone', *Powder Technology*, vol. 339, pp. 947-57.

Xu, G, Luxbacher, KD, Ragab, S, Xu, J & Ding, X 2016, 'Computational fluid dynamics applied to mining engineering: a review', *International journal of mining, reclamation and environment*, vol. 31, no. 4, pp. 251-75.

Xu, X, Wei, J, Wang, M, Jiang, W, Wen, Z & Liu, Y 2022, 'Influence of inclination angle on dust migration and settlement characteristics of excavation roadway', *Environmental Science and Pollution Research*.

Xue, Y, Liu, J, Ranjith, P, Gao, F, Xie, H & Wang, J 2022, 'Changes in microstructure and mechanical properties of low-permeability coal induced by pulsating nitrogen fatigue fracturing tests', *Rock Mechanics and Rock Engineering*, vol. 55, no. 12, pp. 7469-88.

Xue, Y, Ranjith, P, Chen, Y, Cai, C, Gao, F & Liu, X 2023, 'Nonlinear mechanical characteristics and damage constitutive model of coal under CO2 adsorption during geological sequestration', *Fuel*, vol. 331, p. 125690.

Yang, S, Hu, X, Liu, WV, Cai, J & Zhou, X 2018, 'Spontaneous combustion influenced by surface methane drainage and its prediction by rescaled range analysis', *International Journal of Mining Science and Technology*, vol. 28, no. 2, pp. 215-21.

Yang, S, Zhou, B & Wang, C 2021, 'Investigation on coal spontaneous combustion in the gob of Y type ventilation caving face: A case study', *Process Safety and Environmental Protection*, vol. 148, pp. 590-603.

Yang, X, Yu, H, Wang, Y & Cheng, W 2022a, 'Investigation of dust pollution control rules in tunnel excavation based on modularized airflow diverging system', *Building and Environment*, vol. 221.

Yang, X, Yu, H, Zhao, J, Cheng, W & Xie, Y 2022b, 'Research on the coupling diffusion law of airflow-dust-gas under the modularized airflow diverging dust control technology', *Powder Technology*, vol. 407.

Yin, S, Nie, W, Guo, L, Liu, Q, Hua, Y, Cai, X, Cheng, L, Yang, B & Zhou, W 2020, 'CFD simulations of air curtain dust removal effect by ventilation parameters during tunneling', *Advanced Powder Technology*, vol. 31, no. 6, pp. 2456-68.

Yin, S, Nie, W, Liu, Q & Hua, Y 2019, 'Transient CFD modelling of space-time evolution of dust pollutants and air-curtain generator position during tunneling', *Journal of Cleaner Production*, vol. 239.

Yu, H, Cheng, W, Peng, H & Xie, Y 2018a, 'An investigation of the nozzle's atomization dust suppression rules in a fully-mechanized excavation face based on the airflow-droplet-dust three-phase coupling model', *Advanced Powder Technology*, vol. 29, no. 4, pp. 941-56.

Yu, H, Cheng, W, Wang, H, Peng, H & Xie, Y 2017a, 'Formation mechanisms of a dust-removal air curtain in a fully-mechanized excavation face and an analysis of its dust-removal performances based on CFD and DEM', *Advanced Powder Technology*, vol. 28, no. 11, pp. 2830-47.

Yu, H, Cheng, W, Wu, L, Wang, H & Xie, Y 2017b, 'Mechanisms of dust diffuse pollution under forced-exhaust ventilation in fully-mechanized excavation faces by CFD-DEM', *Powder Technology*, vol. 317, pp. 31-47.

Yu, H, Cheng, W, Xie, Y & Peng, H 2018b, 'Micro-scale pollution mechanism of dust diffusion in a blasting driving face based on CFD-DEM coupled model', *Environmental Science and Pollution Research* vol. 25, no. 22, pp. 21768-88.

Yu, H, Cheng, W, Xie, Y & Peng, H 2020, 'Spray dedusting scheme under hybrid ventilation at a fully mechanized excavation face', *Environmental Science and Pollution Research* vol. 27, no. 8, pp. 7851-71.

Yuan, L & Smith, AC 2008, 'Numerical study on effects of coal properties on spontaneous heating in longwall gob areas', *Fuel*, vol. 87, no. 15-16, pp. 3409-19.

Yuan, L & Smith, AC 2009, 'CFD modeling of spontaneous heating in a large-scale coal chamber', *Journal of Loss Prevention in the Process Industries*, vol. 22, no. 4, pp. 426-33.

Yuan, L & Smith, AC 2014, 'CFD modelling of nitrogen injection in a longwall gob area', *International Journal of Mining and Mineral Engineering*, vol. 5, no. 2, pp. 164-80.

Yuan, L, Smith, AC & Brune, JF 2006, 'Computational fluid dynamics study on the ventilation flow paths in longwall gobs'.

Zhang, J, An, J, Wang, Y, Al Mamun, NA & Pan, R 2019a, 'Philosophy of longwall goaf inertisation for coal self-heating control, proactive or reactive?', *International Journal of Heat and Mass Transfer*, vol. 141, pp. 542-53.

Zhang, J, An, J, Wen, Z, Zhang, K, Pan, R & Al Mamun, NA 2020, 'Numerical investigation of coal self-heating in longwall goaf considering airflow leakage from mining induced crack', *Process Safety and Environmental Protection*, vol. 134, pp. 353-70.

Zhang, J, Zhang, H, Ren, T, Wei, J & Liang, Y 2019b, 'Proactive inertisation in longwall goaf for coal spontaneous combustion control-A CFD approach', *Safety Science*, vol. 113, pp. 445-60.

Zhang, W, Xue, S, Tu, Q, Shi, G & Zhu, Y 2022, 'Study on the distribution characteristics of dust with different particle sizes under forced ventilation in a heading face', *Powder Technology*, vol. 406.

Zhang, X & Zou, J 2022, 'Research on collaborative control technology of coal spontaneous combustion and gas coupling disaster in goaf based on dynamic isolation', *Fuel*, vol. 321, p. 124123.

Zhang, Y, Niu, K, Du, W, Zhang, J, Wang, H & Zhang, J 2021, 'A method to identify coal spontaneous combustion-prone regions based on goaf flow field under dynamic porosity', *Fuel*, vol. 288, p. 119690.

Zhang, Y, Wang, J, Xue, S, Wu, J, Chang, L & Li, Z 2016, 'Kinetic study on changes in methyl and methylene groups during low-temperature oxidation of coal via in-situ FTIR', *International Journal of Coal Geology*, vol. 154-155, pp. 155-64.

Zhang, Y, Wu, J, Chang, L, Wang, J, Xue, S & Li, Z 2013, 'Kinetic and thermodynamic studies on the mechanism of low-temperature oxidation of coal: A case study of Shendong coal (China)', *International Journal of Coal Geology*, vol. 120, pp. 41-9.

Zheng, Y, Lan, H, Thiruvengadam, M, Tien, JC & Li, Y 2017, 'Effect of single dead end entry inclination on DPM plume dispersion', *International Journal of Mining Science and Technology*, vol. 27, no. 3, pp. 401-6.

Zhou, C, Zhang, Y, Wang, J, Xue, S, Wu, J & Chang, L 2017, 'Study on the relationship between microscopic functional group and coal mass changes during low-temperature oxidation of coal', *International Journal of Coal Geology*, vol. 171, pp. 212-22.

Zhou, F, Ren, W, Wang, D, Song, T, Li, X & Zhang, Y 2006, 'Application of three-phase foam to fight an extraordinarily serious coal mine fire', *International Journal of Coal Geology*, vol. 67, no. 1-2, pp. 95-100.

Zhou, G, Yang, Y, Jing, B, Sun, B, Hu, S & Liu, Z 2022, 'Study on temporal and spatial evolution law for dust pollution in double roadway ventilation system of short wall continuous mining face', *Environmental Science and Pollution Research* vol. 29, no. 23, pp. 34419-36.

Zhou, X, Yang, Y, Zheng, K, Miao, G, Wang, M & Li, P 2021, 'Study on the spontaneous combustion characteristics and prevention technology of coal seam in overlying close goaf', *Combustion Science and Technology*, pp. 1-22.

Zhou, Z, Hu, P, Qi, C, Niu, T, Li, M & Tian, L 2018, 'The influence of ventilation arrangement on the mechanism of dust distribution in woxi pithead', *Shock and Vibration*, vol. 2018, pp. 1-13.

Zhu, H & Liu, X 2012, 'Theoretical investigation on the relationship between tail roadway methane drainage and distribution of easily spontaneous combustible region in gob', *Safety Science*, vol. 50, no. 4, pp. 618-23.

Zhu, H, Liu, X, Zhang, R & Zhang, S 2011, 'Numerical comparison of coal spontaneous combustion danger influenced by different methane drainage patterns in gob area', *Journal of Coal Science and Engineering (China)*, vol. 17, no. 2, pp. 157-62.

Zhu, P, Li, Q, Li, X, Zhang, G, Zhang, Y & Zheng, Y 2022, 'Investigation on the potential hazard zone of gas explosion in the goaf under longwall top caving coal mining condition', *Combustion Science and Technology*, pp. 1-20.

Zhuo, H, Qin, B & Qin, Q 2021, 'The impact of surface air leakage on coal spontaneous combustion hazardous zone in gob of shallow coal seams: A case study of Bulianta Mine, China', *Fuel*, vol. 295, p. 120636.

Zhuo, H, Qin, B, Qin, Q & Su, Z 2019, 'Modeling and simulation of coal spontaneous combustion in a gob of shallow buried coal seams', *Process Safety and Environmental Protection*, vol. 131, pp. 246-54.

Zosky, GR, Hoy, RF, Silverstone, EJ, Brims, FJ, Miles, S, Johnson, AR, Gibson, PG & Yates, DH 2016, 'Coal workers' pneumoconiosis: an Australian perspective', *The Medical Journal of Australia*, vol. 204, no. 11, pp. 414-8.

Zuo, Q & Li, J 2021, 'Simulation of fire smoke disaster in a goaf during the closure process', *Thermal Science*, vol. 25, no. 5 Part A, pp. 3399-407.